ARCHIVES OF ACOUSTICS
15, 1–2, 3–14 (1990)

OUTLINE OF THE POLISH ACOUSTICIANS HISTORY. PART I (UNTIL 1969)*

LESZEK FILIPCZYŃSKI

This elaboration is devoted to the chronology of the most important events in the scientific life of Polish acousticians. The beginning of Polish acoustics is located in the thirties. Unfortunately, tragical situation of Polish during the Second World War stoped scientific progress on that field. Those scientific and engineering staff suffered the importance personal losses they have been deptived their employments. The staff has been submitted to the dispersion. The laboratories equipment have been destroyed or carried out by the occupant. Libraries and collections of books have been lossed in such way, that now we posses almost any original documentation related to that period. The rememberance to be keep in the form of scanty of notes prepared by Prof. Marek KWIEK (tragical deceased in 1962) and by Prof. Zbigniew ŻYSZKOWSKI (deceased in 1988) and also reminescences of Prof. Ignacy MALECKI allowed to reconstruct in fragmentary form history of the birth of Polish acoustics. After year 1953, the activity of Polish acousticians is well-documented in the form of native and foreign scientific publications, books, handbooks, proceedings, list of papers of Polish acousticians [1–3] and also in the form of easy to attainment reports about scientific activity of Polish institutions, for example [5, 6, 20]. For that reason this period has been treated shortly.

The chronology of significants events has been divided into two periods. The first one of twenty-five years after liberation closed year 1969. This period contains creation of the Polish Society of Acoustics (1963) and Committee of Acoustics of Polish Academy of Sciences (1964) an initiation of the first quarterly periodic "Archives of Acoustics" (1966). At the end of period in the year 1967, it has been published the list of papers of Polish acousticians, to be appeared during the time 1945–1966.

The second part of outline of Polish acoustics history which is now preparing, contains chronological events of major importance to be arised after 1969.

---

* This paper was published in Polish in Proc. of the XXXVI Open Seminar on Acoustics "OSA-89" held in Szczyrk-Biła in September 1989, pp. 27-41

Events of major importance in Polish acoustics

1930

"System of transversaly recording of film sound by using a mirror oscillograph". This system, constructed and patented by Leonid PIMONOW, M. Sc.; graduated from the University of Vilno, was applied in almost all the sound films to be produced during the period 1930–1934 in Poland and next, the system was ransomed by the German firm "Klangfilm".

1933

a) M. KWIEK, M. Sc., graduated from University of Poznań in both different domains: physics and musicology, undertook the research on acoustics at University of Poznań [10–13]. He continued his postgraduate study in Germany under the supervision of Prof. F. TRENDELENGURG and Dr M. GRÜTZMACHER.

b) The first measurement of city noise was carried out in Warsaw, Cracow and Vilno in 1934 by applied the Barckhausen apparatus. The measurement was carried out under the supervision of W. GĄDZIKIEWICZ [24].

c) The Committee of Noise Overcoming was established by Union of Traffic Enterprises and Ministry of Communication. In 1936 the Committee submitted to the ministries and institutions some conclusions concerning the noise overcoming. The Second World War stopped the committee activity [24].

1934

The State Institute of Telecommunication located in Warsaw, Ratuszowa 11, to be supervised by Prof. Janusz GROSZKOWSKI, initiated the work on the telephonometrics and telephonic speaking machines. The work, conducted by T. KORN, M. Sc. was successful and allowed to introduce just before war the speaking clock into the public telephones net, W. FIJAŁKOWSKI, M. Sc., undertook the work on electro-acoustics specially the problem of telephony.

1935

a) The State Industrial Works of Tele- and Radiotechnics, located in Warsaw, Grochowska street, Section of Progress in Research – conducted by Z. ŻYCZKOWSKI, M. Sc., graduated from Electrical Department of Warsaw Technical University, joined the work on the new types of microphone inset with steel diaphragms and powder chambers, as the application to the laryngophones and telephone's receivers, based on the new types of magnets alloy. Previously, it has

been also constructed the dynamic loudspeaker which was applied to the Amplifon and next to the superheterodyne radio receivers.

b) Origin of the laboratory of architecture acoustics located at the Institute of Building Engineering of Civil Engineering Department of Warsaw Technical University. The laboratory was conducted by Prof. Wacław ŻEŃCZYKOWSKI. The measurement of noise and architecture acoustics research has been carried out by Bronisław BUKOWSKI, M. Sc., Irena WASIUTYŃSKA, M. Sc., and J. WOJCIECHOWSKI.

1936

a) The problem of architecture acoustics was carried out at the Research Institute of Building Engineering of Architecture Department of Warsaw Technical University (Head Prof. Stefan BRYŁA) by I. MALECKI [7], M. Sc. graduated from Electrical Department of Warsaw Polytechnics.

b) "Dependence of the sound property on its audibility" – Doctoral Thesis of M. KWIEK, M. Sc., has been promoted by Prof. L. KAMIŃSKI and Dr M. GRÜTZEMACHER at University of Poznań and published in Akustische Zeitschrift [14, 15]. Dr M. KWIEK cooperated as the assistent with Prof. Stanisław KALANDYK – head of the Institute of Physics at Medical Department of University of Poznań. Dr M. KWIEK published a few works on problems of noise and tone quality.

c) Creation of Technical Department at Research Office in Polish Radio Broadcasting in Warsaw under the supervision of I. MALECKI, M. Sc. [19]. I. MALECKI was just coming from Berlin, where he worked at Institut für Schwingungsforschung on the problem of high frequency ultrasonic wave-generation, under the supervision of Prof. E. MAYER.

The main area of interest of Technical Department concerned following problems: acoustics of broadcasting studios and design of the Central Broadcasting of Polish Radio. The department worked on the measurement of acoustic insulation and conditions of broadcasting studios also on testing of microphones and on carring out the theoretical and experimental research on acoustics of interiors. The work was also carried out by Stanisław KOWNACKI, M. Sc., Włodzimierz WORONCOW, M. Sc., and by a few technicians.

1938

Dr Wiktor JANKOWSKI graduated from the Medical Department of the University in Lwów publishes a paper on the internal ear (Pol. Gaz. Lek. **17**, 25, 519–524 (1938)) initiating his scientific activity directed toward acoustics.

Wincenty PAJEWSKI, M. Sc., carried out the research at the State Institute of Telecommunication on the profesional radio receivers, in particular the problem of frequency stability by using the piezoelectric oscillators.

1939

In March, the beginning of building of Central Broadcasting of Polish Radio in Warsaw. The acoustics design was just prepared by the team conducted by I. MALECKI, M. Sc. The architectonics design was worked out by Prof. B. PNIEWSKI.

Dr Tadeusz CEYPEK, graduated from the Medical Department of the University in Lwów, passed the habilitation in the otholaryngology.

1940

a) Closure by the occupant of all High Schools and laboratories.

b) Dr. M. KWIEK after expulsion by occupants from Poznań to Ostrowiec Świętokrzyski began to preserve the church organ. In the same time he worked on the problem of organ's acoustics. He made a few unique research on field of music's acoustics and detaily prepared instructions for the organ builders and musicians.

c) Conspiratorial teaching and researching on acoustics conducted by Prof. S. BRYŁA at Institute of Architecture of Warsaw Technical University which was acted under the sign-board of vocational school. There, I. MALECKI, M. Sc. received his Ph. D. degree on subject "Physics of porous materials" [16] promoted by Prof. S. BRYŁA. The Doctoral Thesis included recapitualation of the research work during the period 1936–1939.

d) After the returning from German captivity, W. PAJEWSKI, M. Sc. worked in private firm on the production of piezo-electric oscillators from where a part of production he supplied to the conspiratorial broadcasting net system in Warsaw District with the aid of engineer; later Prof. S. RYŻKO.

1941

Until 1943, Dr. I. MALECKI led the conspiratorial lecture on acoustics of interiors for students of the third year at the Architecture Department of Warsaw Technical University [16].

1943

a) The habilitation of Dr. I. MALECKI on "Propagation of sounds waves in closed areas" [17] at Architecture Department of Warsaw Technical University promoted by professors S. BRYŁA, R. TRECHCIŃSKI and M. WOLFKE.

b) In November, the occupant partialy revealed the conspiratorial activity of Warsaw Technical University. The lectures became suspended. Prof. S. BRYŁA has been shot.

1944

The total destruction of laboratories of Warsaw Technical University during the Warsaw Insurrection.

1945

a) The habilitation of Dr M. KWIEK on "The monumentary organ of the Kielecko-Sandomierski land" at the Humanistic Department of University of Poznań promoted by professors Józef WITKOWSKI and Adolf CHYBIŃSKI.

b) Creation of the Independent Section of Electro-Acoustics at the State Institute of Telecommunication supervised by Janusz KACPROWSKI, the specialist on the field of telephonometry.

1946

a) Creation of the Chair of Electro-technics and Acoustics at Gdańsk Technical University supervised by Prof. I. MALECKI.

b) Associated Prof. W. JANKOWSKI moves from Lwów to Wrocław organizing there the Clinics of Otolaryngology at the Medical Academy.

c) W. PAJEWSKI, M. Sc. after the returning from the labour camp in Germany organized the Section of Piezo-electric Materials at the State Institute of Telecommunication in Warsaw. At the same time he lectured on "Materials and Piezo-electric elements at Warsaw Technical University.

After emigration from Lwów to Zabrze prof. T. Ceypek organizes in 1950 at the Silesian Medical University the Otholaryngological Chair and Clinics. As the head of that centre he initiates in 1953 the scientific activity in industrial audiology. Cooperating with university acoustical centers he concentrates his activity in acoustic damage problems occurring in the metalurgical and mining industries.

1947

Creation of the Acoustics Section – supervised by doc. M. KWIEK, at the Chair of Experimental Physics of University Poznań, conducted by Prof. Szczepan SZCZENIOWSKI.

1948

Beginning of students education on the field of electro-acoustics at Wrocław Technical University – Z. ŻYSZKOWSKI lectured on the subjects: electro-acoustics and electro-acoustics devices at Telecommunication Section of Electrical Department.

1950

a) Vocation of Prof. I. MALECKI as the Head of Institute of Electro-acoustics at Warsaw Technical University, colaborators Witold STRASZEWICZ, M. Sc., and Stefan BASIŃSKI, M. Sc; students education on film technique and electro-acoustics in broadcasting.

b) Initiation of the Main Institute of Technical Physics in Warsaw. Appointement of Acoustics Section and Laboratory supervised by Prof. I. MALECKI (collaborators Leszek FILIPCZYŃSKI, M. Sc., Jerzy WEHR, M. Sc., [25] and Wacław KOŁTOŃSKI, M. Sc.).

c) The work on the echo sounder's construction for the Radio Ship Service supervised by Zenon JAGODZIŃSKI, M. Sc.

1951

Initiation of the research activity in the Sonochemistry by Prof. Bronisław ZAPIÓR at the Jagiellonian University in Cracow in the Chair of General Chemistry. In 1961 Adam JUSZKIEWICZ, M. Sc. began the collaboration in this field. After prof. B. ZAPIÓR was penssioned off in 1961, dr A. JUSZKIEWICZ took over the Section of Sonochemistry.

1952

a) Creation of the Institute of Acoustics and Vibration Theory supervised by doc. M. KWIEK, at the Chair of Theoretical Physics conducted by Prof. S. SZCZENIOWSKI (collaborators Halina RYFFERT, M. Sc., Antoni ŚLIWIŃSKI, M. Sc., and shortly Helena HARAJDA, M. Sc. just before transition to the Institute of Vibration Research at Academy of Agriculture in Poznań).

b) Creation of the Institute of Vibration Research at Polish Academy of Sciences in Warsaw supervised by Prof. I. MALECKI, the structure of Institute has been based on the team came from the Main Institute of Technical Physics. In the next year Institute has been integrated with the new created Institute of Fundamental Technological Research [5] (the new collaborators J. KACPROWSKI, M. Sc. and W. PAJEWSKI, M. Sc., since 1953 – Jerzy RANACHOWSKI, M. Sc. and Stefan CZARNECKI, M. Sc [4], since 1956 – Ryszard PŁOWIEC, M. Sc., since 1957 – Z. PAWŁOWSKI, M. Sc.).

c) Prof. Z. ŻYSZKOWSKI lectured on electro-acoustics and electro-acoustics transducers at Telecommunication Department of the Technical University in Wrocław.

d) Prof. I. MALECKI won the Third Degree State Prize for the research on acoustics of interiors.

e) W. PAJEWSKI, M. Sc., won the Third Degree State Prize for the research on

materials and piezo-electric elements and for the production implementation of quartz oscillators and piezo-electric crystals.

f) Creation of the Central Laboratory of Polish Radio Broadcasting in Warsaw Head Dr Bolesław URBAŃSKI, which was integrated with the Section of Acoustics (Head S. CZARNECKI, M. Sc.).

1953

a) The First Conference on Ultrasonic Technics to be organized by Institute of Fundamental Technological Research PAN in Warsaw, inaugurated a series of meetings with the wide number of foreign participants. During the years 1953–1966 six conferences took places to be organised by IFTR PAN in Warsaw [18], Międzyzdroje [23], Krynica and Jabłonna [8]. The proceedings were published in Polish and English. During these conferences the all over the world connections have been formed between the participants from Poland, France, Germany, Soviet Union and Czechoslovakia.

b) Creation of the Building Systems and Acoustics Department at Research Office in Polish Radio Broadcasting (since 1959 – Department of Radio and Television Broadcasting conducted by J. SADOWSKI, M. Sc. – graduated at Department of Telecommunication of Warsaw Technical University.

c) The chair of Radio Navigation has been organised by Z. JAGODZIŃSKI, M. Sc., at Gdańsk Technical University. The field of research was extended on ultrasonics and hydroacoustics by constructing the echo sounder and sonar which have been used wreck searching on polish shelf. In the second part of fifties the hydrotelephone has been constructed for diver's wireless communication.

d) Zbigniew KACZKOWSKI, M. Sc., undertook the research on magnetistrictive materials in Department of Electronics (Head Prof. J. GROSZKOWSKI) in the Institute of Fundamental Technological Research in Warsaw.

e) Prof. W. JANKOWSKI takes over the Chair and Clinics of Otolaryngology in Medical Academy of Wrocław developing an intensive cooperation with Polish Acoustical Centers.

1954

a) The First Open Acoustics Seminar has been organized by Prof. M. KWIEK at Department of Acoustics and Vibration Theory of University Poznań. From the Second one up [21, 22] to the Fifth seminars took places yearly at the High School of Agriculture in Olsztyn, organized by the Chair of Physics, conducted by doc. Franciszek KUCZERA (collaborant Aleksander OPILSKI, M. Sc.). At the seminars the Polish and foreign participants took part on the field of physical and technical acoustics. The next seminars took places in Zabrze-Rokitnica, Gliwice, Szczecin, Poznań, Warszawa and Wisła (see the elaboration devoted to the twenty-five years of the Polish Society of Acoustics [26]).

b) The Wire Transmission Chair, supervised by Prof. Z. ŻYSZKOWSKI has been transformed into the chair of Wire Teletransmission together with the Electro-acoustics Institute at the Technical University in Wrocław.

1956

a) At the first time the Polish Acousticians took part in the 2-nd International Congress of Acoustics (ICA) held in Stuttgart.

b) Creation of the Independent Chair of Acoustics and Vibration Theory at University of Poznań (supervised by Prof. M. KWIEK, the new collaborant – Prof. Edmund KARAŚKIEWICZ).

c) Creation of the Department of Technical Acoustics at the Central Institute of Labour Protection in Warsaw the scientific activities of which was concerned with the method of industry noise measurement and acoustical expertises (Head of Czesław PUZYNA, M. Sc.).

d) Dr of English philology Wiktor JASSEM, head of the Phonography Section at the University in Poznań, organized in Poznań the Section of Acoustical Phonetics in the frame of IFTR PAN.

1957

Initiation of the following publications: "Progress in Acoustics" (published in the frame of works of Natural Philosophy Committee at Poznań Society of Science's Friends), single copies of "Acoustics" as the part of Scientific Copies of Poznań University and two volumes of "Bulletin de la Societe des Amis des Sciences et des Lettres" [20].

1958

Creation of the Section of Buildings Acoustics (supervised by Dr Jerzy Sadowski) transformed in 1962 into the Acoustics Department at the Institute of Building Techniques in Warsaw (the new collaborant Barbara SZUDREWICZ, M. Sc., 1962).

1959

a) The quarterly "Proceedings of Vibration Problems" published by Prof. Sylwester KALISKI at the Institute of Fundamental Technological Research PAN concerned the problems of acoustics in the wide range. In 1975 the quarterly changed the title on "Journal of Technical Physics".

b) Creation of the specialization – electro-acoustics at the Department of Telecommunication of Wrocław Technical University.

1961

During the Open Seminar on Acoustics in Szczecin the team of 38 founders decided to establish the Polish Society of Acoustics.

1962

The tragical deceased of Prof. M. KWIEK in airplane's crash. The Head of Chair became Prof. E. KARAŚKIEWICZ and at the next years doc. H. RYFFERT (the new collaborants Edward HOJAN, M. Sc., Edward OZIMEK, M. Sc., and Mikołaj ŁABOWSKI, M. Sc.).

1963

a) The Foundation's Gathering of the Polish Society of Acoustics in Poznań. The first Chairman was Prof. E. KARAŚKIEWICZ.

b) The affiliation of the Polish Society of Acoustics at the Fourth Department of Technical Sciences, Polish Academy of Sciences.

1964

a) Creation of the Committee of Acoustics at the Fourth Department of Technical Sciences, Polish Academy of Sciences. The first chairman became Prof. I. MALECKI (1964–1971), the second Prof. L. FILIPCZYŃSKI (1971).

b) The Chair of Physics "A" of Silesian Technical University since 1971 – Institute of Physics headed by Prof. F. KUCZERA, collaborant Dr. A. OPILSKI organized the research on molecular acoustics of fluids. In 1966 the Department of Electrophysics was formed in which the research on quantum of semiconductors and acousto-optics has been undertaken, the supervision of Prof. A. OPILSKI (collaborant Z. KLESZCZEWSKI, M. Sc).

1965

a) Creation of the Section of Music Acoustics at the Department of State-Managing of the Warsaw High School of Music (head Prof. Andrzej RAKOWSKI, collaborants Tomasz ŁĘTOWSKI, M. Sc., and Antoni JAROSZEWSKI, M. Sc.). In 1968 the Section transformed into the Chair of Musical Acoustics, supervised by the same person (collaborants Prof. Marian RAJEWSKI and Prof. B. URBAŃSKI). In 1979 the High School was renamed on the F. Chopin Academy of Music.

b) The research programme on urban-acoustics was elaborated by the Acoustics Department of ITB (head of Prof. J. SADOWSKI) in collaboration with

Department of Electroacoustics of Warsaw Technical University, Chair of Acoustics of Poznań University, the Warsaw Institute of Automotive Transport, the Warsaw Office of Study and Project in Urban Engineering, the Airport Administration of Air Forces and the others institutions. As the result of this activity the acoustics map of Warsaw, Gdańsk and Poznań and also the basis of urban-acoustics were created.

c) Creation of the Laboratory of Industry Audiology at the Main Institute of Mining in Silesia in which the problems of hearing prophilacticity during the mining process were considered under the supervision of Dr. T. MALINOWSKI. In 1969 Laboratory of Vibroacoustics Menacement was formed, headed by Dr. Adam LIPOWCZAN. In 1976 both laboratories were reorganized into Department of Health Protection and Department of Technical Acoustics under the same menagements.

1966

a) Initiation of the quarterly "Archives of Acoustics" (Archiwum Akustyki) published by Committee of Acoustics PAN and Polish Society of Acoustics (editor Prof. Stefan CZARNECKI).

b) Prof. I. MALECKI has been elected as the Chairman of the International Committee of Acoustics (ICA) for two terms of office 1966–1972. He presided at the meetings of the International Committee of Acoustics held in Tokio – 1968 and Budapest – 1971.

c) The team of Prof. I. MALECKI, Prof. L. FILIPCZYŃSKI, doc. Z. PAWŁOWSKI and doc. J. WEHR won the Second Degree State Prize in Science for works devoted on propagation of ultrasonic waves.

d) Creation of the Department of Acoustics at the Rzeszów High School of Pedagogy, the main scientific programme of which concerned with the theory of acoustics fields (head of Prof. Roman WYRZYKOWSKI, since 1967 collaborant Witold RDZANEK, M. Sc.). In 1984 Prof. W. RDZANEK became the head of Department.

e) Creation of the Institute of Electronic Technology PAN. In 1966–1967 prof. W. PAJEWSKI and doc. Z. KACZKOWSKI organized the Department of Piezotronics with the Piezomagnetic Section.

1967

Bibliographic list of the Polish author's works in the field of acoustics published during the periods 1945–1966 [1], 1966–1971 [2], and 1972–1982 [3].

1968

a) The intensification of research activity on hydro-acoustics at Gdańsk Technical University – formation of the Hydro-acoustics Department at Institute of Telecommunication supervised by Prof. Z. JAGODZIŃSKI, doc. Gustaw BUDZYŃSKI

was the head of the electrophone's problems. In the year 1980, Department of Hydro-acoustics has been divided into Hydroacoustics Department and Sound's Engineering Department, the supervisions by the hitherto persons.

b) Initiation of the book "Speach Analysis and Synthesis" published by the Institute of Fundamental Technological Research PAN and PWN, devoted on problems of the acoustics of speech (editor Prof. Wiktor JASSEM). The next volumes have been edited in the years 1970, 1973, 1976 and 1981.

1969

Creation of the Co-ordination Center of Acoustics Problems Architecture at the Council for Mutual Economic Aid with which the following institutions collaborated: Acoustics Department of Institute of Building Technology in Warsaw, Institute of Acoustics of Poznań University, Institute of Telecommunication of Gdańsk Technical University, Institute of Mechanics and Vibroacoustics of Cracow Academy of Mining and Metallurgy, Institute of Radioelectronics of Warsaw Technical University and Warsaw Academy of Music.

References

[1] *Bibliographic list of the Polish Acousticians's works* 1945–1965 Arch. Akustyki, **2**, 1, 3–68 (1967) (in Polish).

[2] *Bibliographic list of the Polish acoustician's works* 1966–1971. Arch. Akustyki, **7**, 2, 3–77 (1972) (in Polish).

[3] *Bibliographic list of the Polish acoustician's works* 1971–1982 Arch. Akustyki **19**, 1–2 1984 (in Polish).

[4] *"Stefan Czarnecki" — rememberance.* Arch. Akustyki, **17**, 3–4, 209 (1982) (in Polish).

[5] *Scientific Activity of Institute of Fundamental Technological Research PAN in 1962*, PWN Warsaw 1963 (also following years up to the present year).

[6] *Ten years of Electro-acoustics Chair activity.* Offset edition by Technical University of Warsaw. Warsaw 1961 (in Polish).

[7] L. FILIPCZYŃSKI, "I. MALECKI", Nauka Polska, **2**, 67–70 (1962) (in Polish).

[8] L. FILIPCZYŃSKI, J. KACPROWSKI, H. RYFFERT, *The current state and perspective of scientific progress in acoustics in Poland until 1985*, Arch. Akustyki, **8**, 2, (1973). *Chapter III. Progress and current state of acoustics in Poland*, 166–169. Anex. Meetings Activity 224–226 (in Polish).

[9] S. IWANKIEWICZ, *"Prof. dr hab. Wiktor Jankowski"*. Akademia Medyczna, Wrocław 1975.

[10] M. KWIEK, *The initial research on tone quality of vibrating string*, Musicology Annual I, Lwów 1934 or 1935 (in Polish).

[11] M. KWIEK, *The scientific methods of noise overcoming.* The lecture delivered in 1936 Meeting of International Committee for Noise Overcoming acted as the structural part of the League of Nations in Geneve, and at Meeting of the Society of Warsaw Technical University.

[12] M. KWIEK, *Resonance factors in tone quality*, Musicology Annual II, Warsaw 1936 (in Polish).

[13] M. KWIEK, *The admissible noise limit determination in habitable interiors*, Technical Review 14/15 Warsaw 1937 (in Polish).

[14] M. KWIEK, *Über Laustärke und Lautheit*, Akustische Zeitschrift **2**, 170–178 (1937).

[15] M. KWIEK, *Dependence between physical properties of sound and it audibility taking into account musical problems*, The Quarterly of Psychology, **10**, 59–102 (1938) (in Polish).

[16] I. MALECKI, *Fizyka materiałów porowatych*. Wyd. powielone przez Wydział Architektury Politechniki Warszawskiej, Warszawa 1941.
[17] I. MALECKI, *The wave propagation in closed areas*, Editor: Gdańsk Technical University, Gdańsk 1949 in Polish.
[18] *Proceeding of Ultrasonic Technics Conference* 1953, IFTR-PAN PWN Warsaw 1954.
[19] S. MISZCZAK, *History of Radio and Television Broadcasting in Poland*, Warsaw, WKŁ 1972 (in Polish).
[20] E. OZIMEK [Ed.], *Research at the Institute of Acoustics*, Adam Mickiewicz University, Poznań 1984, Serie of Acoustics No. 8
[21] *Proceeding of the II Open Seminar on Acoustics* – Olsztyn 1955, Ed. Olsztyn 1958 (in Polish).
[22] *Proceeding of the III Open Seminar on Acoustics* – Olsztyn 1956, Ed. Olsztyn 1959.
[23] *Proceeding of the II Conference on Ultrasonics*, Międzyzdroje 18–28. VI. 1956, PWN Warszawa 1957 (also in Polish).
[24] J. SADOWSKI, *Architecture's Acoustics*, PWN, Warszawa-Poznań 1976 p. 9 in Polish.
[25] "*J. Wehr*" – *Remembrance*, Arch. Akustyki, **12**, 4 (1977) (in Polish).
[26] J. ETIENNE, Z. JAGODZIŃSKI, *XXV Years of the Polish Acoustical Society (in Polish)*, XXXVI Otwarte Seminarium z Akustyki OSA 89, Szczyrk-Biła, wrzesień 1989, 15–25.

ARCHIVES OF ACOUSTIS
15, 1–2, 15–30 (1990)

ELECTROACOUSTIC SYSTEM IN THE NATIONAL MUSEUM "PANORAMA RACŁAWICKA" IN WROCŁAW

J. BEDNAREK, T. GUDRA, K. RUDNO-RUDZIŃSKI

Institute of Telecommunication and Acoustics, Technical University of Wrocław
(50-370 Wrocław, Wybrzeże Wyspiańskiego 27)

This paper presents a designed and produced electroacoustic system assisting the tour of an exhibition intended for a great number of visitors. The microprocessor operated electroacoustic system fulfills two functions: transfers the commentary to the exhibition and controls the visitor's traffic.

A sound amplification system, which makes it possible to relay at the same time six language versions of the explanatory commentary to different groups of listeners through loudspeakers and earphones, is presented. Such a system enables simultaneous transmission of two different commentaries to two groups in the same interior.

Fundamental elements of technological designs applied in the electroacoustic system are also discussed here.

W pracy przedstawiono opracowany i wykonany system elektroakustyczny wspomagający zwiedzanie obiektu wystawienniczego przeznaczonego dla dużej liczby zwiedzających. System elektroakustyczny, sterowany mikroprocesorem, spełnia dwie funkcje: przekazywanie komentarza objaśniającego wystawę i sterowanie ruchem zwiedzających.

Przedstawiono realizację nagłośnienia umożliwiającą przekazywanie sześciu wersji językowych komentarza objaśniającego jednocześnie dla różnych grup słuchaczy za pomocą głośników i słuchawek. Rozwiązanie systemu nagłośnienia głośnikowego umożliwia równoczesny przekaz dwóch różnych komentarzy dla dwóch grup znajdujących się w tym samym wnętrzu.

Omówiono podstawowe elementy rozwiązań technicznych zastosowanych w systemie elektroakustycznym.

1. Introduction

The group of buildings of the "Panorama Racławicka" was created in order to exhibit the famous battle-scene painted by Kossak and Styka. This work of art with great historical value, which rouses enormous interest from the society, required not only an adequate building for exposition but also technical equipment. The "Panorama Racławicka" consists mainly of the painting, but it is only one of the elements of a complex whole.

The "Panorama Racławicka" exhibition consists of the Rotunda with the painting Small Rotunda with the model of the battle and show-cases with iconographic materials, and hall with video systems and film and slide projection screens (Fig. 1). The surface of the scenic platform in the Rotunda is relatively small, because of the geometry and perspective of the painting. Similar limitations concern

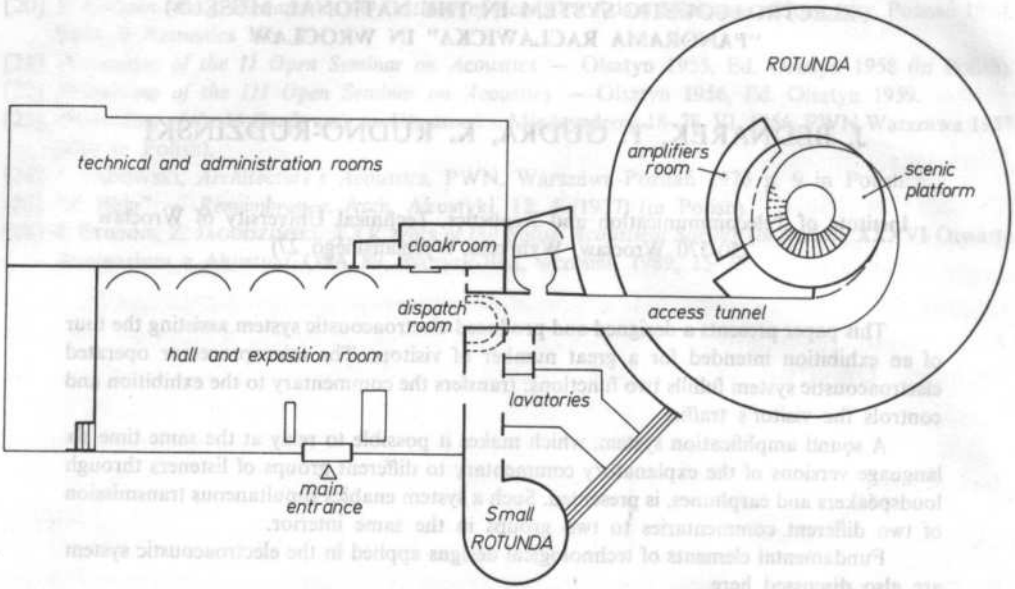

FIG. 1. "Panorama Racławicka" museum — horizontal projection

the Small Rotunda. Therefore, the largest possible capacity of the object with a possible widest commentary on the "Panorama Racławicka" in the conditions of limited space and related safety rules concerning visitors and protection of the painting (e.g stability of climatic conditions inside the building) was the basic problem of the design. Eventually it was accepted that no more than two groups of 40 persons on opposite sides of the platform can be on the scenic platform in the Rotunda at the same time. The touring time of one group was determined at 40 minutes. This time is divided into six intervals corresponding with six sectors the painting is divided into.

On the basis of the nature of the exposition and accepted organization of sightseeing assumptions to the electroacoustic system design were determined. First of all, it has to be made sure that the commentary concerning the painting and the model of the battle is intelligible. It should be possible to transmit the commentary in several languages at the same time. For safety reasons the dispatcher's information had to reach visitors in all possible places. Also, fast communication between the staff of the museum had to be ensured. Furthermore, the whole electroacoustic system should function properly also at different organizations of the visitors'traffic in the

hall, Rotunda and Small Rotunda. It should be noted that the sound amplification system was designed when all designs of interiors were confirmed and could not be changed from the point of view of acoustic requirements. All loudspeakers had to be inperceptible, composed with other elements of interior decorations. Mainly stone, metal and glass were used in interiors of the "Panorama Racławicka" object.

In our work on the electroacoustic system we intended to take advantage of experiences from the exhibition of other panoramas of exhibitions with a similar organization of sight-seeing as accepted for the object under consideration. Unfortunately none were found.

2. Idea of the system

The accepted idea of the system was a result of an analysis of requirements of the organization of visitors' traffic on exhibitions and of other assumptions mentioned in the introduction. It was stated that the system has to be automatic and it has to unite two basic functions:

- transmission of the commentary explaining the exhibition,
- control of the visitors' traffic.

Full synchronization of visitors' traffic has to be ensured for this system to function. In this case the staff of the object has different tasks in classical solutions. In normal work conditions the dispatcher of the object has to start the system and chose the sightseeing course (one-group, two-group or single). The choice of languages of the commentary for a given group and a discret supervision of the group are the tasks of guides. Other functions are fulfilled by the electroacoustic system.

Also the replacement of guides by electroacoustic devices is advantageous because of the constancy of the artistic and emotional side of the commentary.

Figure 2 presents a simplified block diagram of the electroacoustic system. It indicates places in rooms of the object in which individual units are situated.

Intensive exploitation of the electroacoustic system and accepted system of earlier ticket reservation imposed high reliability requirements on the devices on one hand and the necessity of quick defect localization and their immediate repair. This problem was solved with reserve systems switched on in a case of a failure (reserve TTL control system, loop tape recorders, power amplifiers). As for the organization of the system, a fault detection system was applied. Fig. 3 present a full block diagram of the electroacoustic system, containing control, diagnostics and sound signal paths.

Two independent subsystems complement the electroacoustic system. The subsystem of the radio relay centre makes it possible to pass dispatcher's informations and instructions to all places in the buildings of the museum, in which people are present. He can use additional loudspeakers in rooms outside the

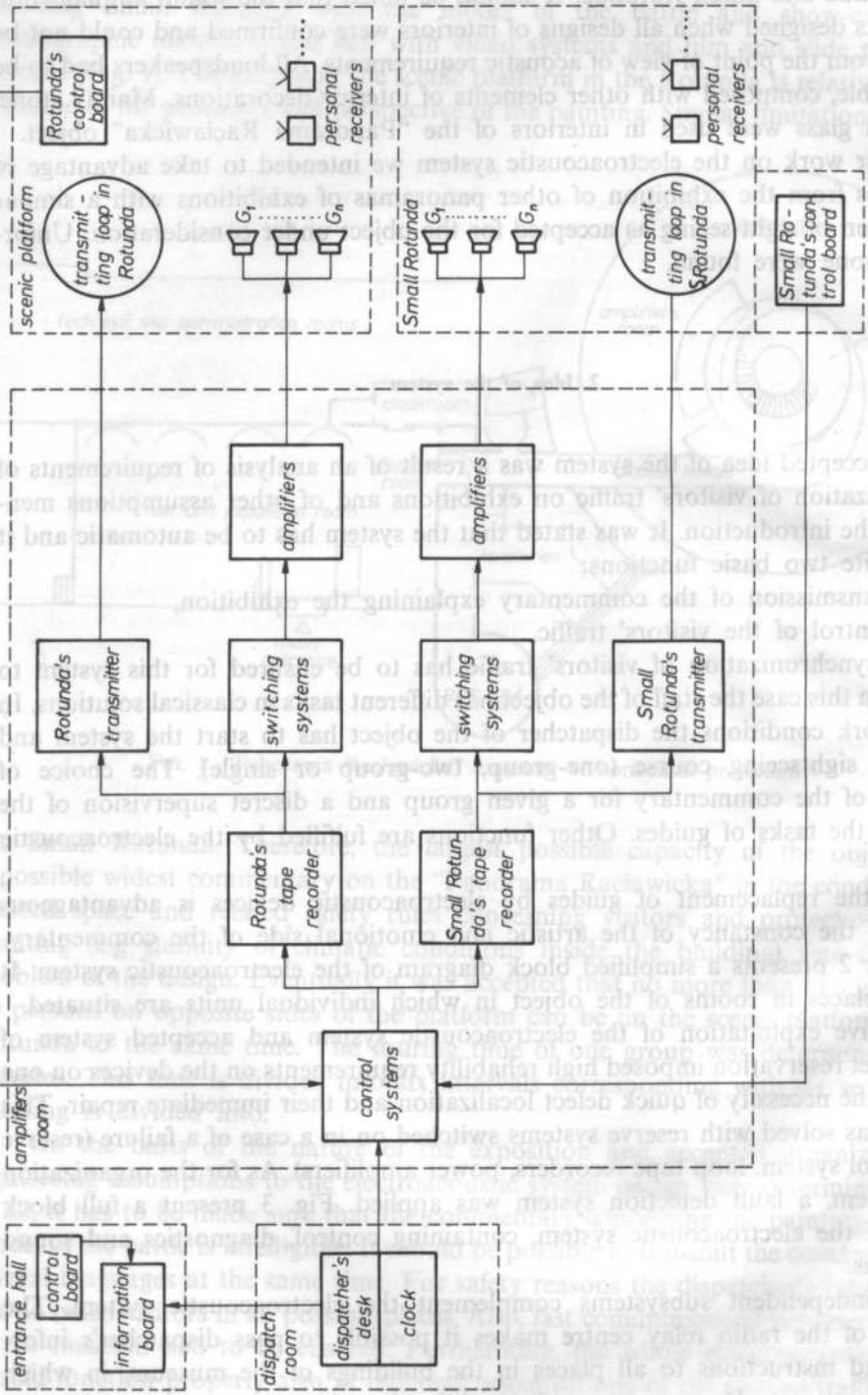

FIG. 2. Simplified block diagram of the electroacoustic system

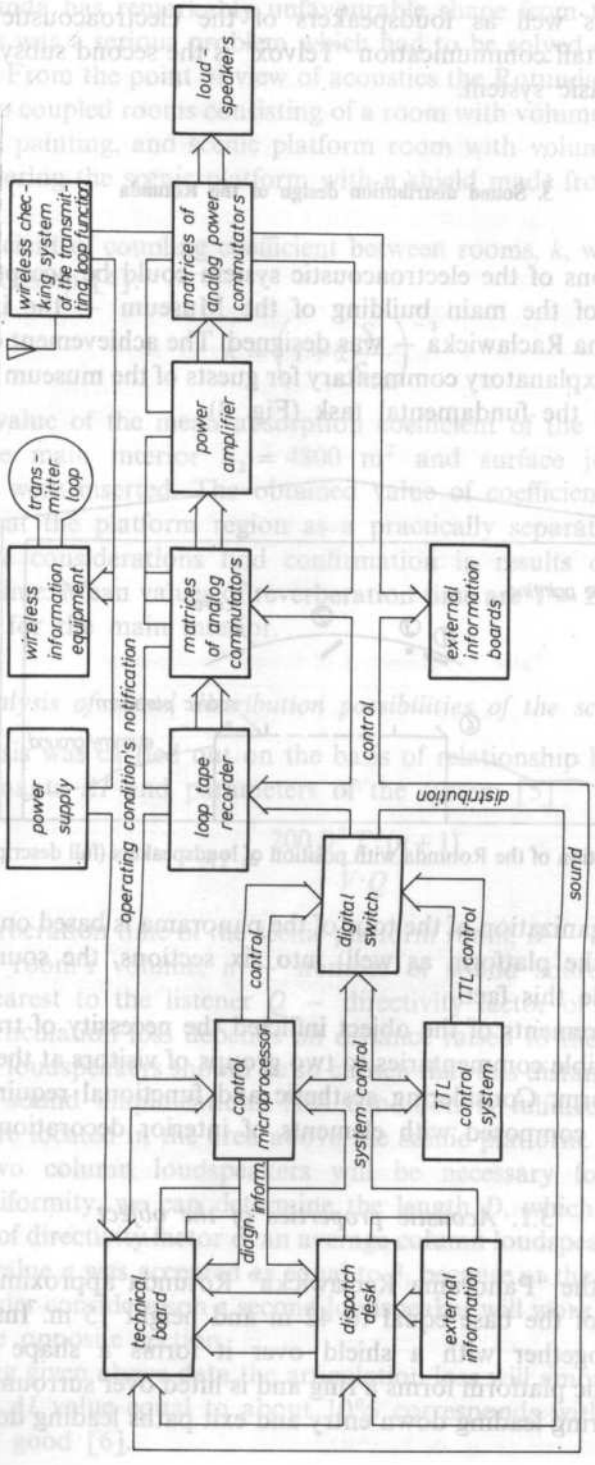

FIG. 3. Block diagram of the electroacoustic system

sightseeing route, as well as loudspeakers of the electroacoustic system. The subsystem of quick staff communication "Telvox" is the second subsystem. It is not connected to the basic system.

3. Sound distribution design of the Rotunda

Detailed solutions of the electroacoustic system could be accepted only when sound distribution of the main building of the Museum – the interior of the Rotunda of Panorama Racławicka – was designed. The achievement of high quality transmission of the explanatory commentary for guests of the museum staying on the scenic platform was the fundamental task (Fig. 4).

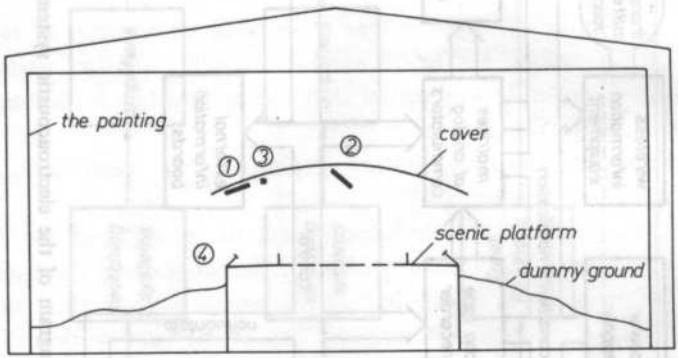

FIG. 4. Diagrammatic section of the Rotunda with position of loudspeakers (full description in the paper)

Because the organization of the tour of the panorama is based on the division of the painting (and the platform as well) into six sections, the sound distribution system must include this fact.

Capacity requirements of the object inflicted the necessity of transmitting two different but intelligible commentaries to two groups of visitors at the opposite sides of the scenic platform. Considering aesthetic and functional requirements, loudspeakers had to be composed with elements of interior decorations.

3.1. Acoustic properties of the object

The shape of the "Panorama Racławicka" Rotunda approximates a cylinder with the diameter of the base equal to 42 m and height 15 m. Inside is a scenic platform, which together with a shield over it forms a shape approximating a cylinder. The scenic platform forms a ring and is lifted over surrounding it artificial ground. Inside the ring leading down entry and exit paths leading down are located (Fig. 1, Fig. 4).

The Rotunda has remarkably unfavourable shape from the point of view of acoustics. This was a serious problem which had to be solved during designing the sound system. From the point of view of acoustics the Rotunda can be described as a system of two coupled rooms consisting of a room with volume of about 20000 m^3, containing the painting, and scenic platform room with volume of about 800 m^3, formed by covering the scenic platform with a shield made from roll formed sheet aluminium.

The coefficient of coupling coefficient between rooms, k, was estimated on the basis of relationship [4]:

$$k = \left(1 + \bar{\alpha}\frac{S_2}{S_{12}}\right)^{-1}$$

in which the value of the mean absorption coefficient of the main room $\bar{\alpha} = 0.1$. Surface of the main interior $S_2 = 4800$ m^2 and surface joining both rooms $S_{12} = 190$ m^2 were inserted. The obtained value of coefficient $k = 0.28$ makes it possible to treat the platform region as a practically separate room.

The above considerations find confirmation in results of measurements of reverberation time. Mean values of reverberation time are $T = 2.2$ s for the platform and $T = 3.8$ s for the main interior.

3.2. Analysis of sound distribution possibilities of the scenic platform

The analysis was carried out on the basis of relationship between articulation loss for consonants AI and parameters of the system [5]

$$AI = \frac{200\,D^2\,T^2(n+1)}{V \cdot Q}$$

where T is reverberation time of the scenic platform room, D – loudspeaker-listener distance, V – room's volume, n – number of sound sources apart from the loudspeaker nearest to the listener Q – directivity factor of sound source.

Because articulation loss depends on distance raised to the second power, the arrangement of loudspeakers should be so chosen that this distance is smallest in the entire area of sound amplification. This condition is fulfilled best of all when loudspeakers are located in the area above the scenic platform. Furthermore, if we accept that two column loudspeakers will be necessary for adequate sound distribution uniformity, we can determine the length D, which is equal to 3.5 m.

The value of directivity factor of an average column loudspeaker, equal to 7, was accepted. The value n was accepted as equal to 3, because at the same time with the loudspeaker under consideration a second loudspeaker will work in the same section and two in the opposite section.

Considering given above data the articulation loss will amount to $AI = 10.9\%$. The calculated AI value equal to about 10% corresponds with quality of speech judged as very good [6].

3.3. Column loudspeaker design

The following assumptions were accepted for the designed column loudspeaker: frequency response uniform in the band from 200 Hz to 5000 Hz and droping below 200 Hz to limit acoustic energy in the range of low frequencies where the reverberation time assumes highest values and it is impossible to achieve high radiation directivity of the column. In order to secure uniform sound distribution of the entire width of the platform, the 6 dB coverage angle should be equal to 45 degrees.

The column loudspeaker was built from GDS 8/4 type broad-band loudspeakers. They have required small dimensions and high quality.

In order to minimize the variability of column directivity due to frequency, a column with active length decreasing with frequency increase was designed. This was achieved with low-pass filters extreme loudspeakers. Since switching off of extreme loudspeakers at higher frequencies gives lower response of the column, a condenser was connected in series before the transformer at the input of the column to equalize the response. The condenser was also secure adequate load for the power amplifier at low frequencies.

Table 1. Parameters of column loudspeaker

Frequency [Hz]	500	1000	2000	4000
Directivity factor Q	3.1	4.3	6.5	9.0
6-dB coverage angle	130°	69°	59°	45°

Required directivity was achieved with a column of 5 loudspeakers. Further extention of the column was inexpedient considering too low sound uniformity in the required coverage angle. Measured parameters of the column are given in Table 1. The sensitivity of the column is equal to 94 dB.

3.4. Comparison of various solutions of sound distribution

When prototypes of column loudspeakers were made, measurements of electroacoustic characteristics of the Rotunda's sound distribution system were performed. The maximal value of local-dependent irregularities of frequency response in a given section in the useful frequency band and crosstalk damping between opposite sections were to be determined from measurements. Pink noise was supplied to loudspeakers. The analysis was carried out in 1/3 octave bands.

The following seven sound distribution systems were tested:

1. 3 units of ZG5c S type loudspeakers located every 20 degrees in the outer railling of the platform (Fig. 4, No. 4),

2. Loudspeakers as above located on the shield above the platform (No. 3).

3. 3 units eight-loudspeaker columns on the shield spaced every 20° over the platform (No. 1).

4. One column as in point 3, installed in an acoustic baffle with dimensions 1 m × 1 m, located in the centre of the shield (No. 2).

5. Single five-loudspeaker column situated in the shield in the centre of the section (No. 1).

6. 3 columns as above spaced every 20° in the shield (No. 1).

7. 2 columns as above spaced every 30° in the shield (No. 1).

Results of measurements of frequency response irregularities measurements indicate two groups of solutions. System 2 and 4 belong to the first group and display much smaller non-uniformity than the rest of the solutions which form the second group. Measured values of crosstalk damping indicate the same repartition of systems; solutions with smallest non-uniformity have smallest crosstalk damping thus worst quality of speech at the same time.

From among other solutions the system with loudspeakers in the railing was rejected as inconvenient from the exploitation point of view and besides sensible to the number of listeners in the section.

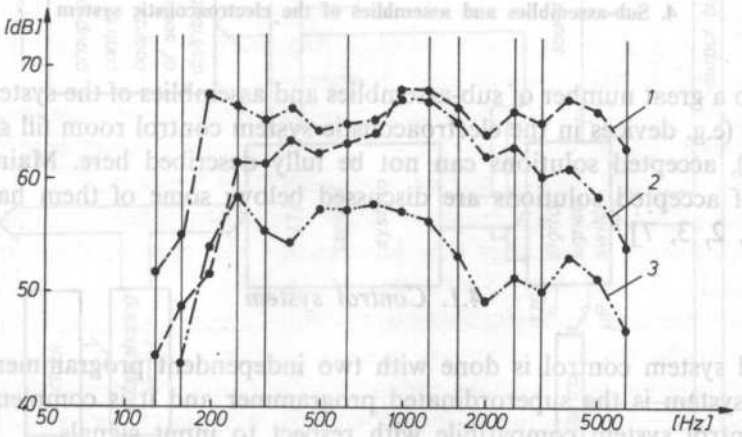

FIG. 5. Level of acoustic pressure under column loudspeaker: 1 – frequency characteristic, 2 – effect of tone quality control, 3 – crosstalk from opposite sector

The chosen previously system with two five-loudspeaker columns reconciles best from among solutions with columns situated above the platform requirements of small non-uniformity high crosstalk damping and minimal number of columns working at the same time. For this system irregularities of frequency response for the entire band is equal to 3 dB, crosstalk damping 9.8 dB (Fig. 5).

3.5. Speech intelligibility testing

Measurements of articulation score for logatoms were a final verification of the accepted sound distribution system. Test logatom lists were applied, structurally and phonetically balanced with each other and in relation to adequate Polish language statistics. Simultaneously with logatoms a speech signal similar to the planned manner of reading the commentary was sent from the column in the opposite section. Levels of the test signal and disturbance in their sectors were equalized and equal to 70 dB.

A group of 19 listeners without previous preparation aged from 25 to 50 years participated in measurements. It consisted of 6 women and 13 men – workers of the Technical University of Wrocław, employed as scientific workers, technical workers and workmen.

An analysis of listeners' records noted on forms proved that they had received correctly 88.4% of sent logatoms. This corresponds with articulation loss for consonants not greater than 11.6%, what is a similar value to the given previously estimation, equal to 10.9%. The measured value of articulation store for logatoms corresponds with practically 100-percent intelligibility of phrases.

4. Sub-assemblies and assemblies of the electroacoustic system

Due to a great number of sub-assemblies and assemblies of the system and their complexity (e.g. devices in the electroacoustic system control room fill six CAMAC type racks), accepted solutions can not be fully described here. Main functional elements of accepted solutions are discussed below; some of them have received patents [1, 2, 3, 7].[1]

4.1. Control system

Sound system control is done with two independent programmers; a microprocessor system is the superordinated programmer and it is complemented with a TTL control system compatibile with respect to input signals.

There are 3 methods of sound system control:
- with a microprocessor programmer (μP),
- with a TTL programmer,
- with both programmers working simultaneously.

Such a solution increases the reliability of the electroacoustic system and makes it possible to repair one programmer without putting the entire system out of action.

[1] All devices within the electroacoustic system are original designs or adaptations of devices produced in Poland.

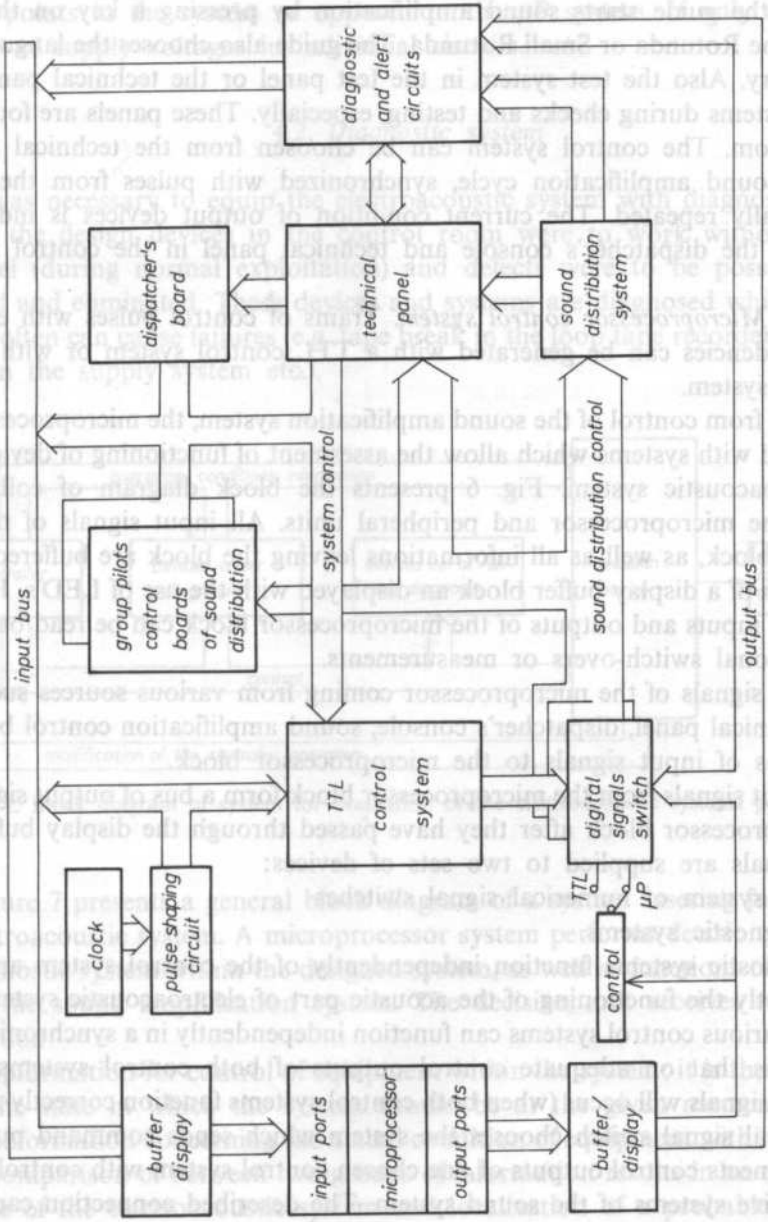

FIG. 6. Block diagram of microprocessor block collaboration with peripheral equipment

Both systems are synchronized with pulses from a clock in the dispatch room. From the console the dispatcher can change the frequency of pulses generated by the clock and allow a single start of sound amplification of the Rotunda or the Small Rotunda; the guide starts sound amplification by pressing a key on the control board in the Rotunda or Small Rotunda. The guide also chooses the language of the commentary. Also the test system in the test panel or the technical panel can be control systems during checks and testing, especially. These panels are found in the control room. The control system can be choosen from the technical panel.

The sound amplification cycle, synchronized with pulses from the clock, is automatically repeated. The current condition of output devices is indicated by LED's on the dispatcher's console and technical panel in the control room.

4.1.1. Microprocessor control system. Trains of control pulses with exact time interdependencies can be generated with a TTL control system or with a microprocessor system.

Apart from control of the sound amplification system, the microprocessor block is equipped with systems which allow the assesment of functioning of devices within the electroacoustic system. Fig. 6 presents the block diagram of collaboration between the microprocessor and peripheral units. All input signals of the microprocessor block, as well as all informations leaving the block are buffered with the application of a display buffer block an displayed with the use of LED's. Hence, the state of all inputs and outputs of the microprocessor block can be read out without any additional switch-overs or measurements.

Input signals of the microprocessor coming from various sources such as the: clock, technical panel, dispatcher's console, sound amplification control boards etc. form a bus of input signals to the microprocessor block.

Output signals from the microprocessor block form a bus of output signals from the microprocessor block after they have passed through the display buffer block. These signals are supplied to two sets of devices:

- to the system of numerical signal switches
- to diagnostic systems.

Diagnostic systems function independently of the control system and do not effect directly the functioning of the acoustic part of electroacoustic system. In this solution various control systems can function independently in a synchronic manner. This means that on adequate control outputs of both control systems identical command signals will occur (when both control systems function correctly of course). A numerical signal switch chooses the system which sends command pulses. This switch connects control outputs of one chosen control system with control inputs of the executive systems of the sound system. The described connection can be done manually by putting the switch in an adequate position or automatically switch operation from the microprocessor block.

4.1.2. TTL control system. The TTL control system is to control sound distribution when the microprocessor system does not function. Output command

signals from the TTL system secure functioning of the electroacoustic system identical as signals from the μP system. The TTL control system also allows certain check or test operations; however it does not secure full control and diagnosis of all delicate points in the system as opposed to the μP system. It only controls the presence of supply voltages in individual circuits.

4.2. Diagnostic system

It was necessary to equip the electroacoustic system with diagnostic systems, because the design devices in the control room were to work without servicing personnel (during normal exploitation) and defects were to be possibly quickly localized and eliminated. These devices and systems are diagnosed which probably most of often can cause failures (e.g. tape break in the loop tape recorder, burnout of a fuse in the supply system etc.).

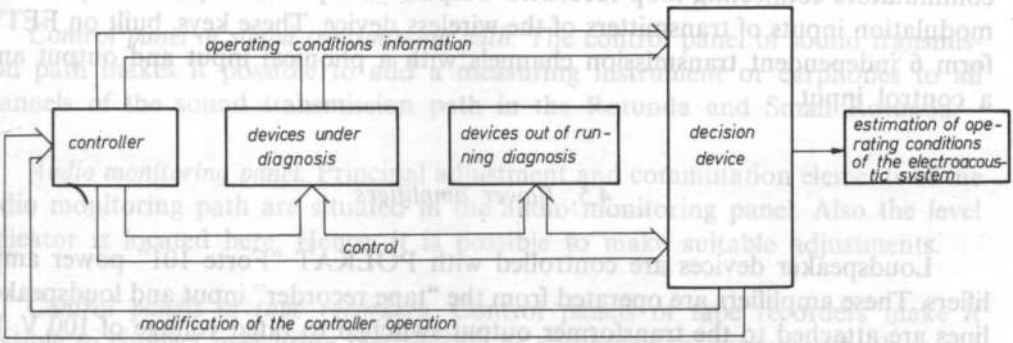

FIG. 7. Block diagram of system for evaluation of the electroacoustic systems performance

Figure 7 presents a general block diagram of a system assesing functioning of the electroacoustic system. A microprocessor system performs decision functions in the diagnostic system within the designed system, as well as functions of a programmer of the sound amplification system. The decision unit receives two kinds of information:

1. information for control of equipment within the system; it is the information about the state in which the system should be at the given moment, and
2. information concerning the actual condition of equipment within the system.

A comparison of between two groups of information results in an estimation of the state of the electroacoustic system and localization of a probable defect. The accuracy of this estimation greatly depends on the number of second kind of information, place of their formation etc.

The control equipment passes the information about the estimation results to the personnel and at the same time it can reduce consequences of the detected failure (e.g. by switching over to a reserve element).

4.3. Loop tape recorders

Double track loop tape recorders equipped with special cassettes which make it possible to reproduce the commentary in a continuous manner without rewinding have been used to reproduce the commentary concerning the painting and model of the battle. The tape recorder is operated by the control system. The beginning and end of the commentary is separated with a piece of transparent tape which causes a photooptic sensor to stop the tape recorder. The tape recorder is provided with control systems which through external diagnostic systems continuously control the tape recorder's functioning and signalize its correctness.

4.4. Switching systems

Switching systems consists of systems of analogue keys acting as phonical signal commutators connecting loop recorders' outputs with power amplifiers' inputs and modulation inputs of transmitters of the wireless device. These keys, built on FET's, form 6 independent transmission channels with a phonical input and output and a control input.

4.5. Power amplifiers

Loudspeaker devices are controlled with POLKAT "Forte 101" power amplifiers. These amplifiers are operated from the "tape recorder" input and loudspeaker lines are attached to the transformer output switched to rated voltage of 100 V. In order to increase reliability the electroacoustic system was equipped with 8 amplifiers; 4 amplifiers make a hot reserve – they are connected with the system for good.

4.6. Commentary transmitting wireless device

A method of wireless information transfer was applied to make it possible to listen to the commentary in a language other than that transmitted through loudspeakers. Therefore, the visitor equipped with a special transistor receiver can listen through earphones to any one of five language versions of the commentary concerning the seen part of painting or model of battle.

Two such devices were applied in the "Panorama Racławicka" object; separate ones for the Rotunda and Small Rotunda. Receivers are identical, five-channel and may be used in the Small Rotunda as well as on the scenic platform in the Rotunda. They are switched on and operated in synchronicity with other appliances of the electroacoustic system.

4.7. *Monitoring systems*

Monitoring systems of the electroacoustic system indicate the functioning of individual elements of the system. They have the form of separate panels placed in stands and have galvanic connections with other elements of the system.

Test panel. The test panel contains a quick-acting test system which starts tape recorders, realizes control connections in phonical channels of the Rotunda and Small Rotunda and also starts reserve tape recorders.

Fast test system's functions are realized in connection with a TTL and microprocessor control system as well as with audio monitoring systems. The fast test system makes it possible (when there is no programme in the phonic channel) to start tape recorders in chosen sector, switch on section keys, switch on zone keys and loudspeaker relays, choice of language for the commentary from loudspeakers. Mentioned functions can be also performed manually or automatically.

Control panel of sound transmission path. The control panel of sound transmission path makes it possible to add a measuring instrument or earphones to all channels of the sound transmission path in the Rotunda and Small Rotunda.

Audio monitoring panel. Principal adjustment and commutation elements of the audio monitoring path are situated in the audio monitoring panel. Also the level indicator is located here. Hence, it is possible to make suitable adjustments.

Control panels of tape recorders. Control panels of tape recorders make it possible to connect measuring instruments or earphones to outputs of both sound transmission paths channels of all tape recorders including the reserve ones.

Technical panel. Information concerning functioning of individual installations of the electroacoustic system can be read-off the technical panel and full servicing of the system can be assured.

Control receivers of the high frequency links. Control receivers constantly check the system for wireless information in the Rotunda and Small Rotunda. They form an unit of five indentical receivers, each tuned in to a different channel and receiving a different language version of the commentary.

Conclusions

The applied system has proved itself functional in practice during over two years of its exploitation. High capacity of the object, amounting to over 0.5 million visitors a year at average time spent inside the museum of about 2 hours, indicates

that the right solution was accepted. The electroacoustic system drivers the traffic inside the object. Acoustic control of the traffic allows precise organization and reservation in advance. A tour of the object in a precisely determined period of time is the only possible solution with such a vast interest in the painting. The acoustic system generally was judged by visitors as good. However, there is a certain discomfort when two groups are touring the museum at the same time. Still, the quality of speech of the commentary transfered to two groups of listeners at the same time is very high. It has been confirmed by measurements.

In 1986 the group of engineers was awarded the Prize of the Minister of Science and Higher Education for the development and realization of the system.

Authors would like to thank all colaborators, who's help made it possible to carry into practice complicated undertaking particularly: M. Sc. R. GODYŃ, M. Sc. J. GOLANOWSKI, M. Sc. Z. IANELLI, Dr. J. JAROSZYŃSKI, M. Sc. J. ŚWIERKOWSKI, Dr. E. TALARCZYK, Dr. J. TARGOŃSKI, eng. K. WARSZAWSKI and M. Sc. A. WORSZTYNOWICZ.

References

[1] J. BEDNAREK, J. GOLANOWSKI, T. GUDRA, Z. IANELLI, J. JAROSZYŃSKI, K. RUDNO-RUDZIŃSKI, J. ŚWIERKOWSKI, E. TALARCZYK, J. TARGOŃSKI, K. WARSZAWSKI, A. WORSZTYNOWICZ, *System for programmed transmission of audio-visual information* (in Polish), Interim Patent PPR no 143080.

[2] J. BEDNAREK, T. GUDRA, Z. IANELLI, *Control system for sources of audio-visual information* (in Polish) Interim Patent PPR no. 143082.

[3] J. BEDNAREK, T. GUDRA, Z. IANELLI, *Diagnostic system of devices in a transmission system of audio-visual information* (in Polish), Interim Patent no 143081.

[4] L. CREMER, H. MÜLLER, *Die wissenschaftlichen Grundlagen der Raumakustik*, Band I, S. Hirzel Verlag, Stuttgart 1978.

[5] D. DAVIES, *Sound system engineering*, Howard W. Sams, Indianapolis 1975.

[6] V. M. A. PEUTZ, *Articulation loss of consonants as a criterion for speech transmission in a room*, J. Audio Eng. Soc., **19**, 915–919 (1971).

[7] K. WARSZAWSKI, *System generating a single pulse after switching on supply voltage* (in Polish), Interim Patent PPR no 141688.

Received on April 26, 1988

ARCHIVES OF ACOUSTICS
15, 1–2, 31–37 (1990)

AN EXTRA COCHLEAR ELECTRO-STIMULATING DEVICE (ECME) USING ATRAUMATIC EXTERNAL MEATAL ELECTRODES AS A COMMUNICATION AID FOR THE DEAFENED

W. BOCHENEK[a], A. CHORZEMPA[b], J. W. P. HAZELL[c]
A. J. KUKWA[d], J. KICIAK[e]

Medical Academy of Warsaw Inst. of Surgery, ENT Dept. Banacha 1a, 02-097 Warszawa[a], Dept. of Nuclear Medecine[b], ENT Dept. Szpital Czerniakowski[d], Royal National Institute for the Deaf, London[c], Military Inst. of Hygiene and Epidemiology[e].

We describe an auditory prosthesis for totally deafened people which stimulates both cochlear via ear canal electrodes. The device emits a square wave pulse matched to the first formant frequency and transposed below 10 Hz. It acts as an aid to lipreading, creates an awareness of environmental sounds, and reduces the isolation of total deafness. It is a cheap non-surgical alternative to cochlear implantation.

Autorzy przedstawiają protezę słuchową dla osób z całkowitą obustronną nabytą głuchotą. Urządzenie, zaopatrzone w atraumatyczne elektrody w obu przewodach słuchowych zewnętrznych, przetwarza sygnały akustyczne na falę prostokątną. Amplituda tej fali jest proporcjonalna do chwilowej intensywności głosek dźwięcznych, ze znacznym ograniczeniem dynamiki, a częstotliwość fali jest proporcjonalna do częstotliwości przejść przez zero pierwszego formantu tych głosek. Z zachowaniem proporcjonalności, częstotliwość na wyjściu jest transponowana w zakres (dobierany indywidualnie) poniżej 100 Hz, tj. w zakres słuchowego reagowania pacjentów na pobudzenie elektryczne przez skórę kanałów usznych. Proteza poprawia sprawność czytania mowy z ust, daje informację o dźwiękach w otoczeniu, zmniejsza wrażenie izolacji. Jest prosta w użyciu i nie wymaga zabiegu chirurgicznego, nawet na uchu środkowym. Może być zastosowana w przypadkach gdy "implant ślimakowy" jest nieosiągalny, lub przeciwwskazany. Koszt protezy jest niski, porównywalny z ceną konwencjonalnej protezy elektroakustycznej.

1. Introduction

Post lingually totally deafened people depend on lipreading to communicate. In speech the number of phonemes exceeds that of vizemes and many efforts have been made to use other sensory modalities to aid lipreading skills [7, 9]. Although VOLTA [12] in 1800 described the auditory sensation that could be achieved by stimulating the ear with an electric current, it was not until the late 1950's that it was used as

a communication aid [8, 10]. Since then many different strategies have been employed at different research centres around the world. These include various single and multi-channel extra and intra cochlear electrode placements as well as many different strategies for speech processing to produce a signal that will be useful to the patient. In all cases the signal must bypass the damaged cochlea to reach the more central, intact, part of the auditory pathway. Our research in this field started in 1976 with electrical stimulation via a transtympanic needle electrode on the promontory overlying the basal turn of the cochlea (BOCHENEK et al [5]).

2. Method

Our philosophy has been that external atraumatic electrodes will avoid any long term ill effects that may arise from internal invasive placement [1, 6]. Tests have been carried out using different electrode positions, but the best results were always obtained with an electrode in each ear canal. These are constructed by passing wires through hearing aid moulds to which is attached a small piece of gauze dipped in saline which lies in contact with the meatal skin (Fig. 1). The system has been tested on subjects with normal hearing, and with moderate and complete deafness. The responses vary, some subjects reporting only a "tweaking" or pressure sensation in the ear. We have already reported on the electrophysiological responses produced by

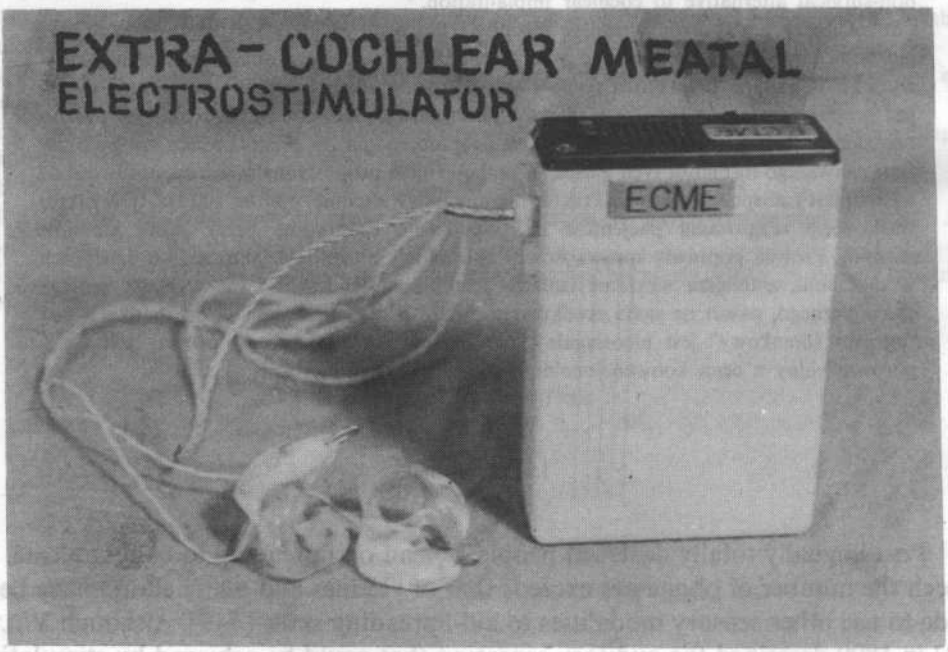

FIG. 1

such stimulation [4]. The device produces an alternating square wave pulse which is an analogue of the speech signal, after frequency transposition to below 100 Hz. Above 100 Hz such transdermal stimulation was found to be ineffective in most individuals. This output is excellent in coping with the narrow (and variable) electrical dynamic range of the ear (Figs 4 and 5).

Various speech processing strategies have been tried:

1. The amplitude of the stimulating signal depends upon the short time average power of the voiced sounds, and its frequency is proportional to the first formant frequency. The voiceless sounds do not produce a signal.

2. The amplitude of the signal depends upon the short time average power of the speech signal filtered by a high pass filter with a cut off frequency of 770 Hz. The frequency of the stimulus is proportional to the second formant of the voiced sounds and to the zero crossing frequency of the voiceless sounds.

3. The frequency of the signal is constant (chosen by the subject) and its amplitude is modulated as in mode 1.

4. The frequency of the signal is constant (chosen by the subject) and its amplitude is modulated as in mode 2.

The frequency of the first and second formant is estimated by analogue filtering and a zero crossing method [3]. The frequency is then divided in order to fit the restricted frequency of electrically evoked auditory sensation.

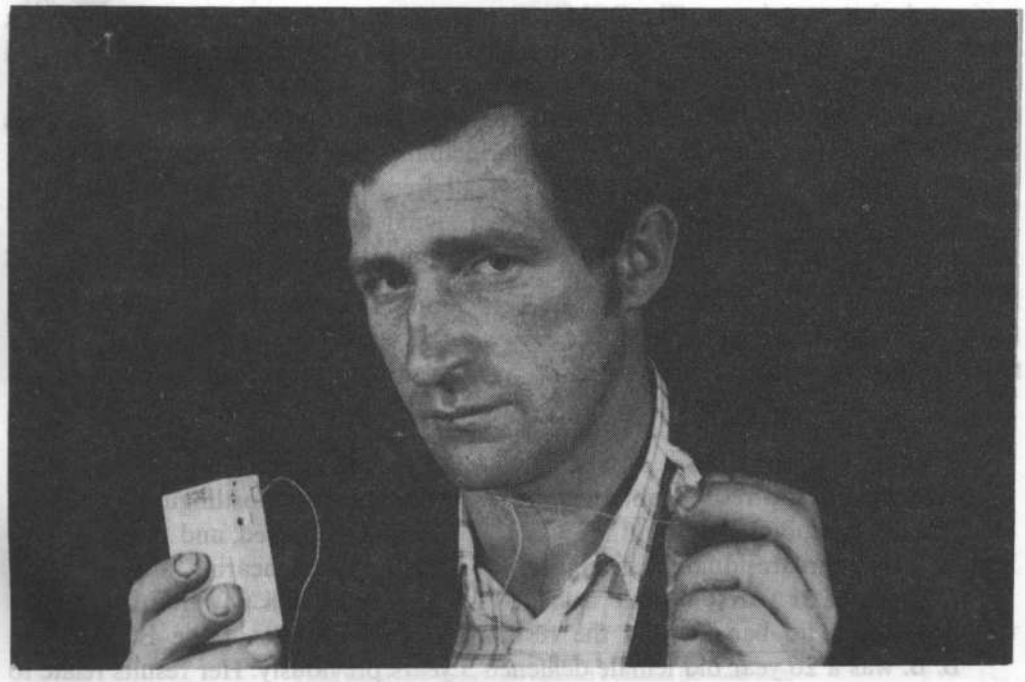

FIG. 2

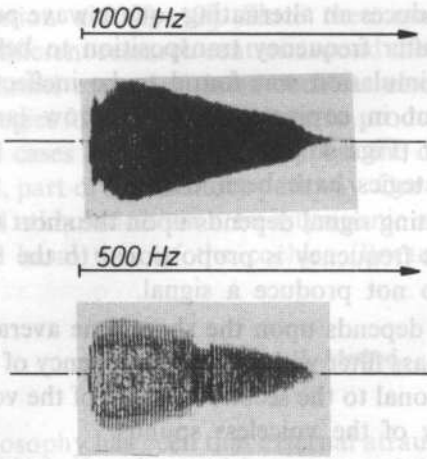

FIG. 3

We have reported on tests made on three patients with total acquired deafness [2]. Signal processing mode 1 was the most successful and has been adopted in current devices now in use. The ECME (Extracochlear (Meatal) Electro-stimulator) is shown in Fig. 2. The device is also being developed and tested at the Royal National Institute for the Deaf, London. The device has the following features:

1. Filtering of the incoming acoustic signal between 200 and 770 Hz. This filters out the fundamental frequency leaving principally the first formant.
2. Variable downard transposition of all frequencies to below 100 Hz.
3. Strong compression of the electrical signal (adjustable).
4. A dynamic threshold to reduce environmental background noise so that continuous signals rapidly decay (Fig. 3).

3. Results

We present the results obtained in two patients with postlingually acquired bilateral deafness, one in whom the ECME device was employed, and the other who had slightly more residual hearing using a high powered hearing aid.

J. Z. was a 31 year old male deafened for 11 years. High powered hearing aid trials produced no benefit, and the results relate to his use of the ECME.

B. B. was a 26 year old female deafened 5 years previously. Her results relate to the use of a high powered hearing aid.

Table 1

Audiograms				
	Auditory Thresholds [kHz]			
Subject	0.5	1	2	4
JZ	100	110	125	–
BB	80	100	105	115

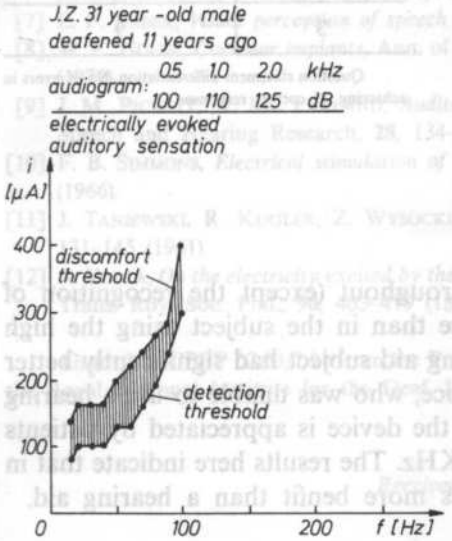

FIG. 4

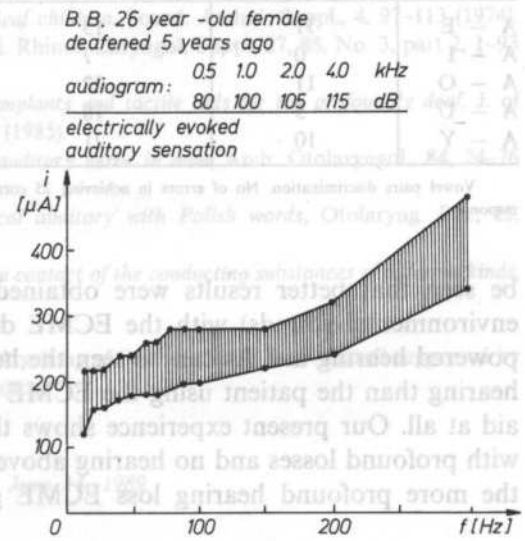

FIG. 5

Table 1 shows the residual hearing on pure tone audiometry obtained in both subjects. Figures 4 and 5 show the frequency and dynamic range of electrically evoked auditory sensation in both subjects. Tests of lipreading were performed with a live speaker, both with and without the ECME/high powered hearing aid. Vowel paired discrimination tests were performed. In each case these were presented until 25 correct responses were obtained. The number of incorrect responses was noted

Table 2

Discrimination tests		
	JZ (ECME)	BB (Hearing Aid)
Lipreading alone	61%	70%
Lipreading & device	79%	76%

Polish two syllable phonetically balanced 5 columns (20 words each) TANIEWSKI et al. (1961) [11].

and the results displayed in Tables 2, 3 and 4. These results indicate that in the case of J. Z. where hearing aids were useless, better discrimination was achieved with ECME than in the case of B. B, a marginal hearing aid user. The same strategy was employed for differentiation between questions and statement presentations. It can

Table 3

	JZ (ECME alone)	BB (Hearing aid alone)
A – E	11	15
A – I	0	7
A – O	11	22
A – U	5	18
A – Y	10	21

Vowel pairs discrimination. No of errors in achieving 25 correct responses.

Table 4

JZ (ECME alone)	BB (Hearing aid alone)
3	9

Question statement differentiation. No of errors in achieving 25 correct responses.

be seen that better results were obtained throughout (except the recognition of environmental sounds) with the ECME device than in the subject using the high powered hearing aid. As can be seen the hearing aid subject had significantly better hearing than the patient using the ECME device, who was unable to use a hearing aid at all. Our present experience shows that the device is appreciated by patients with profound losses and no hearing above 2 KHz. The results here indicate that in the more profound hearing loss ECME gives more benfit than a hearing aid.

4. Conclusion

The ECME is better than a conventional high powered hearing aid in some profoundly deaf patients. It gives an awareness of environmental sounds and reduces the feeling of isolation and sensory deprivation. It is simple to use and avoids surgical implantation. It might be preferred in cases where implantation is not available or contra indicated. It may be useful in a cochlear implant programme to aid assessment and counselling pre-operatively. Its low cost compares favourably with that of a conventional hearing aid.

References

[1] W. BOCHENEK, Z. BOCHENEK (in memoriam), A. CHORZEMPA, *Attempts to rehabilitate totally deafened persons by means of transdermal electrostimulation*, Scand. Audiol. Suppl., **11**, 151–155 (1980).

[2] W. BOCHENEK, A. CHORZEMPA, *Our experiences with the management of young postlingually deafened persons*, Scand. Audiol. Suppl., **17**, 107–111 (1982).

[3] W. BOCHENEK, A. CHORZEMPA, J. W. P. HAZELL, A. KUKWA, J. KICIAK, *Non-invasive electrical stimulation of the ear canal as a communication aid in acquired total deafness*, Accepted for publication in British Journal of Audiology.

[4] W. BOCHENEK, W. SZELENBERGER, A. CHORZEMPA, G. MANOWIEC, *Les "Off" – reponses corticales tardives évoquées par la stimulation électrique*, Société Francaise d'Oto-Rhino-Laryngologie et de Pathologie Cervico-Faciale, Congrés de 1985, Comptes Rendus des Sciences, Librairie Arnette, Paris 1986 pp. 542–547.

[5] Z. BOCHENEK, W. BOCHENEK, J. BIENIEK, *Electrical stimulation of human auditory system with transtympanic electrode* (in Polish) Otolaryng. Pol., **31**, 4, 225-228 (1977).

[6] A. CHORZEMPA, W. BOCHENEK, *The lipreading aids based on utilisation of non-invasive electrostimulation of the hearing tract*, Biocybern. and Biomed. Engineering, **2**, 1/2 15–22 (1982).

[7] E. P. ERBER, *Visual perception of speech by deaf children*, Scand. Audiol. Suppl., **4**, 97–113 (1974).

[8] W. F. HOUSE, *Cochlear implants*, Ann. of Otol. Rhinol. Laryngol, Suppl. 27, **85**, No. 3, part 2, 1–93 (1976).

[9] J. M. PICKETT, W. MC FARLAND, *Auditory implants and tactile aids for the profoundly deaf*, J. of Speech and Hearing Research, **28**, 134–150 (1985).

[10] F. B. SIMMONS, *Electrical stimulation of the auditory nerve in man*, Arch. Otolaryngol., **84**, 24–76 (1966).

[11] J. TANIEWSKI, R. KUGLER, Z. WYSOCKI, *Vocal auditory with Polish words*, Otolaryng. Pol., **15**, 131–145 (1961).

[12] A. VOLTA, *On the electricity excited by the mere contact of the conducting substances of different kinds*, Trans. Roy. Soc. Phil., **90**, 403–419 (1800).

Grant No. CPBP 02.03/7.12 from the Polish Academy of Sciences Mr J. W. P. Hazell supported by the Royal National Institute for the Deaf, London.

Received on June 14, 1989

ARCHIVES OF ACOUSTICS
15, 1–2, 39–43 (1990)

BRIEF NOTE

SAW GENERATED ELECTRIC CHARGE ON A METAL DISK ON PIEZOELECTRICS

E. DANICKI

Institute of Fundamental Technological Research, Polish Academy of Sciences
(00-049 Warszawa, Świętokrzyska 21)

Scattering of a plane SAW by a circular, perfectly conducting disk on a piezoelectric halfspace is considered. A new theoretical approach allows to take into account the electric anisotropy of the substrate and gives the solution for the electric charge density on the disk in a form of fast convergent series for a wide range of wavelength of the SAW.

1. Introduction

Scattering of surface acoustic wave (SAW) by metal disk is exploited in some SAW devices [1], there is also an interest in considering the problem, as it may be helpful in modelling narrow interdigital transducers (IDT) [2].

There are many papers in literature considering electromagnetic wave scattering by a metal disk [3, 4], but they cannot be directly applied to the case of SAW for two reasons:

– in the SAW case the total current flowing to a grounded metal disk is of our major interest for wide range of wavelengths as compared with disk diameter,
– usually, the piezoelectric halfspace must be considered as an highly anisotropic dielectric.

The proposed theoretical approach is based on the known Galerkin's method, but further considerations are quite different and allow evaluation of

– the total current flowing to the grounded metal disk,
– the disk capacitance (anisotropy of the substrate accounted),
– the distribution of electric charge density on the disk in a form of fast convergent series that allows evaluation of the scattered acoustic field outside the disk.

2. The diffraction problem for a circular disk

We consider electric interaction only between the metal disk and SAW with angular frequency ω and wave-number k. The Green's function for a stress-free piezoelectric halfspace expressing the electric potential as dependent on electric charge, both on the substrate surface, can be divided into two terms, the first one describing dielectric properties of the substrate and the second one describing elastic waves, weakly coupled with electric quantities [5, 6].

Let $\mathbf{r}$ be the distance between the point (r, ϑ) where the potential is evaluated and the point (r', ϑ'), where electric charge is placed on the substrate surface (we apply the cylindrical coordinates r, ϑ, z but we confine our considerations to the substrate surface $z = 0$. The ϑ and ϑ' are angular coordinates describing the direction of the corresponding vector on the anisotropic halfspace). It can be shown, that the first above-mentioned dielectric term of the Green's function [7]

$$G(\mathbf{r}, \vartheta) = [2\pi \mathbf{r} \varepsilon_0 \varepsilon_e(\vartheta + \pi/2)]^{-1} \tag{1}$$

is much larger than the second term, if only $k\mathbf{r}K^2 \ll 1$, where K^2, which is usually less than 0.01, describes the piezoelectricity of the substrate. Thus, confining our consideration to disks having diameters of up to about 10 wavelengths, the second term of the Green's function can be neglected. The term $\varepsilon_0 \varepsilon_e$, which is the effective surface permittivity dependent on ϑ for anisotropic piezoelectrics, can be written as follows (n-even)

$$(\varepsilon_0 \varepsilon_e)^{-1} = \sum \chi_n e^{jn\vartheta} \tag{2}$$

Under this simplification the condition that the grounded disk potential is equal to zero takes a form (the disk radius is applied equal to 1, for simplification, S – the disk area)

$$-\Phi^0(r, \vartheta) = \iint_S G(\mathbf{r}, \vartheta) \varrho(r', \vartheta') dS \tag{3}$$

where ϱ is an electric charge distribution on the disk, and

$$\Phi^0 = \exp(jkr \sin \vartheta)$$

is the electric potential coupled with the impingent SAW.

3. Evaluation of charge distribution

Let apply the representation for the charge distribution on the disk in the form (m and n have the same parity, $n \geqslant 0$)

$$\varrho = \sigma_{mn} r^n (1 - r^2)^{-1/2} e^{jm\vartheta} \tag{4'}$$

After some transformations, the right-hand side of (3) can be written in the form (p, s, l – integers, J – Bessel function)

$$\sigma_{pn}\chi_{m-p}[(-1)^l A_s^{m,n}/l^s + (+1)^l B_s^{m,n}/l^s] J_m(\pi r l) e^{jm\vartheta} \tag{5}$$

where $0 \leqslant s \leqslant n$, and there is summation over l in (5), $0 < l < \infty$.

The key observation is, that the second component in the bracket above leads to the inappropriate solution for electric potential under the disk. In fact, it leads to the function like a cone [8]. To avoid such a solution we have to confine the representation (4′) of charge distribution as follows (Appendix)

$$n \geqslant |m| \tag{4''}$$

which is the sufficient condition for vanishing of B in (5).

The left-hand side of (3) can be written in the form

$$\frac{-\sin k}{k} \sum_l (-1)^l \frac{(k/\pi l)^t}{1-(k/\pi l)^2} e^{jm\vartheta} J_m(\pi r l); \qquad \begin{matrix} t = 2 & \text{for} & m = 0 \\ t = |m| & \text{for} & m \neq 0 \end{matrix} \tag{6}$$

In spite of the similarity of both expressions (5) and (6) we can not compare them directly for each l. To do this we have to use Lagrange extrapolation formula, allowing (6) to be approximated as follows ($0 \leqslant s \leqslant N$)

$$(-1)^l C_s^m / l^s e^{jm\vartheta} J_m(\pi r l) \tag{7}$$

if $k < N\pi$, where N is the upper limit of n, applied in the representation (4).

Now, we can compare (5) and (7) for each s-components separately, which results in the set of simultaneous equations for σ_{mn}. There is a triangular set of equations for each m, each set coupled with the other by the term χ_{m-p}. However note, that for isotropic substrate only χ_0 is different from zero, which allows solution of the equations for each m separately.

4. Evaluation of total electric charge generated by SAW

Integration of the charge distribution given in (4) results in the expression for a total charge on the disk of radius R

$$Q = 4(\sin kR/k)\chi_0^{-1} \tag{8}$$

and it follows from the above relation (apply $k = 0$) that the disk capacitance is equal to (see [9] for isotropic case, where $\varepsilon_e = 1 + \varepsilon$)

$$C = 4R/\chi_0 \tag{9}$$

Both relations are correct for arbitrary anisotropic halfspace, where χ_0 is described by the relation (2).

The above formula can be generalized to the case of an elliptic metal disk by

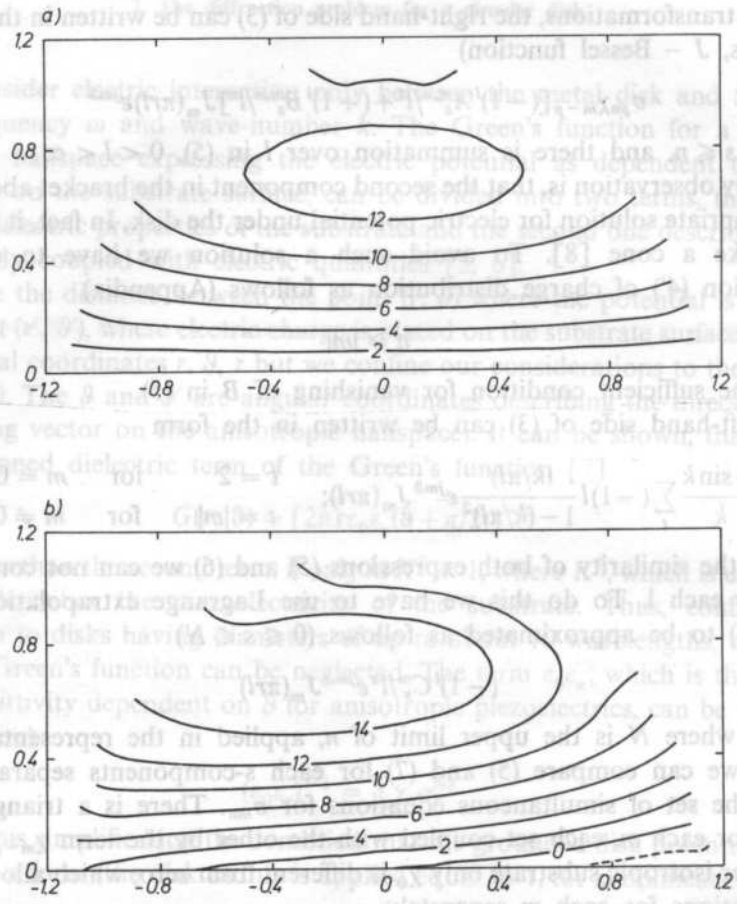

FIG. 1. The diagram of charge distribution for isotropic (a) and anisotropic (b) case. Only the imaginary component of a complex valued charge amplitude is shown, with square root term dropt in (4). The contour line levels are in arbitrary units

introducing the coordinate transformation of an ellipse to the circle. The transformation results in the dependence of ε_e on ϑ, which may become a quite complicated function, so that χ_0 changes, as well.

As a numerical example, Fig. 1 shows the diagram of charge distribution (imaginary part of its complex value), with square root term dropped in (4), for a circular disk on isotropic substrate, and for 4:1 elliptic disk on YZ lithium niobate, the major axis of the disk is rotated about 47 degrees off the Z axis (this orientation is applied for reflecting SAW from Z to X direction). In the latter case the figure shows the charge distribution in the coordinate system transformed as discussed above, so that the charge distribution on the equivalent circular disk is presented. We see considerably different charge distributions in these cases.

Appendix

Consider a charge distribution in somewhat different form

$$\varrho(r, \vartheta) = \sigma_{mn} \frac{T_n(r)}{(1-r^2)^{1/2}} e^{jm\vartheta} \tag{10}$$

which substituted to the right side of (3) yields the following expression for it (after many transformations)

$$\frac{1}{2}\sigma_{kn}\chi_{m-k}c_l^{(k,n)}(\operatorname{sign} k)^k e^{jm\vartheta} J_{|m|}(\pi l r)$$

$$c_l^{(m,n)} = (\pi/2)^2 (\operatorname{sign} m)^m \left[\frac{J_{|m|-n+1}}{2}\frac{J_{|m|+n-1}}{2} + \frac{J_{|m|-n-1}}{2}\frac{J_{|m|+n+1}}{2}\right] \tag{11}$$

where the argument of the Bessel functions J is the $(\pi l/2)$, sign $(m) = +1$ for $m \geqslant 0$ or -1 for $m < 0$. Some further transformations concerning the Bessel functions above, which have half-integer indices, allows to obtain (5), as well as to prove the thesis in the line next to (4').

Acknowledgement

The author would like to thank Prof. A. LAKTAKHIA from Pennsylvania State University for his encouragement and comments concerning electromagnetic diffraction problems.

This work has been performed under the Project CPBP 02.02

References

[1] L. P. SOLIE, *Reflective dot array devices*, IEEE Ultras. Symp. Proc. 309–312 (1976).

[2] E. DANICKI, *Analysis of nearly periodic IDTs by means of scattering matrix for periodic metal strips*, Int. Sch. Phys. Acoustics, Erice, Italy 1988, "Third Course of Ultrasonic Signal Procesing", A. Alippi [ed.), World Sci. Publ., Singapore, 425–440.

[3] W. H. EGGIMANN, *Higher-order evaluation of electromagnetic diffraction by circular disk*, IRE Trans., MTT-9 5, 408–418 (1961).

[4] F. J. SABINA, *General formulation for low frequency acoustic scattering by a soft body or disk*, JASA 81, 6, 1677–1682 (1987).

[5] E. DANICKI, *Scattering of SAW on circular disk*, Winter Sch. on Molec. Acoust., Jaszowiec, Poland 1987, 89–92 (in Polish)

[6] K. C. WAGNER, G. KOVACS, A. R. BAGHAI-WADJI, F. SEIFERT, *Interdigital transducer interaction with SAWs and BAWs*, IEEE Ultras. Symp. Proc. 149–154 (1987).

[7] E. DANICKI, Green's function for anisotropic dielectric halfspace, IEEE. Trans., IFFC-35, 5 (1988), 643 *SAWs and BAWs*, IEEE Ultras. Symp. Proc. 149–154 (1987).

[8] A. P. PRUDNIKOW, J. A. BRICHKOV, O. I. MARICHEV, *Integrals and series* v. 2 p. 678 Nauka, Moscov 1983 (in Russian).

[9] F. OBERHETTINGER, W. MAGNUS, *Anwendung der elliptischen Functionen in Physik und Technik*, Springer, Berlin 1949.

Received on August 10, 1989

ARCHIVES OF ACOUSTICS
15, 1–2, 45–48 (1990)

BRIEF NOTE

NEW APPROACH IN THE THEORY OF MICROSTRIP WAVEGUIDES

E. DANICKI

Institute of Fundamental Technological Research, Polish Academy of Sciences
(00-049 Warszawa, Świętokrzyska 21)

In literature, the Galerkin's method is usually applied in analysis of microstrip waveguides and couplers. Below, a new method is proposed that is a generalization of one developed previously for analysis of SAW waveguides [1] to the electromagnetic case. The proposed approach exploits some identities fulfilling by Fourier series which coefficients are expressed by Legendre functions.

1. Formulation of the problem

Let's consider a periodic system of metal strips on a plane $y = 0$ in vacuum. The period of strips is $2\pi/K$ and they have infinite length along z-axis. Following the Floquet theorem the solution to the Maxwell equations for the system considered has a form (A means an electromagnetic field component)

$$A_n^{\pm} e^{j\omega t} e^{-j r_n x} e^{-j s_n^{\pm} y} e^{-jkz} \tag{1.1}$$

$$r_n = r + nK, \; k_0 = \omega^2 \mu_0 \varepsilon_0 \tag{1.2}$$

$$s_n^{+} = -s_n^{-} = (k_0^2 - k^2 - r_n^2)^{1/2} \tag{1.3}$$

where indices $+$ and $-$ mark the solution in the upper ($y > 0$) and lower ($y < 0$) halfspaces where they fulfill the radiation condition.

Introducing Hertz potentials $\hat{z}\Phi$ and $\hat{z}\Psi$, the electromagnetic field components can be expressed as follows [2]

$$E_x = -\omega \mu_0 s_n \Phi_n - k r_n \Psi_n \tag{2.1}$$

$$E_z = (k_0^2 - k^2)\Psi_n \tag{2.2}$$

$$H_x = -k r_n \Phi_n + \omega \varepsilon_0 s_n \Psi_n \tag{2.3}$$

$$H_z = (k_0^2 - k^2)\Phi_n \tag{2.4}$$

where index n describes the wave-components correspondingly to (1).

The boundary conditions at the plane $y = 0$ are

$$E_x^+ = E_x^- = E_x \quad \text{and} \quad E_x = 0 \quad \text{on metal strips} \tag{3.1}$$

$$E_z^+ = E_z^- = E_z \quad \text{and} \quad E_z = 0 \quad \text{on metal strips} \tag{3.2}$$

$$H_x^+ - H_x^- = 0 \quad \text{between strips} \tag{3.3}$$

$$H_z^+ - H_z^- = 0 \quad \text{between strips} \tag{3.4}$$

2. Construction of the solution

There are known identities [3], [4]

$$\sum_{n=-\infty} e^{-jnKx} \sum_{m=M_1}^{M_2} \alpha_m P^{\mu}_{n-m} = 0, \quad \text{between strips} \tag{4.1}$$

$$\sum_{n=-\infty} e^{-jnKx} \sum_{m=M_1}^{M_2} \beta_m S_{n-m} P^{\mu}_{n-m} = 0, \quad \text{in area covered by strips} \tag{4.2}$$

where P denotes Legendre functions of argument $\Delta = \cos(Kw/2)$, where w is the strip width, and $\mu \leqslant 0$, $S_k = 1$ for $k \geqslant 0$ or $S_k = -1$ for $k < 0$. There are arbitrary coefficients α i β, which allow to express any function in a form of (4.1) or (4.2) in the proper domain under the strips or between the strips, if only this function behaves at the strip edges like $\varepsilon^{-1/2-\mu}$ for $\varepsilon \to 0$.

Then, taking into account (3.2) and (3.1) we can write

$$\Psi_n^+ = \Psi_n^- = \Psi = \Psi_m^{\mu} S_{n-m} P^{\mu}_{n-m} \tag{5.1}$$

$$\Phi_n^+ = -\Phi_n^- = \Phi_n = \phi_m^{\nu} P^{\nu}_{n-m} \tag{5.2}$$

where (5.2) ensure fulfilling (3.4).

The relations (3.1) and (3.3) require fulfilling

$$E_x = -\omega\mu_0 s_n \Phi_n - k r_n \Psi_n = e_m^{\mu} S_{n-m} P^{\mu}_{n-m} \tag{6.1}$$

$$\frac{1}{2}[H_x] = -k r_n \Phi_n - \omega\varepsilon_0 s_n \Psi_n = h_m^{\nu} P^{\nu}_{n-m} \tag{6.2}$$

for every n (above, summation convention concerns μ, ν, m only). The solution of (6) should have a form of (5), that is

$$\phi_m^{\nu} P^{\nu}_{n-m} = \frac{e_m^{\mu} \omega\varepsilon_0 s_n S_{n-m} P^{\mu}_{n-m} + h_m^{\nu} k r_n P^{\nu}_{n-m}}{-\omega^2 \varepsilon_0 \mu_0 s_n^2 - k^2 r_n^2} \tag{7.1}$$

$$\psi_m^{\mu} S_{n-m} P^{\mu}_{n-m} = \frac{e_m^{\mu} k r_n S_{n-m} P^{\mu}_{n-m} - h_m^{\nu} \omega\mu_0 s_n P^{\nu}_{n-m}}{-\omega^2 \varepsilon_0 \mu_0 s_n^2 - k^2 r_n^2} \tag{7.2}$$

The idea of the method [1] is closed in requirement, that the above equations are identities for every $|n| \to \infty$, in approximation for every $n < N_1 < 0$ and for every $n > N_2 > 0$, where $s_n \approx -j|r_n|$ (this approximation makes (7) much simpler). In the remaining area, that is for $N_1 \leqslant n \leqslant N_2$ the relations (7) will be satisfied through properly chosen coefficients ϕ, ψ, e and h.

Consider the area $n < N_1$ or $n > N_2$.

Taking the approximation $s_n \approx -j|nK+r|$ into account and the identity [3]

$$\left(n+\frac{r}{K}\right)P_{n-m}^{(-1)}(\Delta) = \left(m-1/2+\frac{r}{K}\right)P_{n-m}^{(-1)}(\Delta)+\frac{P_{n-(m+1)}^{(0)}(\Delta)-P_{n-(m-1)}^{(0)}(\Delta)}{2(1-\Delta^2)^{1/2}} \tag{8}$$

as well as limiting the representation (5) to the necessary μ and ν, that is in our problem to

$$\phi_m^{(-1)} = \phi_m, \quad \psi_m^{(-1)} = \psi_m \tag{9}$$

only, the relations (7), taken as identities fulfilled for every n in the considered limits, result in

$$e_m^{(-1)} = \left(m-1/2+\frac{r}{K}\right)(j\omega\mu_0\phi_m - k\psi_m) \tag{10.1}$$

$$h_m^{(-1)} = \left(m-1/2+\frac{r}{K}\right)(-k\phi_m - j\omega\varepsilon_0\psi_m) \tag{10.2}$$

$$e_m^{(0)} = [j\omega\mu_0(\phi_{m-1}-\phi_{m+1})-k(\psi_{m-1}-\psi_{m+1})]/[2(1-\Delta^2)^{1/2}] \tag{10.3}$$

$$h_m^{(0)} = [-k(\phi_{m-1}-\phi_{m+1})-j\omega\varepsilon_0(\psi_{m-1}-\psi_{m+1})]/[2(1-\Delta^2)^{1/2}] \tag{10.4}$$

It means that we reduced the unknowns to ϕ i ψ only.

Consider now the relations (7) for $n \in [N_1, N_2]$.

The unknows ϕ i ψ (they are vectors of M_2-M_1+1 dimension) should be chosen from the condition (7) taken for every n in the limits considered. This requires to apply the number of unknows equal the number of equations that is $M_2-M_1+1 = N_2-N_1+1$.

3. An example

The purpose of this example is not to solve any particular problem, but to show the way, the solution can be obtained. Let us then apply the simplest case of $K = 1$, $k_0 = 1$, and $\Delta = 0$, in which $P_{-1}^0 = P_0^{-1} = P_0^0 = 1$, $P_1^0 = 0$, and assume that the wave propagates along z-axis, that is $r = 0$ in (1). What is more, we apply the approximation that $s_n = |n|$ for every $n \neq 0$. Then in our disposal remains one n (namely $n = 0$), for which (7) should be separately considered as the condition for determining ϕ and ψ. In this circumstance it is sufficient to allow unknows ϕ_0 and ψ_0 only in (6).

The relations (10) results in

$$e_c^{(-1)} = -(j\omega\mu_0\phi_0 - k\psi_0)/2 \qquad e_{-1}^{(0)} = (j\omega\mu_0\phi_0 + k\psi_0)/2 = -e_1^{(0)}$$
$$h_c^{(-1)} = (k\phi_0 + j\omega\varepsilon_0\psi_0)/2 \qquad h_{-1}^{(0)} = (k\phi_0 + j\omega\varepsilon_0\psi_0)/2 = -h_1^{(0)}$$

what substituted into (7) taken for $n = 0$ gives

$$\begin{bmatrix} j[(k^2-1)^{1/2}-1] & k\omega\varepsilon_0 \\ -k\omega\mu_0 & -j[(k^2-1)^{1/2}+1] \end{bmatrix} \begin{bmatrix} \phi_0 \\ \psi_0 \end{bmatrix} = 0$$

Finaly, the dispersion relation is $k = 1$. In this simplest case and under the approximation applied we obtained trivial solution.

4. Conclusions

It has been shown how the solution can be constructed for the case of periodic metal strips. But in practice we have a single strip on a layered media and this needs following comments

– for K small considered case of periodic strips can be a sufficient approximation for the case of a single strip,

– for layered structure the relations (1), as well as (6) are much more complicated, but for $|n| \to \infty$ the relations (10) still hold, as well as the method of constructing the solution (5) and (6),

– the generalization to the case of microstrip couplers (the case of few strips) is also possible, by analogy to [5],

– the method can also be generalized to the case of scattering problem of wave on a periodic system of metal strips.

References

[1] E. DANICKI, *Surface acoustic waves, propagation, generation and detection*, Biul. WAT, 11 supplement (in Polish), 1976 see also *Theory of surface acoustic waves slant propagation in periodic system of* electrodes, J. Tech. Phys. **19**, 1, 69–77 (1978).

[2] R. E. COLLIN, *Field theory of guided waves*, Mc Graw-Hill, NY 1960.

[3] H. BATEMAN, A. ERDELYI, *Higher transcendential functions*, Mc Graw-Hill, 1953.

[4] K. BLOTEKJAER, K. A. INGEBRIGTSEN, H. SKEIE, *A method for analyzing waves in structures consisting of metal strips on dispersive media*, IEEE Trans., ED-20, 1, 133–1138 (1973).

[5] E. DANICKI, D. GAFKA, *Propagation, generation and detection of SAW in a multiperiodic system of metal* strips on a piezoelectric substrate (in preparation).

Received on October 31, 1989

ARCHIVES OF ACOUSTICS
15, 1–2, 49–56 (1990)

BRIEF NOTE

SPECIFIC PERFORMANCE OF IDT EDGE FINGERS

E. DANICKI, D. GAFKA

Institute of Fundamental Technological Research Polish Academy of Sciences
(00-049 Warszawa, Świętokrzyska 21)

A rigorous field theory has been developed that allows to analyze the generation and detection performance of each metal strip in a system of a few of them. The theory shows that the edge strips of the system works differently as compared with these positioned inside the system. The familiar δ-function model however, can still be applied provided that the δ-sources of SAW are properly scaled and shifted from their position at the centres of the strips. The scaling factor and the shift magnitude (which are larger for the edge electrodes of IDT) are determined by theory. Some numerical and experimental examples are presented, which seem to agree well.

1. Introduction

Surface acoustic wave (SAW) propagation in a system of metal strips deposited on a piezoelectric substrate occurs in a number of SAW devices:

in interdigital transducers (IDT) consisting of two or more metal strips (fingers), which generate and detect SAW,

in resonators, where metal strips can be used for SAW reflection,

in reflective array compressors (RAC), where the reflection of obliquely propagating SAW from metal strips is exploited,

in convolvers, where a strip is applied to form a waveguide for SAW.

Allowing certain idealization, i.e. neglecting mechanical and certain electrical properties of electrodes (mass, elasticity, finite electric conductance), the mathematical model of the above – mentioned system of metal strips corresponds to the boundary problem with mixed electrical, and homogeneous mechanical boundary conditions. In this work the method for analyzing SAW propagation in a system of metal strips proposed in [1] (for eigenvalue problems) and developed in [2, 3] (for nonhomogeneous problems concerning SAW generation and detection) is applied.

A generalization of the method [1] from the case of periodic split strips to the case of multiperiodic strips (the periodically repeated groups of several metal strips) is given as well as a functional dependence between currents and voltages of the electrodes. The transadmittance relation is derived, expressing the dependence of the current flowing to a given grounded metal strip on the potentials of the other strips. Numerical results for a group of several electrodes are presented, which show the dependence of electromechanical transformation efficiency of a metal strip on the strip position inside the group. These results allow one to take into account the specific performance of edge fingers of IDTs.

2. Formulation of the boundary problem

A piezoelectric half-space is considered. The surface acoustic wave propagation is described by a complex harmonic function

$$e^{j(\omega t - kx_3)} \tag{1}$$

where ω is an angular frequency (the factor $\exp(j\omega t)$ is neglected throughout the paper) and k is the wave-number of SAW (Fig. 1). Neglecting bulk waves, the approximation of the effective surface permittivity that describes sufficiently the piezoelectric halfspace is given by [1, 2]

$$\varepsilon(k) = -j\Delta D_\perp / E_\parallel = \varepsilon_{ef}(k^2 - k_v^2)/(k^2 - k_0^2) \tag{2}$$

where k_0 and k_v are wave-numbers of SAW propagating on metalized and free halfspace, correspondingly. The strip width w and the separation $2p$ between strip centers are equal within every group of N strips, and the groups repeat periodically

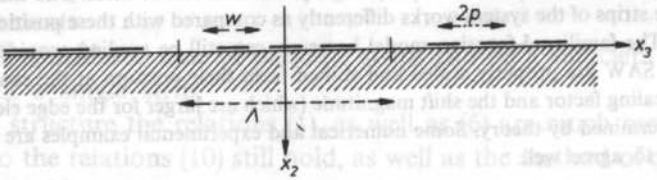

FIG. 1. Multiperiodic system of metal strips ($N = 3$ in the figure)

with period Λ (see Fig. 1). Define $K = 2\pi/\Lambda$ as the wavenumber of the system of the groups of strips. According to the Floquet's theorem, the electric field in the system can be expanded into a series of harmonic components

$$E_\parallel = \sum_{n=-\infty}^{\infty} E_n \exp(-j(k+nK)x_3 \tag{3}$$

and similarly $\Delta D_\perp$ (the difference of the electric flux density). The boundary problem can be formulated as follows:

$$E_\parallel = 0 \quad \text{on the strips,} \quad \Delta D_\perp = 0 \text{ between the strips.} \tag{4}$$

Proceeding in a similar manner as in [1, 2] new functions have been derived

$$G_N(\theta;\alpha) = \sum_{n=-\infty}^{\infty} S_n X_n^N e^{-jn\theta} \qquad F_N(\theta;\alpha) = \sum_{n=-\infty}^{\infty} X_n^N e^{-jn\theta} \tag{5}$$

which fulfill the corresponding conditions

$$G_N(\theta;\alpha) = 0 \text{ on the strips,} \quad F_N(\theta;\alpha) = 0 \text{ between strips,} \tag{6}$$

where parameter $\alpha = Kp$. Details concerning these functions see Appendix A.

Applying the method [1], the quantities $E_{\parallel}$ and $\Delta D_{\perp}$ can be expressed as

$$E_{\parallel} = \sum_{m=-M_1}^{M_2} \alpha_m G_N(Kx_3; Kp) e^{-jmKx_3}, \quad \Delta D_{\perp} = j \sum_{m=-M_1}^{M_2} \beta_m F_N(Kx_3; Kp) e^{-jmKx_3}. \tag{7}$$

3. Currents and potentials of electrodes

The relations (7) allows the calculation of the value of currents flowing to a single metal strip for any wavenumber k as follows

$$\mathbf{I}^k = -2\omega\varepsilon_{\mathrm{ef}} \cdot \sum_{m=-M_1}^{M_2} \alpha_m I_m^k, \; I_m^k = \sum_{n=-\infty}^{\infty} \frac{X_{n-m}^N \sin[(k+nK)w/2]}{k+nK} e^{-j(k+nK)x_k} \tag{8}$$

where $x_k = (2k-N-1)p$, $(k = 1, 2, \ldots N)$ and similarly the l-th strip potential

$$\mathbf{V}^l = -j \sum_{m=-M_1}^{M_2} \alpha_m V_m^1, \quad V_m^l = \sum_{n=-\infty}^{\infty} \frac{S_{n-m} X_{n-m}^N}{k+nK} \cdot e^{-j(k+nK)x_1}. \tag{9}$$

It is noticed, that α_m should satisfy some conditions to ensure that the potential is constant on every strip and the conditions that the strip potentials are $\mathbf{V}^l$ (see Appendix B for details). This allows us to express the unknowns α_m by the values of $\mathbf{V}^l$, which substituted to Eq. (8) gives

$$\mathbf{I}^k = \mathbf{Y}_{kl}\mathbf{V}^l, \; \mathbf{Y}_{kl} = -j2\omega\varepsilon_{\mathrm{ef}} I_m^k [\mathscr{I}^{-1}]_m^l, \text{ (sum after } m, l). \tag{10}$$

4. Transadmittance relations

The relation (10) should be considered as the relation between Fourier transforms $\mathbf{I}^k$, $\mathbf{V}^l$ of discrete functions, namely the discrete set of strip currents I^k and the discrete set of voltages V^1, where indices k or l describe the position of the given strip on the x_3 axis. The transform parameter k is treated as independent variable taking its value from the area of first Brillouin zone $-K/2 < k < K/2$ [2]. The inverse Fourier transform of a discrete function is

$$F^l = \frac{1}{K} \int_{-K/2}^{K/2} \mathbf{F}^l(k) e^{-jkx_3} dk. \tag{11}$$

The following notations are introduced in order to determine the strips uniquely: $s = (m, k)$ and $t = (n, l)$ where k, l – number of metal strip in the group, $k, l \in [1, N]$, and n, m – number of the group, $n, m \in (-\infty, \infty)$. Applying (11) to (10) results in

$$I_s = Y_{st} V_t \quad \text{(sum after } t) \tag{12}$$

Table 1. Relative transformation efficiency b_{kl} of electrodes

N	l \ k	1	2	3	4	5	6	7
2	1	0.6674	0.4834 +j0.0130					
3	1	0.7825	0.7407 +j0.0035	0.6839 +j0.0102				
	2	0.7241 +j0.0122	0.8409	0.7241 +j0.0122				
4	1	0.8409	0.8168 +j0.0012	0.7708 +j0.0011	0.7390 +j0.0026			
	2	0.7772 +j0.0068	0.9036	0.8698 +j0.0013	0.7917 +j0.0053			
5	1	0.8408	0.8168 +j0.0012	0.7934 +j0.0004	0.7707 +j0.0015	0.7392 +j0.0001		
	2	0.7772 +j0.0068	0.9036	0.8698 +j0.0013	0.8373 +j0.0001	0.7922 +j0.0003		
	3	0.8332 +j0.0052	0.9039 +j0.0014	0.9554	0.9039 +j0.0014	0.8332 +j0.0052		
6	1	0.8409	0.8171 +j0.0008	0.8168 +j0.0016	0.7932 +j0.0031	0.7704 +j0.0041	0.7391 +j0.0024	
	2	0.7772 +j0.0068	0.9036	0.8824 +j0.0009	0.8698 +j0.0016	0.8372 +j0.0027	0.7924 +j0.0005	
	3	0.8332 +j0.0052	0.9039 +j0.0013	0.9999	0.9624 +j0.0001	0.9262 +j0.0017	0.8754 +j0.0004	
7	1	0.8409	0.8244 +j0.0002	0.8081 +j0.0022	0.7918 +j0.0041	0.7758 +j0.0059	0.7601 +j0.0075	0.7382 +j0.0076
	2	0.7772 +j0.0011	0.9036	0.8826 +j0.0003	0.8624 +j0.0021	0.8410 +j0.0041	0.8210 +j0.0057	0.7385 +j0.0076
	3	0.8320 +j0.0021	0.9036 +j0.0002	0.9554	0.9271 +j0.0001	0.9017 +j0.0021	0.8752 +j0.0037	0.7933 +j0.0056
	4	0.8752 +j0.0005	0.9263 +j0.0017	0.9612 +j0.0001	0.9999	0.9612 +j0.0001	0.9263 +j0.0017	0.8752 +j0.0005

where

$$y_{st} = -j\frac{2}{K}\cdot\omega\cdot\varepsilon_{ef}\int_{-K/2}^{K/2} R_{kl}e^{j(x_s-x_t)k}\,dk, \qquad R_{kl} = \sum_{m=-M_1}^{M_2} I_m^k[\mathscr{S}^{-1}]_m^l. \tag{13}$$

The integral (13) can be evaluated partly numerically and partly using the Cauchy theorem. Finally, the result of integration can be written as

$$y_{st} = y_{st}^R + y_{st}^C,\ y_{st}^R = b_{kl}[(\Delta v/v)s(1-s)\sin\pi s]e^{-j|x_s-x_t|r_0} \tag{14}$$

where $s = pr_0/\pi$ and r_0 is the wave number of SAW propagating in periodic metal strips with period $2p$. Index C describes terms connected with mutual capacitance of the metal strips. The most interesting term Y_{st}^R, which is the radiation part of transadmittance, is proportional to the parameter characterizing the piezoelectricity of the substrate $(\Delta v/v)$. We recognize the term describing time delay of SAW between the strips s and t in the form $\exp(-j|x_s-x_t|r_0)$, however, b_{kl} can have complex value so that the phase shift between I_s and V_t is described by both the above exponent term and $\arg\{b_{kl}\}$ simultaneously. The values of b_{kl} for a group of N electrodes is shown in Table I for the center frequency $f_0 = v/4p$. It is to be noted that the dependence of b_{kl} on frequency is week so that the values given in Table I can be used for a wide frequency band about f_0.

5. Theory of IDT

Below we consider strips having their widths equal to the spacings between them in the group, and the period of groups is assumed so large, that groups are almost isolated. This models the single group of N metal strips deposited on a piezoelectric substrate, that is exactly the case of interdigital transducer. The result (14) can be

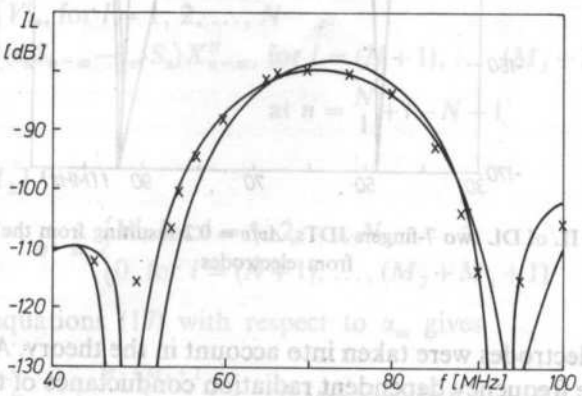

FIG. 2. IL of SAW DL on YX SiO_2 composed of two 7-fingers IDTs: —— the above theory, – – – the δ-function model [2], + + + experimental data (thanks to Dr J. FILIPIAK and Dr A. KAWALEC for experimental data)

easily applied in analysis of interdigital transducers [3]. To do this, one should take into account that some transducer fingers are connected to one transducer bar, while the others are connected to the other bar. Correspondingly, the finger potentials are V_1 and V_2. The currents of transducer bars can thus be evaluated on the strength of Eqs. (12) and (14), and finally, the potentials V_1 and V_2 results from the Kirchoff's laws [4]. Fig. 2 shows the results of analysis of delay line consisting of IDTs having 7 fingers, aperture $A = 4$ mm and $p = 11$ μm. *YX* quartz was applied as the *DL* substrate. Shown are results given by the present theory, the theory [2] for periodic fingers (that is equivalent to δ-function model) and the experimental results, for comparison. The main effect of the specific performance of the each fingers of *DL* transducers (that is the different b_{kl} for different k and l) is the broadenning of *DL* passband and the increasing of *DL* insertion loss, as compared with [2] or δ function model. The results presented in this paper are quite similar to those in [5] however they were obtained on rigorous field theory of propagation and generation of SAW under periodic system of groups of electrodes. Such a second-order effect, as SAW

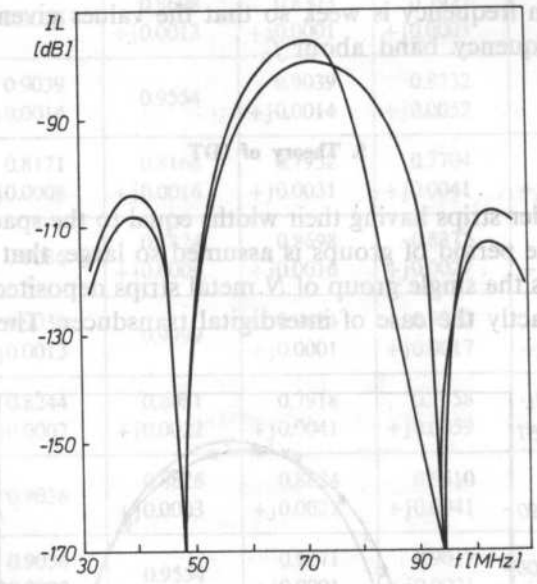

FIG. 3. Distortion of IL of DL two 7-fingers IDTs, $\Delta v/v = 0.2$ resulting from the $\Delta v/v$ reflection of SAW from electrodes

reflection from electrodes were taken into account in the theory. As known [3, 6] this effect distorts the frequency dependent radiation conductance of the transducer. This is illustrated on Fig. 3. The same delay line as presented above was analyzed and $\Delta v/v$ was applied as high as 0.2 in order to make the distortion clearly seen. To our best knowledge, this is the first rigorous theory of that effect.

Appendix A

An expansion of G_N or F_N into the Fourier's series gives

$$G_N(\theta;\alpha)=\sum_{n=-\infty}^{\infty} S_n X_n^N e^{-jn\theta}, \quad F_N(\theta;\alpha)=\sum_{n=-\infty}^{\infty} X_n^N e^{-jn\theta} \tag{15}$$

where

$$\begin{cases} X_n^1 = P_n(\cos\Delta), & \text{for } n\geqslant 0 \quad X_{-n}^N = X_{n-1}^N \text{ for odd } N \\ X_n^2 = \sum_{m=0}^{n-1} P_m P_{n-m-1}\cos[(2m-n+1)\alpha], \quad X_0^2 = 0 & \text{for } n<0 \quad X_{-n}^N = -X_n^N \text{ for even } N \\ \cdots\cdots\cdots\cdots\cdots\cdots\cdots\cdots \\ X_n^N = 2\sum_{m=1}^{n} X_m^2|_{(N-1)\alpha}\cdot X_{n-m}^{N-2}, \end{cases} \tag{16}$$

where $X_m^2|_\beta$ means that X_m^2 are the expansion coefficients of $F_2(\theta;\beta)$.

Appendix B

Assuming, that $\mathbf{V}^l$ are known, the following set of equations is obtained

$$\sum_{m=-M_1}^{M_2} \mathscr{J}_m^1 \alpha_m = jv^l, \quad l=1,2,\ldots,(M_2+M_1+1) \tag{17}$$

where

$$\mathscr{J}_m^1 = \begin{cases} V_m^l, \text{ for } l=1,2,\ldots,N \\ (\varepsilon_n S_{n-m}-\varepsilon_{ef}S_n)X_{n-m}^N, \text{ for } l=(N+1),\ldots,(M_2+M_1+1) \end{cases} \tag{18}$$

$$\text{at } n=\frac{N}{1}+l-N-1$$

for $m\in[-M_1, M_2]$

$$v^1 = \begin{cases} \mathbf{V}^l, \text{ for } l=1,2,\ldots,N \\ 0, \text{ for } l=(N+1),\ldots,(M_2+M_1+1) \end{cases} \tag{19}$$

Solution of the equations (17) with respect to α_m gives

$$\alpha_m = j\cdot \sum_{n=1}^{M_2+M_1+1} [\mathscr{J}^{-1}]_m^n v^n, \; m=-M_1,\ldots,M_2 \tag{20}$$

where $\mathscr{J}^{-1}$ is the inverse matrix to $\mathscr{J}$, what gives next (10).

References

[1] T. AOKI, K. A. INGEBRIGTSEN, *Acoustic surface waves in split strip periodic metal gratings on a piezoelectric surface*, IEEE Trans. SU **24**, 179–193 (1977).

[2] E. DANICKI, *Theory of periodic interdigital transducer (IDT of surface acoustic waves SAW)*, J. Tech. Phys. **19**, 89–102 (1978).

[3] E. DANICKI, *Unified theory of interdigital transducer and SAW reflectors*, J. Tech. Phys. **21**, 387–403 (1980).

[4] E. DANICKI, *Analysis of narrowband dispersive interdigital transducers by scatering matrix method for periodic metal strips*, Arch. Acoustics **13**, 3–4 (1988), pp. 237–253.

[5] W. R. SMITH, W. F. PEDLER, *Fundamental and harmonic frequency circuit model analysis of interdigital transducer with arbitrary metalization and polarity sequences*, IEEE Trans. on MTT, **23**, 853–864 (1975).

[6] W. S. JONES, C. S. HARTMAN, T. D. STURDIVANT, *Second order effects in surface wave devices*, IEEE Trans. on SU, **19**, 368–377 (1972).

Received on October 2, 1989

ARCHIVES OF ACOUSTICS
15, 1–2, 57–68 (1990)

DISLOCATION CONTRIBUTION IN THE ACOUSTOELASTIC EFFECT

J. DEPUTAT

Institute of Fundamental Technological Research of the Polish Academy of Sciences
(00-049 Warszawa, ul. Świętokrzyska 21)

1. Introduction

The acoustoelastic effect consists in the relationship between elastic deformation and velocity of acoustic waves in the medium. Properties of this phenomenon are most frequently observed in the course of measurements of changes of travel time of very small amplitude ultrasonic waves propagating in solids subjected to loading with external forces. A theoretical model is approximated in such experiments by superimposing infinitely small variable displacements on finite elastic deformation. Velocity increments of ultrasonic waves due to stress are usually small and high time resolution apparatus is necessary for their measurement. Velocity changes due to stress are proportional to stress and in a given medium they depend on the direction of wave propagation and orientation of particle vibration in the wave in relation to direction of stress. A 10 MPa increase of tensile stress in steel decreases velocity of longitudinal waves propagating in the direction of stress by about 0.75 m/s; longitudinal waves propagating perpendicular to stress by about 0.1 m/s; transverse waves propagating in the direction of stress by about 0.07 m/s; transverse waves propagating perpendicular to stress and polarized in the direction of stress by about 0.4 m/s, while those polarized perpendicular to the direction of stress by about 0.1 m/s. These changes depend on type of material, and for example in the case of aluminium and its alloys they are approximately twice as big and in plastics many times greater than in steel. The linear theory of elasticity does not lead to a relationship between elastic deformation and the velocity of acoustic waves. According to the linear theory of elasticity velocities of acoustic waves in an isotropic unbounded elastic medium are expressed by:

$$V_L = \sqrt{\frac{E(1-\nu)}{\varrho(1+\nu)(1-2\nu)}}, \qquad V_T = \sqrt{\frac{G}{\varrho}} \tag{1}$$

where: V_L and V_T are velocities of longitudinal and transverse waves, respectively; E and G are longitudinal and shear moduli of elasticity (second-order elasticity constants), respectively; ν – Poisson's ratio; ϱ – mass density. A relationship between velocity of acoustic waves and stress is reached when the non-linear stress-deformation dependence is included. Initial form of expressions relating velocity of elastic waves with low amplitude, and stress for an isotropic medium were given by HUGHES and KELLY [1] in 1953. Their paper initiated wide theoretical and experimental research on the acoustoelastic effect, as well as trials of implementing the stress-velocity relation in measurements of residual stresses in materials and structure elements. An extensive review of theoretical and experimental work concerning the acoustoelastic effect can be found in monographs and review papers [2–5]. The velocity, V, of waves in a body elastically deformed by uniaxial stress, σ, is expressed by second-order elasticity constants, λ and μ (Lamé's constants at $\sigma = 0$), mass density in neutral state, ϱ_0, and third-order elasticity constants, k, l and m. Expressions achieved in paper [1] for longitudinal and transverse waves propagating in the direction of stress have the following form:

$$\varrho_0 V_{111}^2 = \lambda + 2\mu - \frac{\sigma}{3K_0}\left[2l + \lambda + \frac{\lambda+\mu}{\mu}(4m + 4\lambda + 10\mu)\right] \tag{2}$$

$$\varrho_0 V_{121}^2 = \mu - \frac{\sigma}{3K_0}\left[m + \frac{\lambda n}{4\mu} + 4\lambda + 4\mu\right]. \tag{3}$$

Succeeding indexes of V denote the direction of wave propagation, direction of particle's vibrations and direction of stress. Velocity changes due to stress described by formulae (2) and (3) are related with non-linear properties of elastic interaction of particles in the medium. Experiments indicate practical linearity of the σ–v dependence and in stress measurements the expression in used:

$$\frac{v - v_0}{v_0} = \frac{t_0 - t}{t} = \beta \cdot \sigma \tag{4}$$

where: t_0 and t are travel times of waves over a constant path in material in initial and deformed state, respectively; β is the acoustoelastic constant of the material for a given configuration between directions of stress, propagation and polarization of waves in hitherto performed investigations. A symmetry of the effect is observed when the sign of stress is changed. Replacing tension with compression causes a change of sign of velocity increment only. Value changes of the acoustoelastic constant have not been noted when the sign of stress was changed. A frequency dependence of the acoustoelastic constant was not stated. No significant changes of the acoustoelastic constant have been stated for different chemical composition of steel, within limits permissible by standards, and the same β value is accepted for a given grade of steel [6]. Research on the influence of metalurgical phase transformation on the value of the β constant are performed [7].

The dislocation theory indicates the possibility of occurrence of additional

velocity increments due to stress, when dislocations, vibrating in the stress field of propagating acoustic waves, can be found in the crystal. Such dislocations are called active dislocations to tell them from dislocations pinned down on the whole length by point defects and dislocation network points. Active dislocations are introduced into the material through plastic deformation. A hypothesis was made that in plastically deformed construction materials dislocation changes of velocity can occur beside changes due to elastic non-linearity of the crystal lattice. Additional velocity changes due to stress should be taken into account in stress investigations based on velocity measurements of ultrasonic waves.

This paper is dedicated to initial research on the acoustoelastic effect in plastically deformed steel sample. Values of acoustoelastic constants were determined in 24H2MF and 45 steel in initial state and after plastic deformation. The occurence of an additional source of velocity changes due to stress in plastically deformed samples was stated. Properties of additional wave velocity increments were investigated and the dislocation character of this phenomenon was stated. Results were evaluated on grounds of the theory of dislocation modulus defect (changes of the modulus of elasticity) based on the model of dislocations in the form of a vibrating string [8].

2. Experiments

In measurements with waves propagating in the direction of stress, rod-shaped samples with circular crossection diameter of 16 mm and length of 180 mm were used. Sample ends at the length of 18 mm were threaded in order to mount the sample in holders of a machine for tensile tests. Piezoelectric transducers, which were sources of ultrasonic waves, were applyed to the flat surface of the sample's end face. Measurements with waves propagating perpendicular to the direction of stress were made on rod-shaped samples with rectangular section in the measurement part. Piezoelectric transducers were applyed to the flat side surface of samples.

Changes of the travel time of pulses of ultrasonic waves between chosen bottom echos were measured during loading with a tension and compression, when samples were in a state after stress relieving annealing (573 K, 24 h) and after plastic deformation. Plastic deformation was introduced by stretching samples. Measurements were carried out at constant room temperature with a meter of travel time of pulses of ultrasonic waves. The meter provided ± 1 ns resolution. From measured values of travel time a part of time change resulting from wave's path increment due to elastic deformation of sample was subtracted:

$$\left(\frac{t_0-t}{t}\right)_{\sigma} = \left(\frac{t_0-t}{t}\right)_{\text{measured}} - \frac{l_0-l}{l} \tag{5}$$

where: l_0-l is wave's path increment due to elastic deformation. In the case of

measurements with waves propagation along the sample, the stress distribution on the axis of loaded sample was included by introducing the shape coefficient, as it is described in paper [9].

3. Results of measurements

Fig. 1 presents examples of velocity changes of longitudinal waves with frequency of 4 MHz versus time after plastic deformation of a 24 H2MF steel sample. Measurements were done at room temperature. After deformation a recovery of wave velocity is observed. Recovery is practically full after 48 hours.

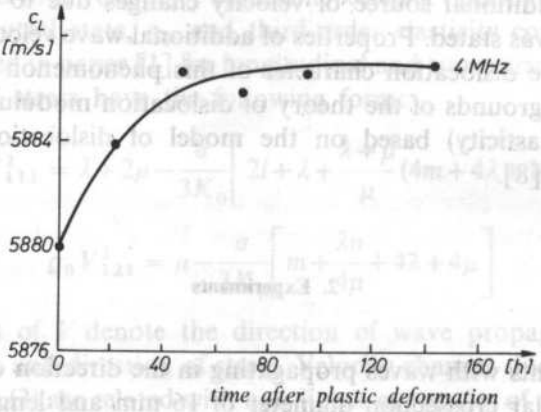

FIG. 1

Fig. 2 presents relative changes of travel time of longitudinal ultrasonic waves with frequency of 4 MHz and 10 MHz, propagating in the direction of stress in terms of stress value in the 24 H2MF steel sample before plastic deformation $\varepsilon = 0$ and after plastic deformation $\varepsilon = 3\%$. Data is arranged along straight segments. The repeatability of results is better than 1%. Tangents of inclinations of these straight lines are acoustoelastic coefficients for individual cases.

The acoustoelastic coefficient for longitudinal waves in a sample before plastic deformation is equal to $\beta = -1.77 \times 10^{-5}$ MPa^{-1} and it has the same value for tension and compression of the sample. Values measured for waves with frequencies of 4 MHz and 10 MHz lie on the same straight line. Due to a 3% plastic deformation the value of the acoustoelastic coefficient changes become depending on the direction of loading. Also a frequency dependence of the coefficient is observed. Values of the coefficient determined during compression are higher than during tension. β values achieved during compression are higher for 10 MHz frequency than for 4 MHz. During tension the β value for waves with frequency of 10 MHz is smaller than for waves with frequency of 4 MHz.

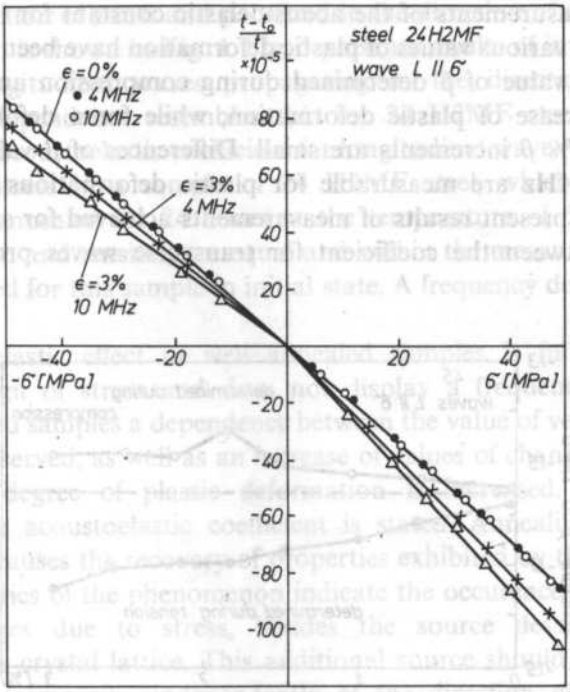
steel 24H2MF
wave L ll 6'
ε=0%
● 4MHz
○ 10MHz
ε=3%
4MHz
ε=3%
10 MHz
-6' [MPa]
6' [MPa]

FIG. 2

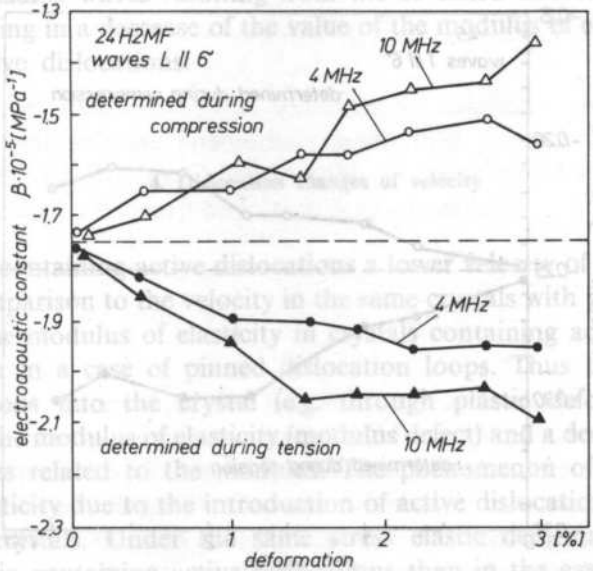
24H2MF
waves L ll 6'
10 MHz
4 MHz
determined during compression
4 MHz
10 MHz
determined during tension
electroacoustic constant
deformation
3 [%]

FIG. 3

Results of measurements of the acoustoelastic constant for longitudinal waves β^L in samples with various values of plastic deformation have been gathered in Fig. 3. Differences in the value of β determined during compression and tension initially grow with an increase of plastic deformation, while for a deformation exceeding approximately 1.5% β increments are small. Differences of β value determined for 4 MHz and 10 MHz are measurable for plastic deformations exceeding 1.5%.

Figs. 4 and 5 present results of measurements achieved for samples of steel 45. A relationship between the coefficient for transverse waves propagating perpen-

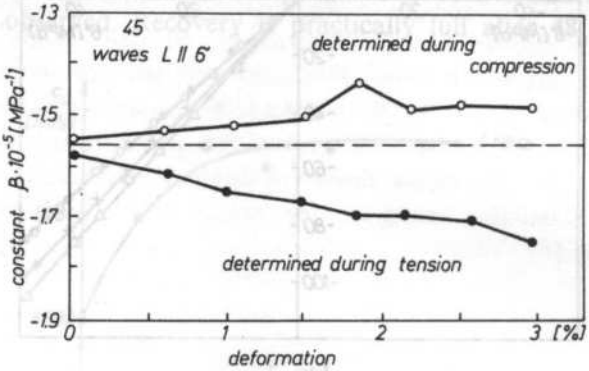

FIG. 4

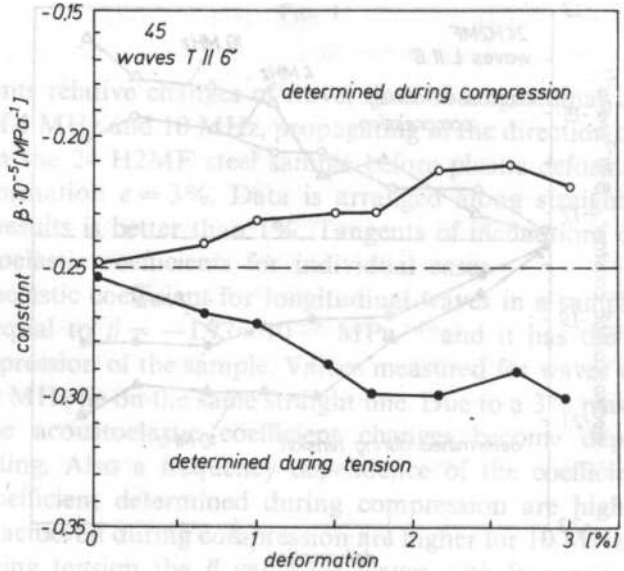

FIG. 5

dicular to the direction of stress and polarized in the direction of stress, and value of plastic deformation is shown in Fig. 4. Fig. 5 presents results of investigations of this coefficient for longitudinal waves propagating in the direction of stress. The character of the dependence resembles that for 24 H2MF steel.

Values of the acoustoelastic coefficient for longitudinal waves propagating along the direction of stress in a sample of 24 H2MF steel, which after 3% plastic deformation was annealed for 24 hours at the temperature of 573 K, determined during compression and tension, are equal and within the measuring error equal to value of β measured for this sample in initial state. A frequency dependence of β was not observed.

The acoustoelastic effect in well annealed samples is fully symmetrical in relation to the sign of stress and does not display a frequency dependence. In plastically deformed samples a dependence between the value of velocity changes and sign of stress is observed, as well as an increase of values of changes under the same stress when the degree of plastic deformation is increased, and a frequency dependence of the acoustoelastic coefficient is stated. Annealing of a plastically deformed sample causes the recovery of properties exhibited by the sample in initial state. Such properties of the phenomenon indicate the occurence of a second source of velocity changes due to stress, besides the source described with elastic nonlinearity of the crystal lattice. This additional source should introduce velocity changes with the same sign independently of the direction of loading (velocity decreases during compression, as well as during tension). Velocity changes introduced by an additional source should be dependent on the degree of plastic deformation and exhibit dispersion. Such properties are demonstrated by velocity changes of ultrasonic waves resulting from the so-called dislocation defect of the modulus consisting in a decrease of the value of the modulus of elasticity due to the presence of active dislocations.

4. Dislocation changes of velocity

In crystals containing active dislocations a lower velocity of ultrasonic waves is observed in comparison to the velocity in the same crystals with pinned dislocations. The value of the modulus of elasticity in crystals containing active dislocations is also lower than in a case of pinned dislocation loops. Thus the introduction of active dislocations into the crystal (e.g. through plastic deformation) leads to diminishing of the modulus of elasticity (modulus defect) and a decrease of velocity of ultrasonic waves related to the modulus. The phenomenon of a decrease of the modulus of elasticity due to the introduction of active dislocations has been known in pure monocrystals. Under the same stress elastic deformation is greater in crystalline media containing active dislocations than in the case when the crystal lattice does not contain dislocations, or when the motion of existing dislocations is

impossible. Total elastic deformation consists of displacement described by the stress-deformation dependence, ε_s, and dislocation deformation, ε_d:

$$\varepsilon = \varepsilon_s + \varepsilon_d \tag{6}$$

The first component of deformation is expressed by:

$$\varepsilon_{(s)kl} = C^{-1}_{klij}\sigma_{ij} \tag{7}$$

where: C – elasticity constants and σ – stress. Deformation due to a dislocation loop with length l in the volume unit is expressed by a product of average displacement $\bar{\xi}$, loop length l and modulus of Burgers vector b. The average displacement of a dislocation $\bar{\xi}$ is determined by:

$$\bar{\xi} = \frac{1}{l}\int_0^l \xi(y)dy \tag{8}$$

where: y is the coordinate along the line of undeformed dislocation (Fig. 6). If Λ is the total length of active dislocation loops in a unit volume, then the dislocation deformation is:

$$\varepsilon_d = \frac{\Lambda b}{l}\int_0^l \xi(y)dy \tag{9}$$

A decrease of the modulus of elasticity due to the presence of dislocations manifests itself by a diminishing of velocity of ultrasonic waves, according to the dependence (1):

$$\frac{\Delta G}{G} = 2\frac{\Delta V}{V} \tag{10}$$

The decrease of the modulus of elasticity is accompanied by an increase of dislocation internal friction. Both these phenomena are described by theories of dislocation internal friction. The most fully verified Granato-Lücke theory [8], based on the string model of dislocation loop, is developed from the equation of dislocation loop's motion:

$$A\frac{\partial^2\xi}{\partial t^2} + B\frac{\partial\xi}{\partial t} - C\frac{\partial^2\xi}{\partial y^2} = b\cdot\sigma_0\sin\omega t \tag{11}$$

where ξ is the coordinate in the direction of displacement in the slip plane, y – coordinate in the direction of line length, $A = \pi\varrho b^2$ – mass of a unit of line length, B – constant of dislocation motion damping, $C = 2Gb/\pi(1-\nu)$ – stress of a bent dislocation line, ϱ – mass density, G – elastic modulus, ν – Poisson's ratio, b – modulus of Burgers vector of dislocations σ_0 – amplitude of applied stress, ω – circular frequency of changes of applied stress.

The solution of the equation leads to an expression for a relative change of wave velocity due to the presence of a dislocation loop with length l:

$$\frac{\Delta V}{V}(l) = \frac{V - V_0}{V_0}(l) = \frac{4 \cdot G \cdot b^2 \Omega}{\pi^2 A} \Lambda \frac{\omega_0^2 - \omega^2}{(\omega_0^2 - \omega^2) + (\omega d)^2} \tag{12}$$

where: V_0 – wave velocity in a crystal without active dislocations; V – velocity in a crystal with dislocations; Λ – length of line of dislocations in a unit-volume; $\omega_0 = \pi / l \sqrt{C/A}$ – resonance frequency of the loop; $d = B/A$, Ω – orientation factor including the dependence between stress in the direction of wave propagation and stresses in individual slipe systems, ω – frequency of ultrasonic wave driving vibrations of the loop. If the distribution of the length of dislocation loop is taken into consideration, then the expression for velocity change will be as follows:

$$\frac{\Delta V}{V}(\omega) = \int_0^\infty \frac{\Delta V}{V}(l) \cdot l \cdot N(l) dl \tag{13}$$

where $N(l)dl$ is the number of loops in a unit of volume with length contained in an interval from l to $l + dl$, and integral of $lN(l)$ substituted dislocation density Λ in equation (12). For a random distribution of pinning points we reach:

$$N(l)dl = \frac{\Lambda}{L_c^2} e^{-l/L_c} dl. \tag{14}$$

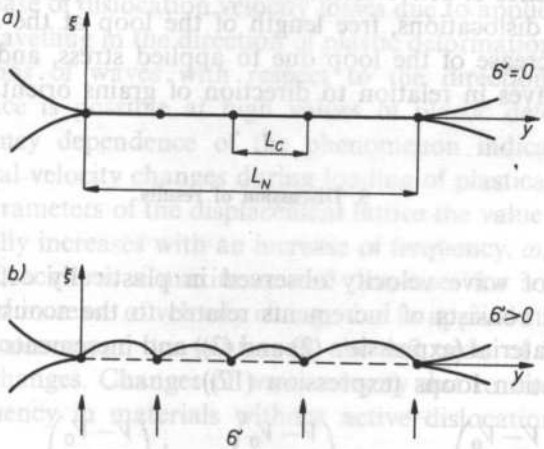

FIG. 6

Due to applied stress loops will bend into arcs (see Fig. 6) and the average free length of the loop will change from L_c to $L_c + \delta L_c$. The influence of stress on changes of damping of ultrasonic waves was analyzed in paper [11]. However, the phenomenon of dislocation changes of velocity due to stress has not been hitherto investigated. If

the increment of the length of a loop δL_c will be small in relation to L_c, then velocity changes of ultrasonic waves due to stress applied to the sample will be noted as:

$$\delta\left[\frac{\Delta V}{V}(\omega)\right] = \frac{\partial}{\partial L_c}\left[\int_0^\infty \frac{\Delta V}{V}(l)\cdot l\cdot N(l)\cdot dl\right]\delta L_c$$
$$= \frac{\Lambda}{L_c^3}\delta L_c \int_0^\infty \frac{\Delta V}{V}(l)\cdot l\left(\frac{l}{L_c}-2\right)e^{l/L_c}dl. \tag{15}$$

Inserting expression (12) in (15) and including the relation between the length increase of the loop and changes of resonance frequency $dl = \pi(\omega_0)^{-1}(C/A)^{-2}$ we reach an expression for measured value of dislocation velocity increment:

$$\delta\left[\frac{\Delta V}{V}(\omega)\right] = \frac{4\cdot G\cdot\Omega\cdot b^2\Lambda^2}{\pi^2 L_c^3 A}\int_0^\infty \frac{\left(\frac{K}{L}-\omega^2\right)\cdot l\cdot\left(\frac{l}{L}-2\right)e^{-l/L_c}}{\left(\frac{K}{L}-\omega^2\right)^2+(\omega d)^2}dl \tag{16}$$

where: $K = \pi^2 C/A$.

The length of the loop Lc (initial state), occuring in expression (14), corresponds to resonance frequency ω_0, while the length of the loop L (state after stress applied) corresponds to lower resonance frequency ω_0'.

Expression (16) indicates that the size of velocity changes of ultrasonic waves related to the presence of active dislocations due to the application of stress depends on the density of dislocations, free length of the loop at the state before stress is applied, length increase of the loop due to applied stress, and on the direction of propagation of waves in relation to direction of grains orientation in the sample.

5. Discussion of results

The change of wave velocity observed in plastically deformed steel samples under elastic load consists of increments related to the acoustoelastic effect of the lattice of tested material (expression (2) and (3)) and increments resulting from length change of dislocation loops (expression (17)):

$$\left(\frac{V-V_0}{V_0}\right)_{\text{measured}} = \left(\frac{V-V_0}{V_0}\right)_{\text{lattice}} + \left(\frac{V-V_0}{V_0}\right)_{\text{dislocation}}. \tag{17}$$

When the direction of vibrations of the medium's particles during the propagation of a wave is consistent with the direction of stress, then during compression the wave velocity is higher than in the initial state and during tension velocity decreases. The sign of the first component of measured velocity changes depends on the direction of applied stress. Elastic tension, as well as compression of a sample containing active dislocations leads to an increment of loop length, and hence to

a velocity decrease. The sign of the second component is independent of the sign of applied stress. The dislocation velocity change increases the acoustoelastic velocity diminishing during stretching and decreases the velocity increment during compression.

The density of dislocation grows during plastic deformation. Research based on the eatched pits count indicate a monotonic increase of the density of dislocations accompanying an increase of plastic deformation [12]. The average free length of loops changes simultaneously with an increase of density of dislocations. However, this change can be in more complex relation with plastic deformation, because the density and distribution of pinning points changes with time due to the diffusion of point defects from the bulk to dislocation lines and diffusion along dislocation lines. In the case of higher values of plastic deformation the motion of dislocations in some slip systems can be hindered (pile-ups of dislocations) and further deformation causes crystalline rotation, so not blocked slip systems are positioned advantageously with respect to the direction of deformation. Surface waves were applied in investigations of the dependence of dislocation velocity changes on plastic deformation in iron [13]. Monotonic velocity changes with regard to deformation have been stated for waves travelling in the direction of the deformation. In the case of waves propagating perpendicular to the direction of deformation the dislocation velocity loss initially increases up to 70% deformation, achieves a maximum and decreases during further deformation. This type of dislocation velocity change suggests that the influence of density of dislocations predominates the effect of the average free length decrease of the loop and an increase of dislocation velocity losses due to applied stress should be expected for waves travelling in the direction of plastic deformation (expression (16)). As to other directions of waves with respect to the direction of displacement a different dependence is possible at high values of plastic deformation.

Also the frequency dependence of the phenomenon indicates a dislocation character of additional velocity changes during loading of plastically deformed steel samples. For fixed parameters of the displacement lattice the value of the dislocation velocity change initially increases with an increase of frequency, ω, of waves passing through the material, achieves a maximum and decreases for a further frequency increase. The observed increase of velocity change due to applied stress indicates that applied frequencies correspond to values on the left side of the minimum of dislocation velocity changes. Changes of wave velocity due to stress increments do not depend on frequency in materials without active dislocations.

6. Conclusions

Changes of wave velocity due to stress in steels with dislocations moving in a field of ultrasonic waves are a sum of changes resulting from inelastic behaviour of an ideal crystal lattice and changes introduced by dislocations.

The lattice part of velocity changes characterizes a given lattice. Its value at given stress is independent of frequency and wave amplitude. An increase of velocity is caused by compressive stress in the direction of particle motion in the wave. Stretching decreases velocity. The size of velocity changes is proportional to stress.

The dislocation part of velocity changes characterizes the dislocation lattice of the crystal and its value depends on density and average free length of the dislocation loops. This means that the value of dislocation velocity changes depends on the degree of plastic deformation, recovery after deformation, content of point defects, as well as frequency and amplitude of ultrasonic waves. The direction of dislocation velocity changes remains the same when the sign of stress is changed.

The value is considered constant for a given sort of material in ultrasonic measurements of stress. Results of this research indicate that such an approach should be limited. In practice a steel sample kept at room temperature during several days from cold plastic deformation exhibits full recovery of the modulus and decay of the dislocation component of velocity changes due to stress. In order to state whether a given material contains the dislocation component of velocity change, the symmetry criterion during stress direction change and frequency test can be used.

References

[1] D. A. HUGHES, G. S. KELLY, Second-order elastic deformation of solids, Phys. Rev., **92**, 1145 (1953).

[2] R. E. GREEN, *Treatise on materials science and technology*, V. 3 – Ultrasonic investigation of mechanical properties, Academic Press, (1973).

[3] В. М. Бобренко, А. М. Куценко, *Акустическая тензометрия* I, *физические основы*, Дефектоскопия, 2, (1980); *Акустическая тензометрия* II, *Методы и устройства*, Дефектоскопия, 12 (1980).

[4] J. DEPUTAT, *Foundations and applications of ultrasonic tensometry*, (in Polish) Dozór Techniczny, 3, 95–100 (1983) and 4, 142–149 (1983).

[5] J. DEPUTAT, *Ultrasonic measurements of welding stress* (in Polish), Przegląd Spawalnictwa, **36**, 7, 10–17 (1984) and **36**, 8, 15–17 (1984).

[6] M. ADAMSKI, J. DEPUTAT, *Structural sensitivity of the acoustoelastic coefficient* (in Polish), Materiały XVIII Otwartego Seminarium z Akustyki OSA-1981, Gliwice 1981, Wyd. Politechnika Śląska.

[7] J. S. HEYMAN, S. C. ALLISON, K. SALAMA, *Influence of carbon content on higher-order ultrasonic properties in steels*, Proc. IEEE Ultrasonic Symposium, 1983.

[8] A. GRANATO, K. LÜCKE, *Theory of mechanical damping due to dislocations*, J. Appl. Phys., **27**, 583 and 789 (1956).

[9] J. DEPUTAT, *Ultrasonic technique for measuring stress in screws*, Proc. 9 World Conference on Nondestructive Testing, Paper 4EDD-2, Melbourne 1979.

[10] G. F. NEWELL, Quart. Appl. Math., **41**, 155, (1958).

[11] A. HIKATA, J. DEPUTAT, C. ELBAUM, *Dislocation interactions with phonons in sodium chloride in the temperature range 70K–300K* Phys. Rev., B, **6**, 4008 (1972).

[12] J. DEPUTAT, *Damping of ultrasound and the photomechanical effect in NaCl crystals* (in Polish) Doctor's thesis, IFTRPAS, Warsaw 1965.

[13] A. BROKOWSKI, J. DEPUTAT, *Ultrasonic testing of the influence of degree of deformation in iron*, (in Polish), Proc. XI National Conf. on Non-destructive Testing, WSI Opole, SIMP, Opole 1982.

Received on January 13, 1987

ARCHIVES OF ACOUSTICS
15, 1–2, 69–92 (1990)

APPLICATION OF THE ACOUSTOELASTIC EFFECT IN MEASUREMENTS OF RESIDUAL STRESSES

J. DEPUTAT

Institute of Fundamental Technological Research Polish Academy of Sciences
(00-049 Warszawa, Świętokrzyska 21)

This paper contains a review of non-destructive methods of residual stress measurements and results of research on the properties of the acoustoelastic effect with regard to its application in investigations of stress fields in technological materials. Values of acoustoelastic constants and temperature coefficients of velocity change were determined in several construction metals for various types of waves. Relations between wave velocity and texture, influence of texture in ultrasonic measurements of stress are presented. Ultrasonic measurement methods of absolute values of stress in screws, railway rails and railway wheels were proposed. Constructed ultrasonic meter of residual stress are described and results of comparative X-ray, ultrasonic and destructive tests are given.

Dokonano przeglądu nieniszczących metod pomiaru naprężeń własnych i opisano wyniki badania własności zjawiska elektroakustycznego pod kątem jego zastosowań w badaniach pól naprężeń w materiałach technicznych. Opisano aparaturę do precyzyjnych pomiarów prędkości fal ultradźwiękowych. Wyznaczono wartości stałych elastoakustycznych i temperaturowych współczynników zmian prędkości w kilku metalach konstrukcyjnych dla różnych typów fal. Przedstawiono związki między prędkością fal i teksturą oraz rolę tekstury w ultradźwiękowych pomiarach naprężeń. Zaproponowano ultradźwiękowe metody pomiaru bezwzględnej wartości naprężeń w śrubach, szynach kolejowych i kołach kolejowych, opisano zbudowane ultradźwiękowe mierniki naprężeń własnych i pokazano wyniki porównawczych badań rentgenowskich, ultradźwiękowych i niszczących.

Notations

a constant dependent on screw's geometry
A constant of acoustic anisotropy of material, birefringence,
A_0 constant of anisotropy in state without stress,
$A\sigma$ constant of stress anisotropy,
E longitudinal modulus of elasticity,
G shear modulus,

$K = \lambda + 2/3\mu$ bulk modulus,
l length, third-order elasticity constant,
L notation of longitudinal waves,
m, n third-order elasticity constant,
N sending head,
0 index referring to the initial state (without stress),
O receiving head,
P force, hydrostatic pressure,
r radius,
R notation of surface waves,
SH notation of transverse waves polarized parallel to surface,
t time,
Δt time increment,
t^w time of flight in the standard material,
V_{ijk} phase velocity of waves propagating in direction i, polarized in direction j, under stress from direction k,
ΔV velocity increment,
w_{ijk} coefficients determining texture,
α angle of incidence,
β_{ijk} elastoacoustic constant of material for waves propagating in direction i, polarized in direction j, under stress from direction k,
λ wave length,
λ, μ Lamé elasticity constants (second-order elasticity constants),
ν Poisson's ratio,
ϱ mass density,
δ stress.

1. Introduction

Residual stresses can occur in elasto-plastic materials in a homogeneous temperature field without external forces. They are formed as a result of structural changes related to mass density changes or when the yield point is exceeded in a partial volume of the material due to mechanical or thermal load. Residual stresses and stresses originating from external loads sum up and frequently have a decisive influence on the mechanical state of material. The strength of construction elements can be adequatly higher or lower, depending on the signs of residual and external stresses. Compressive residual stresses in tension under external loads areas are advantageous.

A quantitative description of residual stresses is essential in studies of strength of material and in the evaluation of exploitation properties of construction elements and machine parts. However, complicated, arduous and expensive destructive measurement methods of these stresses have hindered research work and limited investigations to the most dangerous cases, or cases causing failures most frequently.

The following methods are considered classical methods of measuring stresses: resistance tensommetry, X-ray diffractomme try, photo-elasticity and mentioned destructive methods based on the measurement of deformations during stress release. Among these, only photoelasticity is a direct method. Other methods are based on the linear dependence between measured deformation and determined stress.

Measurement procedures and apparatus for resistance tensommetry have been well developed. However, it is limited by a lack of possibility of measuring absolute values of stress. Only stress increments can be measured with the application of this technique, and solely on the surface of tested object. Photo-elasticity can be used in investigations of stress distributions, but in models made from transparent materials only. With the X-ray technique stresses can be measured only on the surface. Numerous phenomena, influenced by stress, are experimentally applied in stress measurements. The following are most important:

neutron diffraction,
Berkhausen's magnetic noise,
acoustic emission accompanying magnetizing of ferromagnetic materials,
velocity changes of ultrasonic waves during magnetization changes,
microwave absorbtion,
damping of ultrasonic waves,
temperature dependence of velocity of ultrasonic waves,
acoustoelastic effect.

Results of stress measurements done with the application of mentioned phenomena usually are not solely stress dependent, but also depend on other factors, including parameters of the material such as: chemical composition, structure, thermal and mechanical processing, history of the sample. Only investigations of materials with high degree of homogeneity provide reliable quantitative results. Mechanical construction materials rarely meet this requirement.

This paper is concerned with research on the utilization of the relationship between velocity of ultrasonic waves and stress (acoustoelastic effect), which seems promising in practical applications in measurements of residual stress on the surface as well as inside technological materials.

2. Acoustoelastic effect

Velocity of acoustic waves in a solid body depends on forces of atom-atom interactions and mass of atoms transmitting wave motion. The linear theory of elasticity leads to known expressions of velocity of longitudinal and transverse waves in an unlimited isotropic solid:

$$V_{11} = \sqrt{\frac{\lambda+2\mu}{\varrho}} = \sqrt{\frac{E}{\varrho}\frac{1-\nu}{(1+\nu)(1-2\nu)}} \tag{1}$$

$$V_{12} = \sqrt{\frac{\mu}{\varrho}} = \sqrt{\frac{E}{2\varrho}\frac{1}{1+\nu}} = \sqrt{\frac{G}{\varrho}}$$

In these expressions V is the phase velocity of the wave, first index determines the direction of wave propagation in a cartesian coordinates system with axises 1, 2 and 3, second index determines the direction of particles vibrations in the wave, ϱ – mass density, E – and G – shear and elastic moduli, λ – and μ – Lame's constants (second-order elasticity constants) ν – Poisson's ratio.

The classical theory of elasticity assumes infinitesimal deformations of perfectly elastic bodies and does not provide for a velocity-stress dependence. When nonlinear properties of solids are included, the velocity-stress dependence is achieved. In a paper published in 1953 [1] HUGHES and KELLY derivated formulae for velocity of elastic waves in solids subjected to stress (infinitesimal deformations superimposed on finite deformation). They took advantage of Murnaghan's theory of finite deformations, including third-order terms in the expression for elastic energy of a deformed body. Achieved by these authors dependencies between velocity of low amplitude elastic waves and stress are considered fundamental in the description of the elastoacoustic phenomenon:

$$\varrho_0 V_{111}^2 = \lambda+2\mu-(\sigma/3K_0)\left(\frac{\lambda+\mu}{\mu}(4\lambda+10\mu+4m)+\lambda+21\right), \tag{2}$$

$$\varrho_0 V_{113}^2 = \lambda+2\mu-(\sigma/3K_0)\left(\frac{2\lambda}{\mu}(\lambda+2\mu+m)-21\right), \tag{3}$$

$$\varrho_0 V_{131}^2 = \mu-(\sigma/3K_0)\left(4\lambda+4\mu+m+\frac{\lambda n}{4\mu}\right), \tag{4}$$

$$\varrho_0 V_{133}^2 = \mu+(\sigma/3K_0)\left(\lambda+2\mu+m+\frac{\lambda n}{4\mu}\right), \tag{5}$$

$$\varrho_0 V_{132}^2 = \mu+(\sigma/3K_0)\left(2\lambda-m+\frac{n}{2}+\frac{\lambda n}{\mu}\right), \tag{6}$$

Similarly, for hydrostatic pressure

$$\varrho_0 V_{11P}^2 = \lambda+2\mu-(P/3K_0)(61+4m+7\lambda+10\mu), \tag{7}$$

$$\varrho_0 V_{13P}^2 = \mu-(P/3K_0)\left(3m-\frac{n}{2}+3\lambda+6\mu\right), \tag{8}$$

where ϱ_0 – mass density of not deformed medium; v – wave velocity in deformed material; λ and μ – Lamé's elasticity constants; m, n, l – Murnaghan's third-order elasticity constants, σ – uniaxial stress; $K_0 = \lambda + 2/3\mu$ – bulk modulus of not deformed medium, P – pressure. The third index of velocity denotes the direction of stress. Expressions (2) to (8) are used to determine values of third-order elasticity constants on the basis of wave velocity changes due to given stress increments. Including expressions (1) and (2) for velocity of acoustic waves in a not deformed isotropic body, and accepting that velocity increments, $v - v_0$, due to stress are small in comparison to absolute values of velocity, v and v_0 (what leads to an approximation: $V + V_0 \cong 2V_0$), we achieve relationships between relative changes of velocity and stress from equations (2) to (8). Such a relationship for longitudinal waves propagating in the direction of stress is as follows:

$$\left(\frac{V-V_0}{V_0}\right)_{111} = -\frac{\frac{\lambda+\mu}{\mu}(4\lambda+10\mu+4m)+\lambda+21}{2(\lambda+2\mu)(3\lambda+2\mu)} \cdot \sigma_1. \tag{9}$$

Factors of proportionality between stress and relative changes of wave velocity are called acoustoelastic coefficients. These coefficients are expressed by second- (λ, μ) and third-order (l, m, n) elasticity constants. Linearized relationships, like expression (9), ore the fundamental relationships of ultrasonic tensommetry. They have the following form:

$$\begin{aligned} V_{ij} &= V_{ij}^0(1+\beta_{ijk}\sigma_k) \\ t_{ij} &= t_{ij}^0/(1+\beta_{ijk}\sigma_k) \end{aligned} \tag{10}$$

where t and t_0 are travel times over a determined path in a material under stress and material without stress (material in neutral state), respectively, while β is a acoustoelastic coefficient.

Experiments confirm the linearity of the dependence between stress and relative change of wave velocity. Fig. 1 presents increments of travel times of longitudinal L, transverse T and surface R waves propagating in the direction of stress in a St3 steel sample, due to stress. Changes of travel times of waves were measured on a length between receiving heads O_1 and O_2, equal to 196 mm for longitudinal waves, 107 mm for transverse and surface waves.

Table 1 contains values of acoustoelastic constants for several structural metals. The amount of velocity changes due to stress depends on the sort of material, direction of wave propagation and direction of vibration of particles in the wave (direction of polarization) with respect to direction of stress. Longitudinal waves propagating along the direction of stress are most sensitive to stress. The velocity increment of longitudinal waves propagating in the direction of stress in a sample of carbon steel, resulting from a stress change of 10 MPa, is equal to approximately 0.75 m/s. This makes about 0.013 % of the value of velocity of longitudinal waves in steel. The corresponding velocity increment for transverse waves is equal to about

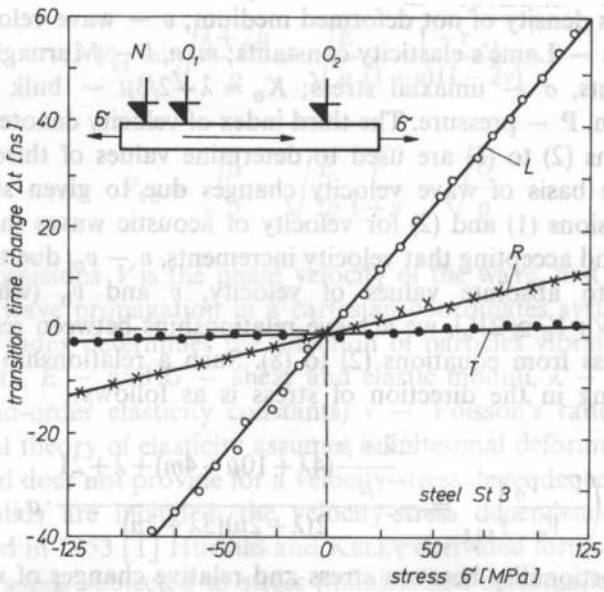

FIG. 1. Changes, Δt, of travel time of longitudinal waves L, transverse waves T, surface waves R, propagating in the direction of stress versus stress δ

0.05 m/s, and for surface waves – about 0.15 m/s. In a state of compound stress the effect of individual stress components on wave velocity sums up. From equations (3), (5) and (6) for waves propagating in the direction of thickness of a plate under biaxial state of stress we achieve the following relationships:

$$\frac{V_{33}-V_{33}^0}{V_{33}^0} = \beta_{331}(\sigma_2+\sigma_3), \tag{11}$$

$$\frac{V_{31}-V_{32}}{\frac{1}{2}(V_{31}^0+V_{32}^0)} = (\beta_{311}-\beta_{321})(\sigma_1-\sigma_2), \tag{12}$$

$$\frac{V_{31}+V_{32}-V\frac{1}{2}(V_{31}^0+V_{32}^0)}{V_{31}^0+V_{32}^0} = (\beta_{311}+\beta_{322})(\sigma_2+\sigma_3). \tag{13}$$

In these formulae V^0 denotes wave velocity for zero stress. Naturally, $V_{31}^0 = V_{32}^0$ for an isotropic material.

Expression (12) describes acoustic birefrigence. Due to stress an isotropic medium becomes anisotropic. The difference of velocity of transverse waves propagating in the direction of plate's thickness and polarized in directions of principal stresses is the measure of anisotropy due to stress.

Diagrams in Fig. 2 present times of flight of longitudinal, t_{33}, and transverse, t_{32},

Table 1. Acoustoelastic constants of aluminium, copper and steel. Consecutive indices of the symbol of the constant denote directions of propagation of a wave beam, polarization of vibrations of particles in the wave and direction of stress

Material	Elastoacoustic constant 10^{-5}MPa^{-1}				
	β_{111}	β_{221}	β_{121}	β_{211}	β_{231}
Aluminium	−7.75	+1.13	−2.19	−4	+0.89
Copper	−1.88	−0.18	0	−1.07	+0.2
Armco iron	−2.69	+0.49	+0.13	−0.48	−3.13
Nickel steel 535	−1.13	+0.06	−0.05	−0.66	+0.03
Steel 60C2H2A	−0.99	+0.14	−0.0	−0.70	+0.17
Steel Hecla 37	−1.39	+0.02	−0.12	−0.73	+0.03
Steel M56	−2.06	+0.15	−0.54	−1.17	+0.47

waves in terms of a force compressing a disc from PA6N alloy. The time of sixteen transitions of a pulse through the thickness of the disc was measured for longitudinal waves and of eight transitions for transverse waves. In effect of a point pressure P, acting along the diameter of the disc, a state of biaxial stress is created in the centre of the disc, where compressive stress is $\delta_1 = -2P/\pi gd$ and tensile stress is $\delta_2 = 6P/\pi gd$ (d is the diameter and g is the thickness of the disc). Linear

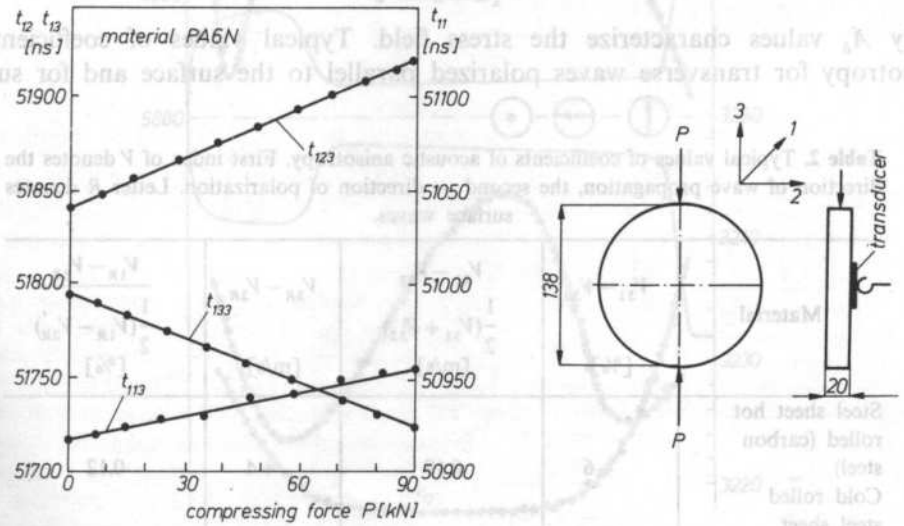

FIG. 2. Changes of travel time of longitudinal waves t_{33}, and transverse waves, t_{31} and t_{32}, versus force P compressing a disc from PA6N alloy

dependencies between stress and relative velocity change can be applied directly in measurements of stress increments. Adequate electroacoustic constants are determined in tensile tests. Because of a significant temperature dependence of the velocity of ultrasonic waves it is necessary to include adequate corrections for temperature in ultrasonic measurements of stress. Fortunately velocity changes are in linear dependence with temperature changes. Technological materials usually exhibit considerable heterogeneity and anisotropy of acoustic properties. In various areas of material free from stress the value of velocity of ultrasonic waves, V_0, can be different. The limits of heterogeneity of acoustic properties of technological metals are not known precisely. Results of wave velocity measurements performed on annealed samples cut out from various areas of the same element indicate the scope of heterogeneity. In the case of NC6 tool steel the greatest velocity difference of longitudinal waves was equal to 3.2 m/s, for surface waves – 5.2 m/s and for transverse waves – 5.4 m/s. In a carbon steel sheet local velocity differences amounted to: 10.8 m/s for longitudinal waves, 6.9 m/s for surface waves and 7.2 m/s for transverse waves. Such velocity differences can be incorrectly attributed to local differences of residual stress. The V_0 value in the area of material under investigation has to be known in order to determine the absolute value of stress. When measurements of acoustic anisotropy are applied in investigations of stress fields, then the anisotropy of the material free from stress has to be considered. Anisotropy in a stress free state in policrystalline materials is related to the preferential orientation of grains (texture) or to the directional arrangement of impurities. The measured coefficient of anisotropy, A, is a sum of anisotropy in a stress free state, A_0, and anisotropy caused by stresses, A_δ,

$$A = A_0 + A_\delta. \tag{14}$$

Only A_δ values characterize the stress field. Typical values of coefficients of anisotropy for transverse waves polarized parallel to the surface and for surface

Table 2. Typical values of coefficients of acoustic anisotropy. First index of V denotes the direction of wave propagation, the second – direction of polarization. Letter R denotes surface waves.

Material	$V_{31}-V_{32}$ [%]	$\frac{V_{31}-V_{32}}{\frac{1}{2}(V_{31}+V_{32})}$ [m/s]	$V_{3R}-V_{2R}$ [m/s]	$\frac{V_{1R}-V_{2R}}{\frac{1}{2}(V_{1R}-V_{2R})}$ [%]
Steel sheet hot rolled (carbon steel)	+6	0.19	+4	0.12
Cold rolled steel sheet (carbon steel)	+280	8.60	+122	3.90
Sheet aluminium	−2.5	0.08	−150	0.05

Table 3. Velocity of ultrasonic waves in a sample of austenitic steel 23 Cr, 12 Ni

Wave	V[m/s]	Wave	V[m/s]	Wave	V[m/s]
V_{33}	5369	V_{32}	3852	V_{23}	3847
V_{22}	5775	V_{31}	3853	V_{12}	2950
V_{11}	5812	V_{21}	2960	V_{13}	3862

waves are given in Table 2. Direction 1 is the direction of rolling, direction 2 is a direction perpendicular to the rolling direction in the plane of rolling.

Table 3 presents velocity values of bulk waves propagating in various directions in a sample cut from austenitic steel. The velocity distribution of ultrasonic waves in the cross section of a railway rail is differentiated. In Fig. 3 velocity changes of longitudinal and transverse waves propagating along the length of the rail versus distance from the rail surface are shown. The velocity distribution reflects texture changes of steel formed in the rolling process. Anisotropy has to be taken into consideration in investigations of stress fields in materials exhibiting anisotropy in

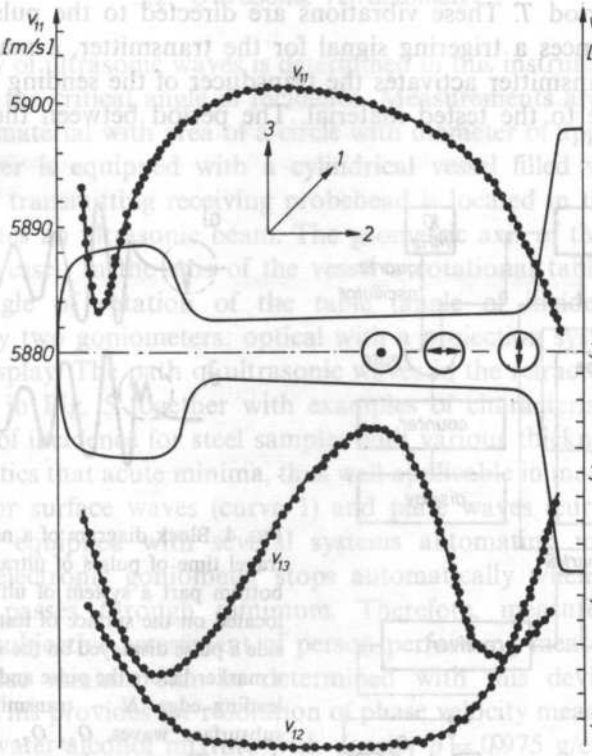

FIG. 3. Velocity changes of longitudinal and transverse waves propagating along the length of the rail and polarized parallel and perpendicular to the height of the rail versus distance from the rails rolling surface

a state free from stress. In certain cases the value of wave velocity, V_0, as well as the coefficient of anisotropy, A_0, in a state free from stress can be measured in an area under test before stress is applied. However, frequently such data is inaccessible and in order to determine stress methods of determining V_0 have to be applied, which are based for example, on measurements of velocities of many types of wares, with velocities to a different degree dependent on stress, or take advantage of such combinations of wave velocities, which are independent of texture.

Several possibilities will be discussed with descriptions of ultrasonic measurements of stresses in technological materials.

3. Measuring technique of velocity of ultrasonic waves

3.1. Nanosecond time meter

A nanosecond mater of transition time of ultrasonic pulses was built for investigations of properties of the elastoacoustic phenomenon. The block diagram of the nanosecond time meter is shown in Fig. 4. The tuned generator produces vibrations with period T. These vibrations are directed to the pulse selector. The pulse selector produces a trigering signal for the transmitter, a marker signal and gate signal. The transmitter activates the transducer of the sending head and sends an ultrasonic pulse to the tested material. The period between the production of

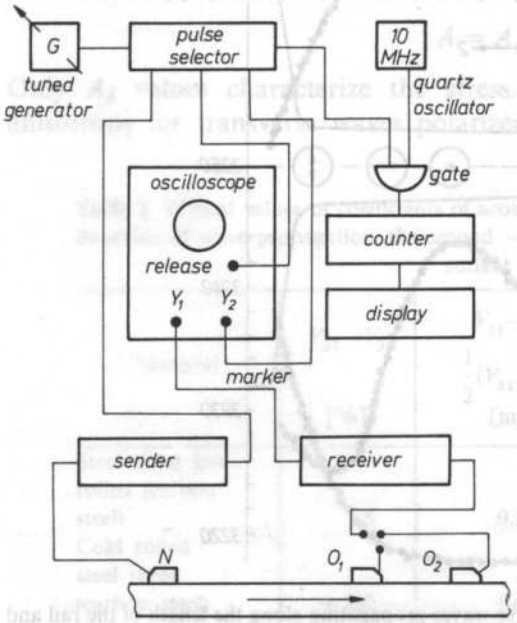

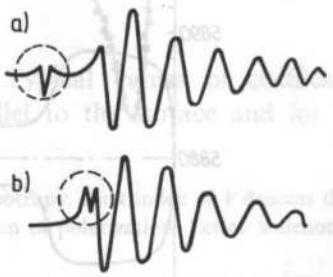

FIG. 4. Block diagram of a nanosecond meter of travel time of pulses of ultrasonic waves. In the bottom part a system of ultrasonic probeheads located on the surface of tested element. On the side a pulse displayed on the screen is shown with a marker before the pulse and guided to the pulse leading edge. N – transmitting transducer of subsurface waves, O_1, O_2, – receiving transducers. The arrow denotes a beam of ultrasonic waves.

successive ultrasonic pulses (repetition time) is equal to 100 T. After a period of time equal to 9 T the time base of the oscilloscope is released. A time marker, appearing after time period 10 T from the release of the transmitter, is superimposed on the received signal, presented on the screen of the oscilloscope tube. By means of fine tuning of generator G, its vibration period T, can be so adjusted, that the time marker is located in a chosen place on the display of received ultrasonic pulse. In this case the transition time of ultrasonic waves will be equal to 10 T. The time measurement with ± 1 ns accuracy is achieved by a pulse count in time equal to 10^4 T from a standard quartz oscillator with 10 MHz frequency and rounding of the indicator of of last counter. Repeatability of successive measurements of time of flight equal to ± 1 ns, for wave frequency 4 MHz, was achieved by using a V-shaped marker (Fig. 4) and by applying the criterion of equal arms in the process of superimposing the marker on the maximum. The accuracy of electronic systems is equal to ± 0.1 ns. The relative error of time measurements is equal to $\Delta t/t = 10^{-5}$ (0.001%) for average measured transition times $t \cong 100$ μs, what corresponds to a 60 cm distance in steel for longitudinal waves.

3.2. Ultrasonic refractometer

The velocity of ultrasonic waves is determined in this instrument on the basis of measurement of the critical angle of incidence. Measurements are performed in the surface layer of material with area of a circle with diameter of approximately 5 mm. The refractometer is equipped with a cylindrical vessel filled with liquid during measurement. A transmitting receiving probehead is located in the side wall of the vessel. It generates an ultrasonic beam. The geometric axis of this beam intercepts the axis of the vessel. In the axis of the vessel a rotational table for specimens is placed. The angle of rotation of the table (angle of incidence) is measured independently by two goniometers: optical with a projection system and electronic with a digital display. The path of ultrasonic waves in the refractometers measuring vessel is shown in Fig. 5 together with examples of characteristics: coefficient of reflection-angle of incidence for steel samples with various thickness. It results from these characteristics that acute minima, thus well applicable in measuremts, occur for critical angles for surface waves (curve 1) and plate waves (curves 2 and 3). The refractometer is equipped with several systems automating measurements. The counter of the electronic goniometer stops automatically when the amplitude of reflected pulse passes through minimum. Therefore, measurement results are independent of subjective assessment of person performing measurements. Angular positions of these minima can be determined with this device with accuracy exceeding $\pm 1'$. This provides for resolution of phase velocity measurements of about 0.01% when a water-alcohol mixture with density $\varrho = 0.975$ g/cm^3 (elimination of temperature influence on velocity of longitudinal waves) is used as standard liquid.

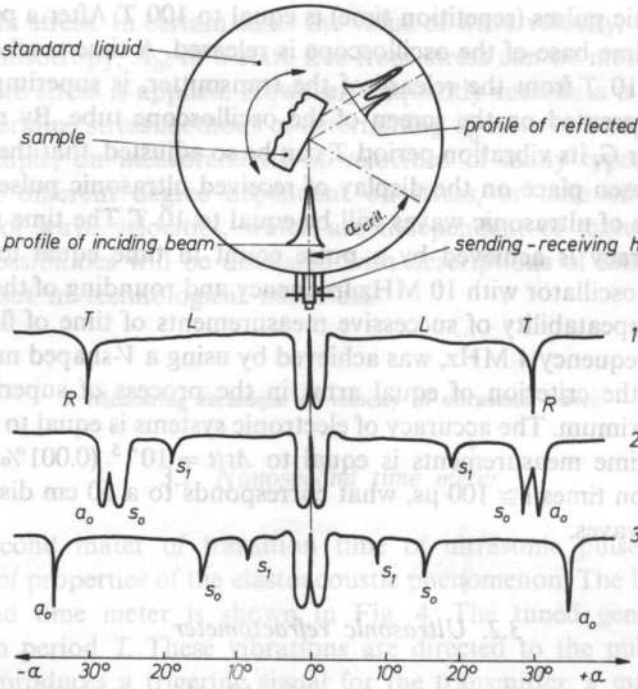

FIG. 5. Principle of measurement of critical angles of incidence on the liquid-solid interface with an ultrasonic refractometer and examples of dependencies of the coefficient of reflection on the angle of incidence α. Curves are for steel samples with thickness 20; 0.5; 0.3 mm respectively. Letters *L*, *T* and *R* denote longitudinal transverse and surface waves, respectively, and critical angles for these waves. a_0, s_0 and s_1 – minima corresponding to successive modes of plate waves

4. Examples of ultrasonic measurements of residual stresses

4.1. Stress measurements in bolts

Stress increment, $\Delta\delta$, in a bolt can be determined from measurements of changes of travel times of ultrasonic waves along the axis of the bolt. If the travel time is measured before ($\delta = 0$) and after ($\delta = 0$) screwing tight the bolt, then the relative change of travel time of waves along the bolt's axis are directly proportional to stress and relationships $\Delta t = f(\Delta\delta)$, determined from experiment for bolted joints in a given construction, can be applied in measurements of stress changes due to screwing.

Fig. 6 presents results of measurements of relative changes of travel times of longitudinal and transverse waves propagating along the length of a screw made of 25H2MF steel during tension [2]. The measured value of relative change of travel time of ultrasonic waves due to path increase of wave resulting from elastic deformation, and to velocity change caused by stress influence on velocity is:

$$\frac{t_0 - t}{t} = \frac{\Delta t}{t_0} = \left(\frac{1}{E} + \beta\right)\sigma \tag{15}$$

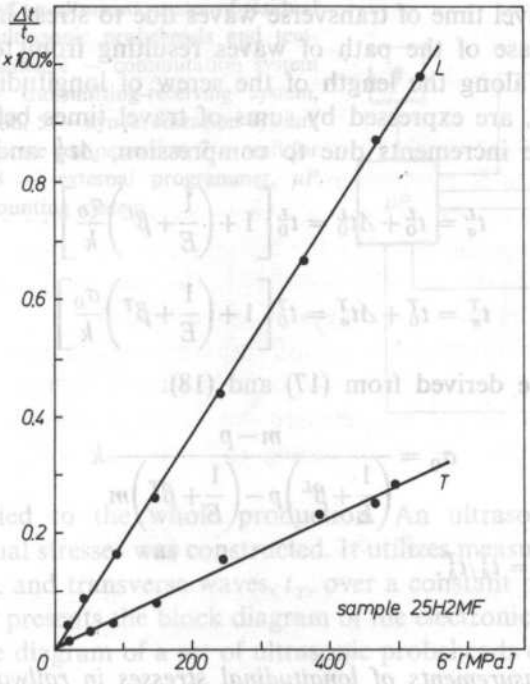

FIG. 6. Relative increments of travel times of longitudinal L and transverse T waves propagating in the direction of stress versus tensile stress. Sample from 25H2MP steel.

where E is the longitudinal modulus and β is an elastoacoustic constant. The relationship is in force when ultrasonic waves propagate along a path in a medium with stress δ. In bolts stresses are distributed along the hickness of the screw and the recorded value $\Delta t/t_0$ is the measure of mean stress, δ_{mid}, along the path of the wave. Stress in the smooth segment of the bolt is

$$\delta_0 = k \cdot \delta_{\text{mid}}. \tag{16}$$

Naturally, coefficient k exceeds unity. As a result of a gross approximation $k = l/(l_0 + a)$, where l is the total length of bolt, l_0 – length of the smooth part with uniform stress, and a – constant dependent on construction parameters of the bolt, such as height off bolt-cap, length of threaded part, parameters of the thread, etc.

The value of coefficient k, dependent on the shape of the bolt and design of bolted joint, can be determined from experiment, as well as from calculations [2]. If we have previously measured the value of travel time, t_0, before screwing the bolt tight, then stress in the bolt can be calculated from expression (15). When the value t_0 remains unknown, then stress in a bolt can be determined on the basis of measurements of times of flight along the length of the bolt of longitudinal as well as transverse waves. The idea of the measurement is based on the effect that longitudinal waves are many times more sensitive to stress than transverse waves.

The increment of travel time of transverse waves due to stress in the bolt is caused mainly by the increase of the path of waves resulting from tension of the bolt.

Times of flight along the length of the screw of longitudinal waves, t_δ^L, and transverse waves, t_δ^T, are expressed by sums of travel times before screwing tight, t_0^L and t_0^T, and time increments due to compression, Δt_δ^L and Δt_δ^T:

$$t_\sigma^L = t_0^L + \Delta t_0^L = t_0^L\left[1+\left(\frac{1}{E}+\beta^L\right)\frac{\sigma_0}{k}\right] \tag{17}$$

$$t_\sigma^T = t_0^T + \Delta t_\sigma^T = t_0^T\left[1+\left(\frac{1}{E}+\beta^T\right)\frac{\sigma_0}{k}\right] \tag{18}$$

The δ_0 value can be derived from (17) and (18):

$$\sigma_0 = \frac{m-p}{\left(\frac{1}{E}+\beta^L\right)p-\left(\frac{1}{E}+\beta^T\right)m}k \tag{19}$$

where: $m = t_0^T/t_0^L$, $p = t_\delta^T/t_\delta^T$.

4.2. *Measurements of longitudinal stresses in railway rails*

Plastic deformations in the process of final straightening of rails are the main source of longitudinal residual stresses in railway rails. A typical distribution of residual stresses in the cross section of a rail after straightening is shown in Fig. 7. Too high tensile stress in the rail head and base promote cracking of rails along the web, while tensile stresses in the rail base sum up with exploitation stresses increasing the danger of fatigue cracking. Previously destructive methods were applied in assessments of the level of residual stresses in rails. These methods are expensive and

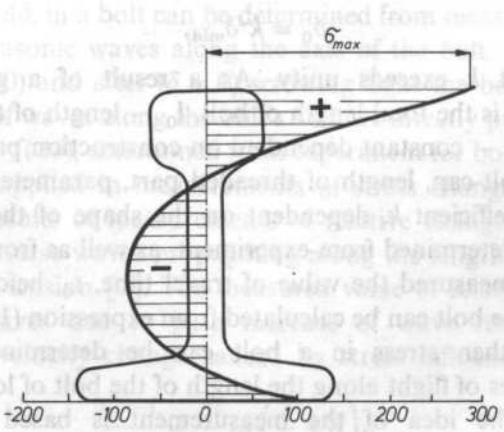

FIG. 7. Typical distribution of average longitudinal residual stresses in a cross-section of a straightened rail

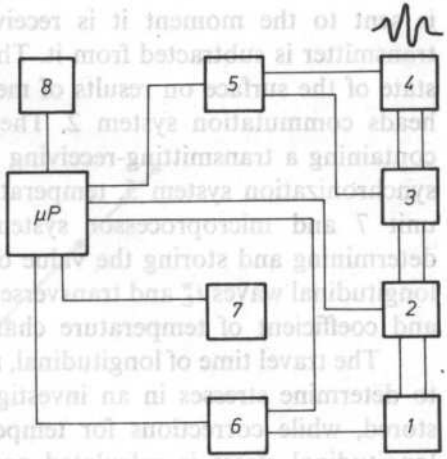

FIG. 8. Block diagram of an ultrasonic meter of residual stresses. 1 – set of ultrasonic probeheads and temperature-sensitive elements, 2 – commutation system for probeheads, 3 – transmitting-receiving system, 4 – visualization system, 5 – synchronization system, 6 – system for temperature compensation, 7 – unit for time measurements, 8 – external programmer, μP – counting system

can not be applied to the whole production. An ultrasonic meter measuring longitudinal residual stresses was constructed. It utilizes measurements of travel time of longitudinal, t_L, and transverse waves, t_T, over a constant path in the material of the rail [3]. Fig. 8 presents the block diagram of the electronic part of the meter and Fig. 9 presents the diagram of a set of ultrasonic probeheads collaborating with the meter.

The transmitting transducer N_L generated pulses of longitudinal waves, which generate in the tested material subsurface longitudinal waves (when the angle of incidence is equal to the first critical angle) or transverse waves (when the angle of incidence is equal to the second critical angle) when they are refracted passing through a plastic wedge. The transition of ultrasonic pulses is registered in turn by separate pairs of receiving transducers for longitudinal waves (O_1^L and O_2^L) and transverse waves (O_1^T and O_2^T). Measurements of travel time on the path between receiving transducers are done with the differential method, i. e., travel time is measured from the moment when the pulse is sent to the moment it is received by the further receiver and then the travel time measured from the moment when the pulse

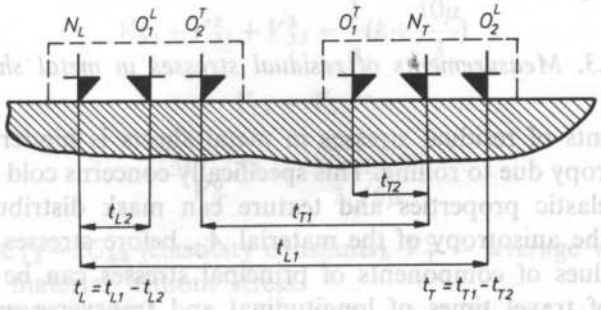

FIG. 9. Arrangement of transducers in a ultrasonic probehead of the stress meter

is sent to the moment it is received by the receiving transducer closer to the transmitter is subtracted from it. This method greatly decreases the influence of the state of the surface on results of measurements. Heads are switched in turn by the heads commutation system 2. They are connected with an electronic apparatus containing a transmitting-receiving system 3, display system of ultrasonic pulses 4, synchronization system 5, temperature compensating system 6, time measurement unit 7 and microprocessor system. Calibration of the instrument consists in determining and storing the value of the acoustoelastic constant β_L, travel times of longitudinal waves t_L^w and transverse waves t_T^w in the standard material without stress and coefficient of temperature changes of wave velocity.

The travel time of longitudinal, t_L, and transverse waves, t_T, is measured in order to determine stresses in an investigated rail. Measured values of travel times are stored, while corrections for temperature are taken automatically. The value of longitudinal stress is calculated according to algorithm (20)

$$\sigma = \frac{1}{\beta_L t_L}[t_L^w + \Delta t_L^s - t_L], \tag{20}$$

where Δt_L^s is the structural correction. This structural correction, calculated for assumed constant bulk modulus, has the following value:

$$\Delta t_L^s = \frac{4}{3}(l_T/l_L)^2 (t_L/t_T)^3 \cdot \Delta t_T \tag{21}$$

where: l_T and l_L are paths of transverse and longitudinal ultrasonic waves, Δt_T is the difference between travel times of transverse waves on the same path in the standard material and in the material of the rail under test.

Fig. 10 presents the dependence of travel time of longitudinal waves between receiving transducers O_1 and O_2, on stress for 90PA steel. This dependence is used in the process of calibration of the stress meter. The value of the acoustoelastic constant is equal $\beta_L = -1.12 \times 10^{-5}$ MPa^{-1} for this material. The correlation coefficient is equal 0.9995. The measurement of stress in one point takes about 1 minute. This allowed full control of the level of residual stresses in rails produced by the Katowice Steel Mill.

4.3. Measurements of residual stresses in metal sheets

Measurements of residual stresses in metal sheets is hindered mainly by the materials anisotropy due to rolling. This specifically concerns cold rolled steel sheets. Differences in elastic properties and texture can mask distributions of residual stresses. When the anisotropy of the material A_0, before stresses are introduced is known, then values of components of principal stresses can be determined from measurements of travel times of longitudinal and transverse waves through the thickness of the sheet. Rolled metal sheets display orthorombic symmetry. The velocity of ultrasonic waves propagating in the direction of anisotropy is expressed

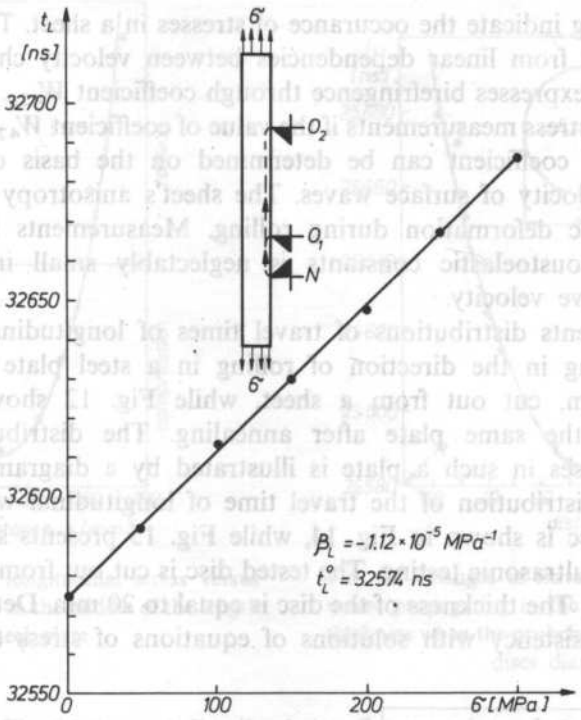

FIG. 10. Acoustoelastic characteristic of 90PA steel for longitudinal waves propagating in the direction of stress

by elasticity constants of the monocrystal and coefficients w_{400}, w_{420} and w_{440}, which determine the distribution of crystallographic orientations grain with respect to selected directions in the sample [4]. Coefficients w_{klm} are coefficients in an expansion into Legendre's multinomials of the function of distribution of orientations of crystal grains. It 1 is the direction of rolling, 2 – direction perpendicular to the direction of rolling, and 3 – direction of thickness, then the following relations occur between velocities of various wave modes in a sheet without stress:

$$V_{33}^2 + V_{31}^2 + V_{32}^3 = \frac{1}{\varrho}\left(k + \frac{10\mu}{3}\right) \tag{22}$$

$$V_{12} = V_{21} \tag{23}$$

$$\frac{V_{31} - V_{32}}{V_T^0} = \frac{16\pi^2 C w_{420}}{7\sqrt{5}\mu} \tag{24}$$

where $C = C_{11} - C_{12} - 2C_{44}$ (elasticity constants), V_T^0 – average velocity of transverse waves in a material without stress.

Expressions (22) and (23) are invariants of texture. Disturbances of the sum of squares (22) or velocity differences between transverse waves polarized parallel to the surface and propagating in the direction of rolling, and perpendicular to the

direction of rolling indicate the occurance of stresses in a sheet. The value of stress can be calculated from linear dependencies between velocity changes and stress. Relationship (24) expresses birefringence through coefficient W_{420}. This relationship can be applied in stress measurements if the value of coefficient W_{420} is known. Then, the value of this coefficient can be determined on the basis of the directional dependence of velocity of surface waves. The sheet's anisotropy changes with an increase of plastic deformation during rolling. Measurements indicate that the anisotropy of acoustoelastic constants is neglectably small in comparison to anisotropy of wave velocity.

Fig. 11 presents distributions of travel times of longitudinal and transverse waves propagating in the direction of rolling in a steel plate with dimensions $40 \times 100 \times 400$ mm, cut out from a sheet, while Fig. 12 shows corresponding distributions in the same plate after annealing. The distribution of residual longitudinal stresses in such a plate is illustrated by a diagram in Fig. 13.

The radial distribution of the travel time of longitudinal waves through the thickness of a disc is shown in Fig. 14, while Fig. 15 presents stress components determined from ultrasonic testing. The tested disc is cut out from a rolled rod with diameter 138 mm. The thickness of the disc is equal to 20 mm. Determined relations exhibit good consistency with solutions of equations of stress equilibrium.

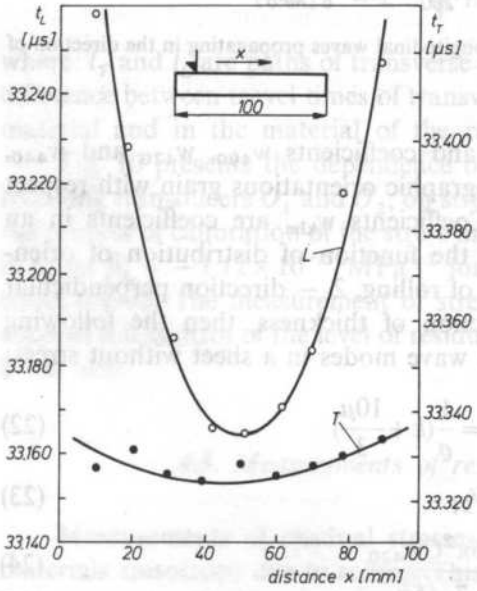

FIG. 11. Changes of travel time of subsurface longitudinal L and transverse T waves when a head is shifted on the plates surface perpendicular to the direction of rolling

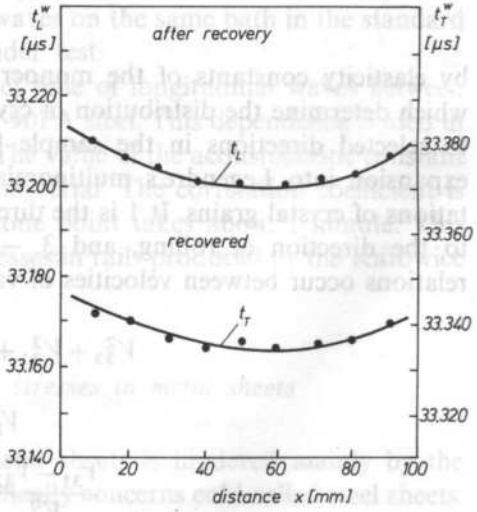

FIG. 12. Changes of travel time of longitudinal L and transverse T waves over a constant path in the direction of rolling in terms of distance from the edge after stress relieving of the plate. Data for the plate before stress relief are presented in Fig. 11

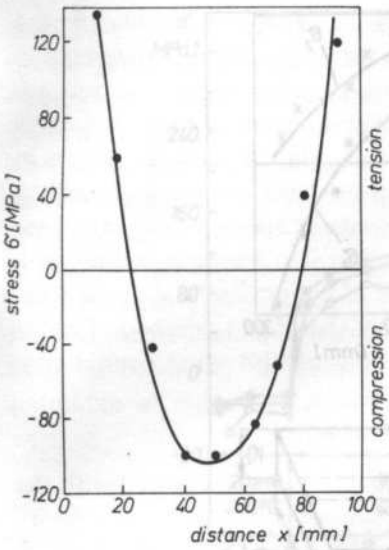

FIG. 13. Changes of longitudinal stress versus distance from the edge in the middle of the length of steel plate

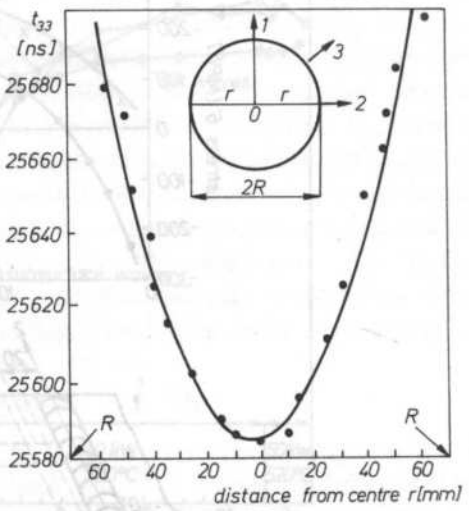

FIG. 14. Changes of travel time of longitudinal waves propagating in the direction of the discs thickness when the probehead is shifted along the discs diameter

Diagrams in Fig. 16 present distributions of stresses introduced into a steel plate due to welding, determined with ultrasonic technique [5]. Ultrasonic measurements of welding stresses can be applied in quick assesments of the degree of stress relief of welded constructions.

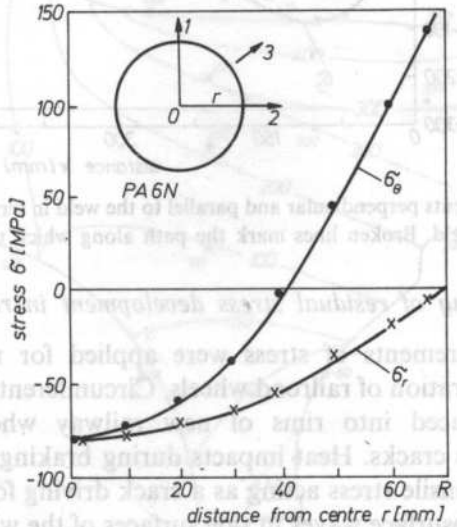

FIG. 15. Changes of radial stress δ_r and circumferential stress δ_θ versus distance from centre of the disc

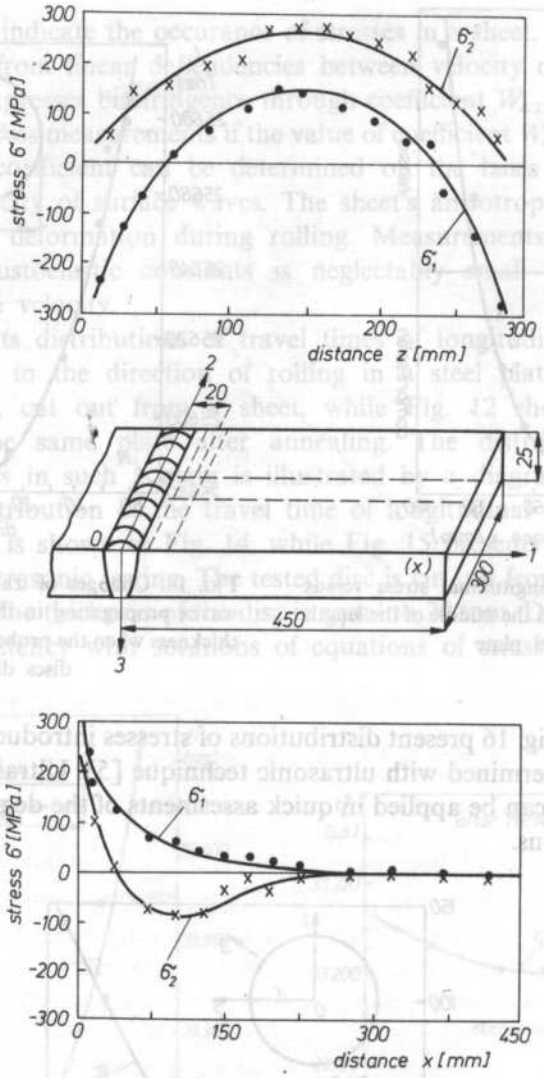

FIG. 16. Changes of components perpendicular and parallel to the weld in terms of distance along the weld and perpendicular to the weld. Broken lines mark the path along which ultrasonic heads were shifted

4.4. *Monitoring of residual stress development in railroad wheels*

Ultrasonic measurements of stress were applied for monitoring of residual stresses during the operation of railroad wheels. Circumferential compressive stresses are purposely introduced into rims of new railway wheels. They hinder the development of fatigue cracks. Heat impacts during braking can cause a change of residual stresses into tensile stress acting as a crack driving forces. At the same time, measurements with subsurface waves in side surfaces of the wheel rim and transverse waves propagating along the width of the rim make it possible to determine distributions of residual stresses in both side surfaces and radial distribution of

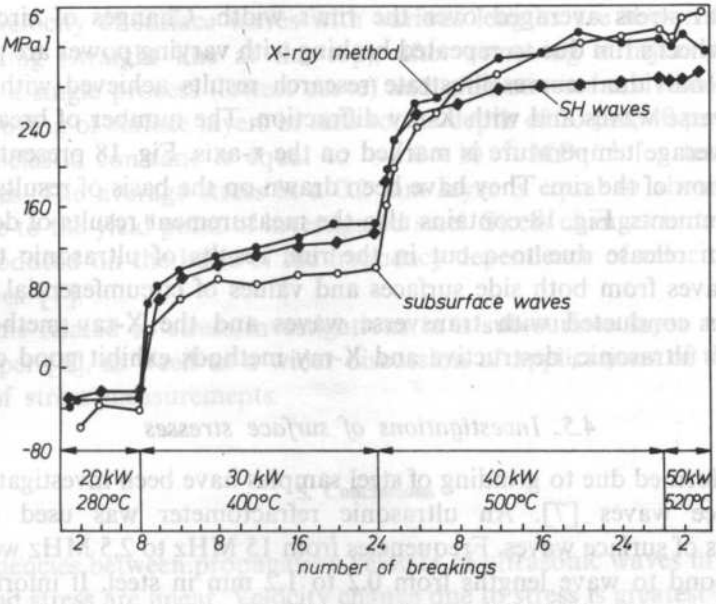

FIG. 17. Changes of circumferential stresses in the rim of a new wheel due to braking in a test banch. The number of brakings is marked on the horizontal axis and circumferential stress is marked on the vertical axis. The power of individual series of brakings and maximal temperature on the tread is noted under the curves

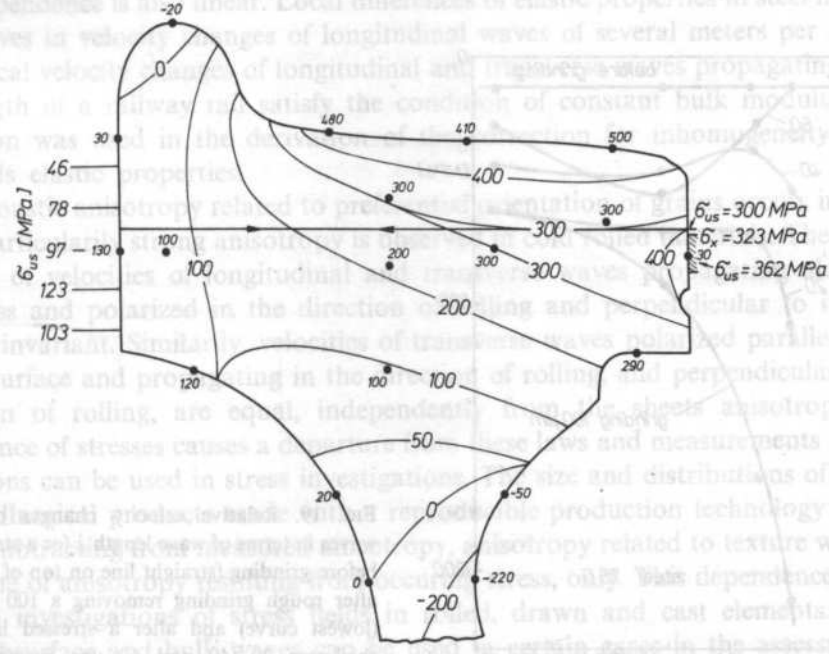

FIG. 18. Distribution of stress on the surface and in the cross-section of a wheel rim after a series of brakings. Comparision of ultrasonic, X-ray and destructive investigations

circumferential stress averaged over the rim's width. Changes of circumferential stress in the wheel's rim due to repeated braking with varying power are presented in Fig. 17 [6]. Individual curves illustrate research results achieved with subsurface waves, transverse waves and with X-ray diffraction. The number of breakings, their power and average temperature is marked on the x-axis. Fig. 18 presents isobars in the cross-section of the rim. They have been drawn on the basis of results of residual stress measurements. Fig. 18 contains also the measurement results of deformations resulting from release due to a cut in the rim, results of ultrasonic testing with subsurface waves from both side surfaces and values of circumferential stress from measurements conducted with transverse waves and the X-ray method. Results achieved with ultrasonic, destructive and X-ray methods exhibit good consistency.

4.5. Investigations of surface stresses

Stresses formed due to grinding of steel samples have been investigated with the aid of surface waves [7]. An ultrasonic refractometer was used in velocity measurements of surface waves. Frequencies from 15 MHz to 2,5 MHz were applied. They correspond to wave lengths from 0.2 to 1.2 mm in steel. If informations on properties of the material collected with the aid of surface waves concern a layer corresponding to one wave length, then in this case collected information concerning stresses was averaged from subsurface layers with thickness from 0.2 mm to 1.2 mm. Residual stresses were introduced into samples in the course of rough grinding without cooling. A layer with thickness 100 μm was removed. In Fig. 19 relative

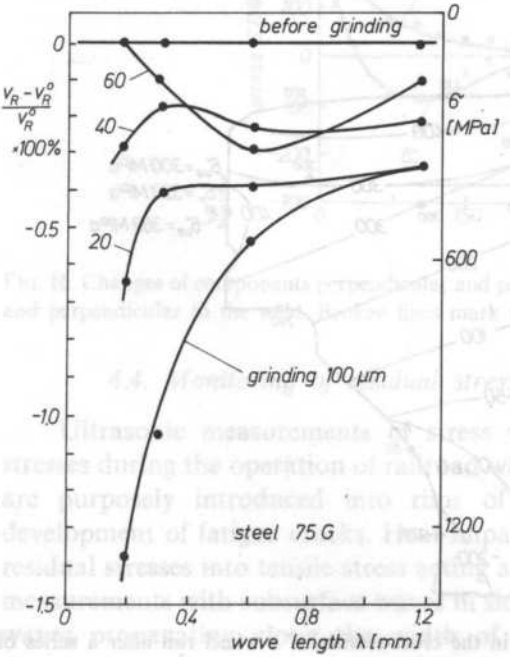

FIG. 19. Relative velocity changes of surface waves in terms of wave length λ for a steel sample before grinding (straight line on top of diagram), after rough grinding removing a 100 μm layer (lowest curve) and after a stressed layer with thickness 20, 40 and 60 μm, respectively, is removed

changes of velocity of surface waves with various lengths are shown for a sample before grinding (straight line at the top), after removing a layer with 100 μm thickness in a single process (lowest curve) and after stresses are removed through delicate removing of surface layers in turn to the depth of 20 μm, 40 μm and 60 μm. The acoustoelastic constant is equal to -1.0×10^{-5} MPa^{-1} for tested steel for surface waves. The average stress in a 0.2 mm layer is equal to about 1400 MPa, what is close to the yield point of investigated steel. Stress changes in terms of depth can be reproduced on the basis of the frequency dependence of velocity changes of surface waves [7].

Problems related to stress investigations in a sub-surface layer are studied in detail in paper [8], as weell as a wider discussion of applications of the ultrasonic technique of stress measurements.

5. Conclusions

Dependencies between propagation velocity of ultrasonic waves in construction materials and stress are linear. Velocity change due to stress is greatest in the case of longitudinal waves propagating in the direction of stress. A 10 MPa increment of tensile stress in steel causes a velocity decrease of longitudinal waves of about 0.75 m/s. Compression leads to a decrease of wave velocity. A temperature increase of steel of 1°C decreases the velocity of longitudinal waves by approximately 0.9 m/s. This dependence is also linear. Local differences of elastic properties in steel manifest themselves in velocity changes of longitudinal waves of several meters per second.

Local velocity changes of longitudinal and transverse waves propagating along the length of a railway rail satisfy the condition of constant bulk modulus. This condition was used in the derivation of the correction for inhomogeneity of the materials elastic properties.

Acoustic anisotropy related to preferential orientation of grains occurs in rolled steel. Particularily strong anisotropy is observed in cold rolled materials. The sum of squares of velocities of longitudinal and transverse waves propagating along the thickness and polarized in the direction of rolling and perpendicular to it is the texture invariant. Similarily, velocities of transverse waves polarized parallel to the sheets surface and propagating in the direction of rolling, and perpendicular to the direction of rolling, are equal, independently from the sheets anisotropy. The occurrence of stresses causes a departure from these laws and measurements of these deviations can be used in stress investigations. The size and distributions of texture in metallurgical products made with a reproducible production technology are the same. Subtracting from measured anisotropy, anisotropy related to texture we reach the value of anisotropy resulting from occuring stress, only. This dependence can be used in investigations of stress fields in rolled, drawn and cast elements.

Subsurface and bulk waves can be used in certain cases in the assessment of stress distributions in the volume of tested element. The application of surface waves

with various frequencies makes it possible to investigate stress gradients in the direction perpendicular to the surface.

Comparative X-ray and destructive testing confirms the correctness of results of ultrasonic measurements of residual stresses.

References

[1] A. HUGHES, G. S. KELLY, *Second-order elastic deformation of solids*, Phys. Rev., **92**, 1145 (1953).

[2] J. DEPUTAT, *Ultrasonic technique for measuring stress in screws*, Proc. 9 World Conference on Nondestructive Testing, Paper 4EDD–2, P235656, Melbourne 1979.

[3] J. DEPUTAT, A. BROKOWSKI, *Ultrasonic measurements of residual stress in rails*, Proc. 11 World Conference on Nondestructive Testing, vol. 1, 592, Taylor Publ. Co., Las Vegas 1985, Dallas 1985.

[4] C. M. SAYERS, *Texture independent determination of residual stress in policrystalline aggregates using Rayleigh waves*, J. Phys. D., Phys. **17**, Li79 (1984)

[5] J. DEPUTAT, *Ultrasonic measurements of welding stresses* (in Polish), Przegląd Spawalnictwa, **15**, 7, 8, 10, (1984).

[6] J. DEPUTAT, A. KWASZCZYŃSKA-KLIMEK, J. SZELĄŻEK, *Monitoring of residual stress in railroad wheels with ultrasound*, Proc. 12 World Conference on Nondestructive Testing, vol. 2, p. 974, Amsterdam 1989.

[7] A. BROKOWSKI, J. DEPUTAT, *Non-destructive testing of grinding stresses* (in Polish), Trybologia, **27** 5/6 (1983).

[8] J. DEPUTAT, *Properties and application of the elastoacoustic effect in residual stress measurements* (in Polish), IFTR–PAS Reports, 28 (1987).

Received on Mai 22, 1989

ARCHIVES OF ACOUSTICS
15, 1–2, 93–105 (1990)

RESOLUTION IMPROVEMENT FILTER FOR SONAR RETURNS[1]

A. DYKA

Technical University of Gdańsk, Institute of Telecommunications
(80–952 Gdańsk, ul. Majakowskiego 11/12)

The concern of this paper is the Single Pulse Resolution Filter – SPRF, which is capable of resolving near-rectangular overlapping pulses. The reason for assuming such pulses is that despite the attractive properties of matched filter pulse compression most operational sonar systems continue to use a finite-length rectangular pulse of constant frequency. The task of the SPRF in such system is to improve the short-range resolution and the target detectability in reverberation. The SPRF here discussed has been synthesized on the basis of the ideal deconvolution filter concept by using the semi-heuristic method of the transformation and the supplementing of input signal spectrum. In order to evaluate the SPRF performance three performance indices have been defined, namely the resolution improvement ratio, the degradation in the output signal-to-noise ratio compared to the maximum which is attainable in the matched filter case, and the processing gain against reverberation. The tradeoffs between the performance indices given in an analytic form have been presented and briefly discussed. The results of tests with the SPRF, both in the laboratory and in sea trials are reported. The first of them proves the resolution capability of the SPRF in the case of two, noise-contaminated overlapping returns. The sea trials were carried out during the FAO sponsored BIOMASS First International Biological EXperiment, (FIBEX 81), programme in Antarctica on board the Polish research vessel "Profesor Siedlecki". A number of echograms produced originally by the Simrad SK–120 echosounder and after having the received signal envelope filtered with the SPRF were recorded simultaneously. Two samples of such echograms recorded on the Brasilian Shelf in April 1981 which show the favourable impact of the SPRF on the picture quality are presented. Finally, the drawbacks of the SPRF are mentioned.

1. Introduction

A problem of considerable importance in many areas of science and technology is the unambiguous resolution of multiple overlapping pulses. General solutions to this problem include deconvolution, (inverse) filtering, (e.g., SENMOTO and CHILDERS,

[1] This paper was presented at International Symposium on Fisheries Acoustics, June 22–26, 1987, Seattle, Washington, USA.

[10]), matched filter pulse compression, (e.g., COOK and BERNFELD, [2], cepstrum analysis, (e.g., OPPENHEIM and SCHAFER [8]), mismatched filtering, (e.g., EVANS and FORTMANN [6]), and the "moments" algorithms, (BAUM 1975; SANDHU and AUDEH [1, 9]). A particular case occurs in sonar and radar where the shape of the transmitted pulse is known. Then, the matched filter pulse compression is superior to any linear method. However, as the pulse compression signals are wideband ones their direct application to a conventional sonar system is difficult, due to the narrow bandwidth of transmitting transducers and the frequency dependent attenuation of ultrasonic waves in sea. For that reason the practically obtainable ratio of signal compression is not expected to exceed 100. This fact and the increased cost and complexity of pulse compression systems as compared to conventional options means that most commercially available sonar systems continue to use a finite-length rectangular pulse of constant frequency. On the other hand, the use of long pulses in such systems, necessary to obtain the desired long-range target detection contributes to poor resolution in range and poor detectability of targets in reverberation. One may partly resolve these conflicting demands by using long pulses, so that detection in range is not compromised and by applying special receiver filtering techniques, which partly recover the short-range resolution and the detectability of targets in reverberation.

The concern of this paper is the Single Pulse Resolution Filter, which from now on will be referred to as the SPRF, intended for use in conventional sonar systems employing a finite-length rectangular pulse. The task of this filter is to improve the short-range resolution and the detectability of targets in reverberation.

2. Formulation and solution to the filtering problem

Prior to the formulation of the filtering problem the input signal is to be defined. A reasonable model of a single return is a near-rectangular, trapezoidal pulse, which can be modelled as the output signal of a low-pass filter, excited by a rectangular pulse. This low-pass filter represents the overall bandwidth of a sonar system and its cut-off frequency is basically limited by the bandwidth of the transmitting transducer. The usual design criterion of maximizing the system output signal-to-noise ratio means, that in practice the matched receiver is mainly responsible for the most severe bandwidth limitation, and converts the envelope of a single return into a near-triangular pulse. However, as from the practical standpoint one can easily manipulate the receiver bandwidth, while in the case of the transmitting transducer one can not do so, it is reasonable to assume that the real, physical limitation of the overall bandwidth is almost entirely due to the transmitting transducer.

Despite the above considerations it is assumed here that the envelope of a single return is a rectangular pulse of the length T. Not only does such an assumption simplify dramatically the design procedure but as is shown later, the results achieved also apply to the more realistic models of the return envelopes considered above.

Basically, an improvement in range resolution can be achieved by filtering which "compresses" the return of the length T into another, possibly the shortest pulse. The ratio of the pulse-lengths prior to the compression and after the compression, respectively is usually referred to as the compression ratio. Taking into account the above assumption about the input signal the best possible filter of this kind should be capable of transforming the rectangular pulse of the length T into a Dirac's delta distribution, (see Fig. 1). Actually, this is a definition of an ideal deconvolution filter. Having formulated the filtering problem in this way we find that the deconvolution filter shown in Fig. 1 is a non-causal and nonlinear one. Unfortunately, the coherent body of knowledge concerning the linear processing of signals has no counterpart in the treatment of nonlinear signal processes. Therefore, any feasible solution of a nonlinear problem may be considered as a reasonable one, although it is usually difficult to prove whether such a solution is an "optimum" one in any sense. Non-causality of the filter is only a minor problem as it can be removed by an appropriate delaying the output signal.

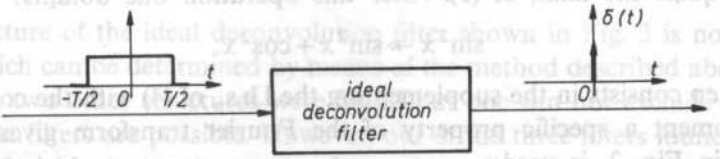

FIG. 1. Definition of the deconvolution filter for a rectangular pulse of the length T. $\delta(t)$ – denotes Dirac's delta distribution

In order to determine a feasible structure of the deconvolution filter shown in Fig. 1 the semi-heuristic method of the transformation and the supplementing of the input signal spectrum in such a way as to obtain the spectrum of the desired output signal was proposed by DYKA, [3]. The transformation and supplementing of the spectrum refer to linear and nonlinear operations, respectively, which are performed on the corresponding signals in the time domain. To illustrate the method briefly, consider the spectrum of the input rectangular pulse as the $\frac{\sin x}{x}$, $x = \omega T/2$, where: ω – is angular frequency, T – is the pulse-length, and the spectrum of the desired output pulse is 1. Then, we can symbolize the filtering procedure as;

$$\frac{\sin x}{x} \twoheadrightarrow 1, \tag{1}$$

where the double arrow denotes all operations performed upon the $\frac{\sin x}{x}$ spectrum, which transform it into 1. The crucial point is, that every operation performed upon

the spectrum in the frequency domain must correspond to its feasible counterpart in the time domain. Consequently, we can rewrite (1) as:

$$\frac{\sin x}{x} \twoheadrightarrow \sin^2 x + \cos^2 x. \tag{2}$$

The first step in transforming the spectrum on the left hand side, (l.h.s.), of (2) into the spectrum on the right hand side, (r.h.s.), consists in removing the denominator from the l.h.s., by multiplying the l.h.s., by jx, where $j = \sqrt{-1}$. In the time domain it corresponds to the operation of differentiation. Thus we get:

$$j\sin x \twoheadrightarrow \sin^2 x + \cos^2 x. \tag{3}$$

The next step is to transform the $j\sin x$ l.h.s., spectrum into the $\sin^2 x$ spectrum. This can be obtained by multiplying the l.h.s., of (3) by $-j\sin x$, which in the time domain corresponds to the filtering with a linear filter, whose impulse response equals $h(t) = \delta(t - T/2) - \delta(t + T/2)$, where $\delta(\cdot)$ denotes Dirac's delta distribution. It is worth noting that this operation is actually the filtering, matched to the signal whose spectrum equals the l.h.s., of (3). After this operation one obtains:

$$\sin^2 x \twoheadrightarrow \sin^2 x + \cos^2 x. \tag{4}$$

The final step consists in the supplementing the l.h.s., of (4) with the $\cos^2 x$ function. At this moment a specific property of the Fourier transform given by (5) and illustrated in Fig. 2, is used;

$$|F^{-1}(\sin^2 x)| = F^{-1}(\cos^2 x). \tag{5}$$

where the $|\cdot|$ bracket denotes the absolute value operation performed upon a signal in the time domain. and F^{-1} denotes the Fourier inverse transform. The three steps described by (3) to (5) enable us to sketch immediately the structure of the

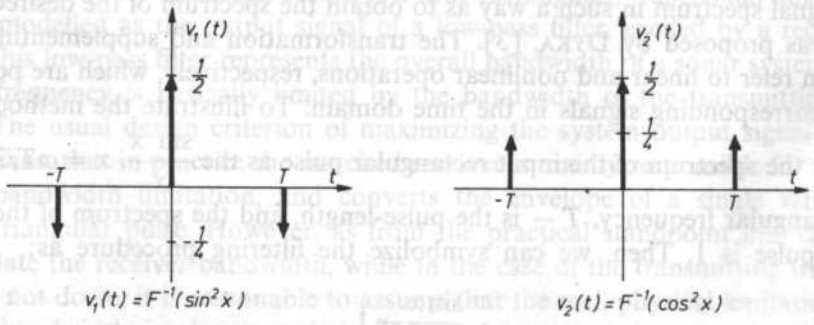

FIG. 2. Illustration of a specific property of the Fourier transform given by formula (5). $v_1(t)$ – denotes the absolute value circuit input signal in the deconvolution filter shown in Fig. 3. $v_2(t)$ – denotes the absolute value circuit output signal in the deconvolution filter shown in Fig. 3. F^{-1} – denotes the Fourier inverse transform. T – denotes the length of a sounding pulse. $x = \omega \cdot T/2$, where ω – denotes the radian frequency

deconvolution filter desired, as shown in Fig. 3. Remarkably the filter shown in Fig. 3 is not causal due to the factor $\delta(t+T/2)$ appearing in the impulse response $h(t)$. However, it can be coerced to be so by introducing the delay of $T/2$ in $h(t)$, which results only in delaying the output signal.

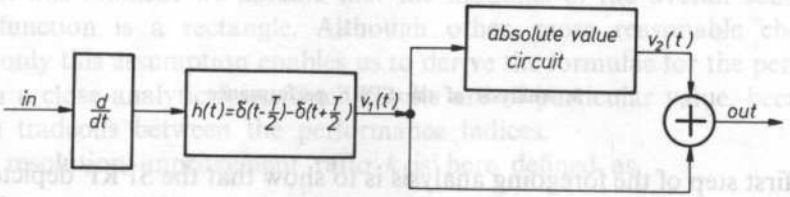

FIG. 3. Ideal deconvolution filter for a rectangular pulse of the length T. $\frac{d}{dt}$ — denotes operation of differentiation, $h(t)$ — denotes impulse response of a linear filter, $v_1(t)$ — denotes the absolute value circuit input signal, $v_2(t)$ — denotes the absolute value circuit output signal, $\delta(\cdot)$ — denotes Dirac's delta distribution, T — denotes the length of a sounding pulse

The structure of the ideal deconvolution filter shown in Fig. 3 is not the only possibility which can be determined by means of the method described above. Apart from this one, two other structures were found but one can not exclude that some other nonlinear filters are possible. However, out of the three filters found, the filter shown in Fig. 3 yields the maximum signal-to-noise ratio and therefore it was chosen for further examinations. One can show that the deconvolution filter depicted in Fig. 3 is equivalent to the filter shown in Fig. 4. The latter from now on will be referred to as the Single Pulse Resolution Filter — SPRF. As can be seen in Fig. 4 the SPRF consists of three basic elements namely the differentiator, the transversal filter, and

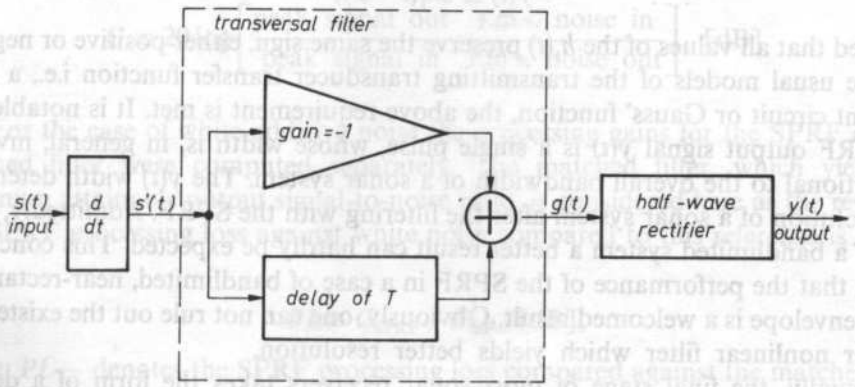

FIG. 4. SPRF circuit diagram, $s(t)$ — denotes the SPRF input signal, $s'(t)$ — denotes the differentiator output signal, $g(t)$ — denotes the transversal filter output signal, $y(t)$ — denotes the SPRF output signal, T — denotes the length of a sounding pulse

the half-wave rectifier. The first two are the linear circuits, while the third one, nonlinear, is a threshold circuit with the threshold voltage of zero volts. It should be pointed out, that the linear part of the SPRF resembles to some extent the pulse-length discriminator, (LAWSON and UHLENBECK [7]), and the High – Pass Sidelobe Reduction Filter, (EVANS and FORTMANN [6]).

3. Analysis of the SPRF performance

The first step of the foregoing analysis is to show that the SPRF depicted in Fig. 4 can be successfully applied to the near-rectangular, trapezoidal input pulses. Such pulses, as already mentioned in the preceeding section, can be assumed as more reasonable models of the sonar return envelope than a rectangular pulse. As has also been pointed out, the transmitting transducer is the main contributor to the limitation of the overall system bandwidth. Taking into account that transmitting transducers are as a rule narrowband ones, one can show that the derivative $s'(t)$ of a single return envelope $s(t)$ is given a

$$s'(t) \cong h_t(t) - h_t(t-T), \tag{6}$$

where $h_t(t)$ denotes the impulse response envelope of a transmitting transducer. Actually, the signal given by (6) is the output signal of the differentiator in the SPRF. One may easily find that the output signal $g(t)$ of the transversal filter in the SPRF equals:

$$g(t) \cong 2h_t(t-T) - h_t(t) - h_t(t-2T). \tag{7}$$

Hence, the output signal $y(t)$ of the SPRF equals;

$$y(t) \cong 2h_t(t-T), \tag{8}$$

provided that all values of the $h_t(t)$ preserve the same sign, either positive or negative. For the usual models of the transmitting transducer transfer function i.e., a single resonant circuit or Gauss' function, the above requirement is met. It is notable, that the SPRF output signal $y(t)$ is a single pulse, whose width is, in general, inversely proportional to the overall bandwidth of a sonar system. The $y(t)$ width determines the resolution of a sonar system after the filtering with the SPRF. Admittedly, in the case of a bandlimited system a better result can hardly be expected. This conclusion means, that the performance of the SPRF in a case of bandlimited, near-rectangular return envelope is a welcomed result. Obviously, one can not rule out the existence of another nonlinear filter which yields better resolution.

Usually, the final stage of most sonar receivers takes the form of a decisive threshold circuit, which basically is a switch that switches "on" when the signal amplitude exceeds a certain pre-fixed value. Therefore, if the SPRF is followed by such a threshold circuit, which actually doubles the task of the SPRF half-wave

rectifier, then the latter can be omitted. Consequently, the SPRF reduces to the linear circuit consisting of the differentiator and the transversal filter only. This conclusion enables us to estimate the SPRF performance indices namely the resolution improvement ratio, the processing loss against white noise compared to the matched filter case, and the processing gain against reverberation, using the linear filtering theory. At this moment we assume that the modulus of the overall sonar system transfer function is a rectangle. Although other, more reasonable choices are possible, only this assumption enables us to derive the formulae for the performance indices in a close analytic form. Such results are of particular value, because they show the tradeoffs between the performance indices.

The resolution improvement ratio k is here defined as,

$$k \equiv \frac{T}{t_0}, \tag{9}$$

where: T – is the pulse-length of the sounding pulse, t_0 – is the pulse-length of the SPRF response to the envelope of a single return.

Notably, k can be also interpreted as the compression ratio defined in Section 2. The assumption about the rectangular shape of the overall system transfer function implies that the response of the SPRF to the input rectangular envelope is the $\frac{\sin x}{x}$ type of function. Having defined t_0 as the width of the "mainlobe" in the SPRF response, we get the following;

$$k = \frac{1}{2} WT, \tag{10}$$

where W denotes the overall bandwidth of a sonar system.

The processing gains were computed using the following definition:

$$G \equiv 20 \log \left[\frac{\text{peak signal out}}{\text{peak signal in}} \cdot \frac{\text{r.m.s. noise in}}{\text{r.m.s. noise out}} \right], \text{ [dB]} \tag{11}$$

For the case of white additive noise the processing gains for the SPRF and the matched filter were computed separately. The matched filter, which yields the maximum attainable output signal-to-noise ratio, is considered here as the reference. The SPRF processing loss against white noise compared to this reference is defined as:

$$PL \equiv G_{\text{SPRF}} - G_{\text{MF}}, \text{ [dB]}, \tag{12}$$

where: PL – denotes the SPRF processing loss compared against the matched filter, G_{SPRF} – denotes the processing gain of the SPRF, G_{MF} – denotes the processing gain of the matched filter.

Routine transformations yield a rather complicated analytic formula for the PL

versus k. However, for $k > 3$ this formula can be well approximated by the asymptotic value it converges to, given as, (DYKA, [3]):

$$PL \cong -10 \log k - 2.2, \text{ [dB]}, \tag{13}$$

In order to estimate the processing gain against reverberation it was assumed that the process of reverberation can be modelled as the convolution of a transmitted sounding pulse with a series of Poisson impulses of random amplitudes. This assumption enables us to derive the formula for the power spectrum of the reverberation squared envelope, and consequently, the processing gain against reverberation G_r as, (DYKA [3]):

$$G_r \cong 10 \log k - 2.1, \text{ [dB]}. \tag{14}$$

This result is basically consistent with conclusions that can be drawn from the phenomenological model of reverberation, (URICK, [11]). According to this model the reverberation level is inversely proportional to the return pulse-length. Therefore, if the SPRF "compresses" the return pulse-length k times then, at the same time it reduces the reverberation level by the same factor. Formulae (10), (13), and (14) show the tradeoffs between the SPRF performance indices. For a given pulse-length T the improvement in resolution expressed by k, (10), and the improvement in target detectability in reverberation, expressed by G_r, (14), do increase with increasing overall bandwidth of a sonar system. At the same time the output signal-to-noise ratio compared to the matched filter case, (expressed by PL, (13)), decreases by the same factor. So, the degradation of the output signal-to-noise ratio can be considered as the price which is to be paid for the "profits" expressed by an improvement in both resolution and target detectability in reverberation.

4. Experiments

With reference to Fig. 4 an analoque model of the SPRF has been constructed. As a delay line the Mullard TDA 1022, CCD integrated circuit has been used. Other elements are standard integrated circuits. First, the SPRF was tested in a laboratory using a return simulator delivering two 1 ms, low-pass filtered, ($f_c = 10$ kHz), rectangular, overlapping pulses. The CRT records in Fig. 5a and 5b show he following: the SPRF input signal (i) and the SPRF output signal (ii), noise free and contaminated by noise, respectively. Remarkably, the input signal, consists of two closely overlapping pulses, which at the presence of noise could not be resolved. In the output signal however, one may distinguish two dominating peaks, which indicate the appearance of two pulses in the input signal.

The sea trials were carried out during the FAO sponsored BIOMASS First International Biological Experiment, (FIBEX 81), programme in Antarctica on board the Polish research vessel "Profesor Siedlecki" in 1981. The parameters and

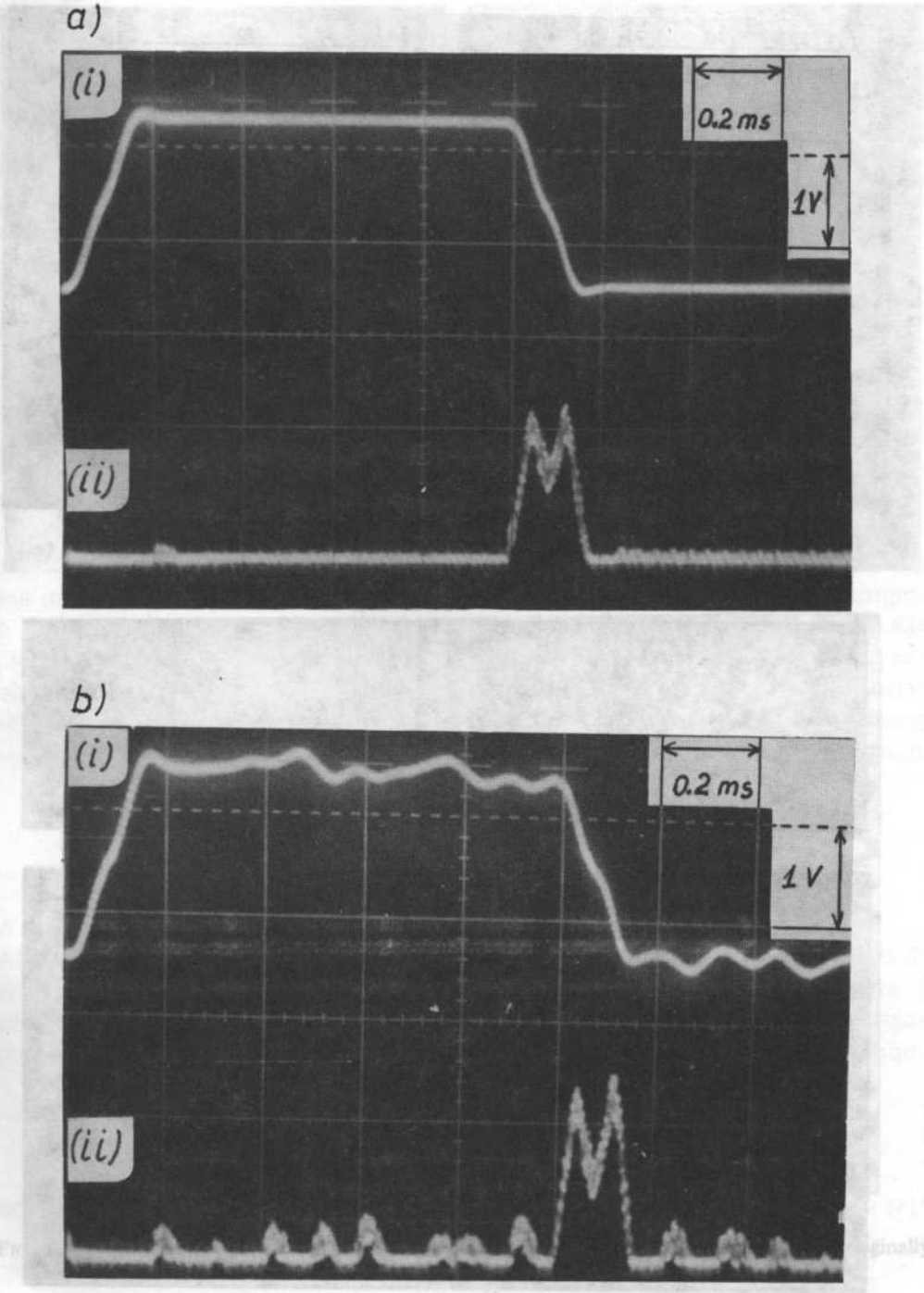

FIG. 5. CRT record of the SPRF input signal, (*i*) and the output signal, (*ii*), a – input signal free of noise, b – input signal contaminated by noise

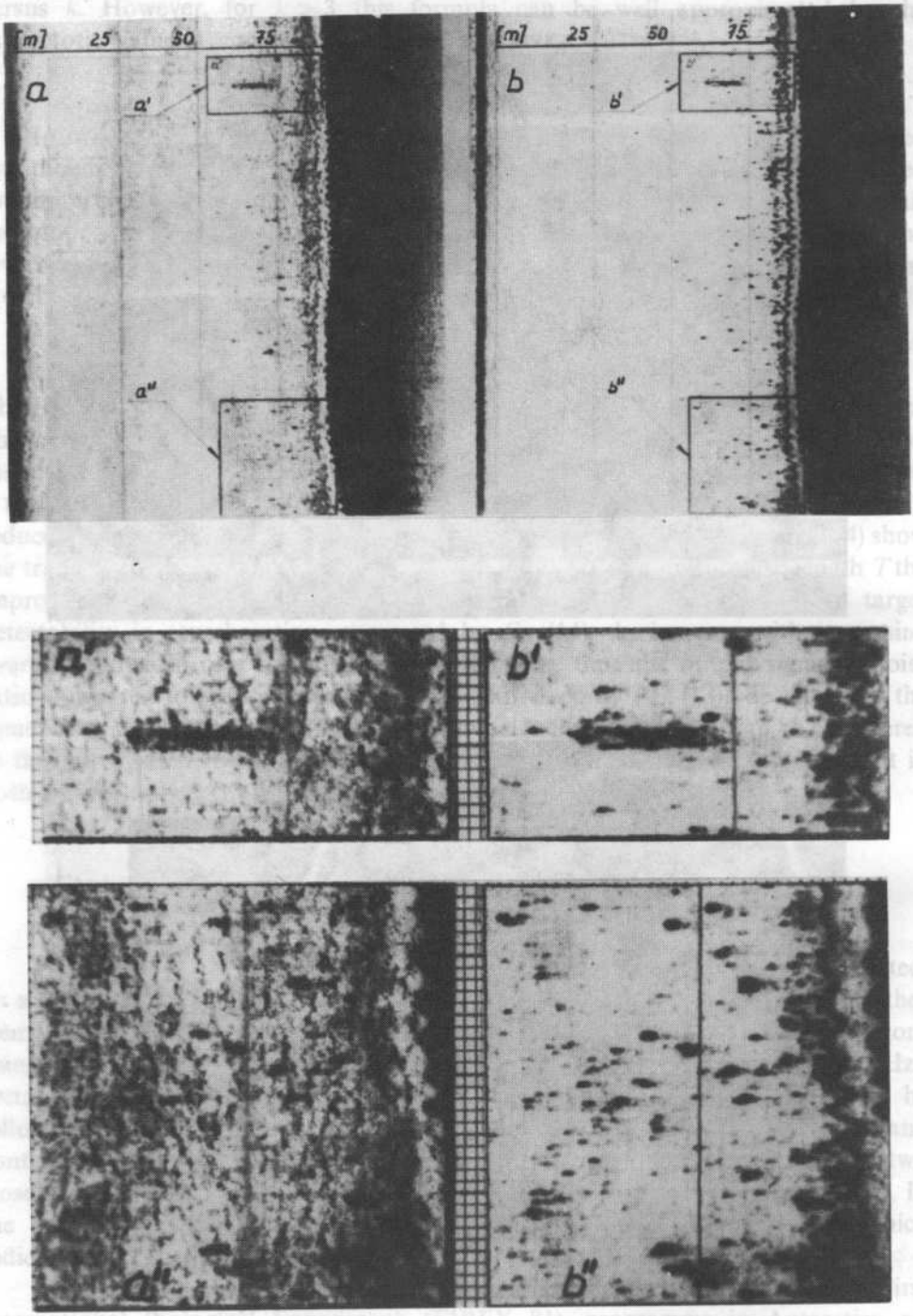

FIG. 6. Echogram of a medium density multiple traget environment Brasilian Shelf. a, a′, a″ — originally recorded by the echosounder; b, b′, b″ — recorded with the use of the SPRF

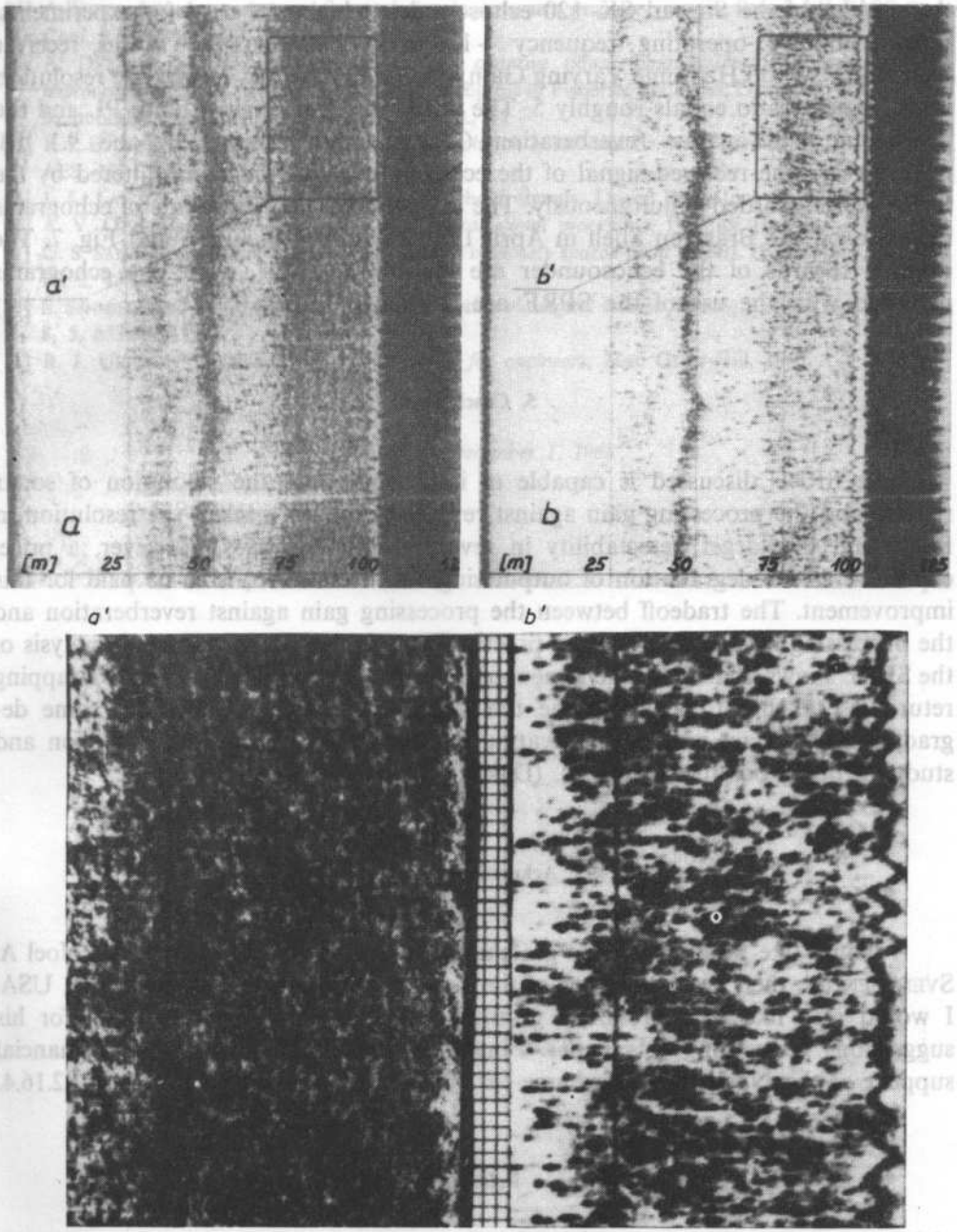

FIG. 7. Echogram of a high density multiple target environment, Brasilian Shelf. *a*, *a'* – originally recorded by the echosounder; *b*, *b'* – recorded with the use of the SPRF

the settings of the Simrad SK–120 echosounder, which was used for experiments, were as follows: operating frequency −120 KHz, pulse-length − 1 ms, receiver bandwidth − 10 kHz, Time Varying Gain, TVG), − 20 log R. Hence, the resolution improvement ratio equals roughly 5. The processing loss against noise PL and the processing gain against reverberation G_r are roughly −9.2 dB and 9.1 dB. respectively. The received signal of the echosounder and the signal filtered by the SPRF were recorded simultaneously. The samples showing fragments of echograms recorded on the Brasilian Shelf in April 1981 are shown in Fig. 6 and Fig. 7. The original records of the echosounder are marked a, a′, a″, while the echograms recorded with the use of the SPRF are marked b, b′, b″.

5. Conclusions

The SPRF discussed is capable of improving both the resolution of sonar returns and the processing gain against reverberation. As a result the resolution in range and the target detectability in reverberation improves. However, a price, expressed as the degradation of output singal-to-noise ratio, is to be paid for this improvement. The tradeoff between the processing gain against reverberation and the processing loss against noise is practically equivalent. More detailed analysis of the SPRF shows, that if the phenomenon of mutual interference between overlapping returns is taken into account, the the SPRF performance undergoes some degradation. This fact was the motivation for developing an improved version and studying other possible solutions. (Dyka [4], [5]).

Acknowledgements

I would like to acknowledge gratefully the practical support given by Noel A. SVENDSEN the then Vice President of the Laitram Corporation, Boston, MA, USA. I would also like to express my gratitude to Prof. Zenon JAGODZINSKI for his suggestions concerning this paper. Finally, I would like to notify the financial support of the National Programme for Fundamental Research C.P.B.P. 02.16.4.

References

[1] R. F. BAUM, *A novel algorithm for resolution of point targets*, IEEE Trans. on AES, **11**, 6, 1260–1268 1975.

[2] C. E. COOK and M. BERNFELD, *Radar signals – an introduction to theory and application*, Academic Press, New York-London 1967.

[3] A. DYKA, *A model of filtering for resolution improvement in sonar systems*, Ph. D., thesis (in Polish) 1984.

[4] A. DYKA, *Filtering techniques for resolution improvement in sonar systems*, Proc. of II FASE Spec. Conf. 221–227 Madrid 1987.

[5] A. DYKA, *Laboratory experiments with an adaptive thresholding system for range resolution improvement in sonar*, accepted for the Conf. Progress in Fisheries Acoustics, Lowestoft, UK, 1988, to be published in Proc. of the Inst. of Acoust., **11**

[6] R. J. EVANS and T. E. FORTMANN, *Optimal resolution of rectangular pulses in noise*, IEEE Trans., on AES, **11,** 3,372–379 (1975).

[7] J. L. LAWSON and G. E. UHLENBECK, Threshold signals, Dover Publ. Inc., New York 1965.

[8] A. V. OPPENHEIM and R. W. SCHAFER, *Digital signal processing*, Prentice Hall Inc., 1975.

[9] G. S. SANDHU and N. F. AUDEH, *Measurement of closely spaced point targets.* IEEE Trans., on AES, **16,** 2, 138–143 1980.

[10] S. SENMOTO and D. G. CHILDERS, *Signal resolution via digital inverse filtering*, IEEE Trans., on AES, **8,** 5, 633–640 1972.

[11] R. J. URICK, *Principles of underwater sound for engineers*, Mac Graw-Hill, 1967.

Received on December 1, 1988

ARCHIVES OF ACOUSTICS
15, 1–2, 107–119 (1990)

EVALUATION OF CALCIFICATION DETECTABILITY IN FEMALE BREASTS BY ULTRASOUND*

L. FILIPCZYŃSKI, T. KUJAWSKA, G. ŁYPACEWICZ

Ultrasonic Department, Institute of Fundamental Technological Research, Polish Academy of Sciences (00–049 Warsaw, Świętokrzyska 21)

The authors investigated detectability of calcifications by means of shadow and echo methods for 5 MHz frequency. Computing the ultrasonic field distribution around a rigid sphere they determined the shadow range and hence the detectability condition for calcification diameter $\phi \geqslant 3$ mm. For the echo method former investigations were continued improving the measurement technique and expanding the analysis. To determine the tissue signal background level measurements were performed on 82 breasts of healthy premenopause women. The boundaries of various tissues and inhomogeneities within cause interfering background and its level limits the detectability. The measurement results, confirmed statistically, were used for detectability determination in normal bresst tissues (attenuation 1.1 dB/cm·MHz). The calculations show that the minimum diameter of a detectable calcification $\phi = 0.4$ mm for a normal breast. JACKSON et al. [18] and KASUMI [19,20] have demonstrated calcifications 0.1–0.5 mm in dia with frequencies of 4 and 7.5 MHz. These results are in general agreement with our theory if one takes into account the high (SD = 8 dB) scattering of the signal background measurement results. When detecting calcifications in the tumor anechoic area one obtains stressing of fine calcification echoes, thus increasing the detectability when comparing with the case of healthy breast tissues.

Autorzy przeprowadzili badania wykrywalności zwapnień za pomocą metody ultradźwiękowej cienia i echa przy częstotliwości 5 MHz. Na podstawie rozkładu pola ultradźwiękowego wokół sztywnej kuli wyznaczyli długość cienia, a na tej podstawie warunek wykrywalności dla zwapnień o średnicy $\phi = 3$ mm. W przypadku metody echa, kontynuując poprzednie badania, autorzy ulepszyli technikę pomiarową i rozszerzyli analizę. W celu wyznaczenia tła poziomu zakłóceń tkankowych przeprowadzili pomiary na 82 piersiach zdrowych kobiet przed menopauzą. Granice różnych rodzajów tkanek piersi oraz ich wewnętrzne niejednorodności tworzą zakłócające tło, którego poziom ogranicza wykrywalność zwapnień. Wyniki pomiarów, potwierdzone statystycznie, wykorzystano do wyznaczania wykrywalności w normalnych piersiach (współczynnik tłumienia 1.1 dB/cm·MHz). Obliczenia wykazały, że minimalna średnica wykrywalnego metodą echa

* The main thesis of the paper were presented during the VI-th International Congress on the Ultrasonic Examination of the Breast. Paris, 29—30 June 1989 [10].

zwapnienia wynosi $\phi = 0.4$ mm. W przypadku piersi normalnych JACKSON et al. [18] oraz KASUMI [19,20] wykrywali w warunkach klinicznych zwapnienia o średnicach 0.1–0.5 mm przy częstotliwościach 4 i 7.5 MHz. Wyniki te są zasadniczo zgodne z naszą teorią, jeśli uwzględnić duży rozrzut pomiarów tła zakłócającego (odch. stan. 8 dB). Gdy zwapnienia znajdują się w obszarze nowotworu pozbawionym wewnętrznych ech, wtedy zwiększa się wykrywalność drobnych zwapnień w porównaniu do przypadku zdrowych tkanek piersi.

Key words: Breast, ultrasound, calcification, shadow, echo

1. Introduction

The ultrasonic echo method is one of the methods for detecting breast cancer. Even at an early phase of the disease, reactions in tissue cells cause microcalcifications to emerge as it can be seen in a mammogram or an X-ray microframe preparation [22]. They usually occur prior to the infiltration phase and as the disease proceeds, the microcalcifications sometimes reach quite considerable size.

Calcifications contain not only calcium but also phosphorus and many elements such as chlorine, sulfur nd various metals. However, probably the particles seen on mammograms, ~ 0.1 mm and larger, contain mainly calcium and perhaps phosphorus. The other particles not containing calcium are too small to be imaged on present state-of-the-art X-ray mammograms [11, 12].

Clinical investigations of breast microcalcifications are based on X-ray mamography. Recently some authors [18–20] successfully detected microcalcifications in some kind of breast tumors by means of ultrasonography. However, diffuse microcalcifications in the breast tissue outside of masses, were not recognized, and if ultrasonography is to be used in the future as a screening modality, vizualization of microcalcifications is essential [18].

The purpose of this study was to analyze the detectability of single small calcifications in female breasts and to answer the question as to what are detectability limits if one uses the ultrasonic shadow and echo methods at a typical frequency of 5 MHz. Thus the former, investigations of the present authors [9] were partially revised and continued by improving the measurement technique and expanding the analysis.

2. The shadow method

In this method one observes a shadow which occurs behind the calcification. The authors did not found papers describing comprehensively the shadow behind a spherical body. Computing the ultrasonic field distribution around a rigid sphere assumed as the calcification model it was possible to determine the shadow range $r_{-6\text{dB}}$ as a function of the sphere diameter ϕ and the wavelength [7, 8]

$$r_{-6\text{dB}} = 0.9\phi^2/\lambda \tag{1}$$

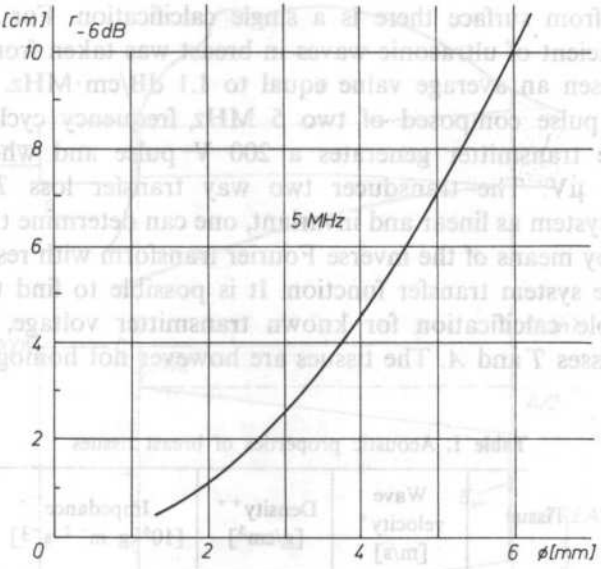

FIG. 1. The shadow range r_{-6dB} as a function of the calcification diameter ϕ calculated for the frequency 5 MHz from the formula 1

which was found to be valid for continuous wave and for the *ka* parameter between 12 and 630 ($k = 2\pi/\lambda$, $a = \phi/2$). The 6dB drop in respect to the pressure of the incident plane wave was asumed to correspond to the shadow range. Figure 1 shows the calculated shadow range for the frequency of 5 MHz.

It follows from this Figure that for obtaining a 2.5 cm long shadow the diameter of the calcification should be equal to 3 mm. The obtained result should be considered as the first approximation of the problem.

3. The echo method

For the echo method former investigations [9] were continued improving the measurement technique and expanding the analysis. We assume that inside a breast

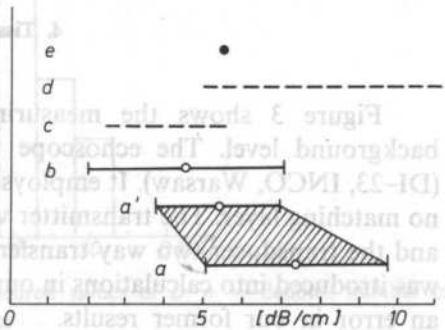

FIG. 2. Attenuation coefficients in normal breast measured or assumed by various authors. Points denote mean value, rods – standard deviation, dashed lines – variation range. a, a′ – after measurements of D'ASTOUS and FOSTER [4], calculated for various ratios of parenhyma to fat content, b – after measurements of CALDERON et al. [3] extrapolated for 5 MHz, c – after supposition of GREENLEAF and BAHN [13], d – after measurements of BAMBER [1], e – assumed by the authors of this paper

at a distance r' from surface there is a single calcification. For our analysis the attenuation coefficient of ultrasonic waves in breast was taken from literature (Fig. 2). We have chosen an average value equal to 1.1 dB/cm·MHz. We assumed an ultrasonic wave pulse composed of two 5 MHz frequency cycles, produced by a scanner whose transmitter generates a 200 V pulse and whose receiver has sensitivity of 10 μV. The transducer two way transfer loss T equals 15 dB. Recognizing the system as linear and invariant, one can determine the pulse reflected from the sphere by means of the inverse Fourier transform with respect to the pulse spectrum and the system transfer function. It is possible to find the radius of the smallest detectable calcification for known transmitter voltage, receiver electric sensitivity and losses T and A. The tissues are however not homogeneous (Table 1)

Table 1. Acoustic properties of breast tissues

Tissue	Wave velocity[+] [m/s]	Density[++] [g/cm^3]	Impedance [10^6kg m^{-2} s^{-1}]
Pectoralis muscle	1545	1.07	1.7
Muscle Connective	1545		
Grandular	1550		
Fat	1470	0.92	1.4

[+] Kossoff et al. [21].
[++] Wells [26].

and in the case of a breast the boundaries of fat, connective, gland and muscle tissues and inhomogeneities within cause interfering signals to mask echoes from small calcifications. These signals form the interfering background, and it is the level of this background, rather than that of the scanner sensitivity which limits the detectability of small calcifications.

4. Tissue background level

Figure 3 shows the measuring principle for determination of the tissue background level. The echoscope used was once designed for materials testing (DI–23, INCO, Warsaw). It employs a 5 MHz plane 5 mm diameter transducer with no matching layer. The transmitter voltage was 200 V, the receiver sensitivity 10 μV. and the transducer two way transfer loss was $T = 30$ dB. The value of 15 dB which was itroduced into calculations in our older paper [9] was erroneous thus introducing an error in our former results.

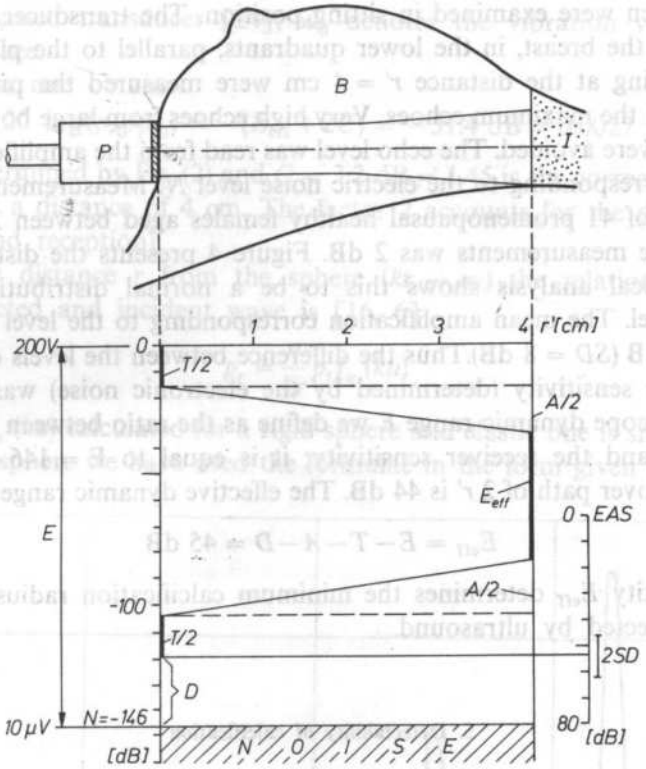

FIG. 3. The principle of determining the level of masking tissue echoes in the breast B showing all signal losses on the way from the probe P to idealized reflectors I and backwarxs. E – echoscope dynamic range, T – transducer two way transfer loss, A – attenuation loss, N – electric noise level, EAS – echoscope amplifications scale, SD – standard deviation, E_{eff} and D – see the text

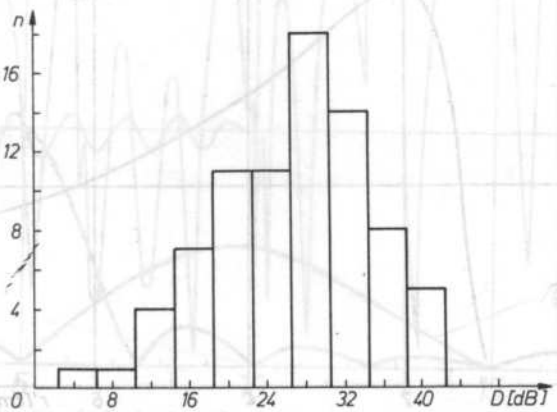

FIG. 4. The histogram showing the distribution of measured values of D. n – denotes number of measurements

The women were examined in sitting position. The transducer was applied at the bottom of the breast, in the lower quadrants, parallel to the plane of the ribs. Echoes occurring at the distance $r' = 4$ cm were measured the probe inclination being to obtain the maximum echoes. Very high echoes from large boundary surfaces of two tissues were avoided. The echo level was read from the amplification scale, the 80 dB level corresponding to the electric noise level N. Measurements were carried on 82 breasts of 41 promenopausal healthy females aged between 20 and 50. The accuracy of the measurements was 2 dB. Figure 4 presents the distribution of the results. Statistical analysis shows this to be a normal distribution at an 0.05 significance level. The mean amplification corresponding to the level of echoes from tissue was 53 dB ($SD = 8$ dB).Thus the difference between the levels of tissue echoes and echoscope sensitivity (determined by the electronic noise) was $D = 27$ bB.

The echoscope dynamic range E we define as the ratio between the transmitter pulse voltage and the receiver sensitivity; it is equal to E = 146 dB. The tissue attenuation A over path of 2 r' is 44 dB. The effective dynamic range (Fig. 3) is thus

$$E_{\text{eff}} = E - T - A - D = 45 \text{ dB} \tag{2}$$

The quantity E_{eff} determines the minimum calcification radius which can be potentially detected by ultrasound.

5. Detectability of calcification

The value of E_{eff} would correspond to the ratio of the reflected wave to that of the incident one, if the beam were parallel and the reflecting object were plane. In the case of a sphere which is small with respect to the beam diameter, one must consider the relative pressure distribution on the beam axis $p_0(r')/\varrho c w_0$ as shown in Fig. 5 for

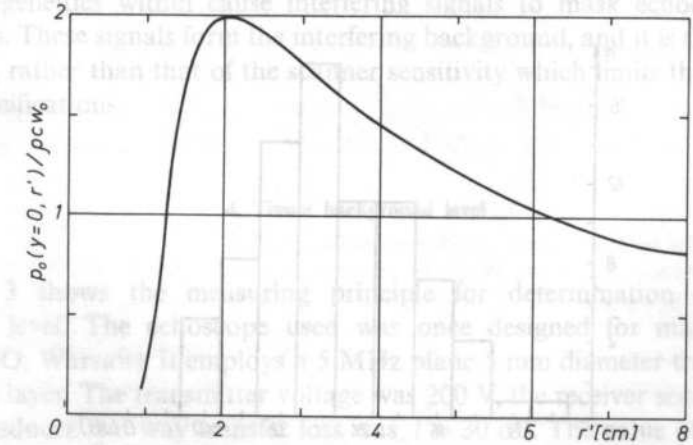

FIG. 5. The relative acoustic pressure amplitude calculated along the beam axis of a plane disc transducer used in measurements

a plane nonfocused transducer [24]; w_0 denotes the vibration velocity on the transducer surface.

In this case one obtains

$$20 \log (p_{r0}/p_{i0}) = -(E_{\text{eff}} + 2C) = -51.4 \text{ dB} \doteq 0.0027 \tag{3}$$

were E_{eff} is determined by Eq. (2) and $C = 3.2$ dB $\doteq 1.45$ is the correction coefficient from Fig. 9 for a distance of 4 cm. The factor 2 accounts for the double gain (in transmission and reception).

At a large distance r from the sphere ($kr \to \infty$) the relation between the backward reflected and incident wave is [16, 6]

$$p_r = \frac{a}{2r} p_i f_\infty(ka) \tag{4}$$

The modulus f_∞ (ka) calculated for a rigid sphere and elastic one is shown in Fig. 6. For the elastic sphere we have used the formulae in the form given by HASEGAWA

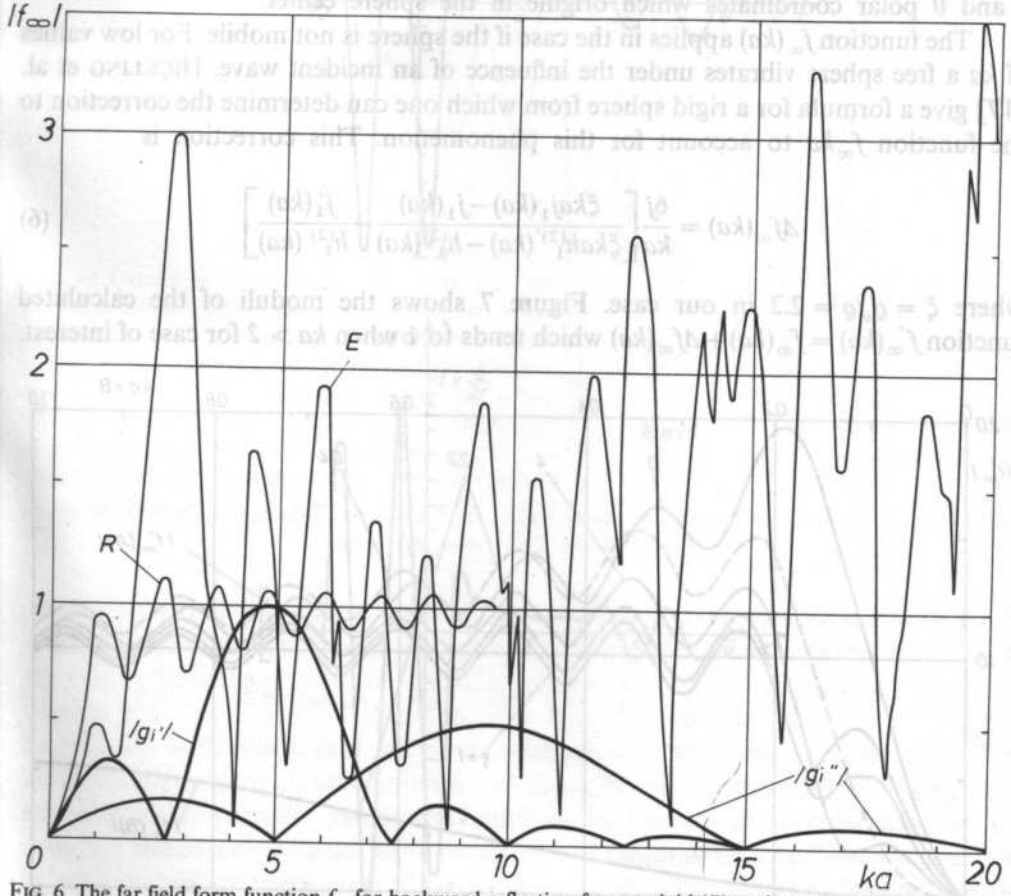

FIG. 6. The far field form function f_∞ for backward reflection from a rigid (R) and an elastic (E) sphere with the Poisson's ratio $\nu = 0.2$; g_i', g_i'' – spectra of the two-cycle sinusoidal pulse for $ka = 5$ and 10, respectively

[14] and HASEGAWA et al. [15]. We assumed that the calcification had the mechanical propeties of scull with density $\varrho_s = 2.2$ g/cm^3 and compressional wave velocity $c_1 = 3.2$ km/s [25]. The Poissons' ratio was assumed as most probable to be $\nu = 0.2$.

One can determine the pulse reflected from the sphere by means of the inverse Fourier transform with respect to the spectrum $g_1(ka)$ and the system transfer function. We define the latter as the ratio between the reflected and the incident harmonic waves [5]. From formula (4) we have for $kr \to \infty$ the pulse backward reflected from the sphere ($\theta = \pi$) in the form

$$p_r(\tau) = \frac{1}{2\pi} \int_{-\infty}^{+\infty} \frac{a}{2r} f_\infty(ka) g_i(ka) \exp(jka\tau) d(ka) \tag{5}$$

where $\tau = (ct - r\cos\theta)/a$ is dimensionless time, c is the wave velocity in breast tissue r and θ polar coordinates which origine in the sphere center.

The function $f_\infty(ka)$ applies in the case if the sphere is not mobile. For low values of ka a free sphere vibrates under the influence of an incident wave. HICKLING et al. [17] give a formula for a rigid sphere from which one can determine the correction to the function $f_\infty ka$ to account for this phenomenon. This correction is

$$\Delta f_\infty(ka) = \frac{6j}{ka}\left[\frac{\xi ka j_1(ka) - j_1(ka)}{\xi ka h_1^{(2)'}(ka) - h_1^{(2)}(ka)} - \frac{j_1'(ka)}{h_1^{(2)'}(ka)}\right] \tag{6}$$

where $\xi = \varrho_s/\varrho = 2.2$ in our case. Figure 7 shows the moduli of the calculated function $f'_\infty(ka) = f_\infty(ka) + \Delta f_\infty(ka)$ which tends to 1 when $ka > 2$ for case of interest.

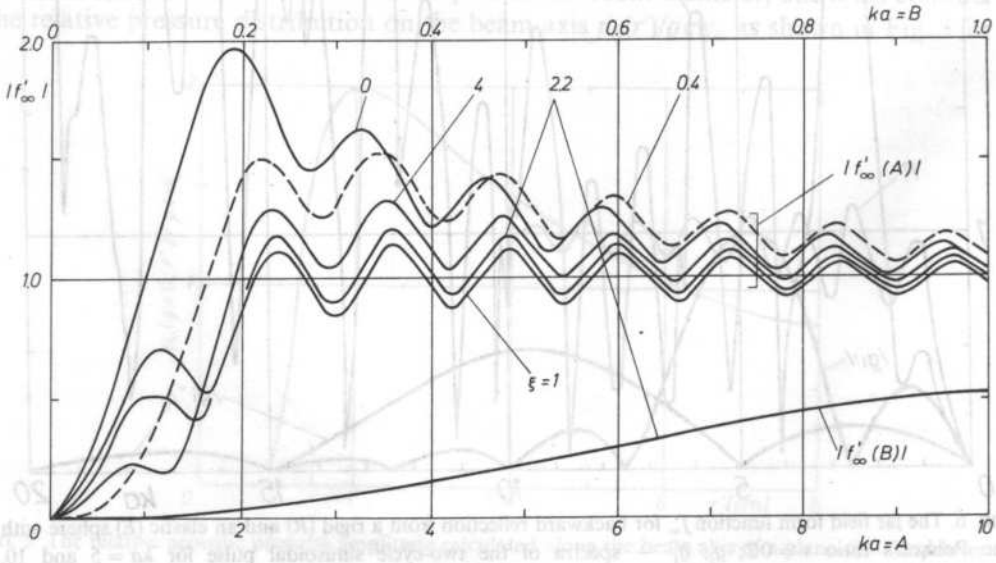

FIG. 7. The function $f_\infty(ka)$ for a movable rigid sphere at various ratios of densities $\xi = \varrho_s/\varrho$, (ϱ_s and ϱ denote densities of the sphere and surrounding tissue, respectively)

Figure 8 shows the ultrasonic pulses reflected from a rigid sphere, as given by Eqs. (5), (6). The reflected waveforms ressemble the incident pulse and there is negligible difference between the immobile and the free sphere. Because of this, one may assume approximately that elastic spheres do not move either, and one can apply for this case an analogous theory of wave reflection.

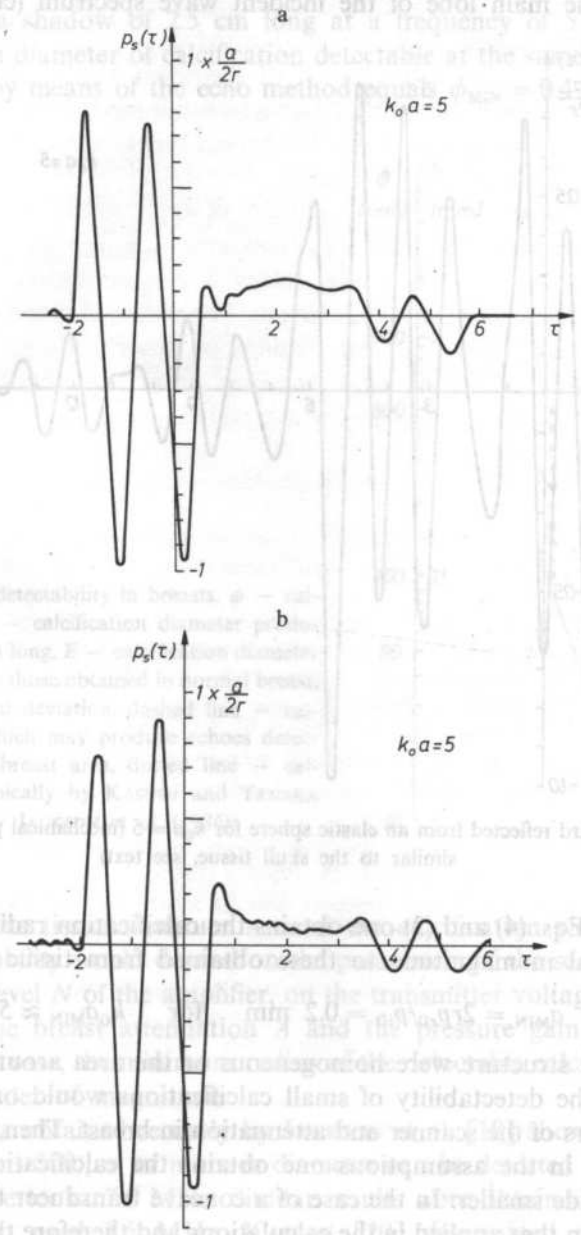

FIG. 8. Pulses backward reflected from rigid spheres for $k_0 a = 5$, a) movable sphere b) immovable sphere. Very small pulses are caused by creeping waves

Figure 9 presents the ultrasonic pulse reflected from an elastic sphere. One can notice much longer duration time of the reflected pulse and some oscillations of its amplitude. For a rigid sphere one can assume $f_\infty(ka) = 1$. This condition can be also assumed for an elastic sphere though the approximation is not so good in this case. One should take into consideration those sections of the curves R and E which correspond to the main lobe of the incident wave spectrum (curve g_i' in Fig. 6).

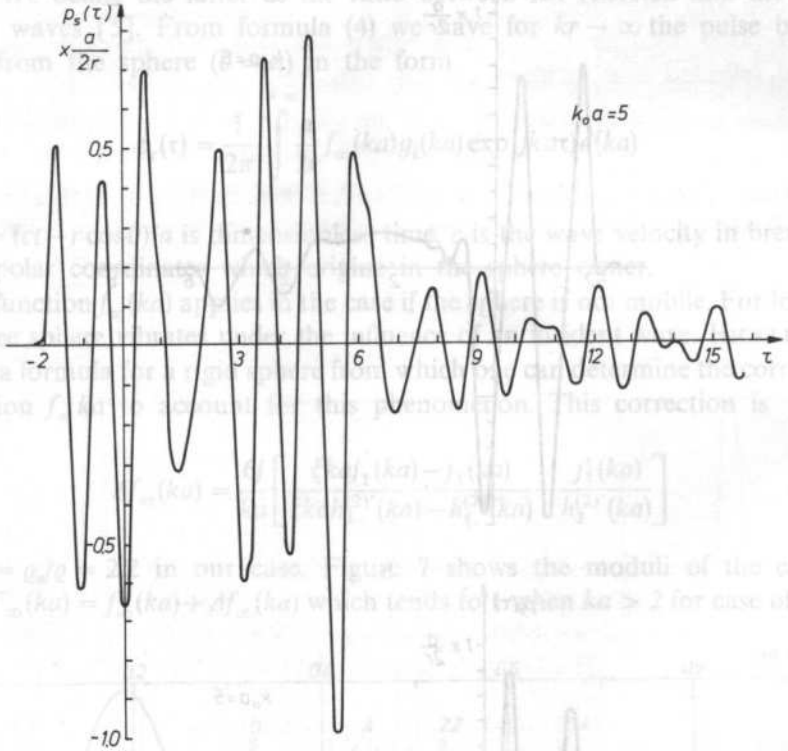

FIG. 9. Pulse backward reflected from an elastic sphere for $k_0a = 5$ (mechanical properties of the sphere similar to the skull tissue, see text)

Then, from Eqs. (4) and (3) one obtains the calcification radius which gives rise to an echo equal in magnitude to these obtained from tissue inhomogeneities

$$a_{\text{MIN}} = 2rp_{r0}/p_{i0} = 0.2 \text{ mm} \quad \text{for} \quad k_0a_{\text{MIN}} \approx 5. \tag{7}$$

If the breast structure were homogeneous or the area around the calcification were anechoic, the detectability of small calcifications would only depend on the electric parameters of the scanner and attenuation in breast. Then, D is 0 and, for the parameters used in the assumptions one obtains the calcification radius $a_{\min}$ one order of magnitude smaller. In the case of a concave transducer the factor C can be much greater than that applied in the calculations and therefore the value of $a_{\min}$ can be even smaller.

6. Discussion and conclusions

The obtained results are presented in Fig. 10.

The calcification detectability of the shadow method is very low when comparing with the echo method. The diameter of the calcification equal to $\phi = 3$ mm gives a shadow of 2.5 cm long at a frequency of 5 MHz.

The minimum diameter of calcification detectable at the same frequency in the distance of 4 cm by means of the echo method equals $\phi_{MIN} = 0.4$ mm ($SD = 8$ dB)

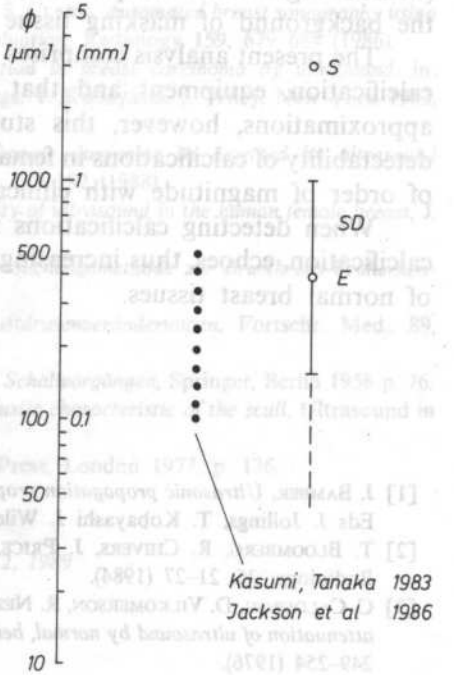

FIG. 10. Calcification detectability in breasts. ϕ – calcification diameter, S – calcification diameter producing the shadow 2.5 cm long, E – calcification diameter giving an echo equal to those obtained in normal breast, tissues, SD – standard deviation, dashed line – calcification diameters which may produce echoes detectable in an anechoic breast area, dotted line – calcification detected clinically by KASUMI and TANAKA (1983) and by JACKSON et al. (1986)

However, if the tissue structure around the calcification were anechoic, the calcification detectability would depend on the parameters of the scanner, namely: on the electric noise level N of the amplifier, on the transmitter voltage, the transducer transfer loss, T, the breast attenuation A and the pressure gain C due to beam focusing. In such a case, the minimum radius of the detectable calcification could be smaller by one order of magnitude.

Clinical results obtained recently by JACKSON et al. [18] showed that inside of tumors calcifications 500 μm or more in diameter can be detected at a frequency of 4 MHz but seen better at 7.5 MHz. Similar results were obtained by KASUMI and TANAKA [19] who used 7.5 MHz, KASUMI [20] determined the diameters of detectable calcifications to be between 100 and 500 μm.

The conditions formulated for the size of detectable calcifications are necessary but not sufficient, for there is still the practical problem of distinguishing calcification echoes greater than comparable tissue echoes. KASUMI and TANAKA [19] always detected calcifications in the tumor anachoic area that stresses fine strong calcification echoes. However, they could not identify calcifications in diffuse benign lessions. JACKSON et al. [18] concluded that diffuse microcalcifications in the breast tissue, outside the masses, were not recognized.

The amplitude of the echo is one of the most important characteristics of calcifications. Therefore it would be desired to use a receiver with a linear response (without logarithmic compression) to distinguish higher calcification echoes against the background of masking tissue echo.

The present analysis comprises a number of approximations with respect to the calcification, equipment and that of tissue masking echoes. Despite the many approximations, however, this study achieved a quantitative evaluation of the detectability of calcifications in female breast. The obtained results agree in the range of order of magnitude with clinical findings of other authors [18–20].

When detecting calcifications in anechoic areas one obtains stressing of fine calcification, echoes, thus increasing the detectability when comparing with our case of normal breast tissues.

References

[1] J. BAMBER, *Ultrasonic propagation properties of the breast*, in: Ultrasonic examination of the breast Eds J. Jollings, T. Kobayashi J. Wiley, New York, 1983 37–44.

[2] T. BLOOMBERG, R. CHIVERS, J. PRICE, *Real-time ultrasonic characteristics of the breast*, Clinical Radiology, **35**, 21–27 (1984).

[3] C. CALDERON, D. VILKOMERSON, R. NEZRICH K. ETZOLD, B. KINGSELY, M. HASKIN, *Differences in the attenuation of ultrasound by normal, benign, and malignant breast tissue*, J. of Clinical Ultrasound, **4**, 249–254 (1976).

[4] F. D'ASTOUS, F. FOSTER, *Frequency dependence of ultrasound attenuation and backscatter in breast tissue*, Ultrasound in Med. and Biol., **12**, 795–808 (1986).

[5] E. DIELESAINT, D. ROYER, *Ondes élastiques dans les solides*, Masson, Paris 1974, p. 36.

[6] L. DRAGONETTE, R. VOGT, L. FLAX, W. NEUBAUER, *Acoustic reflection from elastic spheres and rigid spheres and spheroids. II. Transient analysis*, J. Acoust. Soc. Am., **56**, 1130–1137 (1974).

[7] L. FILIPCZYŃSKI, T. KUJAWSKA, *Isobar distributions and shadow range of spheres immersed in water*, Proc. VI Symposium on Hydroacoustics, Gdynia AMW 1989, 115–120.

[8] L. FILIPCZYŃSKI, T. KUJAWSKA, *Acoustical shadow of a sphere immersed in water. II*, Arch. of Acoustics, **14**, 3–4, 183–192, (1989).

[9] L. FILIPCZYŃSKI, T. KUJAWSKA, G. ŁYPACEWICZ, *Ultrasonic echo method in detection of breast calcification, Transient analysis.* Archives of Acoustics, **11**, 3, 287–298 (1986).

[10] L. FILIPCZYŃSKI, T. KUJAWSKA, G. ŁYPACEWICZ, *Evaluation of calcification detectability in femal breasts by ultrasound.* VI International Congress on the Ultrasonic Examination of the Breast, Paris June 29–30 1989 Abstracts p. 32.

[11] B. GALKIN, S. FEIG, A. PATCHEFSKY, J. RUE, J. GAMBLIN, S. GOMEZ, L. MARCHANT, *Ultrastructure and microanalysis of benign and malignant breast calcifications*, Radiology, **124**, 245–249 (1977).

[12] B. GALKIN, P. FRASCA, A. FEIG, K. HOLDERNESS, *Non-calcified breast particles. A possible new marker of breast cancer*, Investigative Radiology, **17**, 119–128 (1982).

[13] J. GREENLEAF, R. BAHN, *Clinical imaging with transmissive ultrasonic computerized tomography*, IEEE Transactions on Biomedical Engineering, BME-28, 177–185 (1981).

[14] T. HASEGAWA, *Comparison of two solutions for acoustic radiation pressure on a sphere*, J. Acoust. Soc. Am., **61**, 6, 1445–1448 (1977).

[15] T. HASEGAWA, Y. KITAGAWA, Y. WATANABE, *Sound reflection from an absorbing sphere*, J. Acoust. Soc. Am., **62**, 1298–1300 (1977).

[16] R. HICKLING, *Analysis of echoes from a solid elastic sphere in water*, J. Acoust. Soc. Am., **34**, 1582–1592 (1962).

[17] R. HICKLING, H. WANG, *Scattering of sound by a rigid movable sphere*, J. Acoust. Soc. Am., **39**, 276–280 (1966).

[18] V. JACKSON, E. KELLY-FRY, P. TOTSCHILD, R. HOLDEN, S. CLARK, *Automated breast sonography using* 7.5 MHz PVDF *transducer: Preliminary clinical evaluation*, Radiology **159**, 679–684 (1986).

[19] F. KASUMI, H. TANAKA, *Detection of microcalcification in breast carcinoma by ultrasound*, in: Ultrasonic examination of the breast, [Eds]. J. Jellings, T. Kobayashi, J. Wiley, New York 1983, 89–96 (1983).

[20] F. KASUMI, *Can microcalcifications located within breast carcinome be detected by ultrasound imaging?*, Ultrasound in Med. and Biol. **14**, Sup. 1, 175–182 (1988).

[21] G. KOSSOFF, E. KELLY-FRY, J. JELLINS, *Averaged velocity of ultrasound in the human female breast*, J. Acoust. Soc. Am., **53**, 1730–1736 (1973).

[22] V. MENAGES, *Mammographie, die zurverlässigste Untersuchungsmethode zur Brustkrebs-Fruherkennung*, Elęktromedica, **2**, 42–49 (1979).

[23] K. PRECHTEL, *Mastopathie und altersabhängige Brustdrusenveränderungen*, Fortschr. Med., **89**, 1312–1315 (1971).

[24] H. STENZEL, O. BROSZE, *Leitfaden zur Berechnung von Schallvorgängen*, Springer, Berlin 1958 p. 76.

[25] D. N. WHITE, G. R. CURRY, R. J. STEVENSON, *The acoustic characteristic of the scull*, Ultrasound in Med. and Biol., **4**, 225–252 (1978).

[26] P. N. T. WELLS, *Biomedical Ultrasonics*, Academic Press, London 1977, p. 136.

Received on August 12, 1989

ARCHIVES OF ACOUSTICS
15, 1–2, 121–135 (1990)

ANALYSIS OF ACOUSTICS SURFACE WAVE REFLECTION ON THE INTERDIGITAL TRANSDUCER

J. FILIPIAK

Technical Military Academy, Warszawa

By applying the equivalent scheme, the analysis of the acoustics surface wave reflection from the interdigital transducer has been carried out. The explicit form of the coefficient of reflection was found, from which the following terms have been separated – the magnitude of the mechanical wave reflection due to variation of the acoustics impedance in the area of transducer, and magnitude of the wave regeneration by the electrically loaded transducer. The results of calculations has been presented for the coefficient of surface wave reflection from the simple transducer with single and double electrodes as a function of its electrical load. The experimental verification has been undertaken for transducers on $LiNbO_3$.

1. Introduction

The surface acoustic wave (SAW) incident upon the interdigital transducer is submitted to the reflection as result of:

acoustics impendance variation in the transducer domain (the mechanical type reflection),

regeneration by the electrically loaded transducer (the electrical type reflection).

In the case of a pair of two transducers in SAW filters the wave reflection generates multiple echoes, respectively high level of which can caused considerable distortions in amplitude and phase characteristics of filters. The phenomenon of wave reflection from the structure of interdigital transducer can be applied for constructing some SAW devices, for example resonators. On the other hand, by using the exact description of this phenomenon, the effect can be precisely eliminated in the undesirable cases. In this paper the above mentioned aspects of transducers are considered on the strength of its equivalent scheme.

2. A concept of equivalent scheme

The surface wave incident upon the interdigital transducer is submitted to reflection, transmission and convertion into electrical sygnal, Fig. 1a. The analysis of these phenomena can be carried out by using the method of equivalent scheme, [1]. The magnitude of incident wave is identified with a voltage source described by both 2V electromotive force and inner impedance z_N which denotes impedance of free surface of piezoelectric, Fig. 1b, [2]. The simple transducer is a combination of many

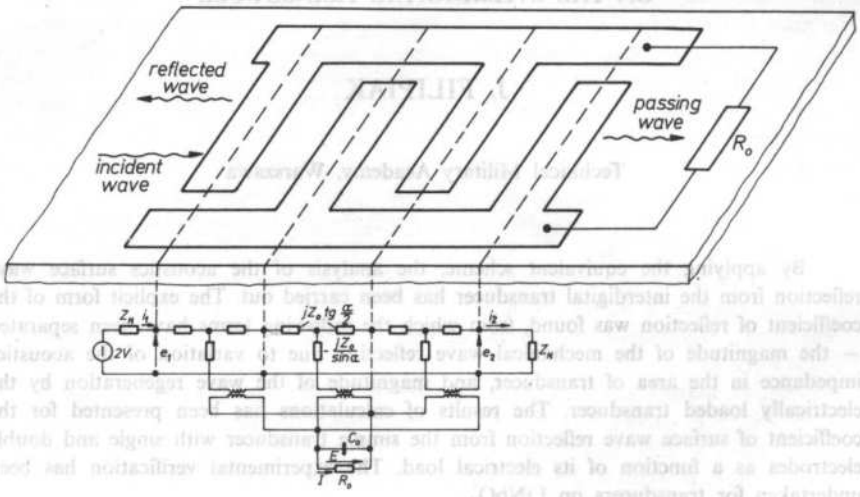

FIG. 1. a) Interdigital transducer, b) Equivalent scheme of transducer

three-port networks each being on equivalent scheme of its single section [3]. Single section corresponds to the area located between centres of two following electrodes. The scheme and notations are presented on Fig. 1b. The acoustics and electrical clamps of separate sections are connected in cascade and in parallel respectively considering polarization of electrodes. On the side of incident wave the three-port network is loaded by the voltage source but on its other side the acoustics clamps are loaded by impedance related to the free surface of piezoelectric. The load of electrical clamps is determined by impedance R_0.

By applying relations introduced in [3], the three-port network can be described in the following way:

$$\begin{aligned} i_k &= i_1\cos\beta+\frac{e_1}{jz_0}\sin\beta-\frac{2r\sin\frac{\alpha}{2}}{jz_0}\sum_{n=1}^{N}E_n\cos\left(N-n+\frac{1}{2}\right)\alpha \\ e_k &= -ji_1z_0\sin\beta+e_1\cos\beta+2r\sin\frac{\alpha}{2}\sum_{n=1}^{N}E_n\sin\left(N-n-\frac{1}{2}\right)\alpha, \end{aligned} \tag{2.1a}$$

where N denotes the number of sections on which transducer is divided,

$$\beta = N\alpha \qquad \alpha = \pi\left(1 - j\frac{\sqrt{(\omega-\omega_3)(\omega-\omega_1)}}{\omega_1}\right)$$

$$\omega_3 = \pi v'_R p^{-1} \qquad \omega_1 = \pi v'_R p^{-1}\left(1+\frac{1}{4}\cos\Delta\right)^{-1} \qquad \Delta = \pi w p^{-1}$$

the notations of V, w and p denote respectively the velocity of surface wave, the width and the period of electrode.

In the electrical side it is

$$I = \sum_{l=1}^{N} \mu(l)\{j\omega C_0 E_l + r(i_{l+1} - i_l)\} \tag{2.1b}$$

where

$$i_l = i_1 \cos l\alpha + \frac{e_1}{jz_0}\sin l\alpha - \frac{2r\sin\frac{\alpha}{2}}{jz_0}\sum_{n=1}^{l} E_l \mu(l)\cos\left(l-n+\frac{1}{2}\right)\alpha.$$

Rel. (2.1) and boundary conditions, derived for the three-port network are presented in the following forms

on the acoustic side

$$i_l z_n = 2V - e_1 \qquad i_k z_n = e_k \tag{2.2a}$$

on the electrical side

$$R_0 I = -E \tag{2.2b}$$

The set of equations (2.2a) and (2.2b) allows to determine all quantities for the three-port network. The reflection and transmission coefficients, derived in [4] can be presented in the following forms

$$\Gamma = \frac{z_n - \frac{e_1}{i_1}}{z_n + \frac{e_1}{i_1}} \tag{2.3}$$

$$T_z = \frac{e_k}{V} \tag{2.4}$$

respectively.

Hence, the identification of Eq. (2.3) and Eq. (2.4) requires finding of both magnitudes – the acoustics impedance of transducer defined by e_1/i_1 to be calculated on the side of incident wave and the value of voltage e_k defined by the loaded acoustic clamps of transducer to be calculated on its other side. A determination of these both magnitudes can be possible by solving the set of equations (2.1) and (2.2) which has been defined for the single three-port network.

3. Reflection and transmission coefficients

By applying relation (2.1a), the coefficient of reflection Γ, Eq. (2.3) can be presented in the following form

$$\Gamma = 1 - \frac{e_l}{V} \tag{3.1}$$

therefore, a determination of above mentioned coefficients requires finding dependence of voltages existed on acoustics clamps of the three-port network upon the value of V. Hence, from relations (2.1a) and (2.2a) a dependence of these voltages on the magnitude of source V and the voltage determined by the loaded transducer can be found in the form

$$\begin{aligned} e_1 &= \frac{(1-R)(1+Re^{-j2\beta})}{1-R^2e^{-j2\beta}} V + \frac{jr(1+R)\sin\frac{\alpha}{2}e^{-j\frac{\beta}{2}}(H^*+Re^{-j\beta}H)}{1-R^2e^{-j2\beta}} E \\ e_k &= \frac{(1-R^2)e^{-j\beta}}{1-R^2e^{-j2\beta}} V + \frac{jr(1+R)\sin\frac{\alpha}{2}e^{-j\frac{\beta}{2}}(H+Re^{-j\beta}H^*)}{1-R^2e^{-j2\beta}} E \end{aligned} \tag{3.2}$$

where

$$R = \frac{z_N - z_0}{z_N + z_0}$$

$$H = \sum_{n=1}^{N} \mu(n) e^{-j\left(\frac{N-1}{2}+l\right)\alpha} \qquad \mu(n) = \frac{A_n - A_{n+1}}{|A_n - A_{n+1}|}$$

Hence, the value of $\mu(n) = 0, 1$ depends on the way in which the bus of transducer is connected to the electrode located in the area of n-th section of transducer. Moreover, the value of $A(n)$ determines position of the end of electrode. By assuming relations (2.1b), (2.2b) and (3.2), a dependence between voltage E of the loaded transducer and the magnitude of incident wave V can be determined in the form

$$E = \frac{2jr(1-R)\sin\frac{\alpha}{2}e^{-j\frac{\beta}{2}}}{z_0(1-R^2e^{-j2\beta})} \frac{(H^*+Re^{-j\beta}H)R_0}{1+Y_N R_0} V \tag{3.3}$$

where Y_N denotes the transducer admittance. By substituting Eq. (3.3) into (3.1), the value of acoustics voltages of the three-port network can be determined as the function of the magnitude of incident wave

$$e_1 = \left\{\frac{(1+R)(1-Re^{-j2\beta})}{1-R^2e^{-j2\beta}} - \frac{2r^2\sin^2\frac{\alpha}{2}(1-R^2)e^{-j\beta}(H^*+Re^{-j\beta}H)^2R_0}{z_0(1-R^2e^{-j2\beta})^2(1+Y_NR_0)}\right\}V$$

$$e_k = \frac{(1+R^2)e^{-j\beta}}{1-R^2e^{-j2\beta}}\left\{1-\frac{2r^2\sin^2\frac{\alpha}{2}(H^*+Re^{-j\beta}H)(H+Re^{-j\beta}H^*)R_0}{z_0(1-R^2e^{-j2\beta})^2(1+Y_NR_0)}\right\}V \tag{3.4}$$

By applying relation (3.4), the reflection and transmission coefficients can be found as

$$\Gamma = \frac{R(1-e^{-j2\beta})}{1-R^2e^{-j2\beta}} - \frac{(1-R^2)e^{-j2\beta}}{1-R^2e^{-j2\beta}}\cdot\frac{2r^2\sin^2\frac{\alpha}{2}(H^*+Re^{-j\beta}H)^2R_0}{z_0(1-R^2e^{-j2\beta})(1+Y_NR_0)}$$

$$T = \frac{(1-R^2)e^{-j2\beta}}{1-R^2e^{-j2\beta}}\left\{1-\frac{2r^2\sin^2\frac{\alpha}{2}(H^*+Re^{-j\beta}H)(H+Re^{-j\beta}H^*)R_0}{z_0(1-R^2e^{-j2\beta})(1+Y_NR_0}\right\} \tag{3.5}$$

In the case of short-circuited transducer ($R_0 = 0$) the magnitudes of wave reflection and transmission depend only on the variation of acoustics impedance of the transducer domain

$$\Gamma_z = \frac{R(1-e^{-j2\beta})}{1-R^2e^{-j2\beta}}$$

$$T_z = \frac{(1-R^2)e^{-j\beta}}{1-R^2e^{-j2\beta}} \tag{3.6}$$

Relations (3.6) are identical with those determined in [5]. The final relations define the reflection and transmission coefficients are presented in the following form

$$\Gamma = \Gamma_z + T_z\frac{2r^2\sin^2\frac{\alpha}{2}(H^*+Re^{-j\beta}H)^2R_0}{z_0(1-R^2e^{-j2\beta})(1+Y_NR_0)}$$

$$T = T_z - T_z\frac{2r^2\sin^2\frac{\alpha}{2}(H^*+Re^{-j\beta}H)(H+Re^{-j\beta}H^*)R_0}{z_0(1-R^2e^{-j2\beta})(1+Y_NR_0)} \tag{3.7}$$

where Γ_z denotes the magnitude of mechanical wave reflection but the term proportional to R_0 denotes electrical wave regeneration by the loaded transducer. The coefficient of wave reflection consists of the "mechanical" and "electrical" terms, Γ_z and Γ_E respectively, where Γ_E is presented in the following form

$$\Gamma_E = \frac{2r^2\sin^2\frac{\alpha}{2}(H^*+Re^{-j\beta}H)^2R_0}{z_0(1-R^2e^{-j2\beta})(1+Y_NR_0)}T_z \tag{3.8}$$

It can be proved that

$$\frac{2r^2\sin^2\frac{\alpha}{2}(H^*+Re^{-j\beta}H)(H+Re^{-j\beta}H^*)}{z_0(1-R^2e^{-j2\beta})} = Re(Y_N) = G \tag{3.9}$$

where G denotes the transducer conductance. Because the transducer admittance has a form

$$Y_N = G+jB \tag{3.10}$$

the coefficient of wave reflection and transmission can be presented in the form

$$\begin{aligned} \Gamma &= \Gamma_z - T_z e^{j\Phi}\frac{GR_0}{1+(G+jB)R_0} \\ T &= T_z - T_z\frac{GR_0}{1+(G+jB)R_0} \end{aligned} \tag{3.11}$$

where

$$e^{j\Phi} = \frac{H^*+Re^{-j\beta}H}{H+Re^{j\beta}H^*}$$

4. Experimental results

The comparison of the theory with experiment has been carried out for both- electrically shorted and opened transducers with single and double electrodes. For these cases the value of R_0 is precisely determined and varied from 1 to ∞ respectively. For the baseband of shorted transducer with double electrodes the value of coefficient of reflection is equal to 0, because $R = 0$, but for the opened one the reflection and transmission coefficients are defined in the form

$$|\Gamma| = \frac{G}{\sqrt{G^2+B^2}} \qquad |T| = \frac{B}{\sqrt{G^2+B^2}} \tag{4.1}$$

By finding the transducer admittance, the value of coefficient of wave reflection can be determined in very simple way. The values of measured admittance of $LiNbO_3$ base transducer with 10 pairs of double electrodes are presented on Fig. 2. Based on the relation (4.1), the coefficient of reflection has been calculated by applying the experimental data of admittance and then the values of coefficient have been compared with the experimental data obtained from [6]. In the case of short-circuited transducer with single electrodes, the coefficient of reflection is identified with Γ_z but for the opened transducer the coefficient has the following form

$$\Gamma = \Gamma_z + T_z \frac{Ge^{j\Phi}}{G+jB} \tag{4.2}$$

The theoretical relations of Γ_z, Γ_E and Γ for simple $LiNbO_3$ base transducer with 10 single electrodes are compared on Fig. 3 with the experimental results obtained from [6]. The worse coincidence between theory and experiment can be explained by the following reasons – the transducer admittance, mainly its static capacitance was defined with the less accuracy, the considery analitical model doesn't contain the phenomenon of the surface wave diffraction.

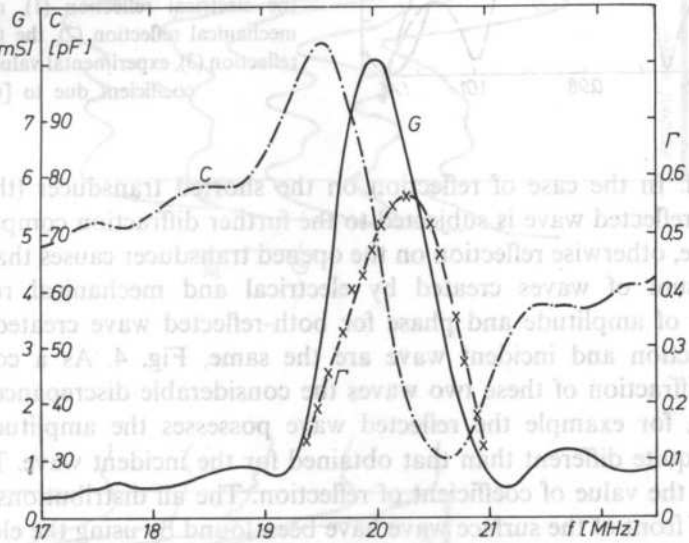

FIG. 2. Experimental dependence of a conductance G and a capacitance G on frequency of the simple $LiNbO_3$ base transducer with 10 pairs of sectional electrodes. Coefficient of the reflected wave, calculated for the opened transducer by applying experimental values of G and C. Experimental values of the reflection coefficient due to [6]

The reflected wave is submitted to the diffraction, evaluation of which is related to its point of generation or its point of regeneration taking into consideration respectively the mechanical or electrical type of reflection. Amplitude and phase distributions of front of the surface wave propagating between two $LiNbO_3$ base transducers with double electrodes are presented on Fig. 4. The distributions of both induced and regenerated wave on the opened transducer are the same in this case. On the contrary, Fig. 5 shows distribution of amplitude and phase of front of the surface wave incident and reflected from shorted and opened simple transducer composed of 10 pairs of single electrodes. These distributions have been obtained at the half distance between transducers in which the surface wave has been induced

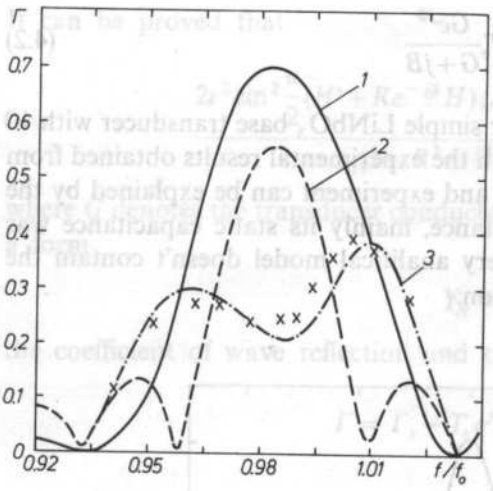

FIG. 3. Theoretical values of the reflection coefficient for wave reflected on the simple transducer with 10 pairs of single electrodes: magnitude of the electrical reflection (1), magnitude of the mechanical reflection (2), the total coefficient of reflection (3), experimental values of the reflection coefficient due to [6] (×).

and reflected. In the case of reflection on the shorted transducer (the mechanical reflection) a reflected wave is subjected to the further diffraction comparing with the incident wave, otherwise reflection on the opened transducer causes that the reflected wave is a sum of waves created by electrical and mechanical reflection. The distributions of amplitude and phase for both-reflected wave created by electrical type of reflection and incident wave are the same, Fig. 4. As a consequence of a different diffraction of these two waves the considerable discrepances occur in its distributions, for example the reflected wave possesses the amplitude and phase distribution quite different than that obtained for the incident wave. This effect can influence on the value of coefficient of reflection. The all distributions of amplitude and phase of front of the surface wave have been found by using the electrical probe, [7]. As shown on Fig. 5 the electrical reflection is bigger than the mechanical one. Simultaneously, the resultant reflection can be less then its components calculated separately. It means that the reflections can eliminat each other. The coefficient of reflection calculated for its electrical type, Eq. (4.2) can be almost equal to 1, if the susceptance of transducer B is setting to zero, what is reached for the greater number of electrodes. The results of admittance of $LiNbO_3$ base transducer with 78 single simple electrodes, presented on Fig. 6 are compliianced to the experimental data obtained from [8]. The susceptance is equal to zero for two values of frequency. The coefficient of reflection, the values of which have been calculated based on the theoretical model, are presented on Fig. 7. The coefficient of reflection calculated for its electrical type is equal to 1, $\Gamma_E = 1$ at points for which the susceptance is setting to zero. Also this coefficient calculated for mechanical type of reflection is almost equal to 1. After all the value of total coefficients of reflection is less than 1 and it reaches the value of 0.34 for $0.99\, f_{00}$. Hence, the value of total coefficient varies with the phase changing of the coefficient of reflection calculated for its electrical type, what can be reached by changing the load impedance R_0. It means that the value

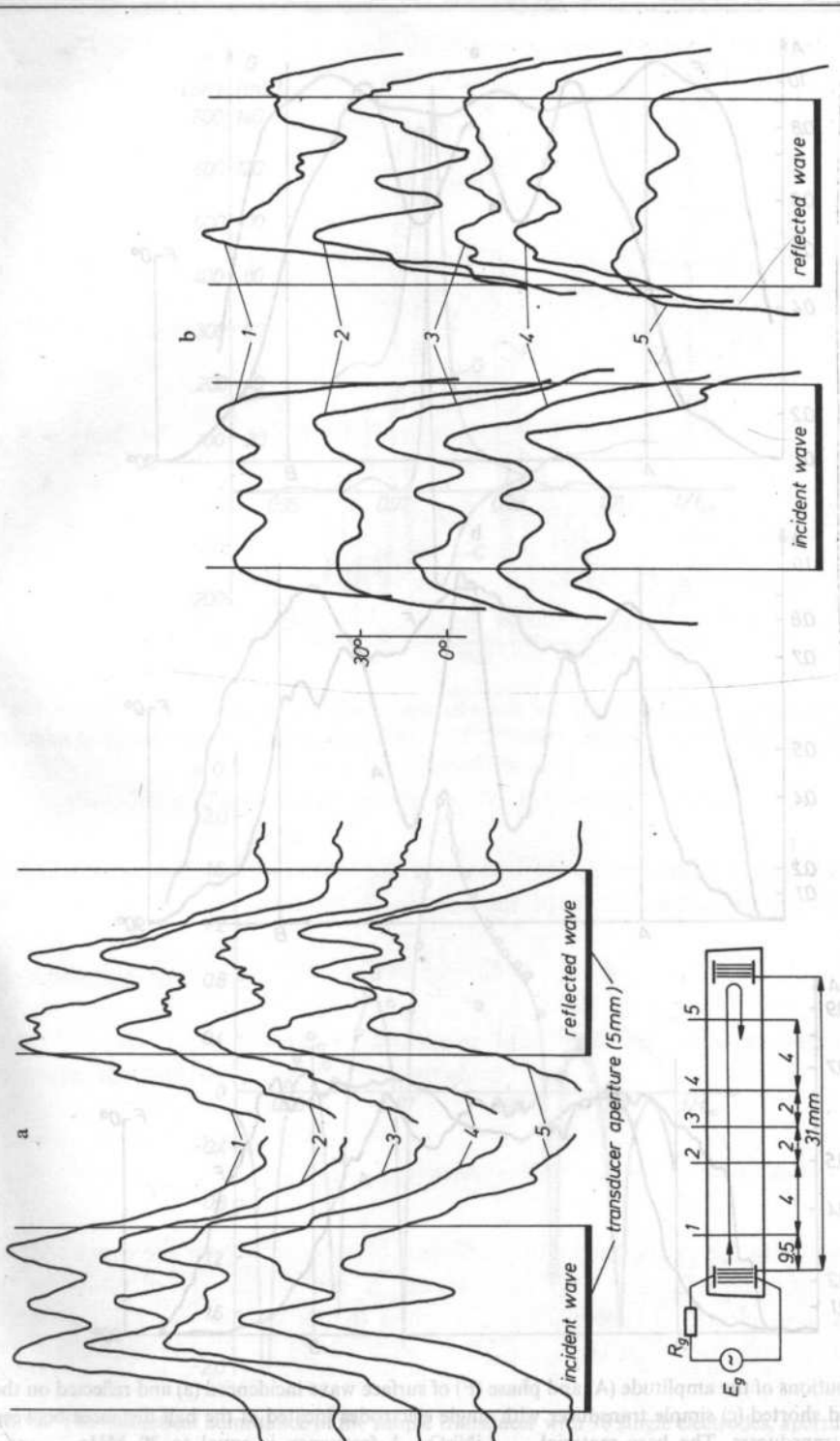

FIG. 4. a) Distributions of amplitude of the surface wave incidenced and reflected on the simple opened $LiNbO_3$ base transducer with double electrodes corresponded to the appropriate distances. Frequency is equal to 30 MHz; b) Distributions of phase of the surface wave corresponded to the distributions of amplitude shown on Fig. 4a

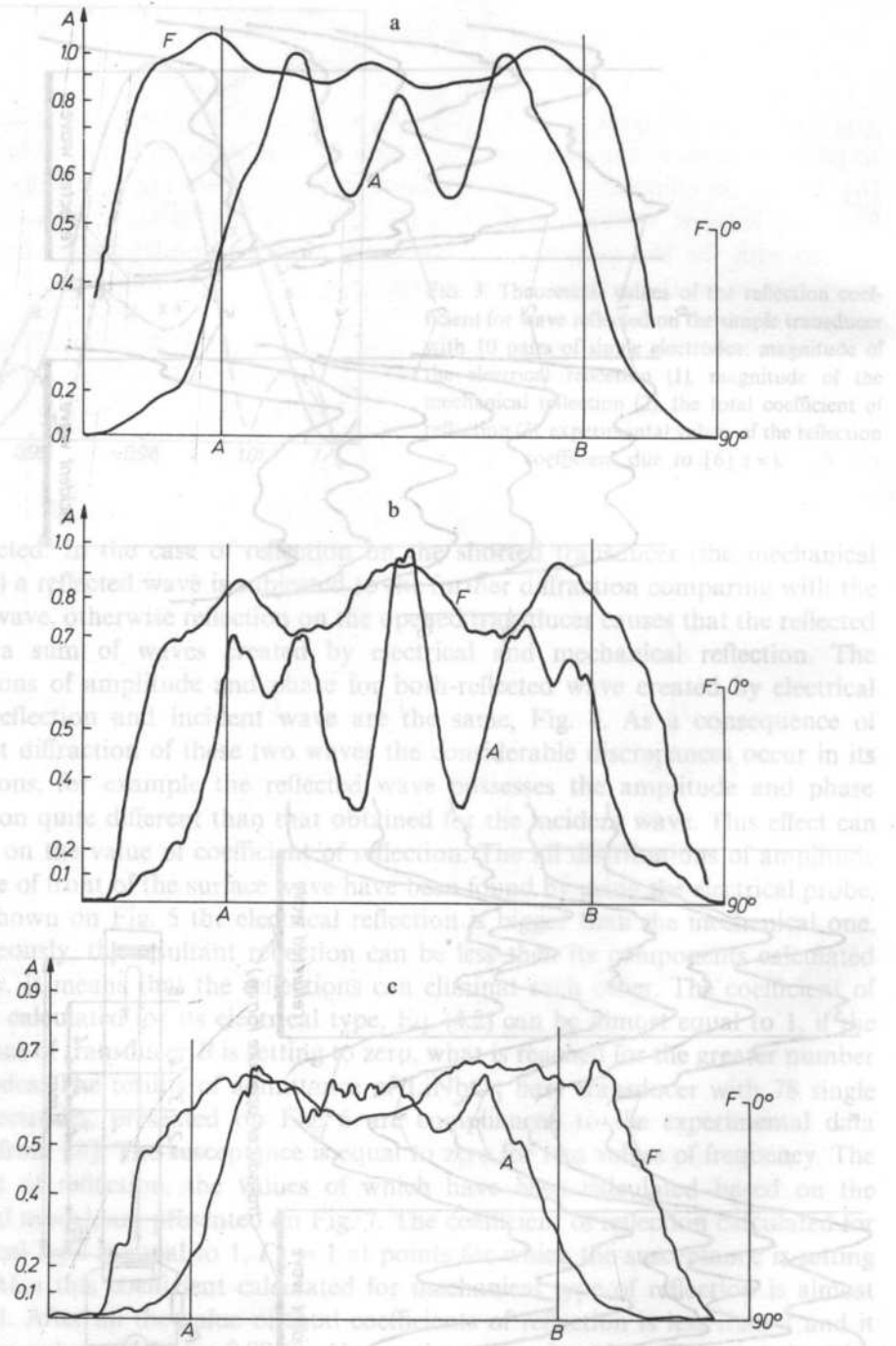

FIG. 5. Distributions of the amplitude (A) and phase (F) of surface wave incidenced (a) and reflected on the opened (b) and shorted (c) simple transducer with single electrodes located at the half distances between the transducers. The base material — $LiNbO_3$. A frequency is equal to 30 MHz

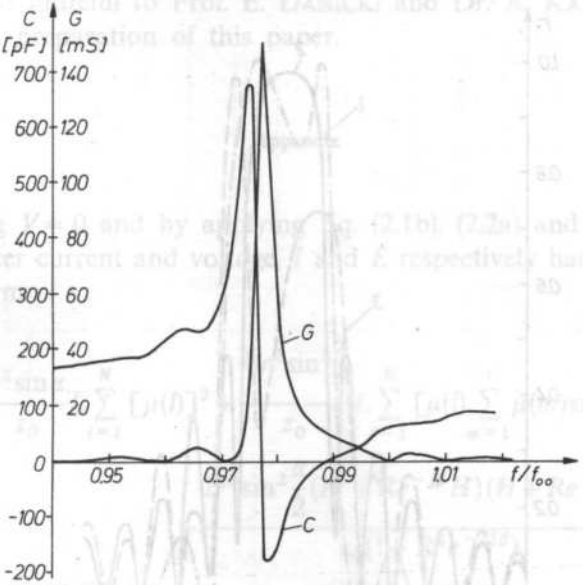

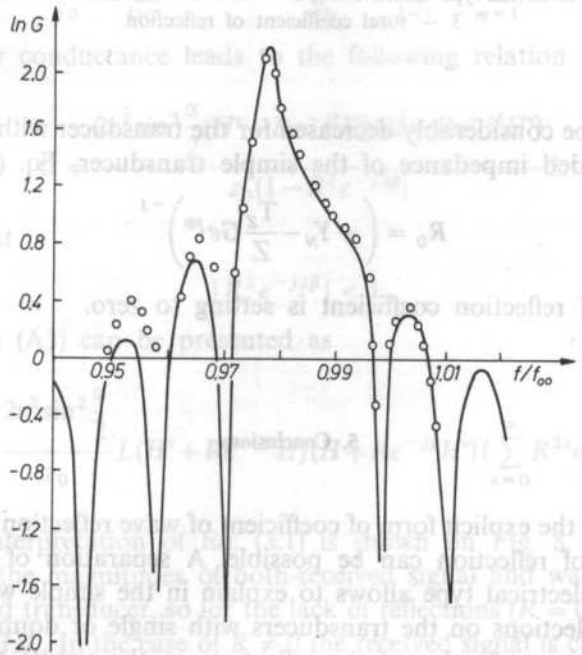

FIG. 6a. The theoretical admittance of the simple transducer with 78 single electrodes, aperture is equal to 0.225 mm. The base material – $LiNbO_3$; b) The experimental data of a conductance due to [8]

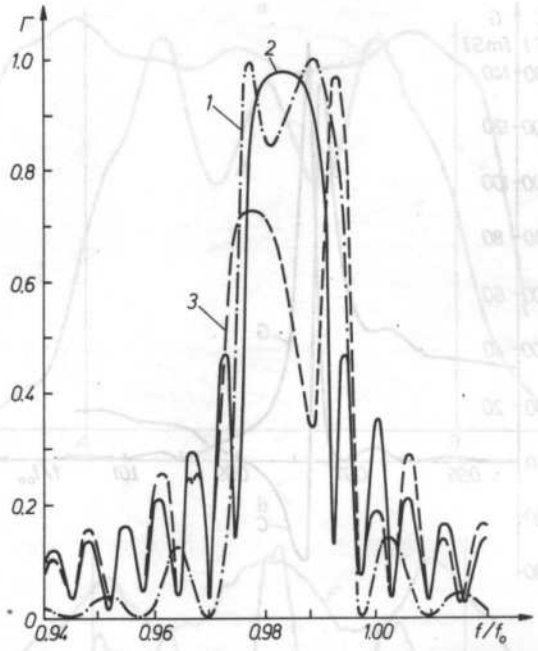

FIG. 7. The theoretical dependence between the reflection coefficients frequency presented on Fig. 5. 1 – coefficient of the electrical type of reflection, 2 – coefficient of the mechanical type of reflection, 3 – total coefficient of reflection

of coefficient can be considerably decreased for the transducer with single electrodes. Hence, if the loaded impedance of the simple transducer, Eq. (3.11) has a form

$$R_0 = \left(-Y_N - \frac{T_Z}{Z} G e^{j\Phi} \right)^{-1}$$

then the value of reflection coefficient is setting to zero.

5. Conclusions

By obtaining the explicit form of coefficient of wave reflection the exact analysis of phenomenon of reflection can be possible. A separation of reflection on the mechanical and electrical type allows to explain in the simple way the differences between wave reflections on the transducers with single or double electrodes. The considerably decrease of value of the reflection on the simple transducer can be reached by its load stimulation. It allows also to apply a transducer as the surface wave reflector.

The author is grateful to Prof. E. DANICKI and Dr. A. KAWALEC for helpful discussion in the preparation of this paper.

Appendix

By assuming $V=0$ and by applying Eq. (2.1b), (2.2a) and (3.2), the relation between transducer current and voltage, I and E respectively has been obtained in the following form

$$I=\left\{j\omega C+j\frac{r^2\sin\alpha}{z_0}L\sum_{i=1}^{N}[\mu(l)]^2+\frac{4jr^2\sin^2\frac{\alpha}{2}}{z_0}L\sum_{l=1}^{N}[\mu(l)\sum_{m=1}^{l}\mu(m)\sin(l-m)\alpha]+\right.$$

$$\left.+\frac{2r^2\sin^2\frac{\alpha}{2}(H^*+Re^{-j\beta}H)(H+Re^{-j\beta}H^*)}{z_0(1-R^2e^{-j2\beta})}L\right\}E \qquad \text{(A1)}$$

where L denotes the transducer aperture. Hence, a transducer susceptance is

$$B=\omega C+\frac{r^2\sin\alpha}{z_0}L\sum_{l=1}^{N}[\mu(l)]^2-\frac{4r^2\sin^2\frac{\alpha}{2}}{z_0}L\sum_{l=1}^{N}\mu(l)\sum_{m=1}^{l}\mu(m)\sin(l-m)\alpha \qquad \text{(A2)}$$

But a transducer conductance leads to the following relation

$$G=\frac{2r^2\sin^2\frac{\alpha}{2}(H^*+Re^{-j\beta}H)(H+Re^{-j\beta}H^*)}{z_0(1-R^2e^{-j2\beta})}L \qquad \text{(A3)}$$

By assuming that

$$|R^2e^{-j2\beta}|<1 \qquad \text{(A4)}$$

then the relation (A3) can be presented as

$$G=\frac{2r^2\sin^2\frac{\alpha}{2}}{z_0}L(H^*+Re^{-j\beta}H)(H+Re^{-j\beta}H^*)(\sum_{n=0}^{\infty}R^{2n}e^{-j2n\beta}) \qquad \text{(A5)}$$

The graphical interpretation of Eq. (3.1) is shown on Fig. 8. A conductance is proportional to the magnitudes of both-received signal and wave induced by the same considerated transducer, so for the lack of reflections ($R=0$) a conductance is proportional to HH^*. In the case of $R\neq 0$ the received signal is changed in terms of the waves to be reflected on the transducer boundary. The every n-th term of infinite series is related to the next twofold wave transmission in the area of whole transducer,

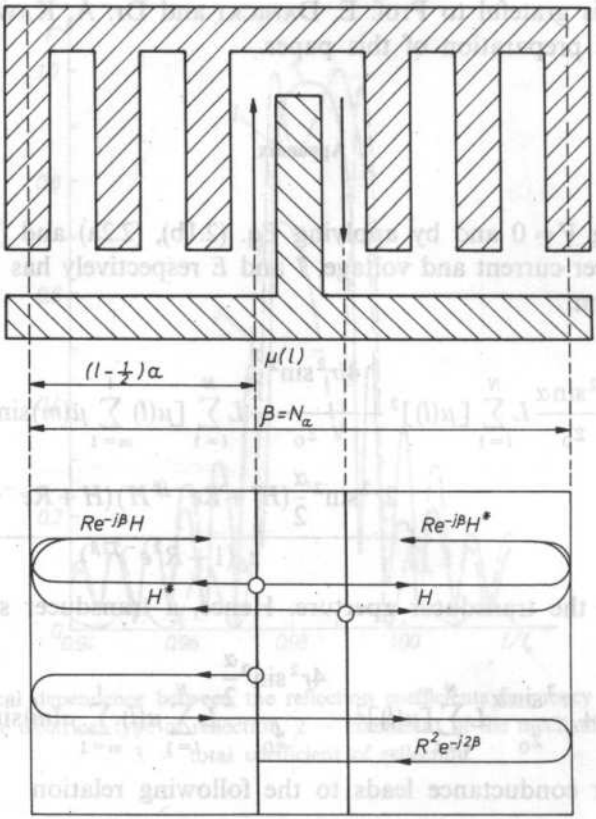

FIG. 8. The graphical interpretation of the components of transducer admittance in terms of the acoustics impedance variation in area of transducer

comparing with the prior (n-1st) term. By considering the simple regular transducer ($\mu_n = (-1)^n$) its conductance has a form

$$G = \frac{\omega\varepsilon_0\varepsilon_\infty k^2 L}{2P^2_{-s}(\cos\Delta)}\left(\frac{\sin Nx}{\operatorname{tg} x}\right)^2 \frac{1+j\dfrac{\omega-\omega_1}{\omega-\omega_3}\operatorname{tg} Nx}{1+j\dfrac{\omega-\omega_3}{\omega-\omega_1}\operatorname{tg} Nx} \tag{A6}$$

and a susceptance

$$B = \omega C_0 + \frac{\omega\varepsilon_0\varepsilon_\infty k^2 L}{2P^2_{-s}(\cos\Delta)}\sqrt{\frac{\omega-\omega_1}{\omega-\omega_3}}\,\frac{\sin 2Nx - 2N\operatorname{tg} x}{2\operatorname{tg}^2 x} \tag{A7}$$

because, due to [3]

$$\frac{r^2}{z_0} = \frac{\omega\varepsilon_0\varepsilon_\infty k^2}{2P^2_{-s}(\cos\Delta)}$$

where

$$X = \frac{\pi(\omega-\omega_1)(\omega-\omega_3)}{2\omega_1}$$

$$S = \frac{\omega}{2\omega_1}$$

and P_{-s} denotes the Legendre's polynomials. A conductance of refular transducer with double electrodes has a form

$$G = \frac{\omega\varepsilon_0\varepsilon_\infty k^2 L}{2P^2_{-s}(\cos\Delta)}\left(\frac{\sin Nx}{\operatorname{tg} x}\right)^2 \tag{A8}$$

and susceptance

$$B = \omega C_0 + \frac{\omega\varepsilon_0\varepsilon_\infty k^2 L}{2P^2_{-s}(\cos\Delta)}\left(\frac{\sin 2Nx - 2N\operatorname{tg} x}{2\operatorname{tg}^2 x}\right) \tag{A9}$$

therefore, the forms of both variables are well-known.

References

[1] W. P. MASON, Physical Acoustics, vol. 1A, Mir, 1966.

[2] W. R. SMITH et al., IEEE Trans. MTT, **17**, 11 (1969).

[3] E. DANICKI, J. FILIPIAK, WAT Report, **4**, 296 (1977).

[4] J. FILIPIAK, *The acoustics wave reflection on piezoelectric transducer in terms of the laminar system* (to be published).

[5] E. DANICKI, *Unified theory of interdigital transducer and SAW reflectors*, J. Tech. Phys., **21**, 3 (1980).

[6] A. J. DEVRIES, S. SUBRAMANIAN, Ultrasonics Symposium Proceedings, pp. 353–358, 1972.

[7] J. FILIPIAK, *Application of the electrical sounder to research on the surface wave in piezoelectrics* (to be published).

[8] W. R. SMITH, *Experimental distinction between crossed-field and in-line three-part circuit models for interdigital transducers*, IEEE Trans., vol. MTT-22, 11 (1974).

Received on June 5, 1988

ARCHIVES OF ACOUSTICS
15, 1–2, 137–149 (1990)

ON THE ACOUSTIC EMISSION IN MOISTED CONCRETS AND THE METHOD OF ITS PRACTICAL APPLICATION

W. KOŁTOŃSKI

Institute of Fundamental Technological Research, Polish Academy of Sciences
00–049 Warszawa, Świętokrzyska 21

The paper presents an attempt to explain mechanism of acoustic emission apperance due to water infiltration into the concrete. Experimental procedure of the *V* tests concerning this phenomenon is presented and obtained results are suported. Practical applications of the presented tests in civil engineering is also discussed.

Przedstawiono próbę wyjaśnienia mechanizmu pojawiania się emisji akustycznej pod wpływem procesu wsiąkania wody w beton. Zaprezentowano i omówiono wyniki badań doświadczalnych nad tym zjawiskiem oraz możliwości ich praktycznego wykorzystania do celów kontrolnych w budownictwie.

1. Introduction

Problems connected with obtaining sufficiently high tightness of buildings constructed nowadays oblige us to look for a new concepts and technologies applicable there. New research project conducted in Kielce branch of the IFTR is a part of this main trend. Investigations are concentrated on new technologies of joints, couplings and barriers together with their application in constructed structers. Experiments considering practical benefits obtained by their application are also conducted on the proper control stand.

Method signalizing water infiltration throughout poor tightenings is needed for this investigations.

Recent experiments as weell as years of observations showed that water infiltration into the concrete is accompanied by excitement of mechanical vibrations in a wide range of frequencies. These vibrations exhibit all the features of acoustic emission and can be applied as a source of information considering appearance and development of the water leaking from concrete precasts into the structure. Special investigations conducted as a project of the general 02.21 research program have been devoted to this problem. This paper presents their description and results.

2. Hypothetical mechanism of the acoustic emission appearance due to the water infiltration into the concrete

According to the commonly used definition, acoustic emission appears when the continuity of the structure of deformed material is destroyed. For this reason it should be examined in which way the water infiltration into the concrete can change its structure.

Professional literature considering technology of concrete its properties and applications does not pay too many attention to the processes taking place in the nature concrete due to its saturation with moisture. Such phenomenon as swelling of concrete, its shrinkage and corrosion are only generaly presented. The most information considering these processes can be found in the paper by Neville [8].

Water adsorption by a cement gel is the reason of concrete swelling. Water makes efforts to separate molecules of concrete evoking pressure of the extending nature. Water infiltration into the decomposed aggregate can be treated as another reason of concrete swelling. Magnitude of swelling mainly depends on the composition of concrete and its degree of moistness hightweighted concrets swell more than dense concrets. In concrete placed for good in the water swelling process is of continuous and long-lasting nature. It begins just after concrete is plunged in the water.

It is probable that the process of microcracks development within the cement building agent is one of the visible consequences of concrete swelling [2, 3, 9–11].

Drying of moistured concrete is accompanied by its shrinkage developing gradually from limit surfaces to interior of the object. Magnitude of shrinkage can varry with its propagation into the concrete mix. The so called heterogeneous shrinkage then takes place. It causes concrete cracking more often than usual shrinkage. Cracking of drying and shrinking concrete is a very slow process [6].

Concrete corrosion under the influence of water mainly consists in leaching and draining off outside components of binding material and in evoking chemical reactions leading to destruction of the concrete structure. Corrosion type phenomena mentioned above can disturb equilibrium of the hardened concrete and cause cracking. Nature and degree of concrete damage depend on the chemical constitution of water and the degree of its purity. Soft water without dissolved mineral salts has a great ability to leach calcium compounds [1, 4, 7].

Concrete strains briefly described above can disturb continuity of its texture and excite vibrations of the acoustic emission in the indirect way. On the other hand, when the basic aims of this paper formulates at the beginning are taken into account, swelling phenomenon seems to be of the greatest importance here. This phenomenon initiates just after water infiltration into the concrete begins and then reflects progress of this process. Suppositions presented herein concerned causes evoking acoustic emission of meistured concrets have their experimental confirmation.

3. Experiments

Formulation of relations between the water infiltration into the concrete and nature as well as intensity of the acoustic emission accompanying to this process have been the basic aim of the conducted experiments. Rectangular prism specimens 200×220 mm cross-section and different length, Fig. 1 of lightweight and dense

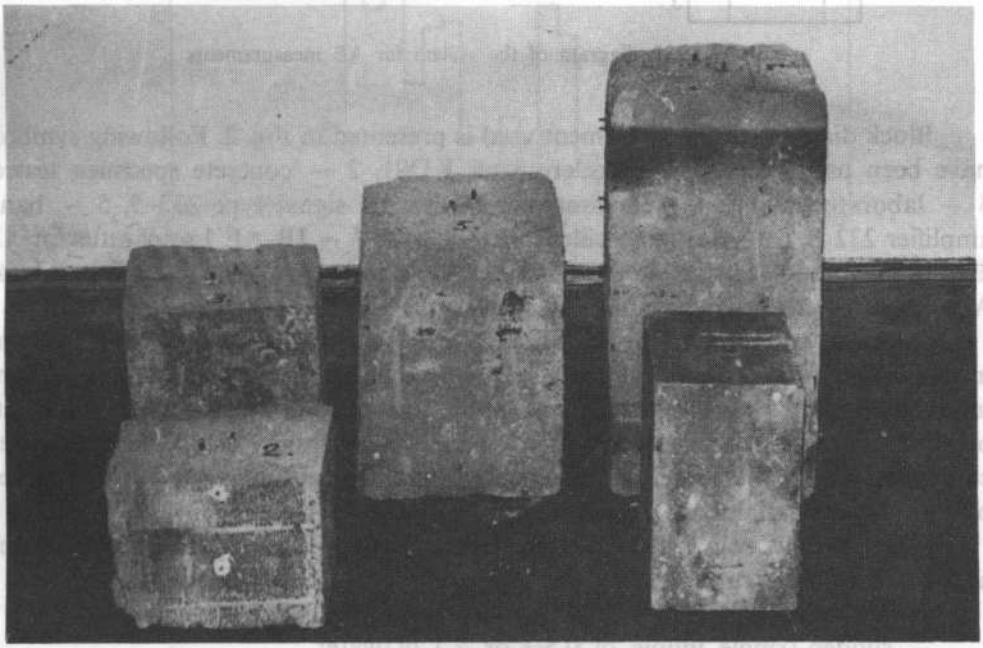

FIG. 1. General view of some concrete samples used for experiments

concrete have been used in tests. All the specimens have short metal bars inserted where needed with acoustic emission (AE) detectors attached to them. Level of the specimen natural AE has been the initial measurement of the experiment. This level has been compensated by the threshold sensitivity of the apparatus. Then specimens have been put in turn in the laboratory tank. Water inflowing the tank has been deaerated and its inflow has been under controll. Simultaneously event rate that is number of AE signals detected in a unit of time has been measured. Maximal amplitude of the signal in a unit of time has been also measured when circumstances allowed. Pictures of the selected AE signals have been photographed. Acoustic emission in the frequency range 15–100 kHz has been used in experiments. Necessity of environment disturbances elimination defined lower value of this band whereas the upper one has been imposed as the AE receiver transmitted band [5].

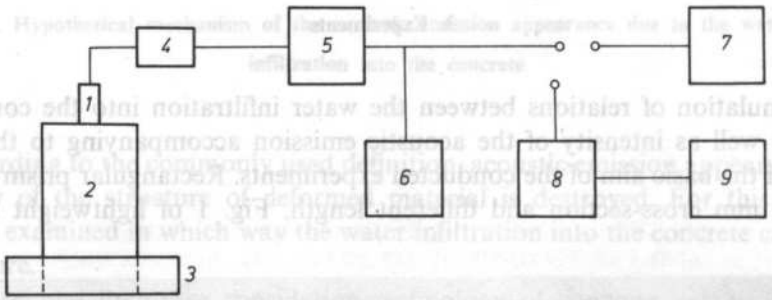

FIG. 2. Block diagram of the system for AE measurements

Block diagram of the equipment used is presented in Fig. 2. Following symbols have been used there: 1 – accelerometer KD91, 2 – concrete specimen tested, 3 – laboratory tank, 4 – preamplifier of the AE signal type 233–5, 5 – band amplifier 232 B, 6 – storage oscilloscope KR7401, 7 – IB–AE 1 apparatus for AE measurement and registration (own original construction), 8 – AE–3 apparatus for AE measurement (own original construction), 9 – B 72 BP analogue plotter.

IB–AE 1 apparatus equiped with IBICO type recorder allowed long-lasting measurement of the AE event rates. Measurement have been carried out in time intervals equal to 1 min, 10 min or 1 hour. Results have been printed. Measurements of short duration of event rate and maximal amplitude of events have been conducted for 10 s time intervals using AE-3 apparatus. Results have been registered by two-channel analogous recorder.

Water inflow below the concrete specimens used in experiments has been accomplished by two ways:

– constant, slow inflow 0.25 l or 1 per hour,
– sudden, single inflow of 0.5 l or 5 l of water.

The first one has been corresponding to the situation when the elements of a building such as walls or ceilings are subjected to the infiltration of water due to badly constructed isolation and long lasting raining or snow melting. The second one has reconstructed results of the rapid shower jointed with stormy wind. Changing intensity of walls and roof sevatering is characteristic for this kind of wheather.

4. Experimental results

Examples of the $\dot{N}_e$ event rate changes registered by the IBAE 1 apparatus for 1 minute time intervals in 1 l/h constant water inflow below the dense concrete sample of small porosity and lightweight concrere sample of high porosity are shown in figures 3 and 4. AE level is significantly lower for the inflow equal to 0.25 l/h. This fact is presented in Figs. 5 and 6 by curves plotted for lightweight and dense concrete.

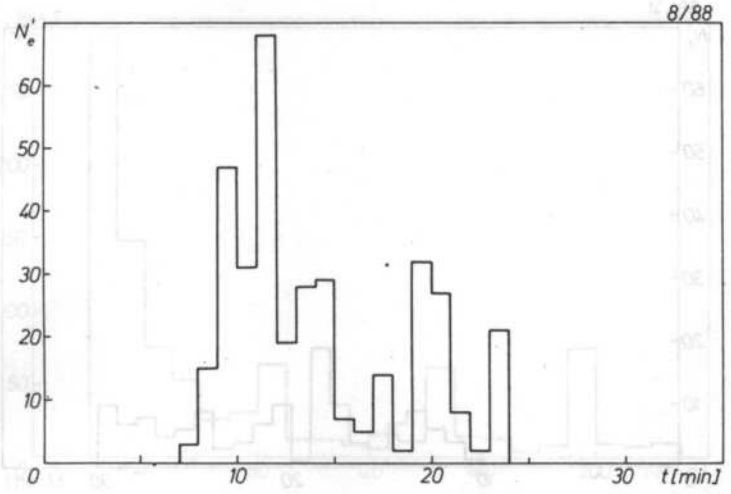

FIG. 3. Results of the measurement of $\dot{N}_e$ event rate conducted for dense concrete of low porosity with water influx equal 1 l/h per hour

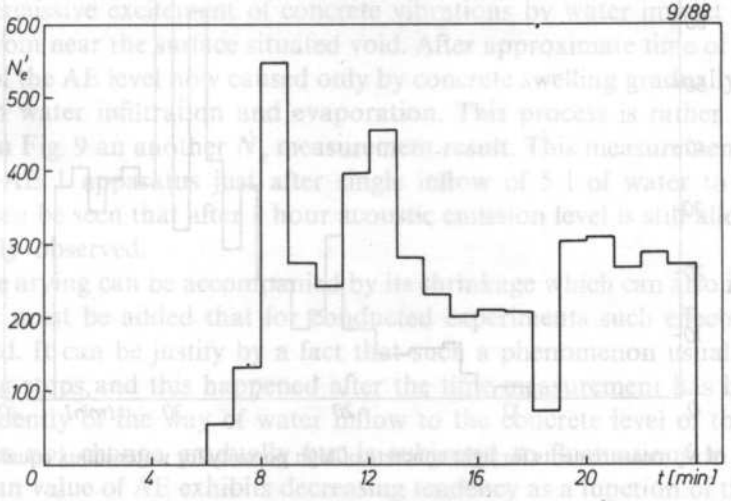

FIG. 4. Results of $\dot{N}_e$ measurements for light concrete of high porosity for water influx equal 1 l per hour

Examples of the results of the $\dot{N}_e$ measurements presented above concern the observations conducted in 30 minutes time periods. Observation time has been so short here because the basic aim of these experiments was to proof that acoustic emission appears soon after water begins to infiltrate into the concrete. Durability and course of this phenomenon in time has been investigated by measurements carried in a few hours, see Fig. 7, for time interval equal to 10 min.

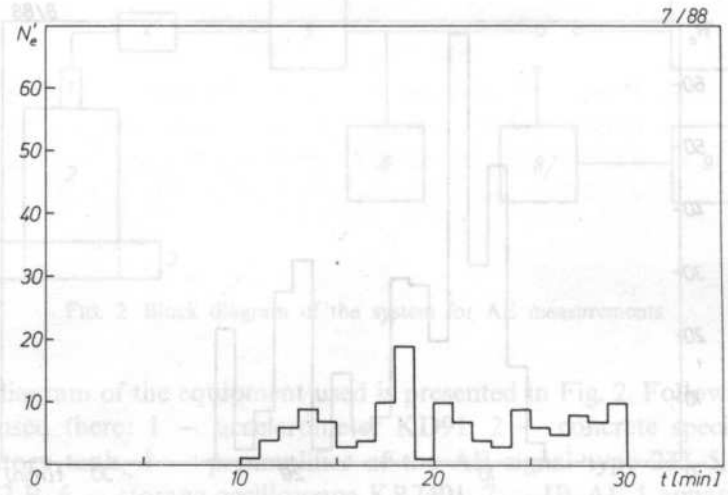

FIG. 5. Results of $\dot{N}_e$ measurement for dense concrete of low porosity for water influx equal 0.25 l per hour

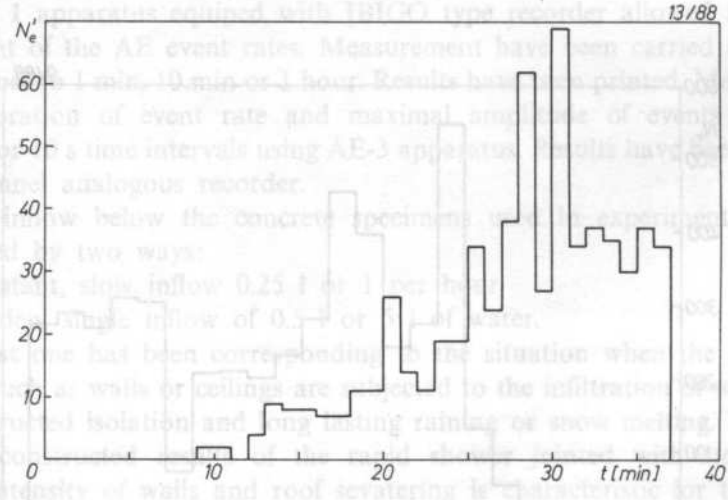

FIG. 6. Results of $\dot{N}_e$ measurements for light concrete of high porosity for water influx equal 0.25 l per hour

In the case of constant slow inflow of water into the concrete, level of AE grows rapidly from the moment of its initiation the seaches maximum and next significantly falls down to be of a variable nature in the end. Peak of the AE level mentioned here can be caused by air pushing out from the concrete subsurface pores by water. Time in which acoustic emission apears and rate of its growth depends on the quantity of water supplied and on porosity of concrete.

Changes of the AE level are completly different in the case of sudden, single water inflow to the concrete. Example is presented in Fig. 8. This figure presents analogous $\dot{N}_e$ record as well as record of AM maximal amplitude measured by AE–3

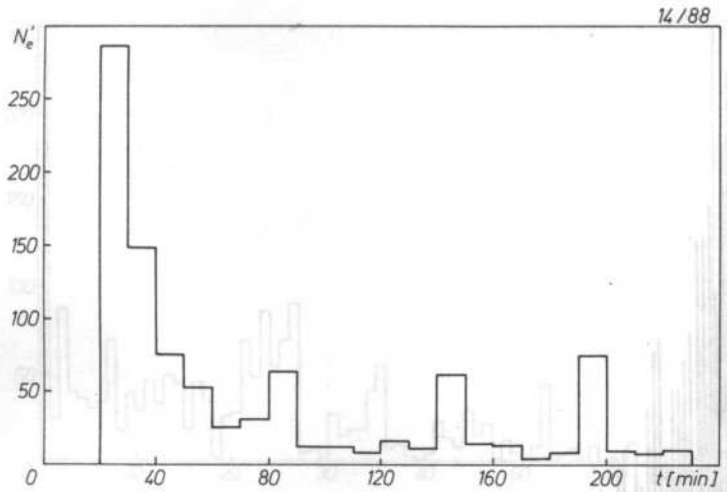

FIG. 7. Results of $\dot{N}_e$ measurements for light concrete after single influx of 1.5 l of water

apparatus for 10 s time intervals. Measurements have been done after single inflow of 5 l of water to lightweight concrete. Initial significant increase of the AE level is caused by percussive excitement of concrete vibrations by water impact and water pushing up from near the surface situated void. After approximate time of 2 to 3 min mean value of the AE level now caused only by concrete swelling gradually decreases together with water infiltration and evaporation. This process is rather long what can be seen in Fig. 9 an another $\dot{N}_e$ measurement result. This measurement has been done by IB–AE 1 apparatus just after single inflow of 5 l of water to the dense concrete. It can be seen that after 1 hour acoustic emission level is still allowed to be experimentally observed.

Concrete arying can be accompanied by its shrinkage which can also initiate AE vibrations. It must be added that for conducted experiments such effects have not been observed. It can be justify by a fact that such a phenomenon usually appears when swelling stops and this happened after the time measurement has been done.

Independently of the way of water inflow to the concrete level of the acoustic emission does not change gradually but is subjected to fluctuations in changing, although mean value of AE exhibits decreasing tendency as a function of time. It can be understood as evidence of irregularity of swelling process of the binding agent, and forming microcracks in that. Intensity of this process decreases with extending of the moistured zone. The increase of the AE signal is not a problem here because AE sources are aproachingthe receiver with extending of the moistured zone so the AE level should grow.

Except of the information considering leakage appearence acquaintance of the range of moistured region is the second important information of practical value. Information concerning situation of this zone with respect to the position of observation is peculiarly helpful here.

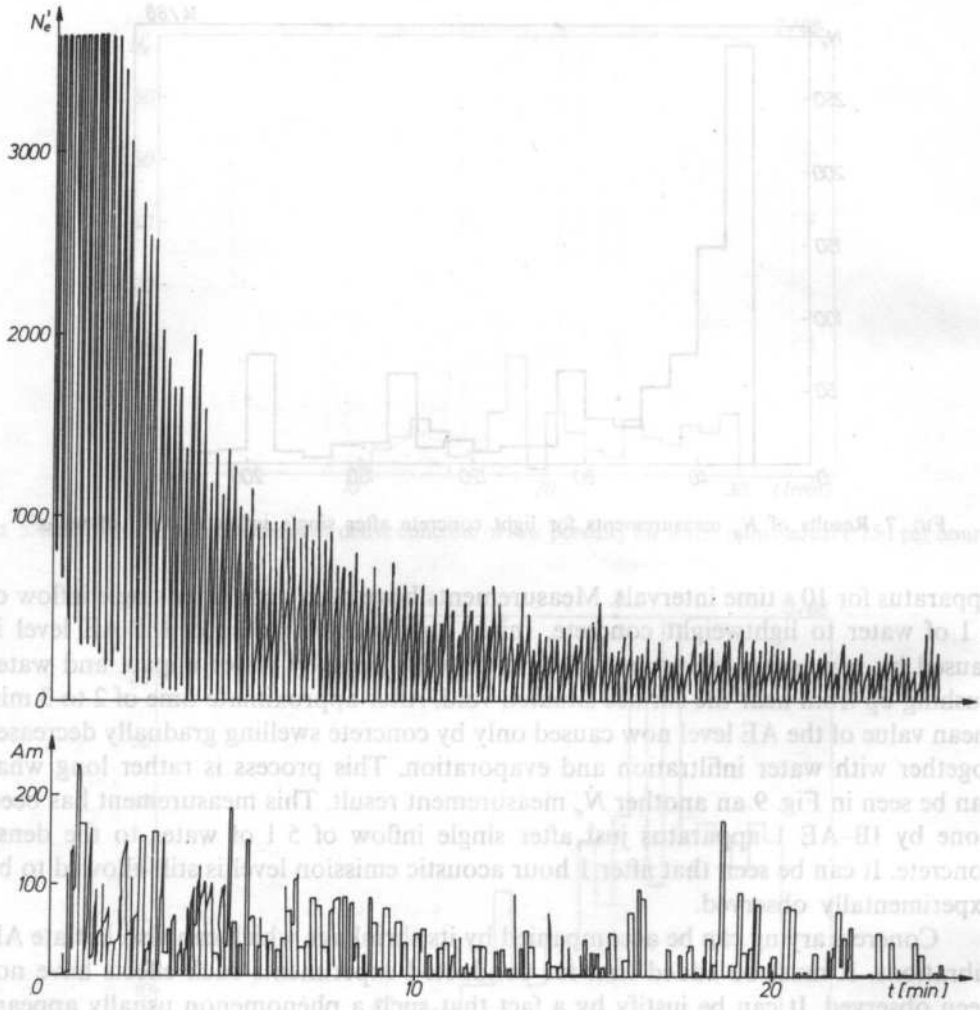

FIG. 8. Analog record of the $\dot{N}_e$ measurement result and maximal amplitude Am of the AE signal after single influx of 5 l of water to the sample of light concrete of a 0.15 m

An attempt to solve this problem has been based an application of relations between AE parameters and distance of its sources of signals from their receivers. To investigate this relations specimens of a 220×220 cross section area and different length have been used. All the specimens have been prepared of the same concrete. It has been assumed that sources of acoustic emission are activated when wall of the specimen contacts with water and within a few minutes time after it. Activation process takes place only in nearest part of the moistured zone that is near this wall. Such an assumption has been practically verified. If AE receiver is placed on the opposite wall of the specimen then the specimen length equals to the distance between sources of AE signals and their receiver.

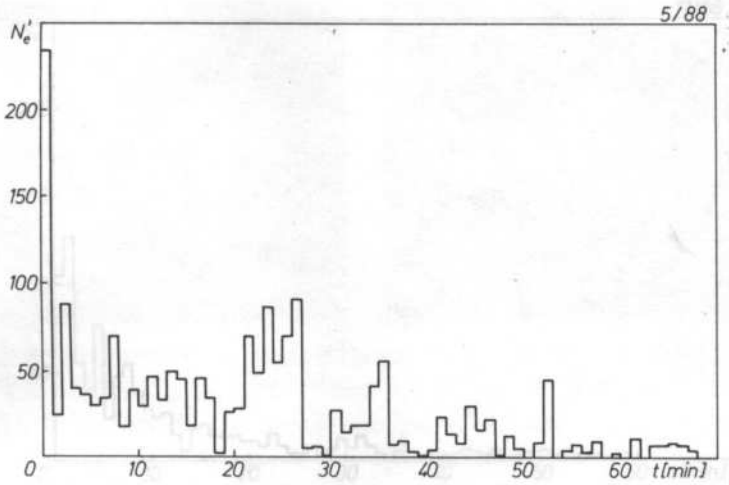

FIG. 9. Result of the $\dot{N}_e$ measurement after single influx of $\dot{5}$ l of water to the sample of dense concrete of a length 0.15 m

N_e and Am measurements have been conducted for analogous testing conditions for samples of growing length when their wall contact with water. Image of the received AE signals have been photographed. Results of measurements are presented in Figs. 8, 10, 11, 12 and 13. First three of them concern. light concrete specimens of a length equal to 0.15, 0.31 and 0.85 m whereas additional two – dense concrete specimens of a length 0.35 and 0.85 m. The increase of AE attenuation with the increasing of the way of the acoustic wave can be seen. It can b supposed that AE signals coming from sources sittuated in distance greater than 1 m of the receiver cannot be registered. In this way AE level can indicate how long is a distance between the place of observation and boundary of moistured zone.

Energy of the AE signal diminishes when the length of its way grows. Spectrum and fundamental frequency of this signal is not constant but changes with this length. It happens due to filtering properties of concrete. Images of two typical AE signals obtained for moistured dense concrete can be seen in Figs. 14 and 15. First signal has been received from the distance of 0.15 m whereas the second one – 0.85 m. Images of three additional typical AE signals but obtained for light weight concrete and received from the distance of 0.15 m, 0.31 m and 0.85 m are shown in Fig. 16, 17 and 18. In the case of dense concrete, increasing length of the way causes change fundamental frequency of AE signal from 30 kHz to 15 kHz. For lightweight concrete corresponding change is from 25 kHz to 7.5 kHz. It must be added here that frequencies lower below than 15 kHz are damped by the apparatus. Apart of this fundamental frequency of the AE signal and, after all, its spectrum can be treated as information concerning the situation of a moistured region boundary with respect to the place of AE reception.

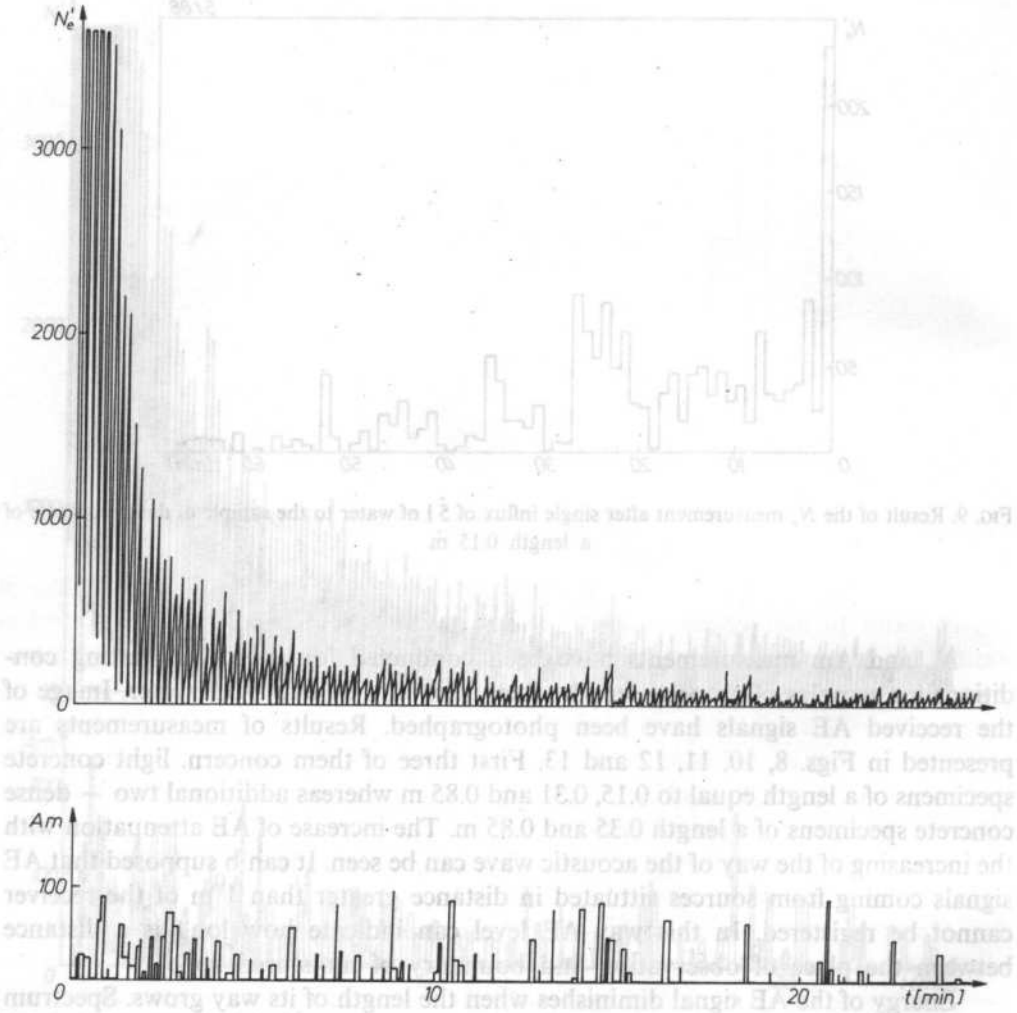

FIG. 10. Analog record of the $\dot{N}_e$ measurement result and Am for the sample of light concrete of a length 0.31 m

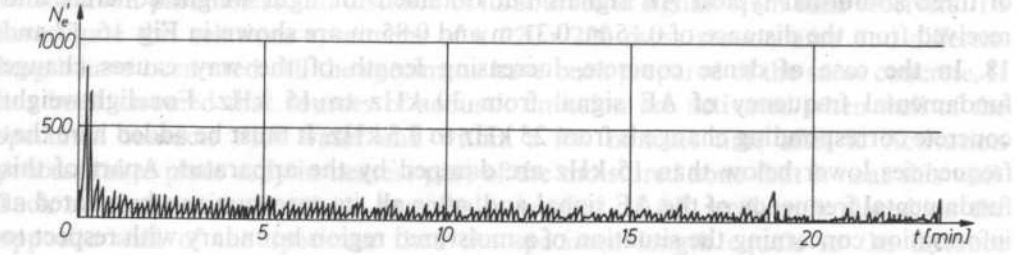

FIG. 11. Analog record of the $\dot{N}_e$ measurement result for a sample of light concrete of a length 0.85 m

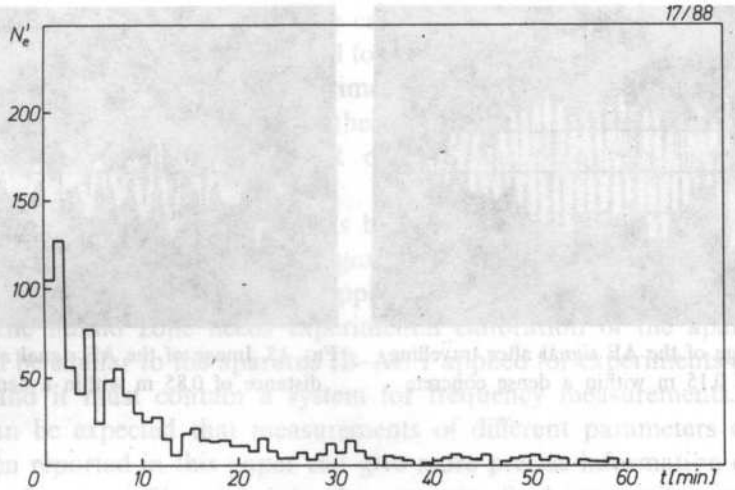

FIG. 12. Results of $\dot{N}_e$ measurement for a sample of dense concrete of a length 0.35 m

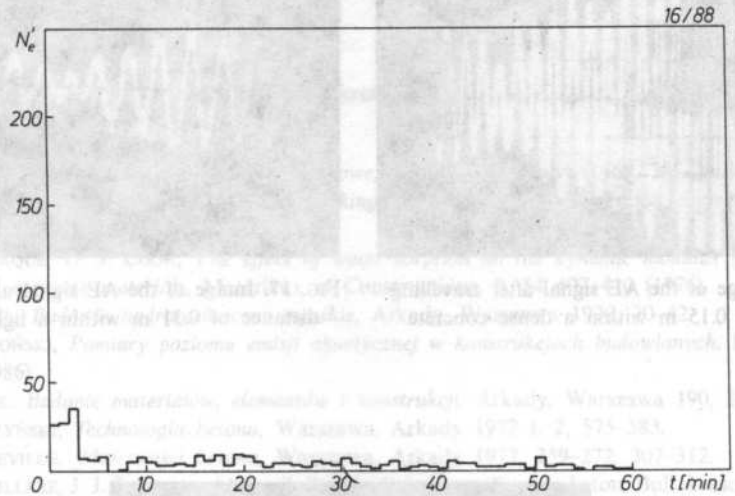

FIG. 13. Results of $\dot{N}_e$ measurement for a sample of dense concrete of a length 0.85 m

5. Conclusions

1. Performed experiments gave evidence supporting assumption presented at the beginning of this paper that acoustic emission accompanying water infiltration into the concrete is caused by its swelling. Fact, that the both acoustic emission and swelling appear with initiation of water infiltration and grow with concrete porosity and its humidity (see Sec. 2) is the reason of this statement.

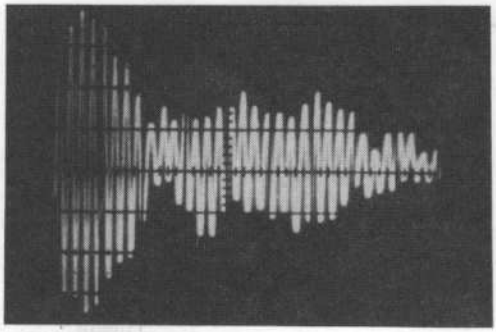

FIG. 14. Image of the AE signal after travelling distance of 0.15 m within a dense concrete

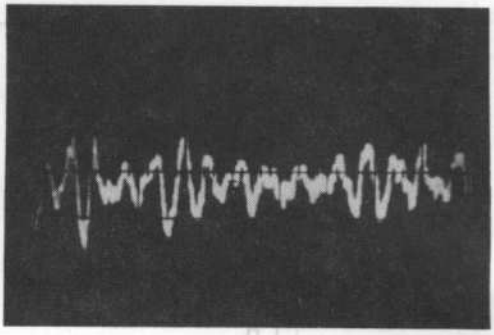

FIG. 15. Image of the AE signal after travelling distance of 0.85 m within a dense concrete

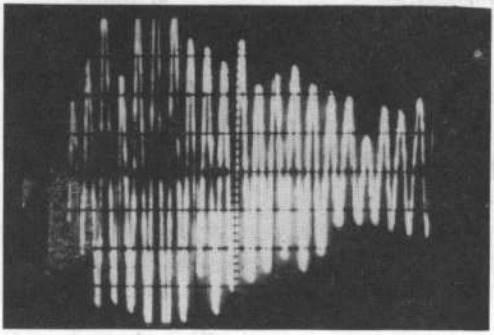

FIG. 16. Image of the AE signal after travelling distance of 0.15 m within a dense concrete

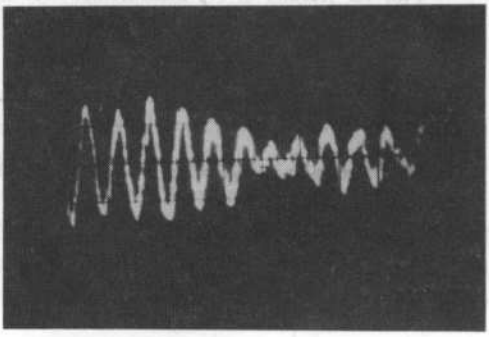

FIG. 17. Image of the AE signal after travelling distance of 0.31 m within a light concrete

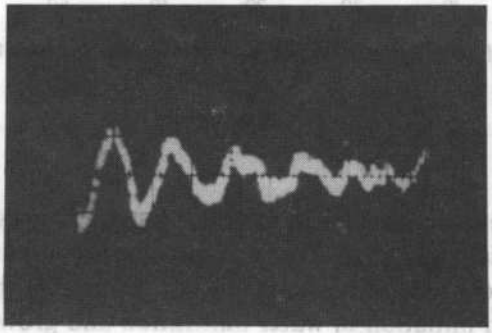

FIG. 18. Image of the AE signal after travelling distance of 0.85 m within a light concrete

2. Measurements of AE event rate can be applied at test stands for remote signalling occurence of water leaking and for observation of its consequences. This is peculiarly helpful in the case of experimental objects such as models of joints, partitions and other structures where their lightness is needed. Aparatus IB–AE 1 constructed and made in the IFTR of PAS has been very usefull for this experiments.

3. Magnitude of $\dot{N}_e$ level as well as basic frequency of the AE signal are the approximate indicators of the humid region boundary with respect to the place of observation at the test stand. Practical applicstion of this AE parameters to defining the size of the humid zone needs experimental calibration of the aparatus. This aparatus can be similar to the aparatus IB–AE 1 applied for experiments reported in this paper and it must contain a system for frequency measurements.

4. It can be expected that measurements of different parameters of acoustic emission then reported in this paper can give more precise information concerning the process of water infiltration into the concrete. Such parameters as maximal amplitude of acoustic emission, its energy and frequency spectrum of the signal could be applied. For this reason, the experiments reported in this paper should be continued.

References

[1] W. BALCERSKI, *Budownictwo wodne śródlądowe*, Arkady, Warszawa 1969, 38–43.

[2] R. H. EVANS, M. S. MARATHE, *Microcracking and stress-strain curves for concrete in tension*, Matèriaux et Structures, 1, 61—64 (1968).

[3] M. N. HAQUE, D. J. COOK, *The effect of water sorption on the dynamic modulus if elasticity of dessicated concrete materials*, Matèriaux et Constructions, **9**, 54 407–410 (1976).

[4] S. HÜCKEL, *Budowle hydrotechniczne morskie*, Arkady, Warszawa 1970, 20–42.

[5] W. KOŁTOŃSKI, *Pomiary poziomu emisji akustycznej w konstrukcjach budowlanych*, Inż. i Bud. 3, 95–97 (1986).

[6] R. KOZAK, *Badanie materiałów, elementów i konstrukcji*, Arkady, Warszawa 190, 244–246.

[7] W. KUCZYŃSKI, *Technologia betonu*, Warszawa, Arkady 1972 t. 2, 575–583.

[8] A. M. NEVILLE, *Właściwości betonu*, Warszawa, Arkady 1977, 259–272, 307–312.

[9] A. M. PAILLERE, J. J. SERRANO, Appareil d'etude de la fissuration du beton, Bull. Liason Labo. P. et Ch. **83**, 29–38 (1976).

[10] G. ROBINSON, *Methods of detecting the formation and propagation of microcracks in concrete*, Intern. Conf. on the Structure of Concrete, Session C, 131–145 (1966).

[11] M. TERRIAN, Emission acoustique et comportement mecanique post-critique d'un beton sollicitéen traction, Bull. Liaison Labo. P. et Ch., 105, 2398, 65–72 (1980).

Received on February 14, 1989

ARCHIVES OF ACOUSTICS
15, 1–2, 151–183 (1990)

DIFFRACTION BY AN IMPEDANCE HALF-PLANE – DEPENDENCE ON THE IMPEDANCE PARAMETER

H. KUDREWICZ

Institute of Fundamental Technological Research Polish Academy of Sciences
(00-049 Warszawa Świętokrzyska 21

The problem of plane wave diffraction by an impedance half-plane is considered. The aim of the paper is to analyze how the solution depends on the complex impedance parameter η. The Senior solution is analytically continued from real positive values of the parameter onto the two-sheeted Riemann surface η. It is shown that the result of the analytic continuation has two branch points of the first order and one pole. The pole is related to incidence angle of the plane wave. The proper choice of the branch is uniquely determined from the outgoing wave condition. Different types of surface waves excited on the impedance half-plane are also discussed.

Praca dotyczy problemu dyfrakcji fali płaskiej na impedancyjnej półpłaszczyźnie. Celem jej jest przeanalizowanie zależności rozwiązania od zespolonego parametru impedancyjnego η. Rozwiązanie Seniora skonstruowane dla wartości rzeczywistych parametru przedłużono analitycznie względem tego parametru. Otrzymano dwupłatową powierzchnię Riemanna η z dwoma punktami rozgałęzienia i biegunem, który jest związany z kątem padania fali płaskiej. Korzystając z warunku fali wybiegającej wyznaczono jednoznacznie gałąź, dla każdej wartości parametru należącej do płaszczyzny zmiennej zespolonej z cięciem. Przedyskutowano występowanie i zależność fali powierzchniowej od parametru.

1. Introduction

This paper is concerned with qualitative study of the solution to the problem of electromagnetic wave diffraction by an impedance half-plane. The analyzed solution is here found by using the Wiener-Hopf method and is expressed by the Fourier-type integral. The factorization is achieved by the Cauchy-type integrals. The function to be factorized depends on the impedance parameter η, and so do the factor functions. We examine the dependence of the solution on this parameter. The same solution was found by SENIOR [1] in 1952. We shall henceforth refer to the solution as the Senior solution.

The factor function is continued analytically with respect to η. A new

representation of this function is obtained. It takes the form of a Cauchy-type integral along a ray in the complex plane.

The result of the continuation is that the Senior solution is analytically continued from real positive η, onto a two-sheeted Riemann surface with two branch-points and one pole. Thus, the continuation produces two possible branches of the solution. The proper branch is chosen using the outgoing wave condition. The solution is valid for both passive and active impedances. The analysis also shows the possibility of excitation of different types of surface waves on the impedance half-plane.

Formulation of the problem is given in Sections 2–3. Section 4 is concerned with mappings of the Riemann surfaces on which the functions involved are defined. Those mappings form a basis for further analysis. In Section 5 the method of analytic continuation of Cauchy-type integrals is given. In Section 6–8 the method is applied to the analytic continuation of factor function depending on two complex variables.

The extension of the Senior solution onto two-sheeted Riemann surface is described in Section 9. Different types of surface waves that emerge from the analysis are discussed in Section 10. Finally, in Appendix A index evaluation of the factorized function is given, and in Appendix B explicit formulas for the factor function are obtained.

2. Formulation of electromagnetic problem

An electromagnetic plane wave $\mathbf{E}^{(i)}$, $\mathbf{H}^{(i)}$ is incident upon an impendance half-plane at an angle Φ_0 to the x-axis, Fig. 1. The direction of propagation is normal

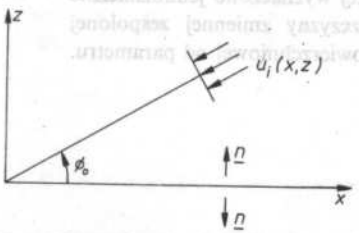

FIG. 1. Geometry of the diffraction problem

to the diffracting edge. The incident plane wave satisfies the Maxwell equations

$$\nabla \times \mathbf{H} = -i\omega\varepsilon\mathbf{E}, \quad \nabla \times \mathbf{E} = i\omega\mu\mathbf{H}. \tag{2.1}$$

A time dependence $e^{-i\omega t}$ is assumed and suppressed throughout.

The impedance half-plane is described by the Leontovich condition

$$\mathbf{n} \times \mathbf{E} = \eta Z[\mathbf{n} \times (\mathbf{n} \times \mathbf{H})], \tag{2.2}$$

where $\mathbf{n}$ is the unit outward normal to the half-plane, $Z = \sqrt{\mu/\varepsilon}$ is the intrinsic impedance of free space, η is the reciprocal of the complex refractive index of the half-plane relative to free space.

The impedance parameter is generally a complex number. If $\operatorname{Re}\eta \geqslant 0$ then the impedance is passive, if $\operatorname{Re}\eta < 0$ then the impedance is active. The value $\eta = 0$ corresponds to a perfectly conducting half-plane.

The total field is a sum of the incident field and a scattered field $E^{(s)}$, $H^{(s)}$. It satisfies the Maxwell equations (2.1) in the whole space, and the Leontovich boundary condition on the half-plane. In addition the scattered field should obey the edge condition and the condition at infinity.

For the purpose of this paper those conditions are formulated in the following way:

(1) each scattered field component $E_j^{(s)}$, $H_j^{(s)}$, $j = x, y, z$, is an integrable function of ϱ (where $x = \varrho\cos\theta$, $z = \varrho\sin\theta$) in a neighbourhood of the point $\varrho = 0$, for every θ, and

(2) the scattered field contains only outgoing waves at infinity.

The above formulation of the edge condition is equivalent to the well known condition that $\int_\tau (\varepsilon|\mathbf{E}^{(s)}|^2 + \mu|\mathbf{H}^{(s)}|^2)\,d\tau = \text{finite}$, [2], provided that each field component is of the form $\varrho^p\Phi(\theta)$, where $\Phi(\theta)$, y) is a bounded function and p is a real number, τ is a finite region of space surrounding the edge.

Splitting the field into TM (transverse magnetic) and TE (transverse electric) in the edge direction, we split the problem into two separate cases: TM, called also E polarization, where

$$\mathbf{E} = (0, E_y, 0), \quad \mathbf{H} = (H_x, 0, H_z). \tag{2.3}$$

and TE, called also H polarization, where

$$\mathbf{H} = (0, H_y, 0), \quad \mathbf{E} = (E_x, 0, E_z). \tag{2.4}$$

For each polarization the electromagnetic field (2.1) can be expressed by one scalar function u satisfying the Helmholtz equation

$$\nabla^2 u + k^2 u = 0, \tag{2.5}$$

where $k^2 = \omega^2\varepsilon\mu$.

For E polarization there is

$$E_y = u, \quad H_x = \frac{i}{\omega\mu}\frac{\partial u}{\partial z}, \quad H_z = -\frac{i}{\omega\mu}\frac{\partial u}{\partial x}. \tag{2.6}$$

For H polarization there is

$$H_y = u, \quad E_x = -\frac{i}{\omega\varepsilon}\frac{\partial u}{\partial z}, \quad E_z = \frac{i}{\omega\varepsilon}\frac{\partial u}{\partial x}. \tag{2.7}$$

From the Leontovich condition we obtain

$$u - i\frac{\eta}{k}\frac{\partial u}{\partial z} = 0 \quad \text{for} \quad z = 0_+, \quad x > 0$$
$$u + i\frac{\eta}{k}\frac{\partial u}{\partial z} = 0 \quad \text{for} \quad z = 0_-, \quad x > 0, \tag{2.8}$$

for E polarization, and

$$u - i\frac{1}{\eta k}\frac{\partial u}{\partial z} = 0 \quad \text{for} \quad z = 0_+, \quad x > 0$$
$$u - i\frac{1}{\eta k}\frac{\partial u}{\partial z} = 0 \quad \text{for} \quad z = 0_-, \quad x > 0 \tag{2.9}$$

for H polarization.

Thus, on replacing η by $\frac{1}{\eta}$ in formulas describing the field for E polarization, we obtain the field for H polarization, and vice versa.

3. *E* polarization

The incident wave is in the form

$$u_i(x, z) = e^{-ik(x\cos\Phi_0 + z\sin\Phi_0)}. \tag{3.1}$$

We seek the solution of (2.5), (2.8), (3.1) as a sum of the incident wave $u_i(x, z)$ and the scattered field $u_s(x, z; \eta) = u_s$

$$u(x, z; \eta) = u_i(x, z) + u_s(x, z; \eta). \tag{3.2}$$

The scattered field satisfies the Helmholtz equation (2.5), where u_s is put in place of u, with boundary conditions for $x > 0$:

$$u_s - i\frac{\eta}{k}\frac{\partial u_s}{\partial z} = -(1 - \eta\sin\Phi_0)e^{ix\alpha_0} \quad \text{for} \quad z = 0_+$$
$$u_s - i\frac{\eta}{k}\frac{\partial u_s}{\partial z} = -(1 + \eta\sin\Phi_0)e^{ix\alpha_0} \quad \text{for} \quad z = 0_-, \tag{3.3}$$

where

$$\alpha_0 = -k\cos\Phi_0. \tag{3.4}$$

We seek the solution to the problem (2.5), (3.3) in the class of functions such that, via (2.6), the edge condition and condition at infinity are fulfilled.

3.1. *The method of solution*

We find the solution for a real η satisfying $0 < \eta < \infty$. We assume that $u_s(x, z; \eta)$ has the following plane wave spectral representation

$$u_s(x, z; \eta) = \int_Q A(\alpha, \eta) e^{i\alpha x} e^{i\gamma z} d\alpha \quad \text{for} \quad z \geqslant 0,$$
$$u_s(x, z; \eta) = \int_Q B(\alpha, \eta) e^{i\alpha x} e^{-i\gamma z} d\alpha \quad \text{for} \quad z \leqslant 0, \tag{3.5}$$

where

$$\gamma = \sqrt{k^2 - \alpha^2}. \tag{3.6}$$

For the unique and continuous relation between α and γ, the variable α belongs to the two-sheeted Riemann surface with branch points $\alpha = \pm k$. The contour Q extends from $-\infty$ to ∞. The necessary condition of convergence of the integrals (3.5) for every x and z has the form

$$\operatorname{Im}\alpha = 0, \quad \operatorname{Im}\gamma > 0 \quad \text{as} \quad |\alpha| \to \infty. \tag{3.7}$$

The Riemann surface α is cut along the lines Γ_0, Γ_π, as in Fig. 2. The sheets are distinguished by the choice

$$\sqrt{k^2 - \alpha} = k \quad \text{for} \quad \alpha = 0 \quad \text{on sheet } \alpha_I, \tag{3.8a}$$

and

$$\sqrt{k^2 - \alpha^2} = -k \quad \text{for} \quad \alpha = 0 \quad \text{on sheet } \alpha_{II}. \tag{3.8b}$$

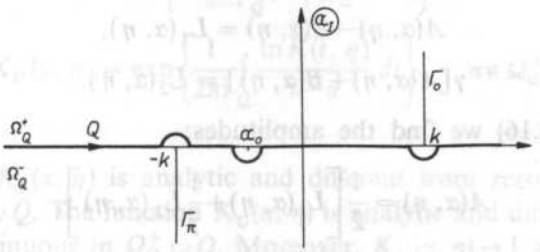

FIG. 2. The α-plane cut along Γ_0, Γ_π lines and the contour Q

The contour Q satisfying (3.7) is put along the real axis of α_I sheet, except for indentations at $\alpha = \pm k$ and $\alpha = \alpha_0$, as in. Fig. 2.

Denote by Ω_Q^+ the domain above (to the left of) the contour Q, and by Ω_Q^- the domain below (to the right of) the contour Q.

Putting (3.5) into boundary conditions (3.3) and into the condition of continuity of the total field and its normal derivative in the aperture $x < 0$, $z = 0$, we get the following integral equations for $A(\alpha, \eta)$, $B(\alpha, \eta)$:

$$\int_Q (1+\frac{\eta}{k}\gamma)\, A(\alpha,\eta)e^{i\alpha x}d\alpha = -(1-\eta\sin\Phi_0)e^{i\alpha_0 x} \quad \text{for} \quad x>0 \tag{3.9}$$

$$\int_Q (1+\frac{\eta}{k}\gamma)\, B(\alpha,\eta)e^{i\alpha x}d\alpha = -(1+\eta\sin\Phi_0)e^{i\alpha_0 x} \quad \text{for} \quad x>0 \tag{3.10}$$

$$\int_Q [A(\alpha,\eta)-B(\alpha,\eta)]e^{i\alpha x}d\alpha = 0 \quad \text{for} \quad x<0, \tag{3.11}$$

$$\int_Q \gamma[A(\alpha,\eta)+B(\alpha,\eta)]e^{i\alpha x}d\alpha = 0 \quad \text{for} \quad x<0. \tag{3.12}$$

There exists a solution of each of these equations according to the following Lemmas:

LEMMA 1. If the point α_0 lies in Ω_Q^+, there exists a solution of the equation (3.9) ((3.10)) such that

$$\left(1+\frac{\eta}{k}\gamma\right)A(\alpha,\eta) = \bar{U}_1(\alpha,\eta)-\frac{1}{2\pi i}\frac{1-\eta\sin\Phi_0}{\alpha-\alpha_0}, \tag{3.13}$$

$$\left(1+\frac{\eta}{k}\gamma\right)B(\alpha,\eta) = \bar{U}_2(\alpha,\eta)-\frac{1}{2\pi i}\frac{1+\eta\sin\Phi_0}{\alpha-\alpha_0}, \tag{3.14}$$

where $\bar{U}_1(\alpha,\eta)$ ($\bar{U}_2(\alpha,\eta)$) is an analytic function of α in the domain Ω_Q^+, and it tends to zero as $|\alpha|\to\infty$ in this domain.

LEMMA 2. Any analytic function $L_1(\alpha,\eta)$ ($L_2(\alpha,\eta)$) in the domain Ω_Q^-, which tends to zero as $|\alpha|\to\infty$ in Ω_Q^- is a solution of the equation (3.11) ((3.12)):

$$A(\alpha,\eta)-B(\alpha,\eta) = L_1(\alpha,\eta), \tag{3.15}$$

$$\gamma[A(\alpha,\eta)+B(\alpha,\eta)] = L_2(\alpha,\eta). \tag{3.16}$$

From (3.15) and (3.16) we find the amplitudes:

$$A(\alpha,\eta) = \frac{1}{2}\left[L_1(\alpha,\eta)+\frac{1}{\gamma}L_2(\alpha,\eta)\right], \tag{3.17}$$

$$B(\alpha,\eta) = \frac{1}{2}\left[\frac{1}{\gamma}L_2(\alpha,\eta)-L_1(\alpha,\eta)\right]. \tag{3.18}$$

The functions $L_1(\alpha,\eta)$ and $L_2(\alpha,\eta)$ are to be found by solving two Wiener-Hopf equations obtained from (3.13)–(3.16):

$$U_1(\alpha,\eta) = \gamma K(\alpha,\eta)L_1(\alpha,\eta)-\frac{k\sin\Phi_0}{\pi i(\alpha-\alpha_0)}, \tag{3.19}$$

$$U_2(\alpha,\eta) = K(\alpha,\eta)L_2(\alpha,\eta)-\frac{k}{\eta\pi i(\alpha-\alpha_0)}, \tag{3.20}$$

where

$$U_1(\alpha, \eta) = \frac{k}{\eta}[\bar{U}_1(\alpha, \eta) - \bar{U}_2(\alpha, \eta)]. \tag{3.21}$$

$$U_2(\alpha, \eta) = \frac{k}{\eta}[\bar{U}_1(\alpha, \eta) + \bar{U}_2(\alpha, \eta)]. \tag{3.22}$$

$$K(\alpha, \eta) = \frac{k + \eta\sqrt{k^2 - \alpha^2}}{\eta\sqrt{k^2 - \alpha^2}}. \tag{3.23}$$

The function $K(\alpha, \eta)$ fulfils all conditions of unique factorization on Q in the class of the factors tending to 1 at infinity:

(i) $K(\alpha, \eta) \to 1$ as $|\alpha| \to \infty$,

(ii) $K(\alpha, \eta) \neq 0$ on Q, (3.24)

(iii) $\operatorname{ind}_Q K(\alpha, \eta) = \frac{1}{2\pi} \int_Q d[\arg K(\alpha, \eta)] = 0$ (the justification is in Appendix A).

Thus, in the cut α-plane there exists the unique representation

$$K(\alpha, \eta) = K_L(\alpha, \eta) K_U(\alpha, \eta), \tag{3.25}$$

where

$$K_L(\alpha, \eta) = \exp\left\{-\frac{1}{2\pi i} \int_Q \frac{\ln K(t, \eta)}{t - \alpha}\, dt\right\}, \quad \alpha \in \Omega_Q^-, \tag{3.26}$$

$$K_U(\alpha, \eta) = \exp\left\{\frac{1}{2\pi i} \int_Q \frac{\ln K(t, \eta)}{t - \alpha}\, dt\right\}, \quad \alpha \in \Omega_Q^+, \tag{3.27}$$

The function $K_L(\alpha, \eta)$ is analytic and different from zero for $\alpha \in \Omega_Q^-$, and is continuous in $\Omega_Q^- \cup Q$. The function $K_U(\alpha, \eta)$ is analytic and different from zero for $\alpha \in \Omega_Q^+$, and is continuous in $\Omega_Q^+ \cup Q$. Moreover, $K_L(\alpha, \eta) \to 1$ and $K_U(\alpha, \eta) \to 1$ as $|\alpha| \to \infty$ in the respective half-planes [3].

By the standard Wiener-Hopf method, we obtain the unique solution of the equations (3.19), (3.20) in the class of the functions tending to zero at infinity.

The solution is

$$L_1(\alpha, \eta) = \frac{k \sin \Phi_0}{\pi i(\alpha - \alpha_0)} \frac{1}{\sqrt{k + \alpha_0}} \frac{1}{\sqrt{k - \alpha}} \frac{1}{K(\alpha_0, \eta)} \frac{K_L(\alpha_0, \eta)}{K_L(\alpha, \eta)}, \tag{3.28}$$

$$L_2(\alpha, \eta) = -\frac{k}{\eta \pi i(\alpha - \alpha_0)} \frac{1}{K(\alpha_0, \eta)} \frac{K_L(\alpha_0, \eta)}{K_L(\alpha, \eta)}, \tag{3.29}$$

$$U_1(\alpha, \eta) = -\frac{k \sin \Phi_0}{\pi i(\alpha - \alpha_0)} \left[1 - \sqrt{\frac{k+\alpha}{k+\alpha_0}} \frac{K_U(\alpha, \eta)}{K_U(\alpha_0, \eta)}\right], \tag{3.30}$$

$$U_2(\alpha, \eta) = -\frac{k}{\eta \pi i(\alpha - \alpha_0)} \left[1 - \frac{K_U(\alpha, \eta)}{K_U(\alpha_0, \eta)}\right], \tag{3.31}$$

Putting (3.28) and (3.29) into (3.17) and (3.18) and then into (3.5) we obtain the solution to the diffraction problem:

$$u(x, z; \eta) = u_i(x, z) - \frac{k}{2\pi i} \int_Q F(\alpha, \eta) e^{i\alpha x} e^{i\gamma|z|} d\alpha, \tag{3.32}$$

where

$$F(\alpha, \eta) = \frac{1}{\alpha - \alpha_0} \frac{1}{\sqrt{k^2 - \alpha^2}} \frac{1}{\eta K(\alpha_0, \eta)} \frac{K_L(\alpha_0, \eta)}{K_L(\alpha, \eta)} \left[1 - \eta \frac{z}{|z|} \sqrt{\frac{k+\alpha}{k+\alpha_0}} \sin \Phi_0\right]. \tag{3.33}$$

If $\eta \to 0_+$, then (3.32) converges to Sommerfeld's solution of Dirichlet problem

$$u(x, z) = u_i(x, z) - \frac{1}{2\pi i} \int_Q \frac{1}{\alpha - \alpha_0} \sqrt{\frac{k+\alpha_0}{k+\alpha}} e^{i\alpha x} e^{i\gamma|z|} d\alpha. \tag{3.34}$$

The convergence is clearly seen if we show that there exists the limit

$$\lim_{\eta \to 0} \frac{K_L(\alpha_0, \eta)}{K_L(\alpha, \eta)} = \sqrt{\frac{k-\alpha}{k-\alpha_0}}. \tag{3.35}$$

This convergence will be verified in Section 9.

4. Conformal mappings. The location of zero-points of the function K

For every $\eta \neq 0$ the function $K(\alpha, \eta)$ given by (3.23) is defined on the two-sheeted Riemann surface α described in Section 3.

Every solution of the equation

$$k + \eta \sqrt{k^2 - \alpha^2} = 0 \tag{4.1}$$

is a zero-point α_d of $K(\alpha, \eta)$. There is

$$\alpha_d = \frac{ik}{\eta} \sqrt{1 - \eta^2}. \tag{4.2}$$

Thus, for a fixed $\eta \neq 0$ and $\eta \neq \pm 1$, the function $K(\alpha, \eta)$ has two zero-points on the Riemann α-surface. Both lie on either the sheet α_I or the sheet α_{II}, depending on η.

Sometimes it is convenient to use the parameter α_d instead of η. In such a case,

we need one-to-one correspondence between η and α_d. The relation (4.2) expresses one-to-one correspondence (mapping) if and only if η belongs to the two-sheeted Riemann surface with branch points $\eta = \pm 1$, and α_d belongs to the two-sheeted Riemann surface with branch points $\alpha_d = \pm k$.

The mapping $\eta \rightleftarrows \alpha_d$ is shown in Fig. 3 abcd. Each surface is divided into sheets, and every sheet is shown separately. The division is arbitrary, but here it is done in the way suitable for further investigations. The sheets η_I and η_{II} are chosen in such a way that the passage from one sheet to the other is through the branch cut along the interval $[-1, 1]$ of the real axis, Fig. 3 ab.

The sheets η_{I} and η_{II} are distinguished by the choice

$$\alpha_d^{(1)} = k\sqrt{2} \quad \text{for } \eta = i \quad \text{on } \eta_I, \text{ and} \tag{4.3a}$$

$$\alpha_d^{(2)} = -k\sqrt{2} \quad \text{for } \eta = i \quad \text{on } \eta_{II}, \tag{4.3b}$$

By the choice of the number (4.3a) we define the branch of the function (4.2) which we also will denote by $\alpha_d^{(1)}$. The second branch we will denote by $\alpha_d^{(2)}$.

There is

$$\alpha_d^{(2)} = -\alpha_d^{(1)} \quad \text{for every } \eta \notin [-1, 1], \tag{4.4}$$

and

$$\operatorname{Re} \alpha_d^{(1)} \geqq 0, \qquad \operatorname{Re} \alpha^{(2)d} \geqq 0 \tag{4.5}$$

Now we present the Riemann surface α_d divided into sheets as in Fig. 3 cd.

The sheets α_{dI} and α_{dII} are chosen in the same way as the sheets α_I and α_{II} described by (3.8). The passage from one sheet to the other is through branch cut lines Γ_0, Γ_π.

By the function (4.2) with chosen branches $\alpha_d^{(1)}$, $\alpha_d^{(2)}$, sheet η_I, is mapped onto $\operatorname{Re} \alpha_{dI} \geqslant 0$, $\operatorname{Re} \alpha_{dII} \geqslant 0$ in Fig. 3 cd, and sheet η_{II} is mapped onto $\operatorname{Re} \alpha_{dI} \leqslant 0$, $\operatorname{Re} \alpha_{dII} \leqslant 0$. The corresponding domains are denoted by the numbers 1–6 and 7–12 respectively.

From (4.1) we have the relation

$$\gamma_d = -\frac{k}{\eta}, \tag{4.6}$$

where $\gamma_d = \sqrt{k^2 - \alpha_d^2}$.

The mappings $\eta \rightleftarrows \gamma_d$ and $\alpha_d \rightleftarrows \gamma_d$ are shown in Fig. 3 abef and Fig. 3 cdef respectively.

The function

$$\beta_d = \cos^{-1}\left(\frac{\alpha_d}{k}\right) \tag{4.7a}$$

defines one-to-one mapping of the two-sheeted Riemann surface α_d onto a cylinder

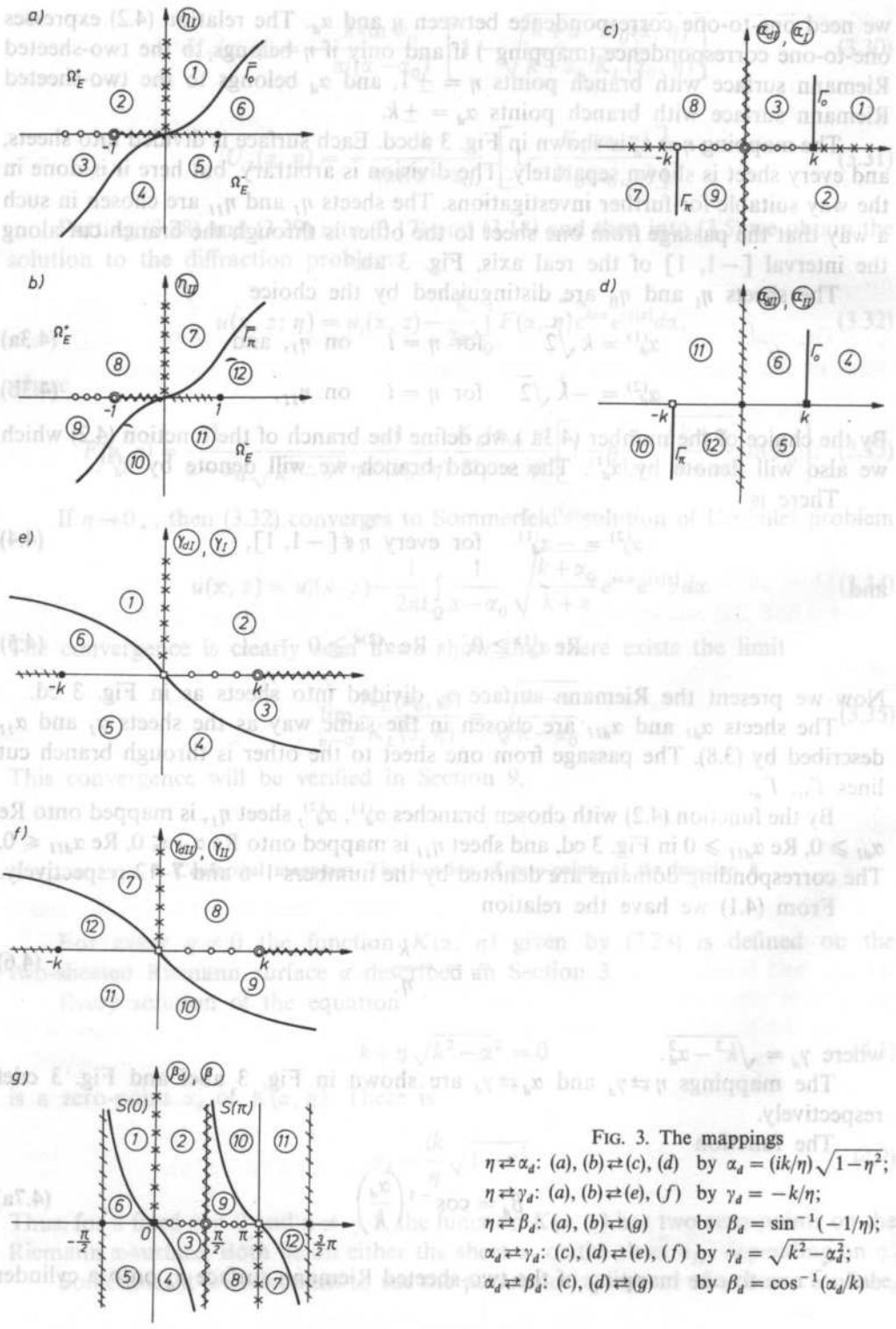

FIG. 3. The mappings
$\eta \rightleftarrows \alpha_d$: (a), (b) $\rightleftarrows$ (c), (d) by $\alpha_d = (ik/\eta)\sqrt{1-\eta^2}$;
$\eta \rightleftarrows \gamma_d$: (a), (b) $\rightleftarrows$ (e), (f) by $\gamma_d = -k/\eta$;
$\eta \rightleftarrows \beta_d$: (a), (b) $\rightleftarrows$ (g) by $\beta_d = \sin^{-1}(-1/\eta)$;
$\alpha_d \rightleftarrows \gamma_d$: (c), (d) $\rightleftarrows$ (e), (f) by $\gamma_d = \sqrt{k^2-\alpha_d^2}$;
$\alpha_d \rightleftarrows \beta_d$: (c), (d) $\rightleftarrows$ (g) by $\beta_d = \cos^{-1}(\alpha_d/k)$

surface β_d, as is shown in Fig. 3 cdg. In Fig. 3 g the cylinder is cut along a generator denoted twice: Re $\beta_d = -\frac{\pi}{2}$, and Re $\beta_d = \frac{3}{2}\pi$.

The cut cylinder can be also unfolded to the plane

$$\beta = \cos^{-1}\left(\frac{\alpha}{k}\right) \tag{4.7b}$$

which will be used in asymptotic evaluation of the solution (3.32). The lines $S(0)$ and $S(\Pi)$ are the steepest descent paths for $\theta = 0$ and $\theta = \Pi$ respectively. In the transformation (4.7) Γ_0 is mapped onto $S(0)$ and $\Gamma(\Pi)$ onto $S(\Pi)$. The sheet α_{dI}, (α_1) is mapped onto the domain contained between $S(0)$ and $S(\Pi)$.

The function

$$\beta_d = \sin^{-1}\left(-\frac{1}{\eta}\right) \tag{4.8}$$

defines one-to-one mapping of the Riemann surface η onto the cylinder β_d, Fig. 3 abg.

The mappings contain valuable information needed for the analysis of the solution as a function of η. Some of them we mention here:

1. Let us treat η as the plane of the complex parameter. If we put sheet η_{I} on sheet η_{II} the curves $\bar{\Gamma}_0$ and $\bar{\Gamma}_\pi$ cover each other. We denote the resulting single curve by S_E; the domain above S_E by Ω_E^+; and the domain below S_E by Ω_E^- respectively. These domains have the following properties:

(i) For $\eta \in \Omega_E^+$ the zero-points $\alpha_d^{(1)}$, $\alpha_d^{(2)}$ lie on the sheet α_I.

(ii) For $\eta \in \Omega_E^-$ the zero-points $\alpha_d^{(1)}$, $\alpha_d^{(2)}$ lie on the sheet α_{II}.

2. Let the function $K(\alpha, \eta)$ be factorized on a contour Q fulfilling (3.7). We denote by $L(Q)$ the set of the points on the η-plane for which the zero points $\alpha_d^{(1)}$, $\alpha_d^{(2)}$ lie on Q. Then we can check the following facts:

(i) For Q put as in Fig. 2 (dotted and crossed real axis in Fig. 3c), we have $L(Q)$ consisting of imaginary semiaxis and a part of negative real semiaxis (dotted and

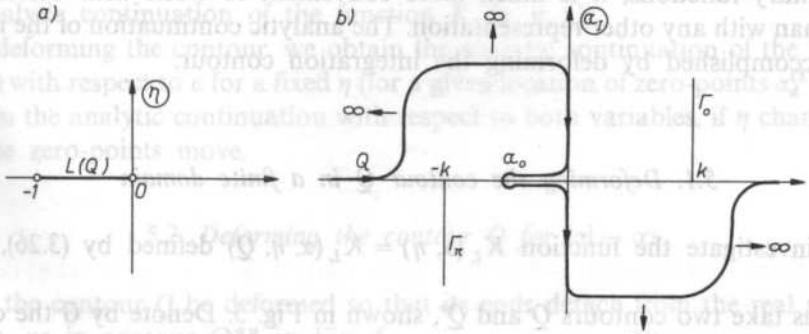

FIG. 4. The η and α-planes, (a) the Line $L(Q)$, and (b) corresponding to $L(Q)$ location of the contour Q

crossed line in Fig. 3 ab)

$$L(Q) = \{\eta: (\mathrm{Re}\eta = 0,\ \mathrm{Im}\eta \geqq 0) \cup (\mathrm{Re}\eta \leqq -1,\ \mathrm{Im}\eta = 0)\}. \tag{4.9}$$

(ii) Every contour Q which passes through $\alpha_I = 0$ and $\alpha_I = \infty$ is mapped onto $L(Q)$ with endpoints $\eta = -1$ and $\eta = 0$.

(iii) For $L(Q)$ which joins the points $\eta = -1$ and $\eta = 0$ in the simplest way, as in Fig. 4a, the contour Q is put along the imaginary axis of α_I. To fulfil the condition (3.7) it has the ends put on the real axis, Fig. 4b. This location of Q will be used in Section 8 and 9.

5. The method of analytic continuation of the factor function

In the following analysis we will treat the parameter η as a variable. Let us return to the solution (3.32) and answer the following questions:

1. For which η does the formula (3.32) have sense?
2. What is the domain of the integrand treated as a function of two complex variables α and η?
3. Is the integrand an analytic function of η there?

Let us focus our attention on $K_L(\alpha, \eta)$. All the remaining functions are easy to analyze. The function $K_L(\alpha, \eta)$ is given by the formula (3.26) which has a sense for every η for which the conditions of unique factorization (3.24) are fulfilled. For such η there exists the Cauchy-type integral which is an analytic function of η and analytic function of α in the domain Ω_Q^-. The condition (i) is fulfilled for $\eta \neq 0$. The condition (ii) is fulfilled for $\eta \notin L(Q)$. The condition (iii) is fulfilled for $\eta \neq 0$ and $\eta \neq \infty$. So we can claim that the function (3.26) is the analytic function of α and η in the Cartesian product $(\alpha \in \Omega_Q^-) \times (\eta \notin L(Q))$.

We are now going to continue $K_L(\alpha, \eta)$ analytically with respect to α, which is necessary to study the physical properties of the solution. Usually this is done by evaluation of the Cauchy-type integral in (3.26). Aa this integral cannot be expressed by elementary functions, it is much more convenient to work with Cauchy-type integral than with any other representation. The analytic continuation of the integral will be accomplished by deforming the integration contour.

5.1. Deforming the contour Q in a finite domain

We investigate the function $K_L(\alpha, \eta) = K_L(\alpha, \eta, Q)$ defined by (3.26), where $\eta \notin L(Q)$.

Let us take two contours Q and Q^*, shown in Fig. 5. Denote by G the domain contained between the contours, and by δG its boundary.

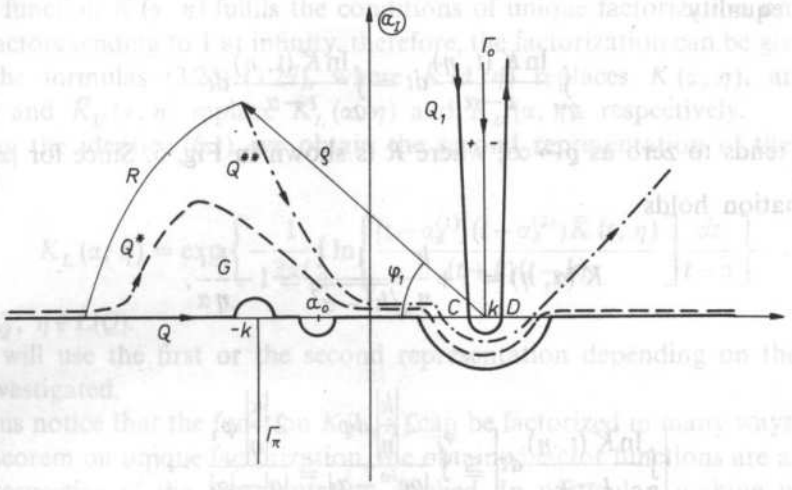

FIG. 5. The contour Q and its deformations for analytic continuation of the factor function

Let us take difference of the integrals

$$\int_{Q^*} \frac{\ln K(t,\eta)}{t-\alpha}\,dt - \int_{Q} \frac{\ln K(t,\eta)}{t-\alpha}\,dt = \oint_{\delta G} \frac{\ln K(t,\eta)}{t-\alpha}\,dt. \tag{5.1}$$

If $\alpha \in \Omega_Q^-$ and $K(t,\eta)$ is analytic and different from zero for $t \in G$, then $\oint_{\delta G} = 0$ and we have

$$\int_{Q} \frac{\ln K(t,\eta)}{t-\alpha}\,dt = \int_{Q^*} \frac{\ln K(t,\eta)}{t-\alpha}\,dt \quad \text{for } \alpha \in \Omega_Q^-. \tag{5.2}$$

As a consequence

$$K_L(\alpha, n, Q) = K_L(\alpha, \eta, Q^*) \quad \text{for } \alpha \in \Omega_Q^-. \tag{5.3}$$

Since the function $K_L(\alpha, \eta, Q^*)$ is analytic in the domain $\Omega_Q^- \cup G$, $K_L(\alpha, \eta, Q^*)$ is an analytic continuation of the function $K_L(\alpha, \eta, Q)$.

By deforming the contour, we obtain the analytic continuation of the function $K_L(\alpha, \eta)$ with respect to α for a fixed η (for a given location of zero-points $\alpha_d^{(1)}$, $\alpha_d^{(2)}$) or we obtain the analytic continuation with respect to both variables, if η changes and hence the zero-points move.

5.2. *Deforming the contour Q for $|\alpha| \to \infty$*

Let the contour Q be deformed so that its ends detach from the real axis and move up, as in contour Q** in Fig. 5.

The equality

$$\int_{Q^{**}} \frac{\ln K(t,\eta)}{t-\alpha}dt = \int_{Q} \frac{\ln K(t,\eta)}{t-\alpha}dt \tag{5.4}$$

holds if $\int_R$ tends to zero as $\varrho \to \infty$, where R is shown in Fig. 5. Since for $|\alpha| \to \infty$ the approximation holds

$$K(\alpha,\eta) = 1 + \frac{k}{\eta}\frac{1}{\sqrt{k^2-\alpha^2}} \simeq 1 - \frac{k}{\eta}\frac{i}{\alpha}, \tag{5.5}$$

therefore

$$\left|\int_R \frac{\ln K(t,\eta)}{t-\alpha}dt\right| \leqq \int_0^{\varphi_1} \frac{2\left|\frac{k}{\eta}\right|d\varphi}{|\varrho e^{i\varphi}-\alpha|} \leqq \frac{2\left|\frac{k}{\eta}\right|\varphi_1}{|\varrho|-|\alpha|} \underset{\substack{\varrho\to\infty \\ \eta\neq 0}}{\to} 0. \tag{5.6}$$

As a result, we have the equality

$$K_L(\alpha,\eta,Q) = K_L(\alpha,\eta,Q^{**}) \quad \text{for} \alpha \in \Omega_Q^-. \tag{5.7}$$

Corollary. The function $K_L(\alpha,\eta)$ can be continued analytically by deforming the contour Q towards Ω_Q^+ into a domain which contains neither a branch-point nor a zero-point of the function $K(\alpha,\eta)$. The ends of the contour Q can be moved above the real axis.

For $\eta \in \Omega_E^-$ we can deform the contour Q to the contour Q_1, Fig. 5. For $\eta \in \Omega_E^+$ the zero-point $\alpha_d^{(1)}$ does not allow us to shift Q so far. In this case we will use different representation of $K_L(\alpha,\eta)$.

6. The alternative representation of the factor function

Let us introduce the function $\bar{K}(\alpha,\eta)$ defined by the following identity with respect to α and η:

$$\bar{K}(\alpha,\eta) \equiv \frac{K(\alpha,\eta)(\alpha+k)(\alpha-k)}{(\alpha-\alpha_d^{(1)})(\alpha-\alpha_d^{(2)})}, \tag{6.1a}$$

$$\bar{K}(\alpha,\eta) = \frac{\eta\sqrt{k^2-\alpha^2}}{\eta\sqrt{k^2-\alpha^2}-k}. \tag{6.1b}$$

The function $\bar{K}(\alpha,\eta)$ has the same branch points $\alpha = \pm k$ as $K(\alpha,\eta)$ does, and has two poles $\alpha = \alpha_d^{(1)}$, $\alpha = \alpha_d^{(2)}$, which unlike the zeros of $K(\alpha,\eta)$ are located for $\eta \in \Omega_E^-$ on the sheet α_I, and for $\eta \in \Omega_E^+$ on the sheet α_{II}.

The function $\bar{K}(\alpha, \eta)$ fulfils the conditions of unique factorization on Q in the class of factors tending to 1 at infinity, therefore, the factorization can be given by the use of the formulas (3.25)–(3.27), where $\bar{K}(\alpha, \eta)$ replaces $K(\alpha, \eta)$, and where $\bar{K}_L(\alpha, \eta)$ and $\bar{K}_U(\alpha, \eta)$ replace $K_L(\alpha, \eta)$ and $K_U(\alpha, \eta)$, respectively.

Using the identity (6.1), we obtain the second representation of the function $K_L(\alpha, \eta)$.

$$K_L(\alpha, \eta) = \exp\left\{-\frac{1}{2\pi i}\int_Q \ln\left[\frac{(t-\alpha_d^{(1)})(t-\alpha_d^{(2)})\bar{K}(t, \eta)}{(t+k)(t-k)}\right]\frac{dt}{t-\alpha}\right\} \tag{6.2}$$

for $\alpha \in \Omega_Q^-$, $\eta \notin L(Q)$.

We will use the first or the second representation depending on the domain being investigated.

Let us notice that the function $K(\alpha, \eta)$ can be factorized in many ways, and yet, by the theorem on unique factorization, the obtained factor functions are always the same, irrespective of the representation applied. In particular, making use of the identity (6.1a) and the properties of the factor functions, we can write

$$K_L(\alpha, \eta) = \frac{\alpha-\alpha_d^{(1)}}{\alpha-k}\bar{K}_L(\alpha, \eta) = \frac{\alpha-\alpha_d^{(1)}}{\alpha-k}\exp\left\{-\frac{1}{2\pi i}\int_Q \frac{\ln \bar{K}(t, \eta)}{t-\alpha}dt\right\} \tag{6.3}$$

for $\eta \notin L(Q)$, $\alpha \in \Omega_Q^-$, where $\alpha_d^{(1)} \in \Omega_Q^+$.

$$K_U(\alpha, \eta) = \frac{\alpha-\alpha_d^{(2)}}{\alpha+k}\bar{K}_U(\alpha, \eta) = \frac{\alpha-\alpha_d^{(2)}}{\alpha+k}\exp\left\{-\frac{1}{2\pi i}\int_Q \frac{\ln \bar{K}(t, \eta)}{t-\alpha}dt\right\} \tag{6.4}$$

for $\eta \notin L(Q)$, $\alpha \in \Omega_Q^+$, where $\alpha_d^{(2)} \in \Omega_Q^-$.

The functions (6.3) and (3.26) are equal as well as the functions (6.4) and (3.27) are.

7. Analytic continuation of $K_L(\alpha, \eta)$ onto the Cartesian product $(\alpha \notin \Gamma_0) \times (\eta \notin L(Q))$

Theorem 1. *There exists the analytic continuation of the factor function* $K_L(\alpha, \eta)$ *given by* (3.26) *onto the Cartesian product of cut* α*-plane and cut* η*-plane. For* $\alpha \notin \Gamma_0$ *this analytic continuation has the representation in the form*

$$K_L(\alpha, \eta) = \exp\left\{-\frac{1}{2\pi i}\int_{\Gamma_0} \frac{\ln K^*(t, \eta)}{t-\alpha}dt\right\} \tag{7.1a}$$

for $\eta \in \Omega_E^-$, and

$$K_L(\alpha, \eta) = \frac{\alpha-\alpha_d^{(1)}}{\alpha-k}\exp\left\{-\frac{1}{2\pi i}\int_{\Gamma_0} \frac{\ln K^*(t, \eta)-2\pi i}{t-\alpha}dt\right\} \tag{7.1b}$$

for $(\eta \in \Omega_E^+) \cap (\eta \notin L(Q))$,

where

$$K^*(\alpha, \eta) = \frac{\eta\sqrt{k^2-\alpha^2}+k}{\eta\sqrt{k^2-\alpha^2}-k}, \tag{7.2}$$

$\mathrm{Im}\,(\ln K^*) \in (-\pi, \pi$, for $\eta \in \Omega_E^-$ the line Γ_0 is directed as in Fig. 5, $\alpha_d^{(1)} \in \Omega_Q^+$.

Proof. Let $\eta \in \Omega_E^-$. According to the Corollary in Section 5, for $\eta \in \Omega_E^-$, $\alpha \in \Omega_Q^-$ we have the equality

$$\int_Q \frac{\ln K(t, \eta)}{t-\alpha} dt = \int_{Q_1} \frac{\ln K(t, \eta)}{t-\alpha} dt. \tag{7.3}$$

In the neighbourhood of $\alpha = k$ we have $K(\alpha, \eta) = O[(k-\alpha)^{-1/2}]$ and, therefore, the integral on a half-circle CD, Fig. 5, tends to zero as its radius tends to zero. Thus, we have

$$\int_Q \frac{\ln K(t, \eta)}{t-\alpha} dt = \int_{\Gamma_0} \ln \frac{K_+(t, \eta)}{K_-(t-\eta)} \Big] \frac{dt}{t-\alpha}. \tag{7.4}$$

The subscripts "+" and "−" denote the values of the function $K(t, \eta)$ from the right hand side and left hand side of Γ_0, respectively. According to (3.8), we have

$$(\sqrt{k^2-t^2})_+ = \sqrt{k^2-t^2}, \quad (\sqrt{k^2-t^2})_- = -\sqrt{k^2-t^2}, \tag{7.5}$$

and, therefore,

$$\frac{K_+(t, \eta)}{K_-(t, \eta)} = K^*(t, \eta). \tag{7.6}$$

Substituting (7.6) into (7.4), and then into (3.26) we obtain (7.1a).

Let $\eta \in \Omega_E^+$. We use the representation (6.3). In exactly the same way as above, we obtain the equality:

$$\int_Q \frac{\ln \bar{K}(t, \eta)}{t-\alpha} dt = \int_{\Gamma_0} \ln \left[\frac{\bar{K}_+(t, \eta)}{\bar{K}_-(t, \eta)}\right] \frac{dt}{t-\alpha}. \tag{7.7}$$

From (6.1b) and (7.5), we have

$$\frac{\bar{K}_+(t, \eta)}{\bar{K}_-(t, \eta)} = K^*(t, \eta). \tag{7.8}$$

Substituting (7.8) into (7.7) and then into (6.3) we obtain (7.1b).

The branch of logarithm is chosen such that the function $K_L(\alpha, \eta)$ is as singular at the point $\alpha = k$, as the function $K(\alpha, \eta)$ is:

$$K_L(\alpha, \eta) = O[(\alpha-k)^{-1/2}] \text{ at } \alpha = k. \tag{7.9}$$

Then the integrals in (7.1) are convergent.

The values of $K_L(\alpha, \eta)$ for $\eta \in S_E$ can be obtained as a limit in the formula (7.1a) or (7.1b) as $\eta \to S_E$

8. Analytic continuation of $K_L(\alpha, \eta)$ onto the second sheet of the Riemann surface η

Theorem 2. *For fixed* α *the function* $K_L(\alpha, \eta)$ has two branch points $\eta = -1$, $\eta = 0$ *of the first order.*

Proof. As far as the point $\eta = -1$ is concerned the conclusions follows immediately from (7.1b). Since the exponential function is regular at $\eta = -1$, the function $K(\alpha, \eta)$ is as singular as $\alpha_d^{(1)}$ is and, therefore it behaves like $\sqrt{1-\eta^2}$. This is illustrated in Fig. 6 a, b. As η circulates twice round the point $\eta = -1$ along a closed line C_1 on the plane η (Fig. 6a), the zero point α_d circulates once round the point $\alpha_d = 0$ along the line $\bar{C}_1$ (Fig. 6b), and returns to the initial position, so that the value $K_L(\alpha, \eta)$ returns to the initial value.

It is much more difficult to prove the thesis at $\eta = 0$. For $\eta = 0$ the formulas (7.1a, b) do not hold because the Cauchy-type integral is divergent. Moreover, there is no "uniform" description of the function $K_L(\alpha, \eta)$ in the neighbourhood of $\eta = 0$. This neighbourhood is cut by the lines S_E and $L(Q)$ which are the branch cuts of the logarithm and of the function α_d, respectively. We will show, however, that the analytically continued function $K_L(\alpha, \eta)$ returns to the initial value after η has circulated twice round the point $\eta = 0$ along a closed line C_2, as in Fig. 6a. In the first circulation η goes from the point 1 to 6, and in the second circulation from 6 to 1 (11).

The line C_2 encloses also the point $\eta = +1$ (a regular point of $K_L(\alpha, \eta)$, because the neighbourhood of $\eta = 0$ is cut from $\eta = -1$ to $\eta = +1$ by the transformation $\eta \rightleftarrows \alpha_d$ (4.2). In fact, the line C_2 is put on the two-sheeted Riemann surface η; the continuous line on the sheet η_{I}, the dashed on the sheet η_{II}. In the η–plane these two parts of the line cover each other.

Using the mapping presented in Fig. 3 abcd, we find the trajectory of the zero-point α_d on the Riemann surface α_d for η moving along C_2. This is the line $\bar{C}_2$ in Fig. 6b. It begins at the point 1 on the sheet α_{II}, and it returns to the initial point 1 (11), Fig. 6b. The dashed line indicates the part of the trajectory on the sheet $\alpha_{d\mathrm{II}}$, the continuous line on the sheet $\alpha_{d\mathrm{I}}$. The line C_2 is also mapped into the β_d–plane – the line C_2 in Fig. 6c.

Having determined the trajectory α_d we can find the analytic continuation of the function $K_L(\alpha, \eta)$ (defined by (3.26)) in the neighbourhood of $\eta = 0$. Three contours selected from eleven ones $Q = Q_i$, $i = 1, 2, \ldots, 11$, that result from pushing Q by the moving point α_d are shown in Fig. 7. The contour Q_i corresponds to the location α_d in the point $i = 1, 2, \ldots, 11$, as in Fig. 6b. This is the realization of analytic continuation of the Cauchy–type integral on Q. The $\alpha_d^{(1)}$, $\alpha_d^{(2)}$ points are additional, dependent on η branch points of the logarithm in this integral.

Looking at the trajectory of α_d, Fig. 6b, we can draw the contour Q_{11}. Although it is in the form of a very long loop it can be shown that the Cauchy–type integral on Q_{11} is equal to the Cauchy–type integral on Q_1, since the integral along a part of the contour "pushed" by $\alpha_d^{(1)}$in first circulation is reduced by the integral along the same

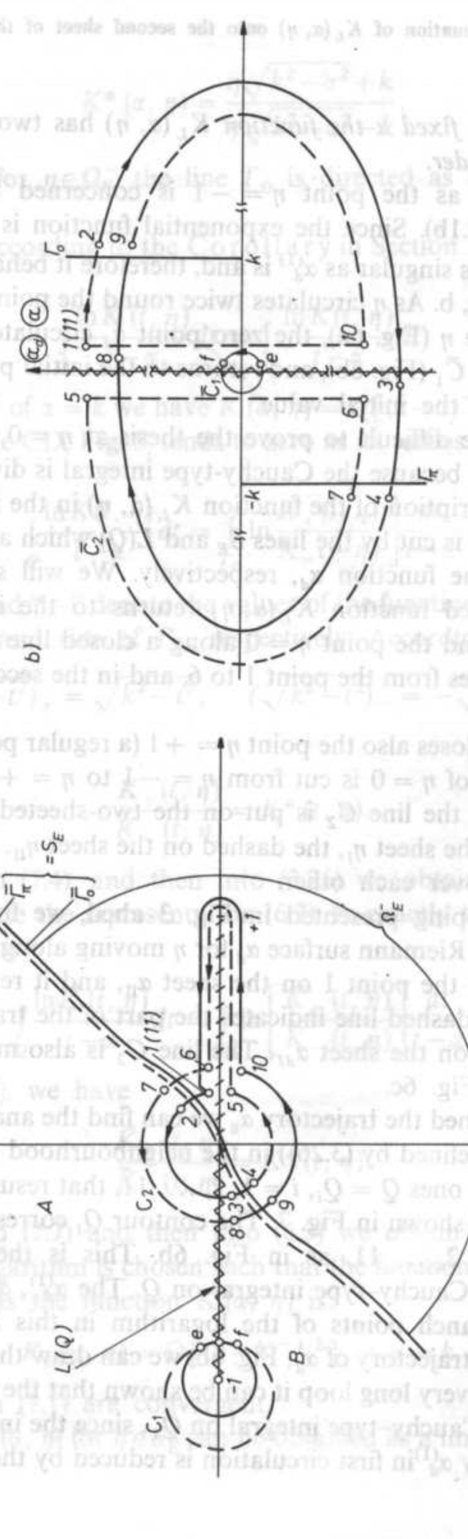

8. Analytic continuation of $K_1(\alpha, \eta)$ onto the second sheet of the Riemann surface η

Theorem 2. *For fixed α the function* $K_1(\alpha, \eta)$ has two branch points $\eta = -1$, $\eta = 0$ *of the first order.*

P r o o f. As far as the point $\eta = -1$ is concerned the conclusions follows immediately from (7.1b). Since the exponential function is regular at $\eta = -1$, the function $K(\alpha, \eta)$ is as singular as $\alpha_z^{(1)}$ is and, therefore it behaves like $\sqrt{1-\eta}$. This is illustrated in Fig. 6 a, b. As η circulates twice round the point $\eta = -1$ along a closed line C_1 on the plane η (Fig. 6a), the zero-point α_z circulates once round the point $\alpha_z = 0$ along the line C_1 (Fig. 6b) and returns to its initial position, so that the value $K_1(\alpha, \eta)$ returns to the initial value.

It is much more difficult to prove the thesis at $\eta = 0$. For $\eta = 0$ the formulas (7.1a, b) do not hold because the Cauchy-type integral is divergent. Moreover, there is no "uniform" description of the function $K_1(\alpha, \eta)$ in the neighbourhood of $\eta = 0$. This neighbourhood is cut by the lines S_E and $L(Q)$ which are the branch cuts of the logarithm and of the function α_z, respectively. We will show, however, that the analytically continued function $K_1(\alpha, \eta)$ returns to the initial value after η has circulated twice round the point $\eta = 0$ along a closed line C_2 as in Fig. 6a. In the first circulation η goes from the point 1 to 6, and in the second circulation from 6 to 1 (11).

The line C_2 encloses also the point $\eta = +1$ (a regular point of $K_1(\alpha, \eta)$), because the neighbourhood of $\eta = 0$ is cut from $\eta = -1$ to $\eta = +1$ by the transformation $\eta = \alpha_z$ (4.2). In fact, the line C_2 is put on the two-sheeted Riemann surface η; the continuous line on the sheet η_I, the dashed on the sheet η_{II}. In the η-plane these two parts of the line cover each other.

Using the mapping described in Section 2, we can find the trajectory of the zero-point α_z on the Riemann surface α_z for η moving along C_2. This is the line C_2 in Fig. 6b. It begins at the point 1 on the sheet α_I, and it returns to the initial point 1 (11), Fig. 6b. The dashed line indicates the part of the trajectory on the sheet α_{II}, the continuous line on the sheet α_I. The line C_2 is also mapped into the β_2-plane – the line C_2 in Fig. 6c.

Having determined the trajectory α_z, we can find the analytic continuation of the function $K_1(\alpha, \eta)$ defined by (5.2b) in the neighbourhood of $\eta = 0$. Three contours selected from eleven ones $Q = Q_i$, $i = 1, 2, \ldots, 11$, that result from pushing Q by the moving point α_z are shown in Fig. 7. The contour Q_i corresponds to the location α_z in the point i ($i = 1, 2, \ldots, 11$) in Fig. 6b. This is the realization of analytic continuation of the Cauchy-type integral on Q. The $\alpha_z^{(1)}$, $\alpha_z^{(2)}$ points are additional, dependent on η branch points of the logarithm in this integral.

Looking at the trajectory of α_z in Fig. 6b, we can draw the contour Q_{11}. Although it is in the form of a very long loop it can be shown that the Cauchy-type integral on Q_{11} is equal to the Cauchy-type integral on Q_1, since the integral along a part of the contour "pushed" by $\alpha_z^{(1)}$ in first circulation is reduced by the integral along the same

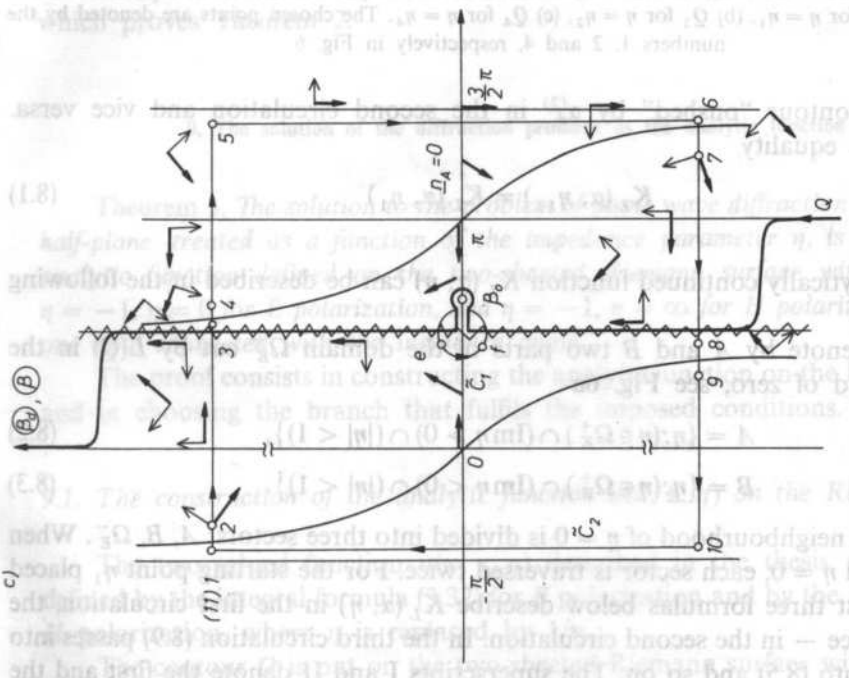

FIG. 6. (a) Two-sheeted Riemann surface η cut along the interval $[-1, +1]$ of the real axis. The line C_1 as the trajectory of η running arround $\eta = -1$ and the line C_2 as the trajectory arround $\eta = 0$ with $\eta = +1$ inside. Also the η-plane cut along $L(Q)$ with the sectors A, B, and Ω_E^- in the neighbourhood of $\eta = 0$ as described in Section 8; (b) The lines $\tilde{C}_1$ and $\tilde{C}_2$ as the mapping of C_1 and C_2 respectively into the Riemann surface α_d; (c) The lines $\tilde{C}_1$ and $\tilde{C}_2$ as the mapping of C_1 and C_2 respectively into β_d-plane. The vectors $\mathbf{n}_A \to$ and $\mathbf{n}_P \to$ characterise a surface wave described in Section 9. The outgoing wave is shown by $\mathbf{n}_P$ in the region $-\frac{\pi}{2} < \operatorname{Re}\beta \leqq \frac{\pi}{2}$. The location of the contour Q corresponds to that in Fig. 4(b)

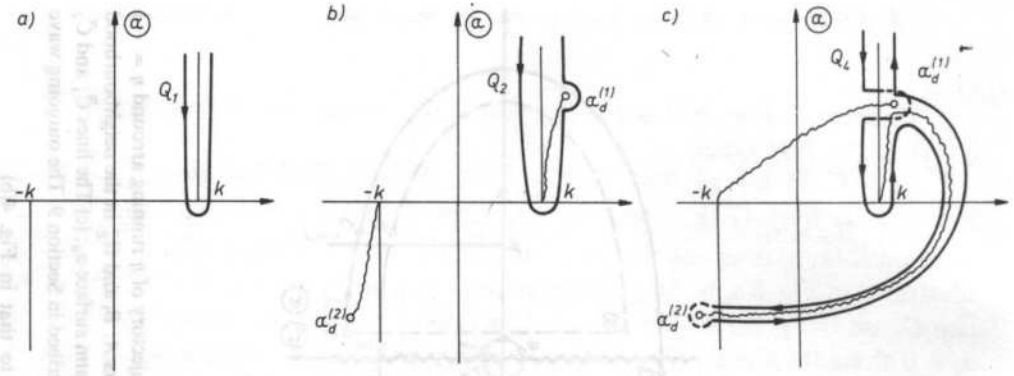

FIG. 7. The deformed contour Q as a realization of analytic continuation of $K_L(\alpha, \eta)$ in the neighbourhood of $\eta = 0$, (a) Q_1 for $\eta = \eta_1$, (b) Q_2 for $\eta = \eta_2$, (c) Q_4 for $\eta = \eta_4$. The chosen points are denoted by the numbers 1, 2 and 4, respectively in Fig. 6

part of the contour "pushed" by $\alpha_d^{(2)}$ in the second circulation and vice versa. Therefore the equality

$$K_L(\alpha, \eta_{11}) = K_L(\alpha, \eta_1) \tag{8.1}$$

holds.

The analytically continued function $K_L(\alpha, \eta)$ can be described in the following way:

Let us denote by A and B two parts of the domain Ω_E^+ cut by $L(Q)$ in the neighbourhood of zero, see Fig. 6a

$$A = \{\eta : (\eta \in \Omega_E^+) \cap (\operatorname{Im}\eta > 0) \cap (|\eta| < 1)\}, \tag{8.2}$$

$$B = \{\eta : (\eta \in \Omega_E^+) \cap (\operatorname{Im}\eta < 0) \cap (|\eta| < 1)\}. \tag{8.3}$$

Then the neighbourhood of $\eta = 0$ is divided into three sectors: A, B, Ω_E^-. When η goes around $\eta = 0$, each sector is traversed twice. For the starting point η_1 placed in Ω_E^- the first three formulas below describe $K_L(\alpha, \eta)$ in the first circulation, the remaining three – in the second circulation. In the third circulation (8.9) passes into (8.4), (8.4) – into (8.5) and so on. The superscripts I and II denote the first and the second branch of two-valued function $K_L(\alpha, \eta)$, respectively. We have for $\alpha \notin \Gamma_0$

$$K_L^{\mathrm{I}}(\alpha, \eta) = \exp\left\{-\frac{1}{2\pi i}\int_{\Gamma_0}\frac{\ln K^*(t, \eta)}{t-\alpha}dt\right\} \text{ for } \eta \in \Omega_E^-, \tag{8.4}$$

$$K_L^{\mathrm{I}}(\alpha, \eta) = \frac{\alpha-\alpha_d^{(1)}}{\alpha-k}\exp\left\{-\frac{1}{2\pi i}\int_{\Gamma_0}\frac{\ln K^*(t, \eta)-2\pi i}{t-\alpha}dt\right\} \text{ for } \eta \in A, \tag{8.5}$$

$$K_L^{II}(\alpha, \eta) = \frac{\alpha-\alpha_d^{(2)}}{\alpha-k}\exp\left\{-\frac{1}{2\pi i}\int_{\Gamma_0}\frac{\ln K^*(t, \eta)-2\pi i}{t-\alpha}dt\right\} \text{ for } \eta \in B, \tag{8.6}$$

$$K_L^{\mathrm{II}}(\alpha, \eta) = \frac{(\alpha-\alpha_d^{(1)})(\alpha-\alpha_d^{(2)})}{(\alpha-k)^2} \times \tag{8.7}$$

$$\times \exp\left\{-\frac{1}{2\pi i}\int_{\Gamma_0}\frac{\ln K^*(t,\eta)-4\pi i}{t-\alpha}dt\right\} \text{ for } \eta\in\Omega_E^-, \qquad (8.7)[\text{cd.}]$$

$$K_L^{II}(\alpha,\eta)=\frac{\alpha-\alpha_d^{(2)}}{\alpha-k}\exp\left\{-\frac{1}{2\pi i}\int_{\Gamma_0}\frac{\ln K^*(t,\eta)-2\pi i}{t-\alpha}dt\right\}\text{for } \eta\in A, \qquad (8.8)$$

$$K_L^{I}(\alpha,\eta)=\frac{\alpha-\alpha_d^{(1)}}{\alpha-k}\exp\left\{-\frac{1}{2\pi i}\int_{\Gamma_0}\frac{\ln K^*(t,\eta)-2\pi i}{t-\alpha}dt\right\}\text{for } \eta\in B, \qquad (8.9)$$

In the formulas above the line Γ_0 is directed as in Fig. 5, $K^*(\alpha,\eta)$ is given by (7.2), and $\alpha_d^{(1)}$ and $\alpha_d^{(2)}$ are described by (4.3)–(4.5).

The derivation of the formulas (8.4)–(8.9) can be found in Appendix B.

This procedure of analytic continuation gives for $K_L(\alpha,\eta)$ exactly two branches which proves **Theorem** 2.

9. The solution of the diffraction problem as the analytic function of η

Theorem 3. *The solution to the problem of plane wave diffraction by an impedance half-plane, treated as a function of the impedance parameter η, is a branch of the analytic function defined on the two-sheeted Riemann surface with branch points $\eta=-1$, $\eta=0$ for E polarization, and $\eta=-1$, $\eta=\infty$ for H polarization, except for one pole connected with the incidence angle.*

The proof consists in constructing the analytic function on the Riemann surface, and in choosing the branch that fulfils the imposed conditions.

9.1. The construction of the analytic function $u(x,z;\eta)$ on the Riemann surface η

The two-valued function $u(x,z;\eta)$ described in the thesis of **Theorem** 3 is defined by the integral formula (3.32) for E polarization and by the same formula for H polarization, where η is replaced by $1/\eta$.

The contour Q is put on the two-sheeted Riemann surface with branch points $\alpha=\pm k$, where the sheets are chosen as described in Section 3. The condition (3.7) requires that the branch cut pass through infinity, but its location Γ_0, Γ_π, as chosen here is directed only by the convenience of writing formulas for the amplitudes $A(\alpha,\eta)$, $B(\alpha,\eta)$ which makes the asymptotic analysis of the integral easier.

We impose two conditions: $\alpha_0\in\Omega_Q^+$, and (3.7) for a location of Q. The condition (3.7) places the ends of Q on the real axis of the sheet α_1.

By fixing the contour Q, we get the first branch u_I of the function (3.32), where the integrand $F^I(\alpha,\eta)$ is described by (3.33), (8.4), (8.5), (8.9) in the domain $|\eta|<1$ for E polarization, and in the domain $|\eta|>1$ for H polarization (if η is replaced by $1/\eta$ in the formula (3.32)).

In the second branch to be denoted by u^{II}, the contour of integration is a function of η. It is "pushed" by the pole $\alpha_d^{(2)}$ of the integrand. It can be reduced,

however, to Q by "picking up" the pole at $\alpha = \alpha_d^{(2)}$.

Thus

$$u^{II}(x, z; \eta) = u_i(x, z) - k\left\{\frac{1}{2\pi i}\int_Q F^{II}(\alpha, \eta)e^{i\alpha x}e^{i\gamma|z|}d\alpha + \right.$$

$$\left. + \operatorname*{res}_{\alpha_d^{(2)}} [F^{II}(\alpha, \eta)]e^{i\alpha_d^{(2)}x}e^{i\gamma_d^{(2)}|z|}\right\}, \quad (9.1)$$

where $F^{II}(\alpha, \eta)$ is described by (3.33), (8.6)–(8.8) in the domain $|\eta| < 1$ for E polarization, and in the domain $|\eta| > 1$ for H polarization when $1/\eta$ is substitutied for η.

This two-valued function on the η-plane, is single-valued on the two-sheeted Riemann surface, as shown in Fig. 8. We pass from one sheet to the other through the branch cut $L(Q)$.

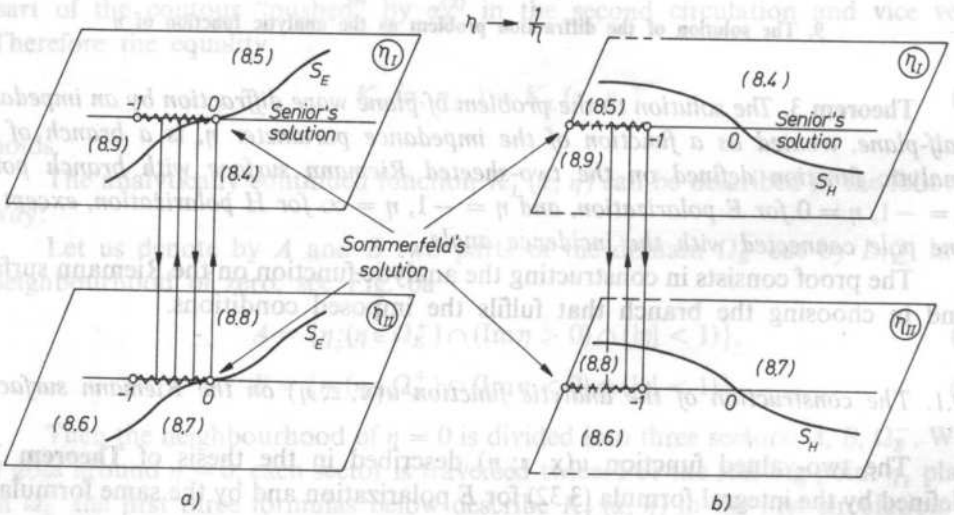

FIG. 8. The Riemann surface of the function $u(x, z; \eta)$ treated as a function of η, (a) for E polarization, (b) for H polarization

Senior's solution lies on the sheet I below the line S_E for E polarization and above the line S_H for H polarization, where S_H is described by the equation

$$\operatorname{Im}\eta = -\frac{\operatorname{Re}\eta}{\sqrt{1-(\operatorname{Re}\eta)^2}}. \quad (9.2)$$

The lines S_E and S_H map one onto the other by the function $w = 1/\eta$.

The location of the contour Q corresponding to $L(Q)$ lying on the real axis is presented in Fig. 4b.

9.2. The properties of $u(x, z; \eta)$ as an analytic function of η

LEMMA. The point

$$\eta_0 = -\frac{1}{\sin\phi_0} \tag{9.3}$$

is a pole of the function $u(x, z; \eta)$ for E polarization, and the point

$$\eta_0 = -\sin\phi_0 \tag{9.4}$$

is a pole of the function $u(x, z; \eta)$ for H polarization.

Proof. We show the thesis for E polarization. Let us examine the function $F(\alpha, \eta)$ as given by (3.33) and extract the quotient $\frac{K_L(\alpha_0, \eta)}{K(\alpha_0, \eta)}$ in each branch of the function $u(x, z; \eta)$ in the sector A.

From (8.5) and (6.1a) we obtain for branch I

$$\frac{K_L^{\mathrm{I}}(\alpha_0, \eta)}{K(\alpha_0, \eta)} = \frac{\alpha_0 + k}{\alpha_0 - \alpha_d^{(2)}} \bar{K}(\alpha_0, \eta) \exp\left\{-\frac{1}{2\pi i}\int_{\Gamma_0} \frac{\ln K^*(t, \eta) - 2\pi i}{t - \alpha_0} dt\right\}. \tag{9.5}$$

From (8.8) and (6.1a) we obtain for branch II

$$\frac{K_L^{\mathrm{II}}(\alpha_0, \eta)}{K(\alpha_0, \eta)} = \frac{\alpha_0 + k}{\alpha_0 - \alpha_d^{(1)}} \bar{K}(\alpha_0, \eta) \exp\left\{-\frac{1}{2\pi i}\int_{\Gamma_0} \frac{\ln K^*(t, \eta) - 2\pi i}{t - \alpha_0} dt\right\}. \tag{9.6}$$

The branch $u^{\mathrm{I}}(x, z; \eta) = u^{\mathrm{I}}(x, z; \alpha_d^{(2)})$ as described by (3.32), (3.33) and (9.5), and treated as a function of the parameter α_d, has the pole

$$\alpha_d^{(2)} = \alpha_0. \tag{9.7}$$

The branch $u^{\mathrm{II}}(x, z; \eta) = u^{\mathrm{II}}(x, z; \alpha_d^{(1)})$ as described by (3.32), (3.33) and (9.6), and treated as a function of the parameter α_d, has the pole

$$\alpha_d^{(1)} = \alpha_0 \tag{9.8}$$

Let us come back to the parameter η. From (9.7) the equality (9.3) for $0 \leqslant \phi_0 \leqslant \frac{\pi}{2}$ results, and vice versa. From (9.8) the equality (9.3) for $\frac{\pi}{2} \leqslant \phi_0 \leqslant \pi$ results and vice versa (this can be seen in Fig. 3 abg).

Since $u(x, z; \eta) \to \infty$ as $\eta \to \eta_0$ on the first or on the second sheet and since it is an analytic function in a ring neighbourhood of η_0, the point $\eta = \eta_0$ is a pole.

Summary: 1. The function $u(x, z; \eta)$ treated as a function of the impedance parameter has two algebraic branch points of the first order and one pole. These

singular points are $\eta = 1$, $\eta = 0$, $\eta = \eta_0 = -1/[\sin \phi_0]$ for E polarization, and $\eta = -1$, $\eta = \infty$, $\eta = \eta_0 = -\sin \phi_0$ for H polarization.

2. Sommerfeld's solution is the limit of $u(x, z; \eta)$ at the branch point $\eta = 0$ (the limit (3.35) exists as η tends to zero in every section of the neighbourhood of $\eta = 0$).

3. If $\phi_0 \neq \frac{\pi}{2}$ then there exists a finite limit of $u(x, z; \eta)$ at the branch point $\eta = -1$. For $\phi_0 = \frac{\pi}{2}$ the limit is infinite.

9.3 The properties of $u(x, z; \eta)$ as a function of x and z

1) The edge condition: Each branch of $u(x, z; \eta)$ treated as a function of x and z belongs to the same class of functions, which derivatives (2.6) have the Fourier transforms tending to zero at infinity. From the half-range Fourier transforms (3.28), (3.29) we find

$$u_s(x, 0_+) - u_s(x, 0_-) = O(x^{1/2}) \quad \text{as } x \to 0_+, \tag{9.9}$$

and

$$\lim_{x \to 0_+} \left\{ \frac{\partial u_s}{\partial z}(x, 0_+) - \frac{\partial u_s}{\partial z}(x, 0_-) \right\} = -\frac{2ik}{\eta} \frac{K_L(\alpha_0, \eta)}{K(\alpha_0, \eta)}. \tag{9.10}$$

From the half-range Fourier transforms (3.30), (3.31) we find

$$\lim_{x \to 0} u_s(x, 0) = \frac{1}{K_U(\alpha_0, \eta)} \tag{9.11}$$

if the limit exists, and

$$\frac{\partial u}{\partial z}(x, 0) = O(x^{-1/2}) \tag{9.12}$$

as $x \to 0_-$.

2) The condition at infinity: In order to verify the condition at infinity, we change the contour Q in the formula (3.32) to the steepest descent path $\bar{S}(\theta)$, Fig. 9, where $0 < \theta < \pi$.

According to the Cauchy theorem and by applying Jordan's Lemma we have in the domain $0 < \theta < \pi$:

$$u_s^I(x, z; \eta) = -k \left[\frac{1}{2\pi i} \Psi^I(x, z; \eta) + H(\pi - \phi_0 - \theta) \operatorname*{res}_{\alpha_0} F^I(\alpha, \eta) e^{i(\mathbf{n}_0 \cdot \varrho)} \right] \tag{9.13}$$

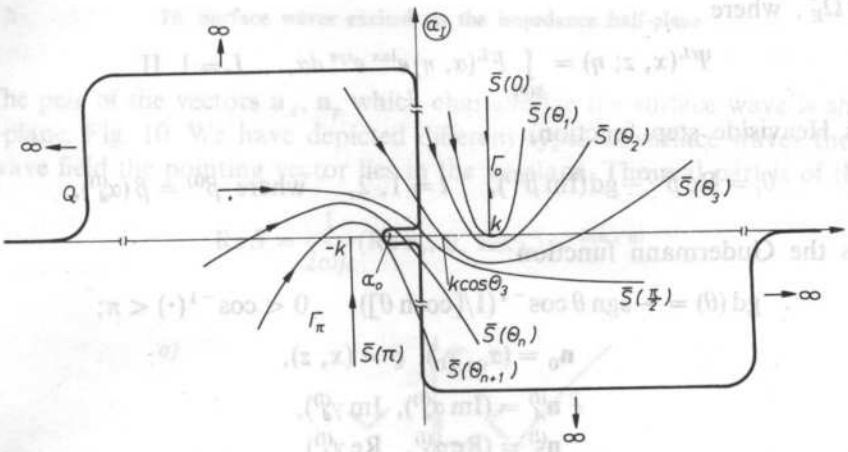

FIG. 9. The steepest descent paths. $\bar{S}(0)$ for $0 \leqq \theta \leqq \pi$ in α-plane cut along $\bar{S}(0)$, $\bar{S}(\pi)$ paths

for $\eta \in \Omega_E^-$, and

$$u_s^{\mathrm{I}}(x, z; \eta) = -k\left[\frac{1}{2\pi i}\Psi^{\mathrm{I}}(x, z; \eta) + H(\pi - \phi_0 - \theta)\operatorname*{res}_{\alpha_0} F^{\mathrm{I}}(\alpha, \eta)\, e^{i(\mathbf{n}_0 \cdot \mathbf{Q})} + H(\theta_1 - \theta)\operatorname*{res}_{\alpha_d^{(1)}} F^{\mathrm{I}}(\alpha, \eta)\, e^{-(\mathbf{n}_A^{(1)} \cdot \mathbf{Q})} e^{i(\mathbf{n}_P^{(1)} \cdot \mathbf{Q})}\right] \tag{9.14}$$

for $\eta \in \Omega_E^+$.

$$u_s^{\mathrm{II}}(x, z; \eta) = -k\left[\frac{1}{2\pi i}\Psi^{\mathrm{II}}(x, z; \eta) + H(\pi - \phi_0 - \theta)\operatorname*{res}_{\alpha_0} F^{\mathrm{II}}(\alpha, \eta)\, e^{i(\mathbf{n}_0 \cdot \mathbf{Q})} + H(\theta_2 - \theta)\operatorname*{res}_{\alpha_d^{(2)}} F^{\mathrm{II}}(\alpha, \eta)\, e^{-(\mathbf{n}_A^{(2)} \cdot \mathbf{Q})} e^{i(\mathbf{n}_P^{(2)} \cdot \mathbf{Q})}\right] \tag{9.15}$$

for $\eta \in \Omega_E^+$, and

$$u_s^{\mathrm{II}}(x, z; \eta) = -k\left[\frac{1}{2\pi i}\Psi^{\mathrm{II}}(x, z; \eta) + H(\pi - \phi_0 - \theta)\operatorname*{res}_{\alpha_0} F^{\mathrm{II}}(\alpha, \eta)\, e^{i(\mathbf{n}_0 \cdot \mathbf{Q})} + \operatorname*{res}_{\alpha_d^{(2)}} F^{\mathrm{II}}(\alpha, \eta)\, e^{-(\mathbf{n}_A^{(2)} \cdot \mathbf{Q})} e^{i(\mathbf{n}_P^{(2)} \cdot \mathbf{Q})}\right] \tag{9.16}$$

for $\eta \in \Omega_E^-$, where

$$\Psi^L(x, z; \eta) = \int_{S(\theta)} F^L(\alpha, \eta)\, e^{i\alpha x} e^{i\gamma z}\, d\alpha, \quad L = \mathrm{I}, \mathrm{II}, \tag{9.17}$$

$H(\cdot)$ is Heaviside step function,

$$\theta_l = \operatorname{Re}\beta^{(l)} - \operatorname{gd}(\operatorname{Im}\beta^{(l)}), \quad l = 1, 2, \quad \text{where } \beta^{(l)} = \beta(\alpha_d^{(l)}),$$

$\operatorname{gd}(\theta)$ is the Gudermann function:

$$\operatorname{gd}(\theta) = -\operatorname{sgn}\theta \cos^{-1}(1/[\cosh\theta]), \quad 0 < \cos^{-1}(\cdot) < \pi;$$

$$\mathbf{n}_0 = (\alpha_0, \gamma_0), \quad \varrho = (x, z),$$

$$\mathbf{n}_A^{(l)} = (\operatorname{Im}\alpha_d^{(l)}), \ \operatorname{Im}\gamma_d^{(l)}),$$

$$\mathbf{n}_P^{(l)} = (\operatorname{Re}\alpha_d^{(l)}, \ \operatorname{Re}\gamma_d^{(l)})$$

for $l = 1, 2$. (9.18)

On evaluating (9.17) for large $k\varrho$ we obtain

$$\int_{S(\theta)} F^L(\alpha, \eta)\, e^{i\alpha x} e^{i\gamma z}\, d\alpha \sim \sqrt{\frac{2\pi}{k\varrho}}\, F^L(k\cos\theta)\, e^{i(k\varrho - \pi/4)} \quad \text{for } L = \mathrm{I}, \mathrm{II}. \tag{9.19}$$

Each function represents the cylindrical wave which decays exponentially at infinity if small positive imaginary part is inserted in k.

The residue term at α_0 gives rise to the reflected wave. The residue term at $\alpha_d^{(l)}$, $l = 1, 2$ gives rise to the nonhomogeneous plane wave called here a surface wave. The surface wave propagates in the direction defined by $\mathbf{n}_p$, and its amplitude decays in the direction defined by $\mathbf{n}_A$.

For some selected points of the η–Riemann surface, as in Fig. 6a, the corresponding pairs of the vectors $\mathbf{n}_A$, $\mathbf{n}_p$ are shown in the β–plane, Fig. 6c. The components of the vectors are found using (9.18) and the mappings in Fig. 3.

A surface wave generated by the pole lying in the strip $-\frac{\pi}{2} < \operatorname{Re}\beta \leqq \frac{\pi}{2}$ belongs to u_s^{I}. It is an outgoing wave. It propagates in an angular domain from the edge into the half-space $x > 0$. A surface wave generated by the pole lying in the strip $\frac{\pi}{2} < \operatorname{Re}\beta \leqq \frac{3}{2}\pi$ belongs to u_s^{II} and can be treated as an incoming one. As could be expected, the outgoing wave condition is fulfiled for u_s^{I} only.

In conclusion we state that the branch u^{I} of the function as shown in Fig. 8, is the solution to our diffraction problem for every η. This completes the proof of Theorem 3.

10. Surface waves excited on the impedance half-plane

The pair of the vectors $\mathbf{n}_A$, $\mathbf{n}_p$ which characterize the surface wave is shown in the η–plane, Fig. 10. We have depicted different types of surface waves there. For each wave field the pointing vector lies in the xz plane. The real part is of the form

$$\operatorname{Re} \boldsymbol{S} = \frac{1}{2\omega\mu}(\operatorname{Re}\alpha_d,\ 0,\ \operatorname{Re}\gamma_d)\, e^{-2(\mathbf{n}_A \cdot \boldsymbol{\varrho})} \tag{10.1}$$

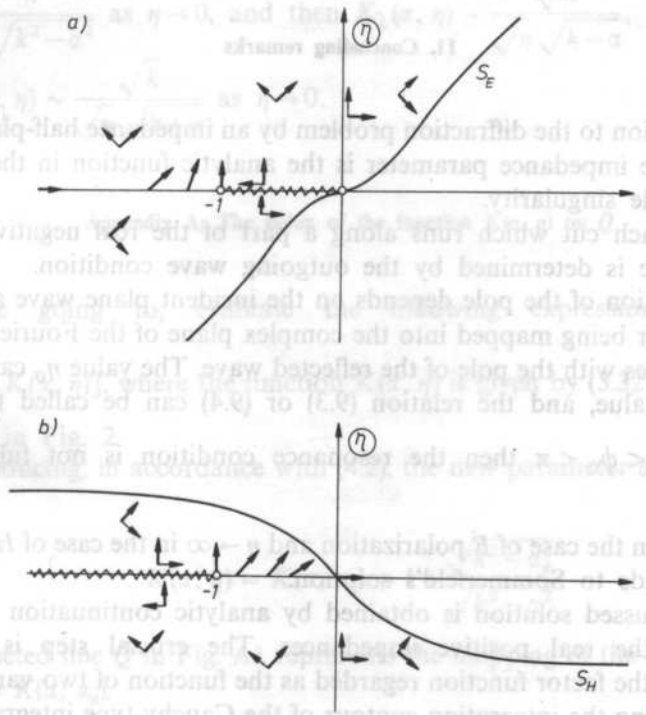

FIG. 10. Impedance plane showing the surface waves: (a) for E polarization, (b) for H polarization, $\rightarrow \mathbf{n}_p$ shows the direction of wave propagation, $\rightarrow \mathbf{n}_A$ shows the direction of wave amplitude decaying

which implies that the power flow vector is directed along $\mathbf{n}_p$. Thus, the wave carries energy towards the half-plane for passive impedances except $\operatorname{Re}\eta = 0$, and it carries energy away from it for active impedances except for $\eta \neq \infty$ for E–polarization and $\eta \neq 0$ for H–polarization. In these exceptional cases, the power-vector is parallel to the half-plane.

The direction of $\mathbf{n}_A$–vector shows, that the amplitude of the surface wave exponentially decays in the directions of both x and z–axis for passive impedances, $\operatorname{Re}\eta = 0$ excluded, while for active impedances the situation is different. The

amplitude exponentially grows in one direction and decays in the other direction. One vector component is negative, the second one is positive, and they change the signs on the real negative semiaxis.

One more difference between passive and active impedances is, that no surface wave exists for passive impedances belonging to the domain bounded by S_E and S_H lines (see also BOWMAN [6]). On the contrary, for active impedances belonging to the domain bounded by S_E and S_H lines there exists a surface wave of E polarization as well as that of H polarization.

11. Concluding remarks

1. The solution to the diffraction problem by an impedance half-plane treated as a function of the impedance parameter is the analytic function in the cut η–plane except for a pole singularity.

2. The branch cut which runs along a part of the real negative axis in the complex η–plane is determined by the outgoing wave condition.

3. The location of the pole depends on the incident plane wave angle ϕ_0. The pole $\eta = \eta_0$, after being mapped into the complex plane of the Fourier transformed solution, coincides with the pole of the reflected wave. The value η_0 can be regarded as a resonant value, and the relation (9.3) or (9.4) can be called the resonance condition. If $\frac{\pi}{2} < \phi_0 < \pi$ then the resonance condition is not fulfiled for any impedance.

4. As $\eta \to 0$ in the case of E polarization and $\eta \to \infty$ in the case of H polarization, the solution tends to Sommerfeld's solution.

5. The discussed solution is obtained by analytic continuation of the Senior solution from the real positive impedances. The crucial step is the analytic continuation of the factor function regarded as the function of two variables. This is done by deforming the integration contour of the Cauchy-type integral. Earlier, the same idea was used by Hurd to derive Wiener-Hopf-Hilbert equations.

6. Analytically continued factor function (8.4)–(8.9) is also an analytic continuation of the solution of the Wiener-Hopf-Hilbert equation on Γ_0, onto two-sheeted Riemann surface η. Another representation of analytic continuation of this solution from Ω_E^- into Ω_E^+ is given by NASALSKI [8]. Analytic continuation of the factor function was first done by MARCINKOWSKI [9] in application to numerical calculations.

7. The function $K_L(\alpha, \eta)$ can be expressed in terms of Maliuzhinets function [10]. Such representation is suitable for computations which are performed in different ways by several authors. The most complete information can be found in [11].

8. It should be noted, that the function $K(\alpha, \eta)$ used in this paper differs by the

factor $1/\eta$ from the function $K(\alpha)$ introduced by SENIOR [1], that is $K(\alpha, \eta) = \frac{1}{\eta} K(\alpha)$, hence $K_L(\alpha, \eta) = \frac{1}{\sqrt{\eta}} K_-(\alpha)$, $K_U(\alpha, \eta) = \frac{1}{\sqrt{\eta}} \cdot \frac{1}{K_+(\alpha)}$.

9. It should be also emphasized, that while the solution to the diffraction problem for the impedance half-plane tends to Sommerfeld's solution as $\eta \to 0$, the factorized function used here does not tend to the factorized function in Sommerfeld's problem. The same refers to the factor functions. That is:

$$K(\alpha, \eta) \sim \frac{k}{\eta \sqrt{k^2 - \alpha^2}} \text{ as } \eta \to 0, \text{ and then } K_L(\alpha, \eta) \sim \frac{\sqrt{k}}{\sqrt{\eta}\sqrt{k-\alpha}},$$

$$K_U(\alpha, \eta) \sim \frac{\sqrt{k}}{\sqrt{\eta}\sqrt{k+\alpha}} \text{ as } \eta \to 0.$$

Appendix A. The index of the function $K(\alpha, \eta)$ on Q

We are going to, evaluate the following expression: $\operatorname{ind}_Q K(\alpha, \eta) = \frac{1}{2\pi} \int_Q d[\arg K(\alpha, \eta)]$, where the function $K(\alpha, \eta)$ is given by (3.32) and the contour Q is shown in Fig. 2.

By introducing, in accordance with (4.2), the new parameter α_d instead of η we have

$$K(\alpha, \eta) = K(\alpha, \alpha_d) = 1 + \frac{\sqrt{k^2 - \alpha_d^2}}{\sqrt{k^2 - \alpha^2}} \tag{A1}$$

The directed line $\bar{Q}$ in Fig. A1 represents the mapping of the contour Q by the function $w = K(\alpha, \alpha_d)$.

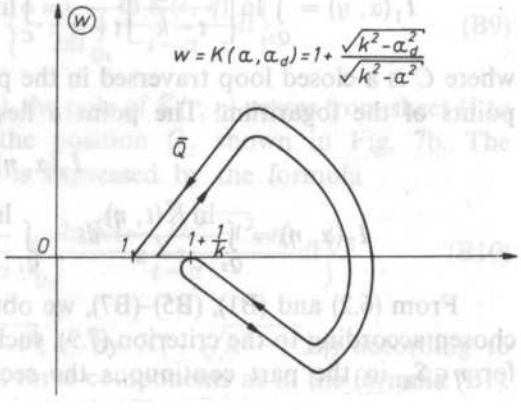

FIG. A1. The directed line $\bar{Q}$ as the mapping of the contour Q by the function $K(\alpha, \eta) = K(\alpha, \alpha_d)$

The increase of the argument of $K(\alpha, \alpha_d)$ on the contour Q is equal to the increase of the argument of the vector $w(Q)$, the initial point of which is (0, 0), and the end-point moves along the directed line $\bar{Q}$. This increase can be easily read from the picture, and is equal to zero. In conclusion $\operatorname{ind}_Q K(\alpha, \eta) = 0$

Appendix B. Derivation of the formulas (8.4) – (8.9)

The first two formulas (8.4) and (8.5), are already known as coinciding with (7.1ab). We shall derive (8.5) once again by using a different method which also works in each of the remaining sectors of η.

For $K_L(\alpha, \eta)$, we use the representation (6.2), where the contour Q shifted to the location Q_2 is shown in Fig. 7b. We write the Cauchy-type integral as a sum of three components

$$\int_{Q_2} \ln\left[\frac{(t-\alpha_d^{(1)})(t-\alpha_d^{(2)})\,\bar{K}(t,\eta)}{(t+k)(t-k)}\right]\frac{dt}{t-\alpha} = I_1(\alpha,\eta)+I_2(\alpha,\eta)+I_3(\alpha,\eta), \tag{B1}$$

where

$$I_1(\alpha,\eta) = \int_{Q_2} \ln\left[\frac{t-\alpha_d^{(1)}}{t-k}\right]\frac{dt}{t-\alpha}, \tag{B2}$$

$$I_2(\alpha,\eta) = \int_{Q_2} \ln\left[\frac{t-\alpha_d^{(2)}}{t+k}\right]\frac{dt}{t-\alpha}, \tag{B3}$$

$$I_3(\alpha,\eta) = \int_{Q_2} \frac{\ln \bar{K}(t,\eta)}{t-\alpha}\,dt, \tag{B4}$$

and where $\alpha \in \Omega^-_{Q_2}$ in every integral above.

We evaluate these integrals succesively.

$$I_1(\alpha,\eta) = \int_{Q_2} \ln\left[\frac{t-\alpha_d^{(1)}}{t-k}\right]\frac{dt}{t-\alpha} = \oint_C \ln\left[\frac{t-\alpha_d^{(1)}}{t-k}\right]\frac{dt}{t-\alpha} = -2\pi i \ln\frac{\alpha-\alpha_d^{(1)}}{\alpha-k}, \tag{B5}$$

where C is a closed loop traversed in the positive direction, containing both branch points of the logarithm. The point α lies outside of C.

$$I_2(\alpha,\eta) = 0, \tag{B6}$$

$$I_3(\alpha,\eta) = \int_{Q_2} \frac{\ln \bar{K}(t,\eta)}{t-\alpha}\,dt = \int_{Q_1} \frac{\ln \bar{K}(t,\eta)}{t-\alpha}\,dt = \int_{\Gamma_0} \frac{\ln K^*(t,\eta)}{t-\alpha}\,dt. \tag{B7}$$

From (6.2) and (B1), (B5)–(B7), we obtain (8.5). The branch of the logarithm is chosen according to the criterion (7.9), such that the function $K_L(\alpha, \eta)$ is continuous for $\eta \in S_E$ in the part continuous the sector A, Fig. B1.

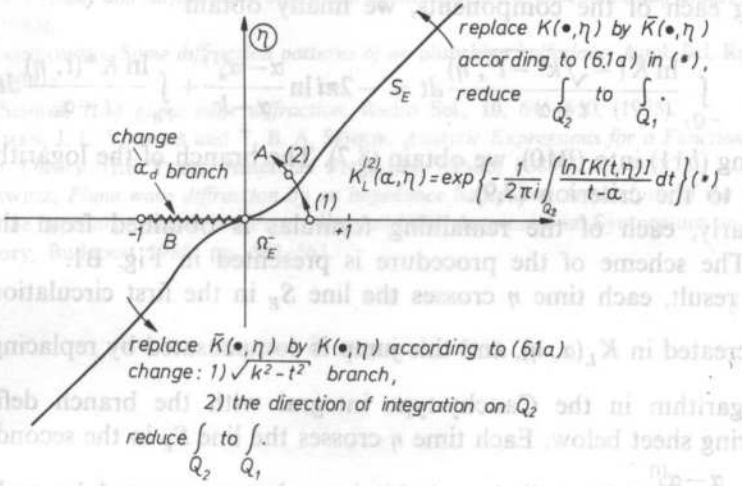

FIG. B1. The scheme of evaluation of $K_L(\alpha, \eta)$ in the neighbourhood of $\eta = 0$, while η goes around $\eta = 0$, starting from the point (1)

The formula (8.6) is obtained from (8.5) by changing the branch α_d thus leading to the continuity of the function $K_L(\alpha, \eta)$ for $\eta \in [-1, 0)$, Fig. B1.

For $\eta \in \Omega_E^-$ now, the contour Ω partially lies on the sheet α_{II}, Fig. 7c. We are going to continue analytically the function (8.6)

If we change $\sqrt{k^2-t^2}$ to $-\sqrt{k^2-t^2}$ in (8.6), we have to change the direction of integration on Γ_0 according to the equality

$$\int_{\Gamma_0} \frac{\ln K^*(\sqrt{k^2-t^2}, \eta)}{t-\alpha} dt = \int_{-\Gamma_0} \frac{\ln K^*(-\sqrt{k^2-t^2}, \eta)}{t-\alpha} dt. \tag{B8}$$

We rewrite the formula (8.6) in the form (6.3) (where $\alpha_d^{(1)}$ is replaced by $\alpha_d^{(2)}$), and continue it analytically by deforming the contour of integration Q to Q_1:

$$K_L(\alpha, \eta) = \frac{\alpha-\alpha_d^{(2)}}{\alpha-k} \exp\left\{-\frac{1}{2\pi i} \int_{Q_1} \frac{\ln \bar{K}(t, \eta)}{t-\alpha} dt\right\} \tag{B9}$$

When η passes from B to Ω_E^- (Fig. B1), the pole of $\bar{K}(t, \eta)$ passes from sheet II to sheet I. It pushes the contour Q_1 to the position Q_2 shown in Fig. 7b. The analytically continued function $K_L(\alpha, \eta)$ is expressed by the formula

$$K_L(\alpha, \eta) = \frac{\alpha-\alpha_d^{(2)}}{\alpha-k} \exp\left\{-\frac{1}{2\pi i} \int_{-Q_2} \frac{\ln \bar{K}(-\sqrt{k^2-t^2}, \eta)}{t-\alpha} dt\right\}. \tag{B10}$$

We replace the function $\bar{K}(-\sqrt{k^2-t^2}, \eta)$ by $K(-\sqrt{k^2-t^2}, \eta)$ according to (6.1a), and rewrite the integral as a sum of three components as in the formula (B1).

Evaluating each of the components, we finally obtain

$$\int_{-Q_2} \frac{\ln \bar{K}(-\sqrt{k^2-t^2}, \eta)}{t-\alpha} dt = -2\pi i \ln \frac{\alpha-\alpha_d^{(1)}}{\alpha-k} + \int_{\Gamma_0} \frac{\ln K^*(t, \eta)}{t-\alpha} dt. \tag{B11}$$

Putting (b11) into (B10), we obtain (8.7). The branch of the logarithm is chosen according to the criterion (7.9).

Similarly, each of the remaining formulas is obtained from the preceding formula. The scheme of the procedure is presented in Fig. B1.

As a result, each time η crosses the line S_E in the first circulation, the factor $\frac{\alpha-\alpha_d^{(i)}}{\alpha-k}$ is created in $K_L(\alpha, \eta)$, and this jump is compensated by replacing the branch of the logarithm in the Cauchy-type integral with the branch defined on the neighbouring sheet below. Each time η crosses the line S_E in the second circulation, the factor $\frac{\alpha-\alpha_d^{(i)}}{\alpha-k}$ is cancelled, and this jump is compensated by replacing of the branch of logarithm with that defined on the neighbouring sheet above.

After the two circulations the value of the analytically continued function $K_L(\alpha, \eta)$ returns to the initial value.

Acknowledgement

The author wishes to thank Professor S. PRZEŹDZIECKI for his discussions helpful suggestions and encouragement which prompted the study leading to the results presented here. The author also wishes to thank Dr. A. CIARKOWSKI for critical reading of the manuscript and his valuable comments.

References

[1] T. B. A. SENIOR, *Diffraction by a semi-infinite metallic sheet*, Proc. Roy. Soc. London A. **213**, 436–458, (1952).

[2] L. FELSEN, M. MARCUVITZ, *Radiation and Scattering of Waves*, Prentice-Hall, Inc., Englewood Cliffs, New Jersey 1973.

[3] M. G. KREJN, *Integral equations on a half-line with a kernel depending on the difference of arguments*, Usp. Matem. Nauk, XIII, No 5 (83), 3, (1958), (in Russian).

[4] A. SOMMERFELD, *Mathematishe Theorie der Diffraction*, Math. Ann. **47**, 317–374, (1986).

[5] N. J. MUSKHELISHVILI, *Singular integral equations*, Noordhoff, Groningen 1953.

[6] John J. BOWMAN, *High frequency backscatering from an absorbing infinite strip with arbitrary face impedances*, Can. J. Phys. **45**, 2409–2429, (1967).

[7] R. A. HURD, *The Wiener-Hopf-Hilbert method for diffraction problems*, Can. J. Phys. **54**, 775–780, (1976).

[8] W. NASALSKI, *Leaky and surface wave diffraction by an asymmetric impedance half-plane*, Can. J. Phys. **61**, 906, (1983).

[9] C. J. MARCINKOWSKI, *Some diffraction patterns of an absorbing half-plane*, Appl. Sci. Res. **B9**, No 3, 189–198, (1961).

[10] T. B. A. SENIOR, *Half plane edge diffraction*, Radio Sci., **10**, 645–650, (1975).

[11] M. I. HERMAN, J. L. VOLAKIS and T. B. A. SENIOR, *Analytic Expressions for a Function Occuring in Diffraction Theory*, IEE Trans. Antennas Propagat., **AP-35**, 1083–1086, (1987).

[12] H. KUDREWICZ, *Plane wave diffraction by an impedance half-plane. An analysis of the solution with respect to the impedance parameter*, Proceedings of URSI International Symposium on Electromagnetic Theory, Budapest 1986, pp. 561–563.

Received on August 10, 1989

ARCHIVES OF ACOUSTICS
15, 1–2, 185–192 (1990)

INFORMATION CONTENTS OF THE ACOUSTIC EMISSION EXEMPLIFIED BY THE SELECTED PHYSICO-CHEMICAL PROCESSES

W. MIKIEL, J. RANACHOWSKI, F. REJMUND, J. RZESZOTARSKA

Institute of Fundamental Technological Research, Polish Academy of Sciences
(00–049 Warszawa, Świętokrzyska 21)

1. Introduction

The main sources of the acoustic emission (AE) signals in the physico-chemical processes are the phase transitions, gas evolution and heat of the reaction [1, 2]. Measurements of AE signals in solutions are more difficult than in solids because of low energetic levels. Energies of AE measured for the reactions in solutions are not much higher than the noise level of measuring apparatus; beside this, such interferences as wavy motion, liberation of dissolved gas and liquid mixing noise are present. This is why the investigation of chemical reactions in the solution with AE method necessitates for the application of highly sensitive measuring sets and computer data processing systems.

2. Sources of AE signals in chemical reactions

Acoustic emission is generated and can be measured in chemical reactions of various types [1–5]. In general, the relation of the AE signal energy to the number of events as a function of time is recorded. The graphs shapes of these relations are usually close to the distributions of other parameters which are recorded as time – dependent functions with other measuring methods, as e.g. potentiometric, thermal or calorimetric methods. The hitherto experimental results can be treated mainly as qualitative identification of physical effects which result in strain energy generation in the form of AE signals. BATTERIDGE et al. [3] studied about 50 diverse chemical reactions. Among them the exothermic and heterogenic reactions exhibit acoustic activity; particularly acoustically active are the reactions with gas liberation. In the seventies, Biełousow and Żabotyński discovered the reactions in which the

system does not tend to the stable state but repeats periodically the dynamical stages of the process. The classical oscillatory reaction (B–Ż) of oxidation of the malonic acid with bromates can be catalyzed by the cerium ions (III), manganium ions (II) or ferroine [6]. In the reaction (B–Ż) catalyzed by cerium (III) four mutually related processes can be distinguished. In the presence of H^+:

$$BrO_3^- + Br^- + 2H^+ \rightarrow HBrO_2 + HOBr \quad (1)$$

$$HBrO_2 + Br^- + H^+ \rightarrow 2HOBr \quad (2)$$

$$HOBr + Br^- + H^+ \rightarrow Br_2 + H_2O \quad (3)$$

$$Br + CH_2(COOH)_2 \rightarrow BrCH(COOH)_2 + Br^- + H^+ \quad (4)$$

The general reaction is represented by the equation

$$BrO_3^- + 2Br^- + 3CH_2(COOH)_2 + 3H^+ \rightarrow 3BrCH(COOH)_2 + 3H_2O \quad (A)$$

The second oscillatory reaction recorded by the authors with the use of AE was the reaction of decomposition of hydrogen peroxide catalyzed by iodates the Bray –Liebhafsky (B–L) reaction. The hydrogen peroxide plays a dual role in this reaction: the role of the oxidation (5) and reduction (6):

$$5H_2O_2 + I_2 \rightarrow 2HIO_3 + 4H_2O \quad (5)$$

$$5H_2O_2 + 2HIO_3 \rightarrow I_2 + 5O_2 + 6H_2O \quad (6)$$

$$H_2O_2 \rightarrow H_2O + \frac{1}{2}O_2 \quad (B)$$

The emerging reaction products periodically drive the system nearer and farther from the balance point. The oscillation period depends on the concentration of substrates. Oscillatory reactions are carried out in closed systems with diffusion reactant transport or with continuous mixting, and also in the systems with the flow of a passive gas which removes the gas products from the vessel [7]. The oscillatory reactions which take place in the presence of redox-type catalysts are tested mainly with the potentiometric, and less frequently with the colorimetric method. The acoustic emission method makes it possible to distinguish a number of processes which take place in these reaction, as the local disturbance of thermal equilibrium and gas phase liberation.

3. Measurements of acoustic emission in physico-chemical reactions

Experimental investigations of the acoustic emission AE in physico-chemical processes are carried out as a cycle of measurements realized in time which include only AE. signal measurements or also other parameters transformed into the magnitudes of voltage, as the optic density of liquid, specific resistance, pH and

temperature. Regarding the time relations of these signals (as functions of temperature and concentrations) it is necessary to find at the first stage of the experiment, the variations of which of the measured quantities are the quickest. The measuring cycle quantization time should be chosen shorter by an order of magnitude. The results of measurements obtained with such assumptions allow to find, with the numerical methods, the basic parameters of time periodicity of the processes (spectral analysis), or to approximate them with the apperiodic functions (polynomials). The typical scientific measuring data processing software packages make it also possible to study mutual correlations between the magnitudes measured in the experiment.

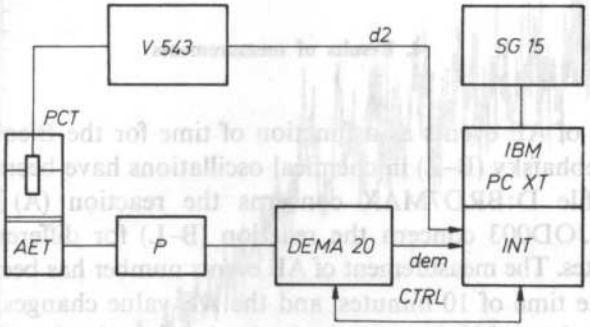

FIG. 1. Block diagram of the measuring set

The measurements have been carried out with the system displayed in the Fig. 1. The glass vessel containing the reactant mixture has been coupled with the acoustic emission transducer AET and the physico-chemical parameters transducer PCT, which co-operates with the numerical voltage or resistance meter, type MERATRONIK V 543. The AET transducer co-operates with the DEMA 20 analyzer through preamplifier P. Both measuring devices have 5–digit numerical outputs in the BCD code and a set of control signals. As an output, the three data blocks are obtained:

dem – block of data on the number of AE events counted in the intervals of 0.1, 1 or 10 s;

d2 – block of data on the physical quantity defined by the type of the PCT transducer, which varies much slower then the AE and is measured at the time of transmission of DEM data;

CTRL – block of the signals which control the cycle of transmission, dependent in time on the signals which control DEM; these signals, in turn, are software controlled by the *I/O* parallel interface of the IBM PC/XT. The parallel interface card, designed and manufactured specially for this purpose, enables simultaneous transmission of 12 bytes of data and 2 bytes of control signals in both directions.

The real-time process of measuring and storing the data during the experiment is realized by the program DEMASCII, which contains the following functional blocks:

1. Automatic measurement and loading the data to the operating memory.
2. Plotting the graph on a parameter-time or parameter-parameter plane.
3. Printout of the plot in the graphic mode.
4. Storing the data as a binary disk file with a chosen name.
5. Reading the data from the disk file to the memory buffer.
6. Conversion of the binary data sers to the ASCII code with separators between data and writing such strings with a name to the disk file.

4. Results of measurements

The numbers of AE events as a function of time for the Bieołusow–Żabotyński (A) and Bray–Liebhafsky (B–Ż) in chemical oscillations have been displayed in Figs. 2–8. The data file D:BRO7MAX concerns the reaction (A) whereas the files D:JOD103 and JOD003 concern the reaction (B–L) for different initial concentrations of substrates. The measurement of AE events number has been carried out every second during the time of 10 minutes, and the AE value changes from 5 to 400 for iodates and from 5 to 1200 have been obtained. After plotting the distributions of measured data, it has been observed that the scatter of data points was very large, what made impossible the interpretation and comparisons of the results. In the next stage of the analysis, carried out offline, the data have been transformed to the ASCII

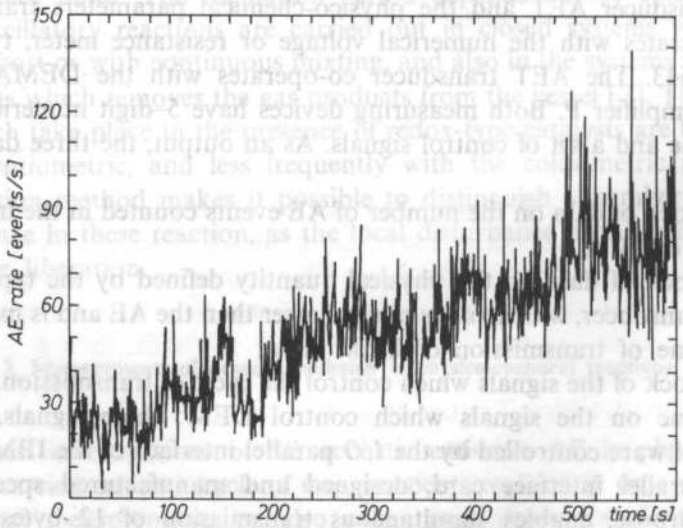

FIG. 2. The plot of AE events number for B–L reaction (D:JOD103)

code and subjected to some numerical processing. In the Figs. 2 and 3 the graphs of numbers of AE events for the data D:JOD103 and D:BRO7MAX have been shown. The plots were obtained by connecting the subsequent data points with sectors. The general AE increase tendency in time can be observed; the differences consist in that for bromium the AE increase is quicker and the oscillations take place after 5 minutes. In order to discriminate the periodical AE changes the moving average

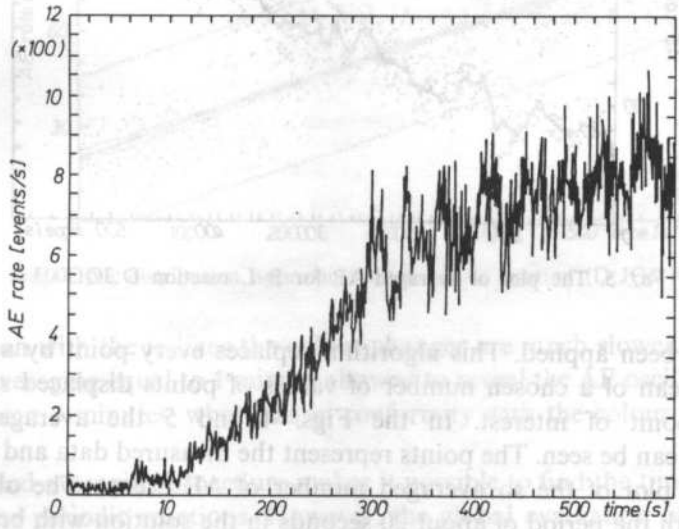

FIG. 3. The plot of AE events number for B–Ż reaction (D:BRO7MAX)

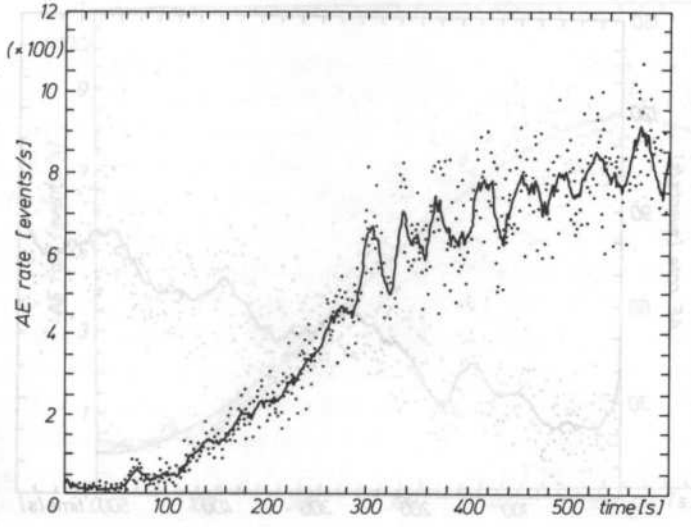

FIG. 4. The plot of averaged AE for B–Ż reaction (D:BRO7MAX)

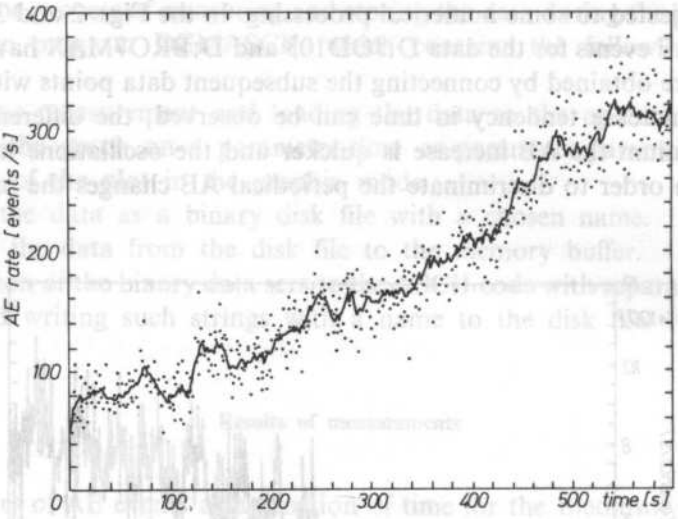

FIG. 5. The plot of averaged AE for B–L reaction D:JOD003

algorithm has been applied. This algorithm replaces every point by a point which value is the mean of a chosen number of values of points displaced symmetrically around the point of interest. In the Figs. 4 and 5 the averaged results of measurements can be seen. The points represent the measured data and the solid line represents the plot of the so averaged number of AE events. The observation of oscillations with the period of about 20 seconds in the solution with bromates takes place simultaneously with the emergence of periodic change of the solution colour.

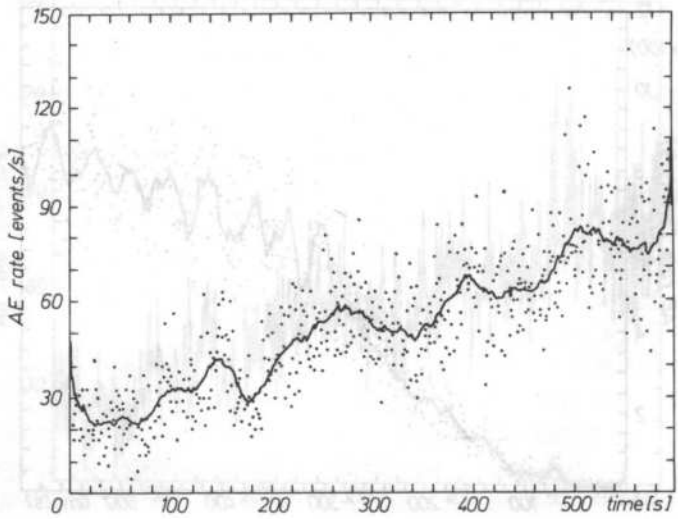

FIG. 6. The plot of averaged AE for B–L reaction (D:JOD103)

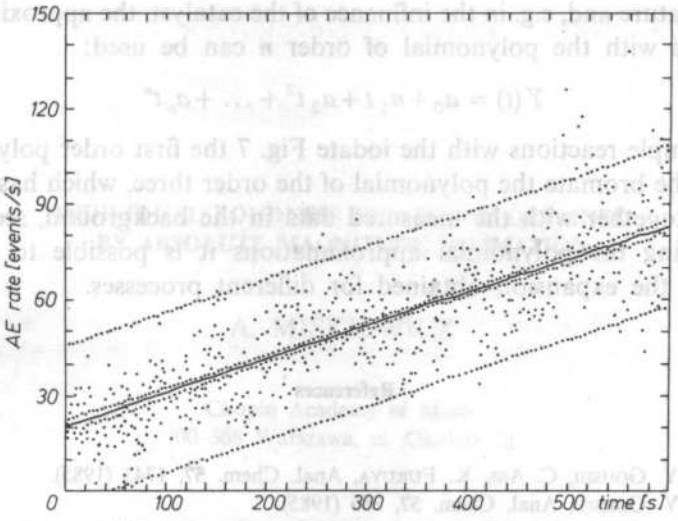

FIG. 7. AE distribution approximation for B–L reaction (D:JOD103)

In the solution with the iodates the colour changes are much slower. Application of the time of averaging equal to 1 minute allowed to reveal the AE oscillations with the period of about 3 minutes, what was in conformity with the colour changes period (Fig. 6).

The applied averaging procedure makes it possible to find the time parameters of the AE in the periodic reactions. However, the global evaluation of the process is difficult. To enable the comparison of various experiments which differ in concent-

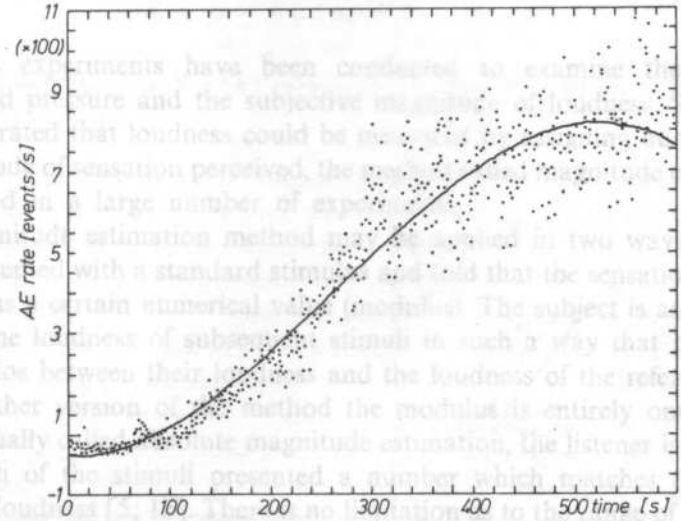

FIG. 8. AE distribution approximation for B–Ż reaction (D:BRO7MAX)

ration, temperature and, e.g. in the influence of the catalyst, the approximation of the AE (t) process with the polynomial of order n can be used:

$$Y(t) = a_0 + a_1 t + a_2 t^2 + \ldots + a_n t^n$$

In the example reactions with the iodate Fig. 7 the first order polynomial is the best, and for the bromate the polynomial of the order three, which has been plotted in the Fig. 8 together with the measured data in the background, seems the most expedient. Using the polynomial approximations it is possible to compare the coefficients of the expansion obtained for different processes.

References

[1] T. Sawada, Y. Gohshi, C. Abe, K. Furuya, Anal. Chem. **57**, 1743 (1985).
[2] T. Sawada, Y. Gohshi, Anal. Chem. **57**, 366 (1985).
[3] D. Betteridge, M. T. Joslin, T. Lilley, Anal. Chem. **53**, 1064 (1981).
[4] R. N. Belchamber, D. Betteridge, M. P. Collins, T. Lilley, C. Z. Marczewski, A. P. Wade, Anal. Chem. **58**, 1973 (1986).
[5] A. N. Smirnow, A. N. Dementiew, Ż. Fiz. Chem. 59, 1972 (1985).
[6] O. Gurel, D. Gurel, Topics in current chemistry, Springer Verlag, Berlin, vol. 118 (1984).
[7] V. Ševčik, L. Adamcikowa, J. Phys. Chem. **8**, 9, 5178 (1985).

Received on March 20, 1989

ARCHIVES OF ACOUSTICS
15, 1–2, 193–200 (1990)

INDIVIDUAL LOUDNESS FUNCTIONS OBTAINED BY ABSOLUTE MAGNITUDE ESTIMATION

A. MIŚKIEWICZ

Chopin Academy of Music
(00–368 Warszawa, ul. Okólnik 2)

Six subjects estimated, in individual listening sessions loudness of 1/3–octave noise band centered at 1 kHz. The results confirm that numerical estimates of loudness are unique characteristics of individual observers. In the present study no evidence for the existence of an absolute loudness scale could be observed.

W eksperymencie opisanym w niniejszej pracy przeprowadzono badania przebiegu wartościowania głośności szumu pasmowego o szerokości tercji i częstości środkowej 1 kHz. W pomiarach uczestniczyło 6 słuchaczy. Stwierdzono znaczne zróżnicowanie osobniczych funkcji wartościowania głośności. Uzyskane wyniki nie potwierdzają hipotezy o absolutnej zależności między wielkością wrażenia głośności i wartościami liczbowymi przypisywanymi głośności w skalowaniu.

1. Introduction

Numerous experiments have been conducted to examine the relationship between sound pressure and the subjective magnitude of loudness. Since STEVENS [11] demonstrated that loudness could be measured by assigning numbers directly to the magnitude of sensation perceived, the method called magnitude estimation has been employed in a large number of experiments.

The magnitude estimation method may be applied in two ways. In one, the listener is presented with a standard stimulus and told that the sensation of loudness it produces has a certain numerical value (modulus). The subject is asked to assign numbers to the loudness of subsequent stimuli in such a way that his judgments reflect the ratios between their loudness and the loudness of the reference tone [4; 11]. In the other version of the method the modulus is entirely omitted. In this procedure, usually called absolute magnitude estimation, the listener is instructed to assign to each of the stimuli presented a number which matches the subjective magnitude of loudness [5; 15]. There is no limitation as to the range of numbers: the subject is allowed to use any positive number that appears appropriate.

It has been demonstrated in numerous investigations that loudness scales derived from magnitude estimation data obey the formula known as "Stevens' Power Law", that is, $L = kp^n$, where L represents the magnitude of loudness, p the sound pressure, k is an arbitrary constant which depends on the scale unit, and n, the power exponent.

STEVENS [11] observed that the form of loudness functions obtained by magnitude estimation was dependent on the intensity of the reference tone. HELLMAN and ZWISLOCKI [4] confirmed in a more elaborated study that the chosen sensation level of the reference stimulus had a substantial effect on the shape of the loudness function (Fig. 1). The form of the loudness function was also affected when the loudness of the reference tone was associated with different numbers.

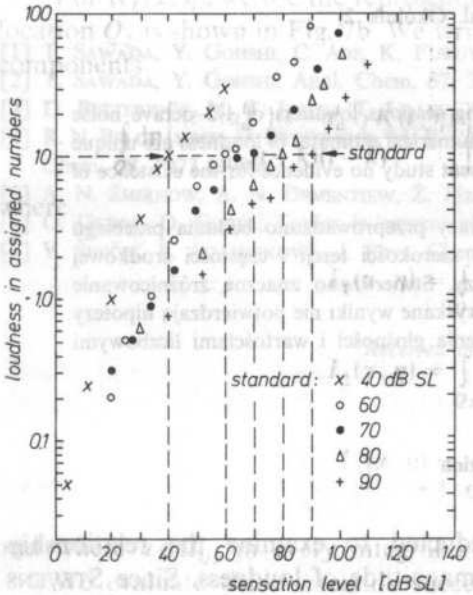

FIG. 1. Median loudness estimates of a 1-kHz tone obtained with the reference number 10 associated with five different sensation levels. (Data from [5], quoted in [15])

HELLMAN and ZWISLOCKI [4] argued that the observed influence of the modulus value on the shape of the loudness function is evidence that subjects make numerical judgments of loudness on an absolute rather than a ratio scale. If numbers assigned to loudness represented a ratio scale, the intensity of the reference tone or the number associated with the modulus, should have only influenced listeners' judgments in changing them by a multiplicative constant. The observed nonlinearity between responses obtained with different modulus results from the existence of a natural, absolute coupling between loudness and its numerical estimates. Subjects assign numbers to loudness in such a way that their subjective impression of how large a number is matches the subjective magnitude of loudness. If loudness of the reference stimulus and the reference number are not in agreement with the natural, absolute scale, listeners tend subconsciously to correct their responses to converge

with the absolute loudness function that is obtained without a designated modulus and data normalization.

The concept of an "absolute" scale has been derived from Stevens' classification of scales based on permissible mathematical transformations that leave the scale form invariant. The highest level scale in Stevens' classification is the ratio scale which allows the scale values to be multiplied by a constant. The absolute scale, as stated by ZWISLOCKI and GOODMAN [15] "implies a fixed unit and, therefore, an absolute coupling between numerals and psychological magnitudes."

ZWISLOCKI and GOODMAN [15] pointed out that the absolute scaling hypothesis may also be supported by the convergence of magnitude estimation and magnitude production data obtained in experiments which were conducted in different laboratories on separate groups of subjects. The results compared in Fig. 2 show that on the average, two different groups of listeners associated approximately the same numbers with the same sensation levels. On the basis of the data shown in Fig. 2, ZWISLOCKI and GOODMAN presented a loudness function which reflects the absolute (constant) relationship between the sensation level of a 1 kHz tone and the numbers assigned to its loudness (Fig. 3).

The absolute scaling hypothesis was suggested from the convergence of average data obtained on groups of subjects, however, it has been demonstrated in a number of investigations that among listeners with normal hearing the exponents of

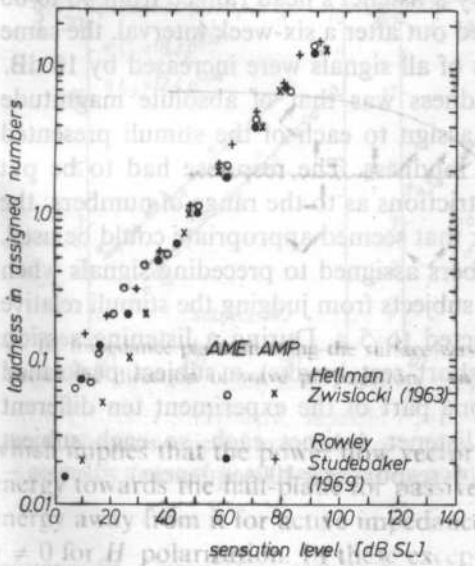

FIG. 2. Loudness of a 1-kHz tone in monaural presentation. Absolute magnitude-estimation (AME) and absolute magnitude-production (AMP) results obtained in two independent studies (Data from [5] and [8], quoted in [15])

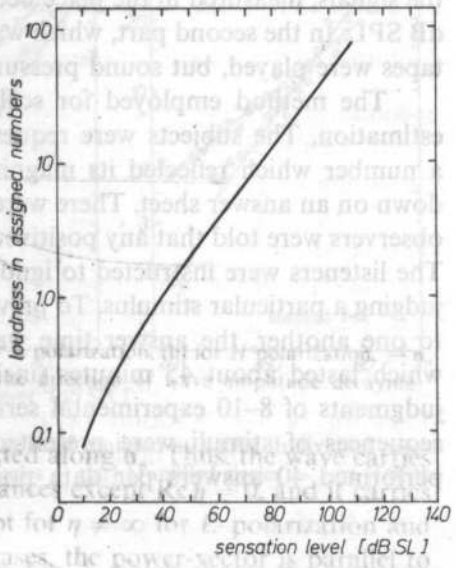

FIG. 3. Loudness function of a 1-kHz tone in binaural presentation. Absolute relationship between the sensation level of the tone and numbers assigned to its loudness. (After [15])

individual loudness functions vary within a large range [2; 3; 6; 7; 9]. The variability of individual loudness functions leads to the conclusion that not all listeners perform absolute magnitude estimates of loudness in accordance with the function presented in Fig. 3. If subjects made numerical estimates of loudness on an absolute scale, it could therefore be assumed that the loudness function shown in Fig. 3 represents the mean of different, individual absolute loudness scales.

The aim of the present study was to examine whether the tendency to couple numbers with loudness on a constant, absolute scale may also be observed in judgments by individual observers.

2. Procedure

Six students aged 20 to 24 years estimated, in individual listening sessions, the loudness of 1/3–octave noise bursts centered at 1 kHz. The stimuli, recorded on tape were played back through a loudspeaker placed in a listening room, 2 m from the subject. The noise signals were presented in series comprising 21 stimuli of different sound pressure levels. The duration of each noise burst was 1 s with an interstimulus interval of 5 s. Ten tapes with stimuli recorded in different, randomly chosen sequences were used.

The experiment was conducted in two parts. In the first, sound pressure levels of the signals, measured in the place occupied by a listener's head ranged from 40 to 80 dB SPL. In the second part, which was carried out after a six-week interval, the same tapes were played, but sound pressure levels of all signals were increased by 10 dB.

The method employed for scaling loudness was that of absolute magnitude estimation. The subjects were requested to assign to each of the stimuli presented a number which reflected its magnitude of loudness. The response had to be put down on an answer sheet. There were no restrictions as to the range of numbers: the observers were told that any positive number that seemed appropriate could be used. The listeners were instructed to ignore numbers assigned to preceding signals when judging a particular stimulus. To prevent the subjects from judging the stimuli relative to one another, the answer time was restricted to 5 s. During a listening session which lasted about 45 minutes (including short rest breaks), a subject performed judgments of 8–10 experimental series. In one part of the experiment ten different sequences of stimuli were presented to a listener 4 times each, so each subject performed 40 answers per data point (i.e. 4 responses $\times$ 10 sequences).

3. Results

Figure 4 shows individual results of loudness estimation obtained in the first and second part of the experiment. Each point indicates the geometric mean of 40 judgments. The data are approximated by a power function determined by a least

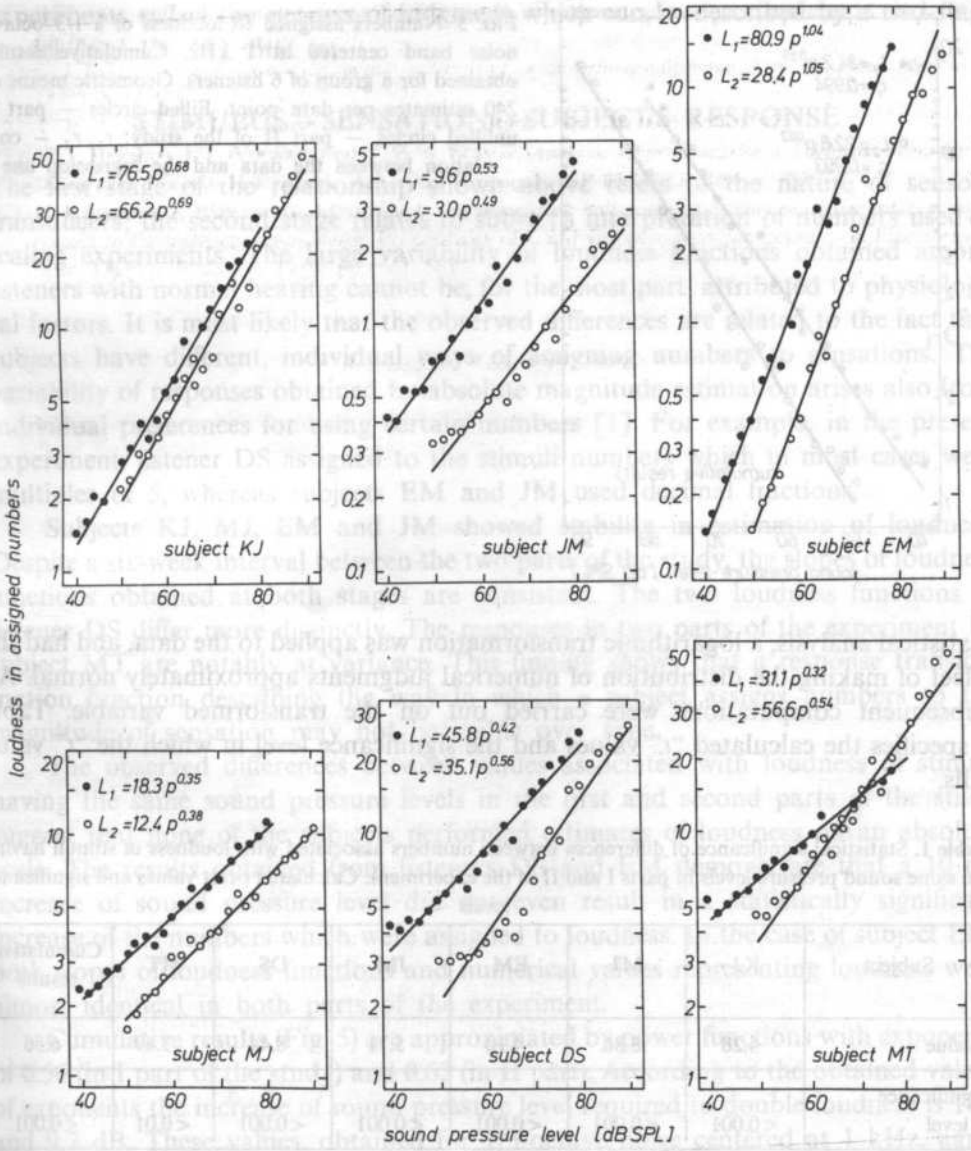

FIG. 4. Numbers assigned to loudness of a 1/3–octave noise band centered at 1 kHz. Individual results – geometric means of 40 estimates per data point. Filled circles – part I, unfilled circles – part II of the study

squares fit. Cumulative results are presented in Fig. 5 which shows the geometric means of 240 estimates (6 listeners × 40 judgments).

In order to examine the statistical significance of the differences between numbers assigned to stimuli having the same sound pressure levels in both parts of the experiment, a *t*-test analysis of the data was carried out. For the purpose of

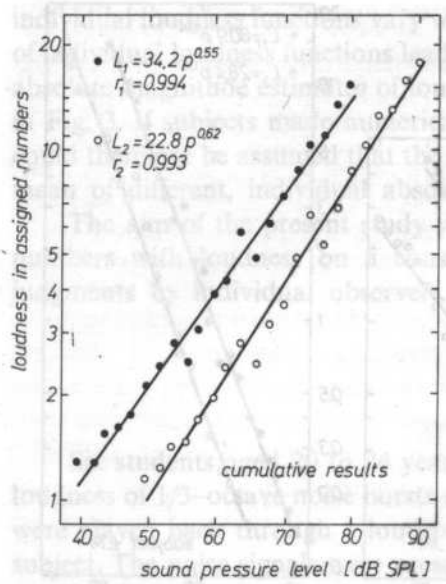

FIG. 5. Numbers assigned to loudness of a 1/3-octave noise band centered at 1 kHz. Cumulative results obtained for a group of 6 listeners. Geometric means of 240 estimates per data point. Filled circles – part I, unfilled circles – part II of the study; r_1, r_2 – correlation between the data and the regression line

statistical analysis, a logarithmic transformation was applied to the data, and had the effect of making the distribution of numerical judgments approximately normal. All subsequent computations were carried out on the transformed variable. Table 1 specifies the calculated "t" values and the significance level in which the "t" value falls.

Table 1. Statistical significance of differences between numbers associated with loudness of stimuli having the same sound pressure levels in parts I and II of the experiment. Calculated t-test values and significance levels

Subject	KJ	MJ	EM	JM	DS	MT	Cumulative results
t-value	4.28	8.86	4.10	5.71	8.44	3.49	6.36
Significance level	<0.001	<0.001	<0.001	<0.001	<0.001	<0.01	<0.001

4. Discussion and conclusions

The exponents of individual loudness functions range from 0.32 to 1.04 (in I part of the experiment) and from 0.35 to 1.06 (in II part). Variability of individual exponents observed in the present investigation is similar in range to that reported in previous studies [2; 3; 6; 9].

It has been stated in the literature that responses performed in sensory scaling

experiments reflect the process of judgment which can be described by a two-stage model [e.g. 12; 13], that is:

STIMULUS → SENSATION → SUBJECT'S RESPONSE

The first stage of the relationship shown above refers to the nature of sensory transducers; the second stage relates to subject's interpretation of numbers used in scaling experiments. The large variability of loudness functions obtained among listeners with normal hearing cannot be, for the most part, attributed to physiological factors. It is most likely that the observed differences are related to the fact that subjects have different, individual ways of assigning numbers to sensations. The variability of responses obtained by absolute magnitude estimation arises also from individual preferences for using certain numbers [1]. For example: in the present experiment, listener DS assigned to the stimuli numbers which in most cases were multiples of 5, whereas subjects EM and JM used decimal fractions.

Subjects KJ, MJ, EM and JM showed stability in estimation of loudness. Despite a six-week interval between the two parts of the study, the slopes of loudness functions obtained at both stages are consistent. The two loudness functions of listener DS differ more distinctly. The responses in two parts of the experiment by subject MT are notably at variance. This finding shows that a response transformation function describing the way in which a subject assigns numbers to the magnitude of sensation may not be stable over time.

The observed differences between values associated with loudness of stimuli having the same sound pressure levels in the first and second parts of the study suggest that none of the subjects performed estimates of loudness on an absolute scale. The results obtained from listeners DS and EM demonstrate that a 10 dB increase of sound pressure level did not even result in a statistically significant increase of the numbers which were assigned to loudness. In the case of subject EM, both slopes of loudness functions and numerical values representing loudness were almost identical in both parts of the experiment.

Cumulative results (Fig. 5) are approximated by power functions with exponents of 0.56 (in I part of the study) and 0.62 (in II part). According to the obtained values of exponents the increase of sound pressure level required to double loudness is 10.8 and 9.7 dB. These values, obtained for 1/3-octave noise centered at 1 kHz, agree fairly well with the standard loudness function of a 1 kHz tone, based on the experimental data which have been compiled by STEVENS [10] from numerous sources. Just as it has been found in individual data, the comparison of cumulative results obtained in both parts of the experiment does not demonstrate evidence of estimating loudness on an absolute scale.

What then are the reasons for the failure to obtain estimates of loudness on an absolute scale in the present work? ZWISLOCKI [14] pointed at the difference between a formally defined scale and its experimental realization. A scale formally defined as absolute should not be considered as being less susceptible to experimental biases

than any other scale. Therefore the experimental conditions should be arranged so that the subjects would be able to respond according to the scale definition.

The present investigation was conducted according to the procedure specified by ZWISLOCKI and GOODMAN [15]. This procedure is very convenient for use in loudness scaling experiments. However, the failure to obtain results that would support the absolute scaling hypothesis leads to a conclusion that conditions under which an absolute scale can be proved to exist need to be determined in more detail. The variability of individual data obtained in experimental conditions arranged in the present investigation argues that further attempts to examine the absolute scaling hypothesis should also include results of loudness scaling obtained from individual observers.

This work was supported by a grant from the Polish Academy of Sciences (CPBP 02.03.7.9).

References

[1] J. C. BAIRD, *Numbers and exponents*, Proc. 2nd Annual Meeting of the International Society for Psychophysics – "Fechner Day". Cassis (1986)

[2] C. M. de BARBENZA, M. E. BRYAN, W. TEMPEST, *Individual loudness functions*, J. Sound. Vib., **11**, 399–410 (1970).

[3] R. P. HELLMAN, *Stability of individual loudness functions obtained by magnitude estimation and production*, Percept. Psychophys, **29**, 63–70 (1981).

[4] R. P. HELLMAN, J. J. ZWISLOCKI, *Some factors affecting the estimation of loudness*, J. Acoust. Soc. Am., **33**, 687–694 (1961).

[5] R. P. HELLMAN, J. J. ZWISLOCKI, *Monaural loudness function at* 1000 cps and interaural summation, J. Acoust. Soc. Am., **35**, 856–865 (1963).

[6] A. W. LOGUE, *Individual differences in magnitude estimation of loudness*, Percept. Psychophys., **19**, 279–280 (1976).

[7] W. J. McGILL, *The slope of the loudness function. A puzzle*, In: Psychological scaling, [eds] H. Gulliksen, S. Messick. Wiley, New York 1960.

[8] R. ROWLEY, G. STUDEBAKER, *Monaural loudness-intensity relationships for a* 1000-Hz *tone*, J. Acoust. Soc. Am., **45**, 1186–1192 (1969).

[9] J. C. STEVENS, M. GUIRAO, *Individual loudness functions*, J. Acoust. Soc. Am., **36**, 2210–2213 (1964).

[10] S. S. STEVENS, *The measurement of loudness*, J. Acoust. Soc. Am., **27**, 815–827 (1955).

[11] S. S. STEVENS, *The direct estimation of sensory magnitudes – loudness*, Am. J. Psychol., **69**, 1–25 (1956).

[12] M. TREISMAN, *Sensory scaling and the psychological law*, Quart. J. Exper. Psychol. **16**, 11–12 (1964).

[13] J. J. ZWISLOCKI, *Group and individual relations between sensation magnitudes and their numerical estimates*, Percept. Psychophys., **33**, 460–468 (1983).

[14] J. J. ZWISLOCKI, *Absolute and other scales: Question of validity*, Percept. Psychophys., **33**, 593–594 (1983).

[15] J. J. ZWISLOCKI, D. A. GOODMAN, *Absolute scaling of sensory magnitudes: A validation*, Percept. Psychophys., **28**, 28–38 (1980).

Received on October 27, 1989

ARCHIVES OF ACOUSTICS
15, 1–2, 201–209 (1990)

A NEW ATTEMPT AT THE ESTIMATION FOR THE NOISE LEVEL PROBABILITY DISTRIBUTION BASED ON SPECIFIC L_x NOISE EVALUATION INDICES

M. OHTA, Y. MITANI

Faculty of Engineering, Hiroshima University Shitami, Saijo-cho, Higashi-hiroshima City, 724 Japan

In this paper, a new attempt at the estimation for the noise level probability distribution is proposed based on the known values of several specific L_x noise evaluation indices. Here, the effect of the restricted amplitude fluctuation range matched to the actual stochastic phenomenon on the estimation accuracy is reasonably taken into consideration. The effectiveness of the proposed method is experimentally confirmed by applying it to the actually measured road traffic noise data.

1. Introduction

It is well-known that the actual environmental stochastic noises exhibit various types of probability distributions, due to the diversified causes of the noise fluctuations. Therefore, their stochastic property shows very often the arbitrary non-Gaussian distribution forms. Of course, every noise evaluation index for these stochastic phenomena can be extracted along to its definition as one of the representative values, by grasping precisely the population probability distribution of the original stochastic phenomenon. From this point of view, many researchers already found various types of important relations among more than two noise evaluation indices in close connection with the above population probability distribution [1–4]. In the authors' previous studies [5, 6], a general theory for estimating the original noise level probability distribution as the above population one has been proposed in a generalized form by employing the known values of *Leq* and several specific L_x levels. In this paper, in a similar way, a new attempt at the estimation for the original population distribution for the noise level fluctuation is considered based on several known specific values of only L_x noise evaluation indices. Here, the measured levels fluctuate only in a restricted amplitude fluctuation range. Thus, in the theoretical consideration, the effect of this restricted amplitude fluctuation range on the estimation accuracy is theoretically taken into consideration

in comparison with the ordinary method having no effect of the above amplitude fluctuation range (i.e., its amplitude fluctuation range is within $(-\infty, \infty)$).

Finally, the effectiveness of the proposed method has been experimentally confirmed by applying it to the actually measured road traffic noise data.

2. Theoretical consideration

2.1 Estimation method with no restriction of amplitude fluctuation range

Let us consider the noise level fluctuation, L, with no restriction of an amplitude fluctuation range. In this case, a statistical Hermite series expansion type expression for the cumulative distribution function of the noise level fluctuating within $(-\infty, \infty)$ can be introduced at the starting point of the analysis, as follows [7]:

$$Q(L) = \int_{-\infty}^{L} N(\xi; \mu, \sigma^2)\, d\xi - \sum_{n=3}^{\infty} A_n \sigma N(L; \mu, \sigma^2) H_{n-1}\left(\frac{L-\mu}{\sigma}\right)$$

with

$$\mu \triangleq \langle L \rangle, \quad \sigma^2 \triangleq \langle (L-\mu)^2 \rangle, \quad A_n \triangleq \frac{1}{n!}\left\langle H_n\left(\frac{L-\mu}{\sigma}\right)\right\rangle$$

and

$$N(\xi; \mu, \sigma^2) \triangleq \frac{1}{\sqrt{2\pi}\sigma} \exp[(\xi-\mu)^2/2\sigma^2], \tag{1}$$

where $\langle * \rangle$ denotes an averaging operation with respect to $*$ and $H_n(.)$ denotes the nth order Hermite polynomial. Based on the definition of L_x noise evaluation indices, the following relationship can be derived from Eq. (1):

$$1 - \frac{x}{100} = \int_{-\infty}^{L_x} N(\xi; \mu, \sigma^2)\, d\xi - \sum_{n=3}^{\infty} A_n \sigma N(L_x; \mu, \sigma^2) H_{n-1}\left(\frac{L_x-\mu}{\sigma}\right). \tag{2}$$

Thus, after employing several specific L_x levels to the above relationship, one can construct the N-dimensional simultaneous equations for the coupling coefficient A_n $(n = 3, 4, \ldots, N-2)$. After solving these equations, one can evaluate the objective noise level probability distribution $Q(L)$ by substituting the mean value μ, the variance σ^2 and the estimated expansion coefficient A_n into Eq. (1).

In this case, the specific formulae for estimating A_n are explicitly expressed as follows:

(1) Case for A_3 with use of one reference level L_{x1}:

$$A_3 = \frac{\int_{-\infty}^{L_{x1}} N(\xi; \mu, \sigma^2)\, d\xi + \frac{x_1}{100} - 1}{\sigma N(L_{x1}; \mu, \sigma^2) H_2\left(\frac{L_{x1}-\mu}{\sigma}\right)}. \tag{3}$$

(2) Case for A_3 and A_4 with use of two reference levels L_{x1} and L_{x2}:

$$A_3 = \frac{\left[\int_{-\infty}^{L_{x2}} N(\xi;\mu,\sigma^2)\,d\xi + \frac{x_2}{100} - 1\right] F_2(L_{x1};\mu,\sigma^2) - \left[\int_{-\infty}^{L_{x1}} N(\xi;\mu,\sigma^2)\,d\xi + \frac{x_1}{100} - 1\right] F_2(L_{x2};\mu,\sigma^2)}{\sigma F_1(L_{x2};\mu,\sigma^2) F_2(L_{x1};\mu,\sigma^2) - \sigma F_1(L_{x1};\mu,\sigma^2) F_2(L_{x2};\mu,\sigma^2)}, \quad (4)$$

$$A_4 = \frac{\left[\int_{-\infty}^{L_{x1}} N(\xi;\mu,\sigma^2)\,d\xi + \frac{x_1}{100} - 1\right] F_1(L_{x2};\mu,\sigma^2) - \left[\int_{-\infty}^{L_{x2}} N(\xi;\mu,\sigma^2)\,d\xi + \frac{x_2}{100} - 1\right] F_1(L_{x1};\mu,\sigma^2)}{\sigma F_1(L_{x2};\mu,\sigma^2) F_2(L_{x1};\mu,\sigma^2) - \sigma F_1(L_{x1};\mu,\sigma^2) F_2(L_{x2};\mu,\sigma^2)}$$

with

$$F_1(\xi;\mu,\sigma^2) \triangleq N(\xi;\mu,\sigma^2) H_2\left(\frac{\xi-\mu}{\sigma}\right), \quad (5)$$

$$F_2(\xi;\mu,\sigma^2) \triangleq N(\xi;\mu,\sigma^2) H_3\left(\frac{\xi-\mu}{\sigma}\right).$$

2.2. *Estimation method with restriction of amplitude fluctuation range*

Let us consider the noise level fluctuation, L, with restriction of an amplitude fluctuation range matched to the actually measured amplitude range of a stochastic phenomenon and a dynamic range of a measurement device. In this case, one can employ a statistical Jacobi series expansion type expression as the cumulative distribution function of the noise level fluctuation, as follows [8]:

$$Q(L) = \int_a^L \frac{1}{B(\gamma,\alpha-\gamma+1)(b-a)}\left(\frac{\xi-a}{b-a}\right)^{\gamma-1}\left(1-\frac{\xi-a}{b-a}\right)^{\alpha-\gamma} d\xi$$

$$+ \sum_{n=3}^{\infty} \frac{B_n}{B(\gamma,\alpha-\gamma+1)} \cdot \frac{1}{\gamma}\left(\frac{L-a}{b-a}\right)^{\gamma}\left(1-\frac{L-a}{b-a}\right)^{\alpha-\gamma+1} G_{n-1}\left(\alpha+2,\gamma+1;\frac{L-a}{b-a}\right)$$

with

$$\alpha \triangleq \frac{(\mu-a)(b-\mu)}{\sigma^2} - 2, \quad \gamma \triangleq \frac{(\alpha+1)(\mu-a)}{b-a}$$

and

$$B_n \triangleq \frac{\Gamma(\gamma)\Gamma(\alpha-\gamma+1)}{\Gamma(\alpha+1)} \cdot \frac{(\alpha+2n)\Gamma(\alpha+n)\Gamma(\gamma+n)}{n!\,\Gamma(n+\alpha-\gamma+1)[\Gamma(\gamma)]^2}\left\langle G_n\left(\alpha,\gamma;\frac{L-a}{b-a}\right)\right\rangle, \quad (6)$$

where $B(.)$, $\Gamma(.)$ and $G_n(.)$ denote respectively Beta function, Gamma function and the nth order Jacobi's polynomial. It should be noticed that the above formula is a generalized one including the well-known statistical Hermite series expansion type expression (taking a well-known standard Gaussian distribution as the first expansion term) in a special case when $\gamma \to \infty$ $(a = b \to \infty)$ (see Ref. [8]). According to

the definition of L_x noise evaluation indices, the following relationship can be directly derived from Eq. (6).

$$1-\frac{x}{100}=\int_a^{L_x}\frac{1}{B(\gamma,\,\alpha-\gamma+1)(b-a)}\left(\frac{\xi-a}{b-a}\right)^{\gamma-1}\left(1-\frac{\xi-a}{b-a}\right)^{\alpha-\gamma}d\xi$$
$$+\sum_{n=3}^{\infty}\frac{B_n}{B(\gamma,\,\alpha-\gamma+1)}\cdot\frac{1}{\gamma}\left(\frac{L_x-a}{b-a}\right)^{\gamma}\left(1-\frac{L_x-\mu}{b-a}\right)^{\alpha-\gamma+1}G_{n-1}\left(\alpha+2,\,\gamma+1;\frac{L_x-a}{b-a}\right). \quad (7)$$

Therefore, after employing several specific L_x levels to the above relationship, one can obtain the N-dimensional simultaneous equations for the expansion coefficient B_n ($n=3, 4, \ldots, N-2$). The objective noise level probability distribution can be obtained by substituting the estimated B_n and the known values of μ, σ^2, a and b into Eq. (6).

More explicitly, the explicit formulae for estimating the expansion coefficient B_n can be obtained as follows:

(1) Case for B_3 with use of one reference level L_{x1}:

$$B_3=\frac{1-\frac{x_1}{100}-Q_0(L_{x1};\,\alpha,\,\gamma,\,a,\,b)}{\frac{1}{B(\gamma,\,\alpha-\gamma+1)}\cdot\frac{1}{\gamma}\left(\frac{L_{x1}-a}{b-a}\right)^{\gamma}\left(1-\frac{L_{x1}-a}{b-a}\right)^{\alpha-\gamma+1}G_2\left(\alpha+2,\,\gamma+1;\frac{L_{x1}-a}{b-a}\right)},$$

$$Q_0(\xi;\,\alpha,\,\gamma,\,a,\,b)\triangleq\int_a^{\xi}\frac{1}{B(\gamma,\,\alpha-\gamma+1)(b-a)}\left(\frac{\xi-a}{b-a}\right)^{\gamma-1}\left(1-\frac{\xi-a}{b-a}\right)^{\alpha-\gamma}d\xi. \quad (8)$$

(2) Case for B_3 and B_4 with use of two reference levels L_{x1} and L_{x2}:

$$B_3=\frac{\left[1-\frac{x_1}{100}-Q_0(L_{x1};\,\alpha,\,\gamma,\,a,\,b)\right]J_2(L_{x2};\,\alpha,\,\gamma,\,a,\,b)-\left[1-\frac{x_2}{100}-Q_0(L_{x2};\,\alpha,\,\gamma,\,a,\,b)\right]J_2(L_{x1};\,\alpha,\,\gamma,\,a,\,b)}{J_1(L_{x1};\,\alpha,\,\gamma,\,a,\,b)J_2(L_{x2};\,\alpha,\,\gamma,\,a,\,b)-J_1(L_{x2};\,\alpha,\,\gamma,\,a,\,b)J_2(L_{x1};\,\alpha,\,\gamma,\,a,\,b)},$$

$$B_4=\frac{\left[1-\frac{x_2}{100}-Q_0(L_{x2};\,\alpha,\,\gamma,\,a,\,b)\right]J_1(L_{x1};\,\alpha,\,\gamma,\,a,\,b)-\left[1-\frac{x_1}{100}-Q_0(L_{x1};\,\alpha,\,\gamma,\,a,\,b)\right]J_1(L_{x2};\,\alpha,\,\gamma,\,a,\,b)}{J_1(L_{x1};\,\alpha,\,\gamma,\,a,\,b)J_2(L_{x2};\,\alpha,\,\gamma,\,a,\,b)-J_1(L_{x2};\,\alpha,\,\gamma,\,a,\,b)J_2(L_{x1};\,\alpha,\,\gamma,\,a,\,b)}, \quad (9)$$

with

$$J_1(\xi;\,\alpha,\,\gamma,\,a,\,b)\triangleq\frac{1}{B(\gamma,\,\alpha-\gamma+1)}\cdot\frac{1}{\gamma}\left(\frac{\xi-a}{b-a}\right)^{\gamma}\left(1-\frac{\xi-a}{b-a}\right)^{\alpha-\gamma+1}G_2\left(\alpha+2,\,\gamma+1;\frac{\xi-a}{b-a}\right),$$

$$J_2(\xi;\,\alpha,\,\gamma,\,a,\,b)\triangleq\frac{1}{B(\gamma,\,\alpha-\gamma+1)}\cdot\frac{1}{\gamma}\left(\frac{\xi-a}{b-a}\right)^{\gamma}\left(1-\frac{\xi-a}{b-a}\right)^{\alpha-\gamma+1}G_3\left(\alpha+2,\,\gamma+1;\frac{\xi-a}{b-a}\right). \quad (10)$$

3. Experimental consideration

In order to confirm the effectiveness of the proposed method, it has been applied to two kinds of road traffic noise data measured actually in Hiroshima Prefecture. That is, first, the road traffic noise data have been measured in an urban area with a fairly large traffic volume. From the notational viewpoint, the above case is defined here as "Case *A*". Next, the other road traffic noise data have been measured in a rural area with a small traffic volume. At this time, this case is defined as "Case *B*". Figure 1 shows the actual situation in Case *A* of measuring the road traffic noise in an urban area. Similarly, Fig. 2 also shows the actual situation in Case *B* of measuring the road traffic noise in a rural area.

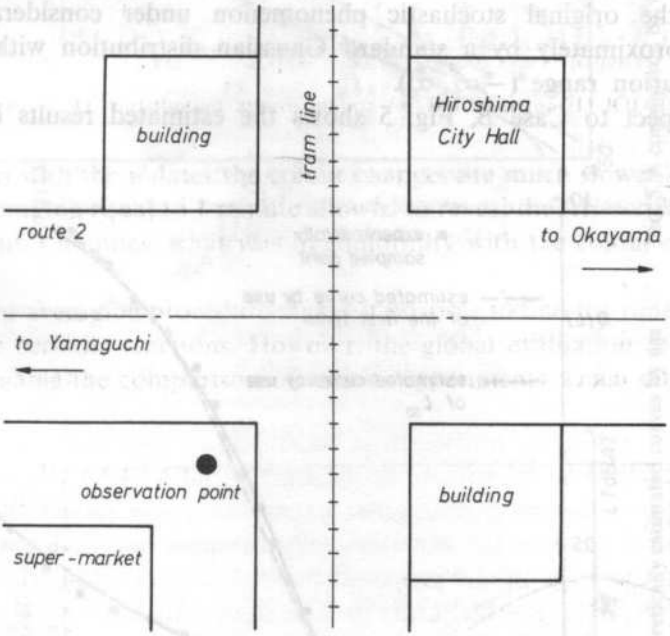

FIG. 1. Actual situation of measuring the road traffic noise in an urban area (Case *A*)

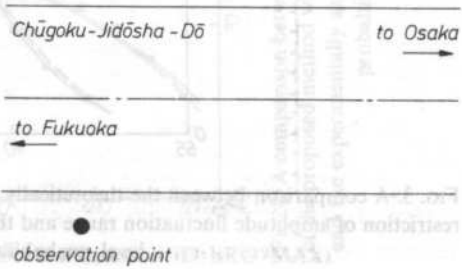

FIG. 2. Actual situation of measuring the road traffic noise in a rural area (Case *B*)

Figure 3 shows a comparison between the theoretically estimated curves by use of the proposed method with no restriction of an amplitude fluctuation range and the experimentally sampled points for the cumulative noise level probability distribution with respect to Case *A*. As shown in this figure, it is obvious that these data exhibit approximately a standard Gaussian distribution corresponding to the first expansion term of Eq.(1). A comparison between the theoretically estimated curves by use of the proposed method with consideration of the restricted fluctuation range and the experimentally sampled points is shown in Fig. 4. From these results, the estimated results due to both methods are in good agreement with the experimental results, because both methods are generally applicable to the case when the objective stochastic phenomenon can be expressed by not only a non-Gaussian distribution but also a standard Gaussian one. In this case, the effect of a constant restriction of an amplitude fluctuation range on the estimation accuracy is not so clear, since the original stochastic phenomenon under consideration can be expressed approximately by a standard Gaussian distribution with an idealized infinite fluctuation range $(-\infty, \infty)$.

With respect to Case *B*, Fig. 5 shows the estimated results by use of the

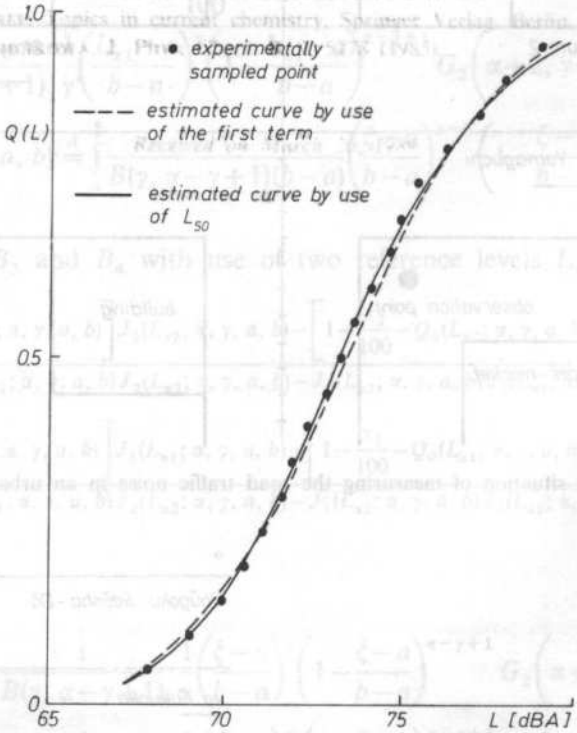

FIG. 3. A comparison between the theoretically estimated curves by use of the proposed method with no restriction of amplitude fluctuation range and the experimentally sampled points for the cumulative noise level probability distribution (Case *A*)

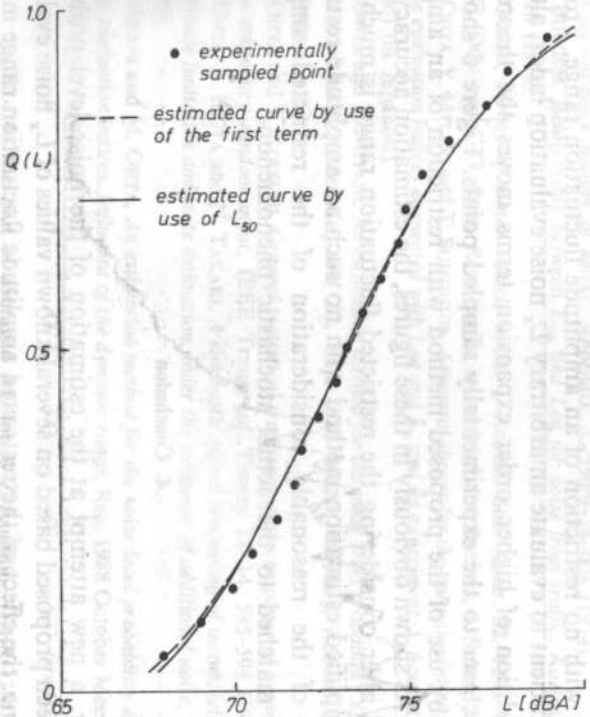

FIG. 4. A comparison between the theoretically estimated curves by use of the proposed method with restriction of amplitude fluctuation range and the experimentally sampled points for the cumulative noise level probability distribution (Case *A*)

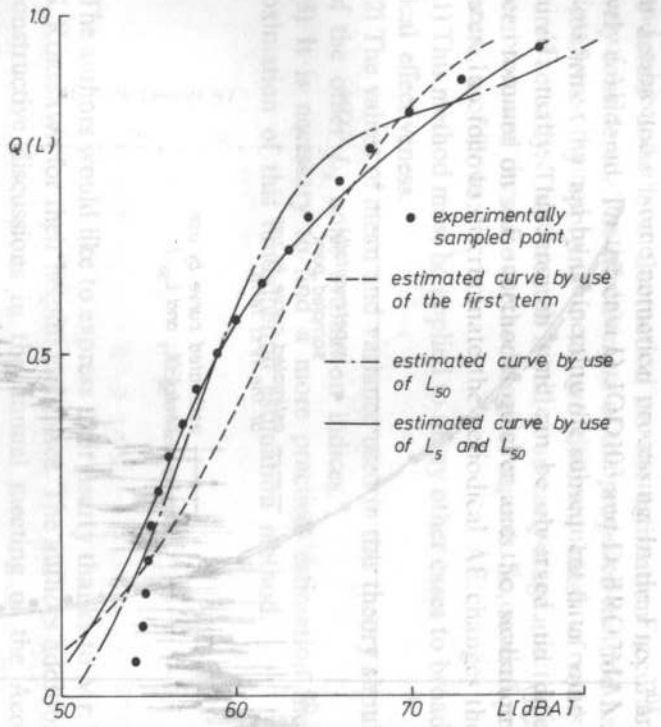

FIG. 5. A comparison between the theoretically estimated curves by use of the proposed method with no restriction of amplitude fluctuation range and the experimentally sampled points for the cumulative noise level probability distribution (Case *B*)

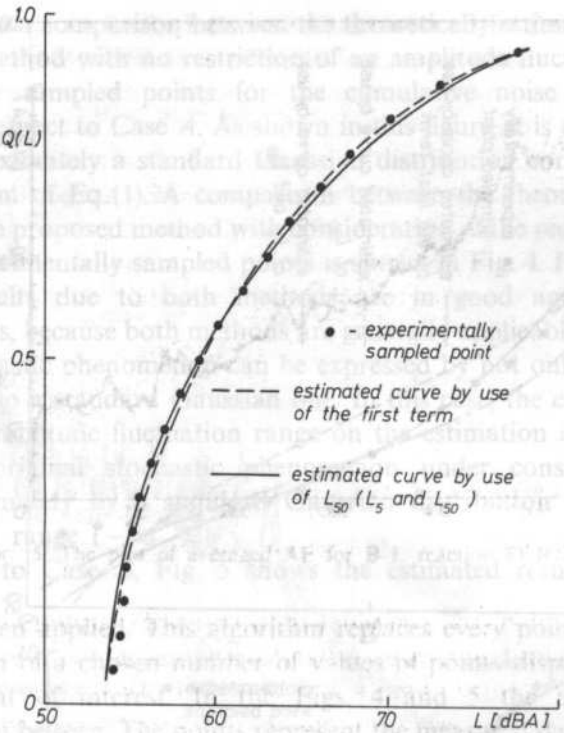

FIG. 6. A comparison between the theoretically estimated curves by use of the proposed method with restriction of amplitude fluctuation range and the experimentally sampled points for the cumulative noise level probability distribution (Case *B*)

proposed method with no restriction of an amplitude fluctuation range. From this figure, it is not sufficient to evaluate an arbitrary L_x noise evaluation index, although the successive addition of higher order expansion terms moves the theoretically estimated curves closer to the experimentally sampled points. Figure 6 shows the estimated results by use of the proposed method with restriction of an amplitude fluctuation range. As shown obviously in these figures, the estimation accuracy of the method proposed after considering the restricted fluctuation range is much better than that of a simplified estimation method with no such an amplitude restriction. This is because of the reasonable consideration of the restricted amplitude fluctuation range matched to the actual stochastic phenomenon.

4. Conclusion

In this paper, a new attempt at the estimation of the noise level probability distribution has been proposed based on several known values of L_x noise evaluation indices. At this time, the effect of the restricted amplitude fluctuation range matched

to the actual noise level fluctuation on the estimation accuracy has been quantitatively considered. The effectiveness of the proposed method has been experimentally confirmed by applying it to two different kinds of road traffic noise data measured actually. This research is still at an early stage and the work reported here has been focussed on some methodological aspects. So, several problems are left for the future, as follows:

(1) This method must be applied to many other cases to broaden and confirm its practical effectiveness.

(2) The values of mean and variance used in this theory should be estimated by use of the other L_x noise evaluation indices.

(3) It is necessary to find a more practical estimation method through the approximation of this fundamental estimation method.

Acknowledgements

The authors would like to express their hearty thanks to Mr. T. KATAYAMA and Mr. S. KORESAWA for their helpful assistance. The authors additionally acknowledge the constructive discussions in the annual meeting of the Acoustical Society of Japan [9].

References

[1] U.S. EPA, *Information on levels of environmental noise requisite to protect public health and welfare with an adequate margin of safety; Appendix A*, 550/9–74–004 (1974).

[2] M. BURGESS, *Relationship between L_{10} and Leq for noise from traffic*, Australian Road Research **8**, 15–18 (1978).

[3] N. OLSON, *Survey of motor vehicle noise*, J. Acoust. Soc. Amer. **52**, 1291–1306 (1972).

[4] C. G. DON and I. G. REES, *Road traffic sound level distributions*, J. Sound Vib. **100**, 41–53 (1985).

[5] M. OHTA, Y. MITANI and T. SUMIMOTO, *A general theory for the mutual relationship among several type noise evaluation indices connected with Leq and L_x and its experiment*, J. Acoust. Soc. Jpn. **41**, 598–607 (1985) (in Japanese).

[6] M. OHTA and Y. MITANI, *An estimation method for the noise level probability distribution based on two noise evaluation indices, Leq and L_x*, Rep. 1988 March Meeting, Acoust. Soc. Jpn. 487–488 (in Japanese).

[7] M. OHTA and T. KOIZUMI, *General statistical treatment of the response of a nonlinear rectifying device to a stationary random input*, IEEE Trans. Inf. Theory IT–14, 595–598 (1968).

[8] M. OHTA, A. IKUTA and N. TAKAKI, *A stochastic signal processing of incomplete observation data with amplitude limitation and state estimation under the existence of additional noise*, Trans. IEICE **71**, 8–15 (1988).

[9] Y. MITANI and M. OHTA, *An estimation method for the noise level probability distribution based on L_x noise evaluation indices. Influence of the dynamic range*, Rep. 1988 October Meeting, Acoust. Soc. Jpn., 555–556 (in Japanese).

Received on January 23, 1989

ARCHIVES OF ACOUSTICS
15, 1–2, 211–226 (1990)

ACOUSTIC EMISSION DURING TENSILE DEFORMATION OF COPPER SINGLE CRYSTALS AND DISLOCATION ANNIHILATION PROCESSES

A. PAWEŁEK[a]*, W. STRYJEWSKI[b], H. DYBIEC[a], W. BOCHNIAK[a]

Institute for Metal Working and Physical Metallurgy, Academy of Mining and Metallurgy
(30–059 Kraków, Al. Mickiewicza 30)[a]
Institute of Molecular Biology, Jagiellonian University
(30–059 Kraków, Al. Mickiewicza 3)[b]

The behaviour of acoustic emission (AE) during the two first stages of the tensile deformation of copper single crystals is investigated using the broad-band piezoelectric transducer for the measurement of AE energy rate $\Delta E/\Delta t$, AE event rate $\Delta N/\Delta t$ (event density) and energy per one AE event $\Delta E/\Delta N$. The existence of some essential correlation between the AE intensity (proportional to $\Delta E/\Delta t$ or $\Delta N/\Delta t$ patterns) and the plastic flow features has been stated. Two large maxima of AE intensity have been observed: the one correlated with the onset of easy glide region and the other one with the onset of stage II of the deformation. Moreover, the mean level of the AE intensity is high in the whole easy glide region and considerably greater than the mean one at the advanced stage II of the deformation, whereas the high mean level is the smaller the smaller is the length of the easy glide region. It has been shown that the observed correlations can be qualitatively quite well explained in terms of the dislocation annihilation component of the transition acoustic radiation.

1. Introduction

The application of acoustic emission (AE) technique to the investigation of the various aspects of the mechanical properties of metals and alloys (mainly plastic deformation, fracture, phase transitions) has already been developing for nearly twenty years [1]. Today there exist many experimental observations of the AE behaviour during tensile deformation of crystals [1, 2] and a common feature of their interpretations is the opinion that the AE during plastic flow is, in general, caused by the dislocation motion. However, these interpretations differ from each other in details and so far there exists no good enough model which would explain most of the experimental observations. The difficulties in their interpretation consist in the fact that there is still no possibility of a quantitative comparison of the results obtained in various laboratories because of the lack of standard engineering devices, and hence no possibility to secure identical conditions for the calibration of the

* Present address: Aleksander Krupkowski Institute for Metals Researche, Polish Academy of Sciences (30–059 Kraków, ul. Reymonta 25)

piezoelectric sensors [1, 3, 4]. Nevertheless, the results obtained using the same apparatus always give some additional information on the nature of plastic deformation, and thus they are interpreted mostly qualitatively.

The first more extensive investigations of the AE during tensile testing of various metals have been carried out by FISHER and LALLY [5]. They suggested that AE was a consequence of the fast collective motion of a large number of dislocations. Similar suggestions appeared in some models proposed later. SEDGWICK [6] has considered two possible AE sources: the operation of the fast dislocation sources and the sudden release of dislocation pile-ups. He discussed the former one in detail and pointed out that there existed a correlation between the length distribution of the dislocation segments (being potential Frank-Read sources) and the observed distribution of the AE intensity as a strain function.

Another model has been proposed by JAMES and CARPENTER [7]. They suggested that the AE event rate is proportional to the rate of the mobile dislocation density increase, $d\varrho_m/dt$. The $d\varrho_m/dt$ rate is, in turn, imposed by the stimulated processes of the dislocation breakaway from the pinning points and to a less degree by the dislocation multiplication. A similar conclusion has been drown by HIGGENS and CARPENTER [8], who suggested that the AE at the yield point is caused also by dislocation unpinning. On the other hand, IMANAKA et al. [9] have observed the increase of the AE intensity with increasing strain rate. They suggested that this was due to the dynamic operation of the Frank-Read sources, and the assumption of the constancy of mobile dislocation density during strain rate change should be reconsidered. Unfortunately, they have not developed their idea in detail. Likewise, KIESEWETTER and SCHILLER [10] suggest that the main cause of the AE is also associated with the operation of Frank-Read sources. A common feature of all the models discussed above as well as of other more recent interpretations of various experimental data [11, 12] (see also [1, 2]) is the supposition that during plastic deformation the AE is induced by non-stationary dislocation motion ("bremsstrahlung" type of accoustic radiation).

On the other hand the series of excellent experiments carried out by BOIKO et al. [13 to 17] strongly suggest that AE should be considered on the basis of the so-called transition type of acoustic radiation, the main component of which arises from the dislocation annihilation processes occuring inside the crystal and at the surface. Likewise our recent experimental observations of the AE behaviour [18, 19], and particularly those of the increase (decrease) of AE intensity induced by increasing (decreasing) strain rate changes [18] during copper single crystals tensile deformation have been also interpreted in terms of dislocation annihilation component of the transition type of acoustic radiation. The annihilation of dislocation at a crystal surface is recently also discussed in [20] as the one of possible causes of AE during the fracture of metals.

Therefore the main aim of this paper is to find further experimental evidences for the dislocation annihilation origin of the acoustic radiation during plastic flow of metals using as an example the tensile deformation of copper single crystals.

2. Theoretical background

The first theoretical predictions on a possibility of acoustic radiation due to the non-stationary dislocation motion was reported much earlier [21 to 27]. The theory was developed by ESHELBY [28] for acoustic radiation by an oscillating dislocation kink (recently see also [29]), and later by KOSEVICH [30–32] for a system of accelerating dislocation loops.

It is interesting to notice here that according ESHELBY [28] the rate of acoustic energy radiation is proportional to the mean value of the square of time derivative of the dislocation kink linear velocity, quite analogously to the electromagnetic radiation from an accelerated electron.

A similar result has been obtained by KOSEVICH [30–32] on the basis of the dislocation model in a continuous medium. The analogy between Kosevich and Eshelby treatment follows from the fact that the second time derivative of the dislocation moment tensor is just proportional to the dislocation loop acceleration. However, Eshelby treatment is of microscopic character and describes rather the high-frequency radiation due to the non-stationary dislocation kink motion since the kink vibration frequency is related with atom vibration in the dislocation core. Kosevich approach, is of macroscopic character and describes rather the low-frequency radiation due to the non-stationary motion of the system of many dislocation loops.

One can see that the acoustic emission induced by non-stationary dislocation motion is of an analogous nature as the electromagnetic bremsstrahlung radiation induced by the charged particles. Thus this type of the AE may be called the "bremsstrahlung" acoustic radiation. It should be noted here that in literature also the Čerenkov type of acoustic radiation is being discussed [33 to 35]. Unfortunately, none of these types of AE has a sufficiently explicit experimental evidence.

On the other hand, NATSIK et al. [36 to 38] were the first to analyse theoretically the acoustic radiation due to the dislocation escape from a crystal or due to the dislocation annihilation. Moreover, NATSIK [36] pointed out, basing on the results obtained by GINZBURG and FRANK [39], that the acoustic radiation due to the dislocation escape from a crystal, again per analogy to the classical electrodynamics, is similar to the transition electromagnetic radiation by a charged particle going through the boundary between two media differing from each other in a dielectric constant. Therefore he called this type of AE the transition acoustic radiation, and this name is accepted at present [40]. Since dislocation escape from a crystal may be considered as the annihilation of dislocations with their virtual images, hence the acoustic radiation due to the dislocation annihilation (irrespective whether it occurs inside the crystal or due to the dislocation escape) is always of a transition character. Moreover, the escape of edge dislocations from a crystal induces additionally the Rayleigh surface waves which are absence, however, in the case of screw dislocation escape.

Furthermore, NATSIK and CHISHKO [37], using the methods of the dislocation theory in a continuous medium, proved that the energy E per unit length, which is released after the annihilation of dislocations is given by

$$E = \alpha \cdot u^2 \ln \frac{L}{b} \tag{1}$$

where u is the relative velocity of dislocations at a time moment of their collision, L is of the order of crystal size and α is the coefficient depending on the medium density, the dislocation species and the magnitude of the Burgers vector b.

In the next sections we shall present briefly the experimental procedure as well as our further experimental results and interpretations which confirm quite well the dislocation-annihilation concept of the acoustic emission.

3. Experimental procedure

The equipment for AE measurement and the method of crystals growth were the same as described in [3, 4] and used in [19, 41]. Some of the obtained crystals were oriented for easy glide (orientations 1, 1′ and 2, 2′) and the others were oriented for multislip (orientation 3). The crystals of a length 50 mm and of rectangular cross section 10 mm × 1 mm for the orientations 1, 1′ and 4 mm × 4 mm for the orientations 2, 2′ and 3 were deformed at a constant strain rate $\dot{\varepsilon} = 1.6 \times 10^{-4}\ \mathrm{s}^{-1}$, $\dot{\varepsilon} = 1.7 \times 10^{-5}\ \mathrm{s}^{-1}$ and $\dot{\varepsilon} = 3.0 \times 10^{-4}\ \mathrm{s}^{-1}$, respectively to the orientations 1, 2, 3. For all the specimens the tensile force F and the following AE parameters: rate of AE events counting $\Delta N/\Delta t$, rate of energy released in events $\Delta E/\Delta t$, and mean energy per one event $\Delta E/\Delta N$, were simultaneously recorded as the strain function. The AE parameters were measured at an amplification of about 88dB and at a threshold voltage $U_d = 1.0$ V, except insolated cases when the values $U_d = 0.75$ V or $U_d = 0.5$ V were used. Moreover, the piezoelectric sensor used was of a broad-band type what allowed to record the AE signals in the frequency range from about 50 to 600 kHz, in contrary to the resonance type of the transducers where only a narrow frequency band (about 20 to 50 kHz) may be recorded. The use of the treshold voltage U_d from 0.5 V to 1.0 V allowed to eliminate the apparatus noise, whereas the minimum frequency (50 kHZ) and the maximum one (600 kHz) ensured in turn the elimination of the noises arising from the tensile machine and radio waves, respectively.

The AE event rate $\Delta N/\Delta t$ was measured by the counting of each events which exceeded the threshold level of the discriminator. Thus the AE detected in our experiments, with regard to the resolution of the apparatus, was always of the burst character. The energy of AE events was measured by using the formula

$$E = \int_0^T f^2(t)\,dt \tag{2}$$

where $f(t)$ describes the shape of the AE signal and T is the duration of the event. The rate $\Delta E/\Delta t$ is thus determined in arbitrary units and therefore only its relative changes during the deformation may be useful for the interpretation. Each of the AE parameters ($\Delta N/\Delta t$, $\Delta E/\Delta t$ and $\Delta E/\Delta N = (\Delta E/\Delta t)/(\Delta N/\Delta t)$) was measured within two-second time periods during each tensile test.

4. Experimental results

Fig. 1 and 2 show the strain dependences of the tensile force F and the AE parameters $\Delta N/\Delta t$, $\Delta E/\Delta t$ and $\Delta E/\Delta N$ for two crystals of type 1 orientations (slightly differing from each other). Within the whole easy glide region the AE intensity, proportional to the $\Delta E/\Delta t$ (or $\Delta N/\Delta t$) parameter, remains at a high mean level, and the onset of the decrease of AE intensity takes place nearly at a strain value corresponding to the point of transition from the easy glide region to the stage II of the deformation. One can observe that in the advanced stage II of the deformation (Fig. 2) the level of the AE is much lower and the curve of AE intensity is of a more discrete character than in the case of easy glide region. A more smooth character of the AE intensity curve within the easy glide region follows from the use of the logarithmic scale.

Fig. 3 and 4 show the dependences similar as in Fig. 1 and 2 for the crystals of type 2 orientations, which also differ in their cross-sections and strain rates from those of the orientations 1. One can see that the difference between the orientations as well as between the cross-sections and strain rates of the crystals leads only to quantitative changes, whereas qualitative features of the AE patterns remain the same.

A comparison of the patterns of the AE intensity illustrated in Fig. 1 to 4 leads to the conclusion that there exists a correlation between a high level of the AE intensity and the length of easy glide region. Moreover, Fig. 1 to 4 reveal two appreciable maxima of the AE intensity. In Fig. 4 these maxima are more clearly visible owing to the decrease of the threshold voltage from 1.0 down to 0.75 V (they are very weekly visible in Fig. 1 and 2 as they are masked due to the use of logarithmic scale). Thus the second maximum is in a quite good correlation with the strain value corresponding to the transition from easy glide region to stage II of the deformation.

Fig. 5 shows also the strain dependence of the force and the AE parameters but merely for a crystal of the multislip orientation 3. One can say that the AE from a multislip oriented crystal behaves quite similarly to the one from single slip oriented crystals if we mentally reject the easy glide region in Fig. 1 to 4. This means that in the case of single slip oriented crystals the first maximum of the AE is related with the onset of the easy glide region and the second maximum of the AE is indeed related with the onset of stage II of the deformation. Therefore in the case of

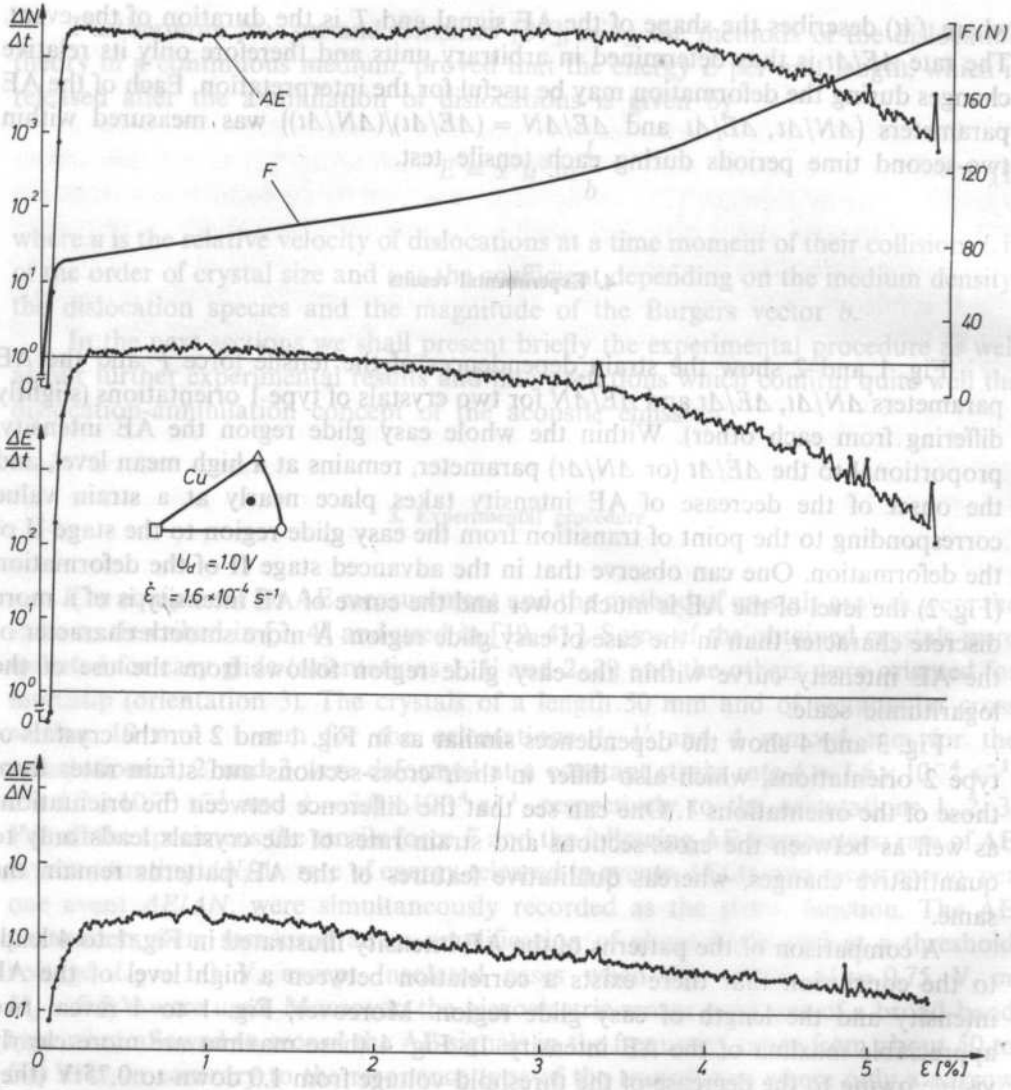

FIG. 1. Strain dependence of the tensile force F and the AE parameters for an easy glide oriented copper single crystal of orientation 1 and of cross-section 10 mm × 1 mm

a multislip oriented crystal, where at least two slip systems are operating from the beginning of the deformation, there exists only one maximum of the AE.

Moreover, the behaviour of the AE within stage II of the deformation is similar for all crystals of various orientations used here. The AE intensity decrease the faster the more advanced is the stage II of the deformation, to attain the mean level which is, however, considerably smaller than the one related with the easy glide region, Fig. 5 brings an additional illustration of the behaviour of the AE intensity during sudden strain rate decrease from $\dot{\varepsilon} = 3.0 \times 10^{-4}\ s^{-1}$ down to $\dot{\varepsilon} = 3.0 \times 10^{-5}\ s^{-1}$ (or increase

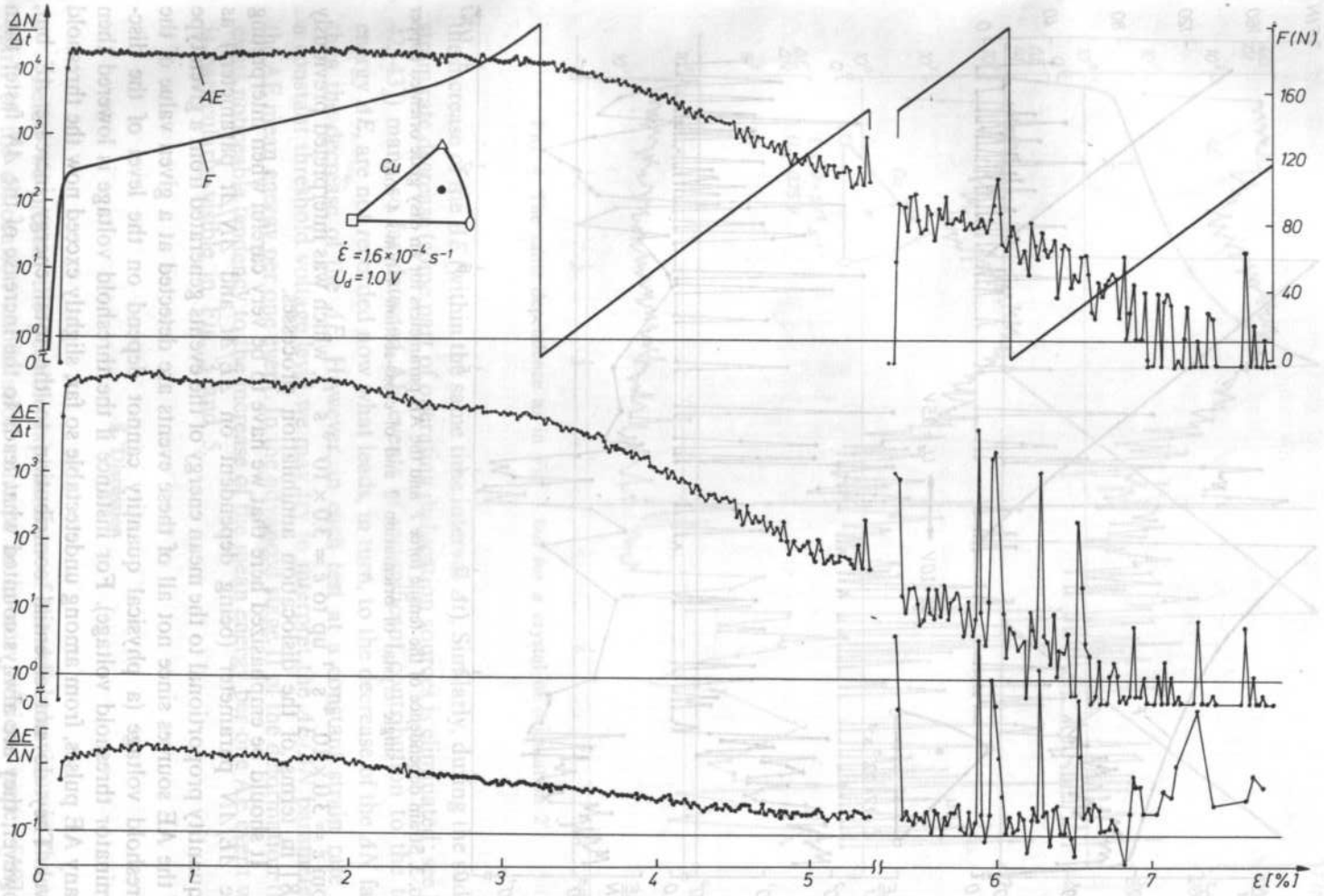

FIG. 2. The same dependence as in Fig. 1 but for a crystal of orientation 1'

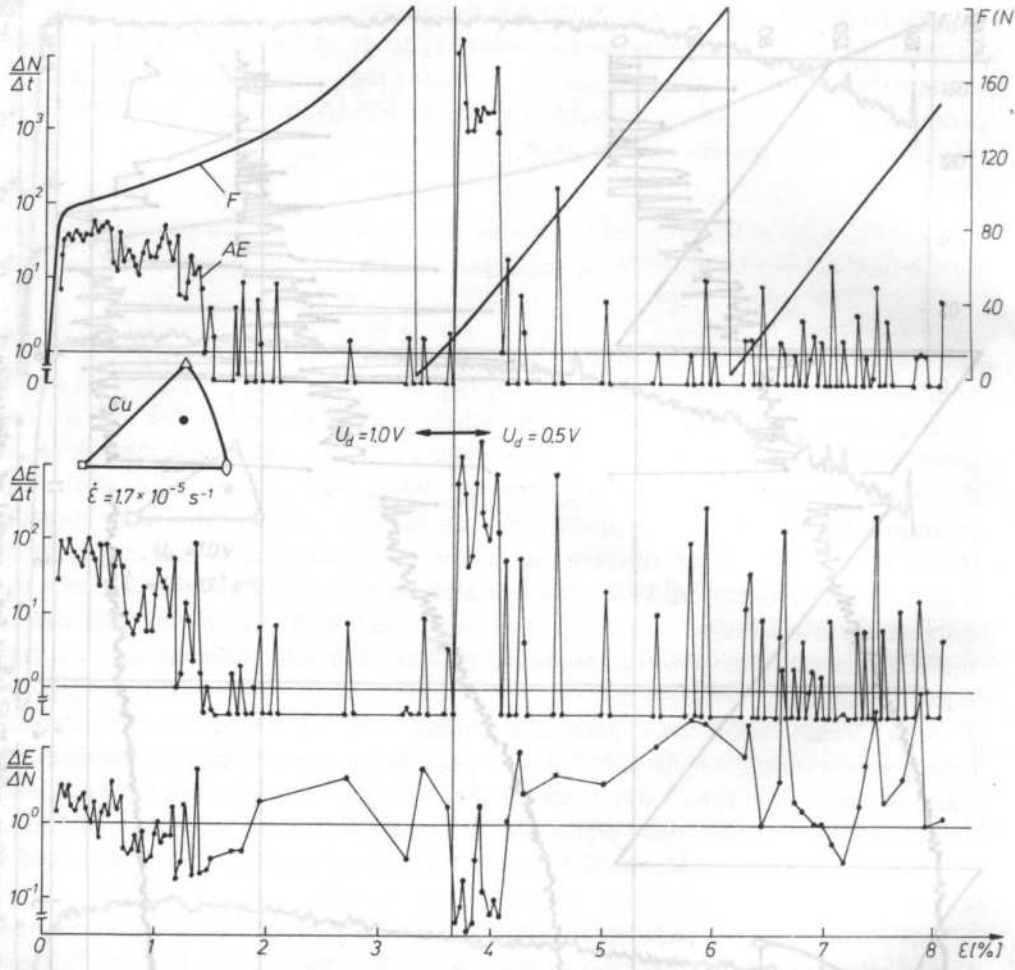

FIG. 3. Strain dependence of the tensile force F and the AE parameters for an easy glide oriented copper single crystal of orientation 2 and of cross-section 4 mm × 4 mm

from $\dot{\varepsilon} = 3.0 \times 10^{-4}\ s^{-1}$ up to $\dot{\varepsilon} = 3.0 \times 10^{-3}\ s^{-1}$), which was interpreted previously [18] in terms of the dislocation annihilation processes.

It should be emphasized here that we have to be very careful when interpreting the $\Delta E/\Delta N$ parameter (being dependent on $\Delta E/\Delta t$ and $\Delta N/\Delta t$ parameters) as a quantity proportional to the mean energy of the events generated from a given type of the AE sources since not all of these events are detected at a given value of the threshold voltage (a physical quantity cannot depend on the level of the discriminator threshold voltage). For instance if the threshold voltage is lowered then many AE pulses, from among undetectable so far, slightly exceed now the threshold level. They do not essential contribution to the total energy increase ΔE but, however, they are always counted what leads to the increase of the ΔN faster than

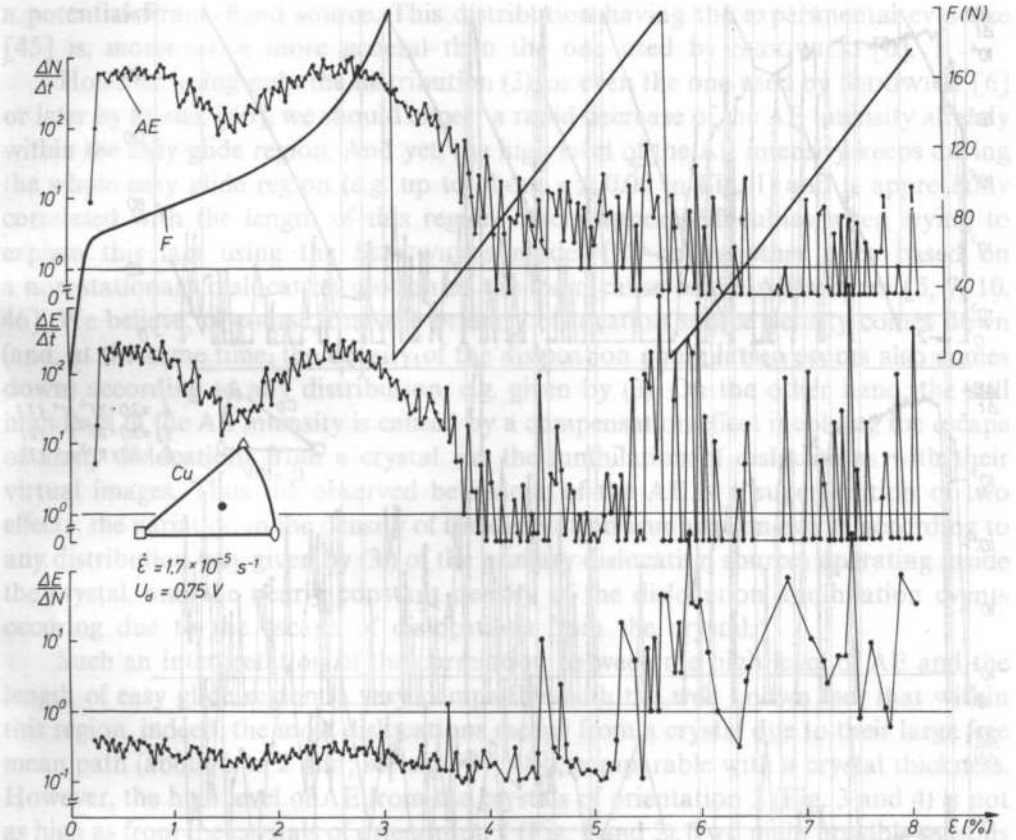

FIG. 4. The same dependence as in Fig. 3 but for a crystal of orientation 2'

the increase of the ΔE (within the same time interval Δt). Similarly, during the sudden strain rate decrease (some part of operating dislocation sources is eliminated; see [18, 42, 43]) many so far detected AE events of insignificant contribution to the total energy ΔE, are not recorded now what leads, in turn, to the decrease of the ΔN faster than the decrease of the ΔE. However, in each test at a constant strain rate and a constant threshold voltage level we may try to interpret the $\Delta E/\Delta N$ parameter as the AE mean energy per one event. In the advanced stage II of the deformation there exists noticeable tendency to the increase of the mean energy per one AE event what is particularly visible in Fig. 3 and 5.

5. Discussion

Below we present the possible explanations of the AE behaviour in the same spirit of the dislocation annihilation concept as in our previous paper [18].

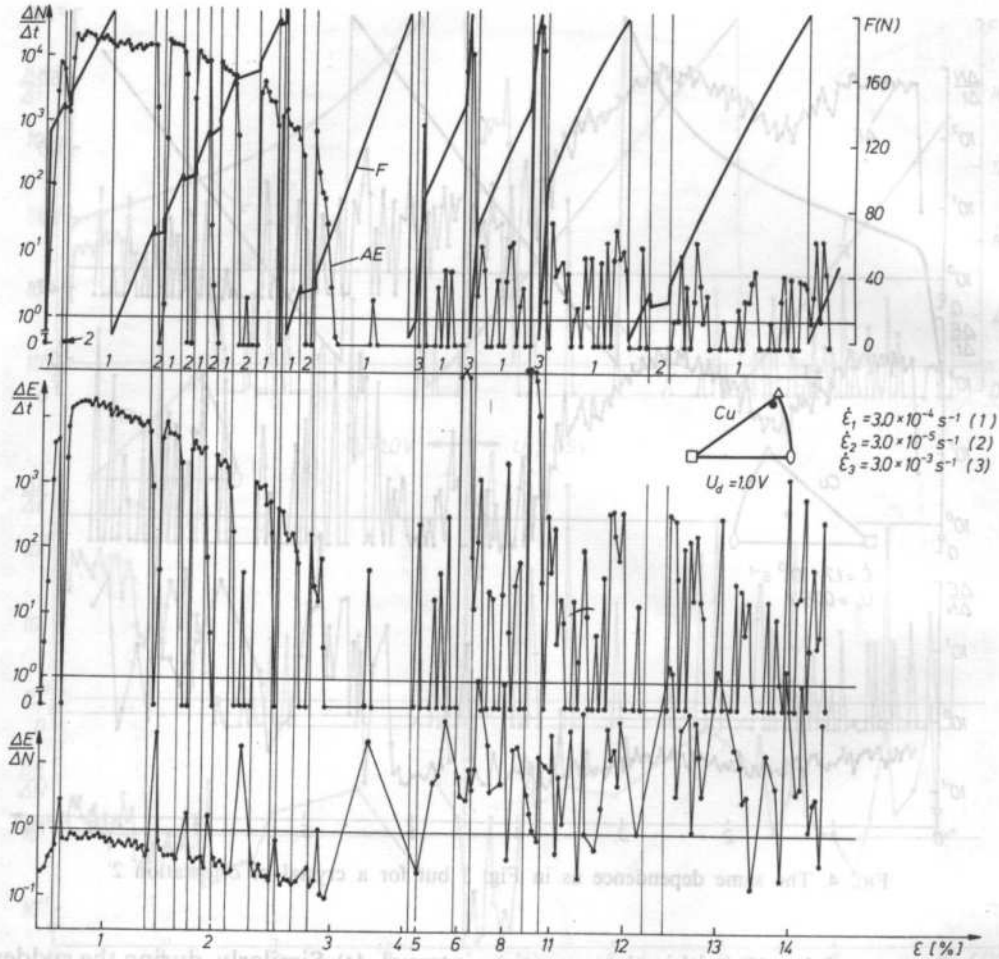

FIG. 5. Strain dependence of the tensile force F and the AE parameters for a multislip oriented copper single crystal of orientation 3 (see also [18])

Let us assume firstly that the high level of the AE intensity at the beginning of the easy glide region (Fig. 1 to 4) may be ascribed only to the high density of the events of the dislocation segment annihilation which proceeds during the closing of each dislocation loop generated due to the start of many dislocation sources of the Frank-Read type. Assume that the primary source density distribution is similar to the one given by GASCA-NERI and NIX [44]

$$N(l) = \frac{n^{n+1}}{n!}\varrho_0^{(n+3)/2} l^n \exp(-n\sqrt{\varrho_0}\, l) \tag{3}$$

where n determines the abruptness of the distribution curve, ϱ_0 is the total initial density of primary dislocations and l is the length of a dislocation segment being

a potential Frank-Read source. This distribution having the experimental evidence [45] is, moreover, a more general than the one used by SEDGWICK [6].

However, using only the distribution (3), or even the one used by SEDGWICK [6] or later by SIEGEL [46], we should expect a rapid decrease of the AE intensity already within the easy glide region. And yet, the high level of the AE intensity keeps during the whole easy glide region (e.g. up to about $\varepsilon \cong 0.05$ in Fig. 1) and is appreciably correlated with the length of this region. There appear difficulties when trying to explain this fact using the SEDGWICK'S model [6] or by other ones based on a non-stationary dislocation motion as the main cause of the AE sources [5, 7, 10, 46]. We believe, of course, that the primary dislocation source density comes down (and, at the same time, the density of the dislocation annihilation events also comes down) according to any distribution, e.g. given by (3). On the other hand, the still high level of the AE intensity is caused by a compensation effect involving the escape of many dislocations from a crystal, i.e. the innihilation of dislocations with their virtual images. Thus the observed behaviour of the AE is a superposition of two effects: the variation in the density of the dislocation annihilation events according to any distribution (say given by (3)) of the primary dislocation sources operating inside the crystal, and the nearly constant density of the dislocation annihilation events occuring due to the escape of dislocations from the crystal.

Such an interpretation of the correlation between the high level of AE and the length of easy glide region is very compatible with the well known fact that within this region, indeed, the most dislocations escape from a crystal due to their large free mean path (about 1 to 2 mm; see e.g. [47, 48]), comparable with a crystal thickness. However, the high level of AE from the crystals of orientation 2 (Fig. 3 and 4) is not as high as from the crystals of orientation 1 (Fig. 1 and 2). Two main possible reasons may be accounted for it. First, there is another well known fact that the length of easy glide region decrease with increasing crystal thickness (e.g. [48]). Thus it is clear that the density of dislocations escaping from the crystals of 2 type orientation is smaller than this density in the case of the crystals of 1 type orientation. Second, the lower strain rate of crystals 2 yields the lower density of dislocation annihilation events inside the crystal since the density of operating Frank-Read sources decreases with decreasing strain rate [18, 42, 43].

In the same spirit we can try to explain the appearance of the second maximum of AE, corresponding to the transition from the easy glide region to the stage II of the deformation. This maximum is followed by the local minimum, especially visible in Fig. 3 and 4 (reproducible in Fig. 1 and 2 too, but masked there due to the use of logarithmic scale). Thus the second maximum can be ascribed in turn to the operation of new dislocation sources in the secondary slip systems, i.e. also to the variation of the events of dislocation segments annihilation inside the crystal according to the distribution analogous to that given by (3) for the primary source density.

Moreover, a further decrease of the AE intensity in the advanced stage II of the deformation to a much lower mean level in comparison to the one in the easy glide

region can be explained in the following way. It is a well known fact that the mean free path of dislocation decreases considerably with increasing strain within stage II of the deformation (e.g. [47]). Thus the number of dislocations escaping from a crystal becomes now considerably limited since the most dislocation remain inside a crystal forming the pile-ups against the Cottrell-Lomer barriers.

We can explain quite similarly the behaviour of AE from the multislip oriented crystal of greater thickness (orientation 3, Fig. 5). However, the high mean level of the AE intensity at the beginning of the deformation, comparable to the one for the crystals of smaller thickness, is mainly as a result of the superposition of the dislocation annihilation events due to a simultaneous operation of primary and secondary dislocation sources.

Using the Eq. (1) obtained by NATSIK and CHISHKO [37] we may try to give an analytical description of our experimental results. Let $\Delta\varrho_i$ and u_i ($i = 1, 2, 3$) denote, respectively, the mean densities and velocities of annihilating dislocations, corresponding to the operation of primary ($i = 1$) and secondary ($i = 2$) sources as well as to the escape ($i = 3$) from a crystal. Then for each of these processes the rate of elastic energy $\Delta E_i/\Delta t$ released per unit volume may be written in the form

$$\frac{\Delta E_i}{\Delta t} = \alpha \frac{\Delta \varrho_i}{\Delta t} u_i^2 \ln \frac{L}{b}. \tag{4}$$

Thus the total rate of acoustic energy radiation, $\Delta E/\Delta t = \Delta E_1/\Delta t + \Delta E_2/\Delta t + \Delta E_3/\Delta t$, varies with increasing strain according to the superposition rule illustrated schematically in Fig. 6.

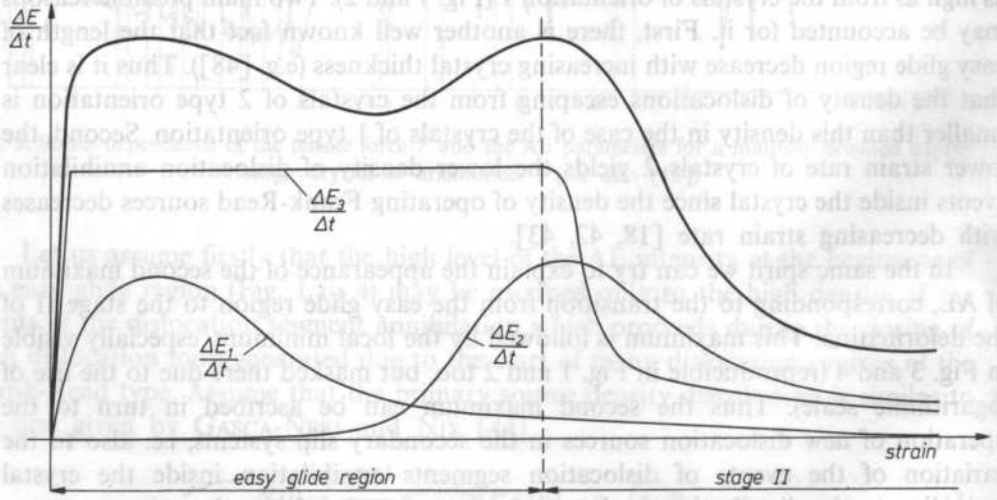

FIG. 6. Schematic illustration of the resultant pattern of the AE behaviour as a superposition of three effects: dislocation annihilation inside a crystal induced by primary ($\Delta E_1/\Delta t$) and secondary ($\Delta E_2/\Delta t$) dislocation source operations, and dislocation annihilation due to the escape of dislocations from a crystal ($\Delta E_3/\Delta t$)

In a similar way we can describe the mean energy $\Delta E_i/\Delta N$ per one event

$$\frac{\Delta E_i}{\Delta N} = \alpha \cdot \Delta d_i \cdot u_i^2 \ln \frac{L}{b} \tag{5}$$

where Δd_i is the mean length of the annihilating segments of dislocation corresponding to each of three discussed processes. Assuming that in the first approximation the mobile dislocation density, ϱ, and the mean dislocation velocity, v, are constant in the easy glide region ($\dot{\varepsilon} = b\varrho v = \text{const}$) then the density of the dislocations escaping from a crystal is constant, too, and thus the mean energy of AE events generated by the corresponding annihilation events is also constant. A slight decrease of the $\Delta E/\Delta N$ till the onset of stage II of the deformation may be related with the decrease of mean dislocation segment length with increasing strain. The lower the segment length the lower is the length of the annihilating dislocation segments during the closing of the dislocation loop generated by the source, what leads to the decrease of the mean energy per one event according to Eq. (5). However, the behaviour of $\Delta E/\Delta N$ parameter is modulated by the appearance of the second maximum (visible in Fig. 3 and 4, but again masked in Fig. 1 and 2). It may be also explained according to Eq. (3) since the lengths of the secondary sources operating at the beginning of stage II are greater than the lengths of primary sources operating at the same time.

Moreover, assuming that in the advanced stage II of the deformation the mobile dislocation density is smaller, and thus the mean dislocation velocity is greater than the corresponding values in the easy glide region, we may suppose that the noticeable increase of the mean event energy is related mainly with the increase of the mean dislocation relative velocity during the annihilation events induced inside the crystal as well as at the surface.

Eventually, we would like to emphasize here once again that there are difficulties in explaining the decrease of the AE intensity during the sudden strain rate decrease (additionally illustrated in Fig. 5; see also [18]) by using any model based on a non-stationary dislocation motion as the main cause of the AE, since the assumption of the "bremsstrahlung" nature of acoustic radiation leads, in this case at least, to the conclusion that a sudden decrease of strain rate should also result in an increase of the AE intensity what is contrary to experimental observations. Nevertheless, we cannot exclude any contribution of this type of acoustic radiation to the AE intensity observed in our experiments. On the other hand, theoretical results obtained not long ago by MALÉN and BOLIN [49] and more recently by JASZCZEWSKI [50], basing after all on the formalism developed by KOSEVICH [30 to 32] and MURA [51], still suggest the possibility of the detection of the "bremsstrahlung" type of acoustic radiation. Also the estimations carried out by JAMES and CARPENTER [7] and also by JASZCZEWSKI [50] show that the dislocations of about 10^2 to 10^3 m length when accelerated simultaneously enough should give a detectable AE signal. And though the annihilation of dislocation at a crystal surface is also considered in terms of non-stationary movement of dislocation (i.e. as a very particular case of

dislocation stopping over the distance corresponding to the length of the step formed at the surface [20]), nevertheless there is still very difficult to state experimentally how much is the part of the observed AE signal which originates from the non-stationary dislocation motion. We believe, however, that more precise measurements of the possible deviation from the symmetrical behaviour of the AE during sudden strain rate jumps and drops should reveal the contribution of the "bremsstrahlung" acoustic radiation to the detected AE signals.

Moreover, we cannot exclude the Rayleigh surface waves contribution to the detected AE signals, either. However, under the conditions of our present experiments it was not possible to extract the Rayleigh wave component. And yet we believe that its contribution, if it exists, should be always additive and the qualitative pattern of the AE behaviour is determined only by the dislocation annihilation component of the transition acoustic radiation.

7. Conclusion

The present observations on the AE intensity patterns during two first stages of the tensile deformation of copper single crystals, reveal some essential correlations with the dislocation mechanisms of plastic flow. They can be qualitatively quite well explained in terms of the dislocation annihilation component of the transition acoustic radiation. Namely:

(i) The correlation between a high level of the AE intensity and the length of the easy glide region (large mean free path of dislocations) is related with the escape of the dislocations from the crystal (annihilation of dislocations with their virtual images).

(ii) The high mean level of AE from single slip oriented crystals of greater thickness deformed at smaller strain rate is much lower than the high mean level of AE from those crystals of smaller thickness deformed at greater strain rate. It is related, firstly, with a smaller density of dislocation annihilation events at the surface of the crystal of greater thickness and, secondly, with a smaller density of dislocation annihilation events induced by the Frank-Read source operation inside the crystal deformed at a smaller strain rate.

(iii) The two maxima of the AE intensity correlate by turns with the onset of the easy glide region and onset of stage II of the deformation. They are related with the dislocation annihilation events inside the crystal induced by the operation of the primary and secondary dislocation Frank-Read sources, respectively (started successively according to any distribution, e.g. similar to the one given by Gasca-Neri and Nix).

(iv) The resultant pattern of the AE intensity is a superposition of the dislocation annihilation effects occuring inside the crystal and due to the dislocation escape from the crystal.

(v) The decrease of the AE intensity to a low mean level within the advanced stage II of the deformation is related with the considerably limited dislocation escape from the crystal (small mean free path of dislocations).

(vi) The explanation of the high level of AE and the existence of only one maximum of the intensity of AE from the multislip oriented crystal, where at least two slip systems are operating simultaneously from the beginning of the deformation, follows from previous conclusions being thus a quite good confirmation of the presented interpretation.

(vii) The proposed qualitative explanation of the strain dependence of event mean energy is also compatible with this interpretation.

This work was supported by the Institute for Fundamental Technical Researches at the Polish Academy of Sciences under the contract CPBP 02.03.

References

[1] H. N. G. Wadley, C. B. Scruby and J. H. Speake, Int. Met. Rev., **249**, 41 (1980).
[2] A. Pawełek, W. Bochniak, H. Dybiec and W. Stryjewski, Archives of Metallurgy, **33**, 645 (1988).
[3] W. Stryjewski and G. Zapalski, Rep. Institute of Nuclear Physics, No. 1204/E, Cracow 1983.
[4] W. Stryjewski, G. Zapalski and A. Pawełek, Archives of Metallurgy, **33**, 485 (1988).
[5] R. M. Fisher and J. S. Lally, Can. J. Phys., **45**, 1147 (1967).
[6] R. T. Sedwick, J. Appl. Phys., **39**, 1728 (1967).
[7] D. R. James and S. E. Carpenter, J. Appl. Phys., **42**, 4685 (1971).
[8] F. P. Higgens and S. H. Carpenter, Acta metall., **26**, 133 (1978).
[9] T. Imanaka, K. Sano and H. Shimizu, Crystal Lattice Defects, **4**, 57 (1973).
[10] N. Kiesewetter and P. Schiller, Phys. Stat. Sol. (a) **38**, 569 (1976).
[11] S. Mintzer, R. Pascual and R. M. Volpi, Scripta metall., **12**, 531 (1978).
[12] C. H. Caceres and H. R. Bertorello, Scripta metall., **17**, 1115 (1983).
[13] V. S. Boiko, R. I. Garber, L. F. Krivenko and S. S. Krivulya, Fiz. tverd. tela, **11**, 3624 (1969).
[14] V. S. Boiko, R. I. Garber, L. F. Krivenko and S. S. Krivulya, Fit. tverd. tela, **12**, 1753 (1970).
[15] V. S. Boiko, R. I. Garber, L. F. Krivenko and S. S. Krivulya, Fiz. tverd. tela, **15**, 321 (1973).
[16] V. S. Boiko, R. I. Garber and L. F. Krivenko, Fiz. .tverd. tela, **16**, 1233 (1974).
[17] V. S. Boiko, R. I. Garber, V. F. Kivshik and L. F. Krivenko, ZhETF, **71**, 708 (1976).
[18] A. Pawełek, W. Stryjewski, W. Bochniak and H. Dybiec, Phys. Stat. Sol. (a), **90**, 531 (1985).
[19] A. Pawełek, H. Dybiec, W. Bochniak and W. Stryjewski, Archives of Metallurgy, **34**, 239 (1989).
[20] S. Pilecki, Arch. Akustyki, **21**, 109 (1986).
[21] J. D. Eshelby, Proc. Roy. Soc. London, **A197**, 396 (1949).
[22] G. Leibfried, Z. Phys., **127**, 144 (1950).
[23] F. R. N. Nabarro, Proc. Roy. Soc. London, **A209**, 278 (1951).
[24] J. D. Eshelby, Philos. Trans. Roy. Soc. London **244**, 87 (1951).
[25] A. Seeger, A. Donth and A. Kochendörfer, Z. Phys., **134**, 173 (1953).
[26] A. Seeger, Z. Naturforsch., **8a**, 47 (1953).
[27] J. D. Eshelby, Phys. Rev., **90**, 248 (1953).
[28] J. D. Eshelby, Proc. Roy. Soc. London, **A 266**, 222 (1962).
[29] A. Pawełek, Report of the International Centre for Theoretical Physics, ICTP (87) 136, Trieste, Italy 1987; J. Appl. Phys., **63**, 5320 (1988).

[30] A. M. KOSEVICH, Usp. Fiz. Nauk, **84**, 579 (1964).
[31] A. M. KOSEVICH, *Dislocations in elasticity*, Nauk. Dumka, Kiev 1970 (in Russian).
[32] A. M. KOSEVICH, *Dislocations in solids*, vol. 1, [Ed.] F. R. N. Nabarro, North-Holland Publ. Co, Amsterdam 1979, p. 33.
[33] J. D. ESHELBY, Proc. Phys. Soc., **B 69**, 1013 (1956).
[34] D. ROGULA, Bull. Acad. Pol. Sc., Sèrie sc. techn., **13**, 337 (1965).
[35] D. ROGULA, Bull. Acad. Pol. Sc., Sèrie sc. techn., **14**, 159 (1966).
[36] V. D. NATSIK, ZhETF Pis. Red., **8**, 324 (1968).
[37] V. D. NATSIK and K. A. CHISSHKO, Fiz. tverd. tela, **14**, 3126 (1972).
[38] V. D. NATSIK and A. N. BURKHANOV, Fiz. tverd. tela, **14**, 1289 (1972).
[39] W. L. GINZBURG and I. M. FRANK, ZhETF, **16**, 15 (1946).
[40] V. I. PAVLOV and A. I. SUHORUKOV, Usp. Fiz. Nauk., **147**, 83 (1985).
[41] J. A. GOLCZEWSKI and W. STRYJEWSKI, Phys. Letters, **92A**, 397 (1982).
[42] A. PAWEŁEK, Phys. Stat. Sol., (a) **85**, K117 (1984).
[43] A. PAWEŁEK, Archives of Metallurgy, **30**, 295 (1985)
[44] R. GASCA-NERI and W. D. MIX, Acta metall., **22**, 257 (1974).
[45] A. ORLOVA, Scripta metall., **16**, 1133 (1982).
[46] E. J. SIEGEL, Phys. Stat. Sol., (a), **5**, 607 (1971).
[47] F. R. N. NABARRO, Z. S. BASINSKI and D. B. HOLT, *The plasticity of pure single crystals*, Advances in Physics, **13**, 193 (1964).
[48] R. W. K. HONEYCOMBE, *The plastic deformation of metals*, Ed. A. Arnold Cambridge 1968.
[49] K. MALÉN and L. BOLIN, Phys. Stat. Sol., (b) **61**, 637 (1974).
[50] M. JASZCZEWSKI, Rep. Institute of Nuclear Physics, No 1149/PS Cracow 1984.
[51] T. MURA, *Advances in materials research*, vol. 3 Ed. H. Herman, Wiley 1968 p. 1.

Received on April 6, 1988

ARCHIVES OF ACOUSTICS
15, 1–2, 227–234 (1990)

DIRECTIONAL CHARACTERISTIC OF A CIRCULAR PLATE VIBRATING UNDER THE EXTERNAL PRESSURE

W. RDZANEK

Institute of Physics, Pedagogical University
(35–310 Rzeszów, Rejtana 16)

In this paper, the problem of acoustic wave radiated and received by a lip restrained circular plate vibrating in a rigid baffle is distributed. The vibratory system is found in the lossless and homogeneous liquid medium. The dynamics influence of the wave emitted by plate on its vibration form has been omitted as well as the losses in plate have been neglected. The axially symmetric vibration induced by the sinusoidal varried in time external pressure has been considered. By assuming the known distribution of pressure forcing vibration, a simple expression has been found allows to determine the directional characteristic.

W pracy rozwiązano zagadnienie promieniowania i odbioru fal akustycznych przez utwierdzoną na obrzeżu w sztywnej odgrodzie płytę kołową. Układ drgający znajduje się w bezstratnym i jednorodnym ośrodku płynnym. Pominięto dynamiczne oddziaływanie promieniowanej przez płytę fali na jej postać drgań oraz zaniedbano straty w płycie. Rozpatrzono osiowosymetryczne drgania wymuszone sinusoidalnie zmiennym w czasie ciśnieniem zewnętrznym. Zakładając znany rozkład ciśnienia wymuszającego drgania, ustalono wyrażenie mające elementarną postać, pozwalającą na wyznaczenie charakterystyki kierunkowości.

1. Introduction

A utilization of circular plates and membranes as the vibratory systems for design of acoustic devices which satisfy a function of sender or receiver of acoustic waves, requires identyfying, between the others, directional characteristic. A relative big attention to be payed to this problem by using the approximation methods as well as the equivalent schemes is however not sufficient in case of an exact analysis [3, 6].

The precisely mathematically formulated basis magnitudes characterizing the circular membrane as a source or a receiver of acoustic energy can be found in [1], the main point of which is focussed on the frequency response of input impedance for the circular membrane stimulated to the forced vibration.

A directional characteristic of a circular membrane excited to a resonance vibration is described, for example in [6, 7] – but in more general case – of nonresonance vibration, in [4].

Describing the problem of radiation of circular plate only the following boundary cases have been analyzed – a focused forced vibration and a vibrated plate modelled by a system of concentrated constants with the equivalent force [3, 6].

The most precisely considerations needed to find acoustic properties of a vibrated plate require undergoing of investigations for the nonresonance vibration, taking into account a time – and position-depended factor forcing the vibration.

In this paper, the problem of acoustic wave emission by a lip restrained circular plate placed in a rigid, planer baffle is considered. A plate is enough thin as well as the effect of medium forcing the vibration is enough large to omitt the influence of losses including the forced vibration created by a self-acoustics field. It has been assumed that the vibratory system is found in the lossless and homogeneous liquid medium with the small value of self-resistance.

Assuming the known sinusoidal varied in time surface distribution of factor forcing the vibration, the directional characteristic has been established.

Expressions, to be here obtained for the resonance frequencies are reduced to the known formulae, formely established in [5].

Results of numerical calculations have been presented graphically.

Based on the results here obtained, the continuation of analysis will be possible in emission of energy vibration, the exact application of which is useful for the sound emission problems of the vibrated plates.

2. Assumptions of analysis

A forced transversal vibration of a homogeneous circular plate for which the energy losses don't occur as well as the local of plate stimulated by the surrounded environment is neglected, can be described by the following equation, [3]

$$B\nabla^4 \eta(r, t) + \varrho h \frac{\partial^2 \eta(r, t)}{\partial t^2} = f(r, t), \tag{1}$$

where

$$B = \frac{Eh^3}{12(1-\nu^2)} \tag{2}$$

denotes the bending stiffness of plate, η denotes transversely displacement of point located on the plate surface, h – denotes the width of plate, E denotes Young modulus, ν denotes Poisson coefficient, ϱ denotes volumen density of plate. A medium, for which the influence of a radiated field of plate on the form of

vibration can be omitted in Eq. (1), is identified, for example with the air possesing small value of the self-resistance. The theory of bending of thin plates is applied for the plate thickness h, fullfield the inequality, [2].

$$h \leqslant 0.1\ D, \tag{2a}$$

where D denotes the diameter of plate.

Assuming that a factor forcing the vibration is identified with the external pressure

$$f(r,\ t) = f(r)\exp(i\omega t), \tag{3}$$

an amplitude of which has the following form

$$f(r) = \begin{cases} f_0 & \text{for} \quad 0 < r < a_0 \\ 0 & \text{for} \quad a_0 < r < a \end{cases} \tag{4}$$

where $f_0 = \text{const}$.

From the practical point of view, this kind of extorsion can be realized for example by two surface circular electrodes parallel to the plate surface with radius $a_0 < a$, where denotes radius of plate.

Equation of vibration (1) for the extortion induced by external factor Eqs. (3), (4) has the following form

$$\begin{aligned} \eta_1(r)/\eta_0 = 1 - \frac{\gamma_0}{2S(\gamma)} \Big\{ & \frac{1}{\gamma} I_1(\gamma_0) + \frac{\pi}{2} I_1(\gamma)\,[J_1(\gamma_0)\,N_0(\gamma) + \\ & - J_0(\gamma)\,N_1(\gamma_0)] - \frac{\pi}{2} I_0(\gamma)\,[J_1(\gamma)\,N_1(\gamma_0) - J_1(\gamma_0)\,N_1(\gamma)] \Big\} \\ & \times J_0(kr) + \frac{\gamma_0}{2S(\gamma)} \Big\{ \frac{1}{\gamma} J_1(\gamma_0) + J_1(\gamma)[I_1(\gamma_0)\,K_0(\gamma) + I_0(\gamma) \\ & \times K_1(\gamma_0)] - J_0(\gamma)[I_1(\gamma_0)\,K_1(\gamma) - I_1(\gamma)\,K_1(\gamma_0)] \Big\} I_0(kr) \end{aligned} \tag{5}$$

for $0 < r < a_0$,

$$\begin{aligned} \eta_2(r)/\eta_0 = & -\frac{\gamma_0}{2S(\gamma)} \Big\{ \frac{1}{\gamma} I_1(\gamma_0) + \frac{\pi}{2} J_1(\gamma_0)[N_0(\gamma)\,I_1(\gamma) + N_1(\gamma)\,I_0(\gamma)] \Big\} J_0(kr) \\ & - \frac{\gamma_0}{2S(\gamma)} \Big\{ \frac{1}{\gamma} J_1(\gamma_0) + I_1(\gamma_0)[K_0(\gamma) \times J_1(\gamma) - K_1(\gamma) J_0(\gamma)] \Big\} I_0(kr) \\ & + \frac{\gamma_0}{2} \Big[I_1(\gamma_0)\,K_0(kr) + \frac{\pi}{2} J_1(\gamma_0)\,N_0(kr) \Big] \end{aligned} \tag{6}$$

for $a_0 < r < a$, furthermore the following notations have been derived

$$\gamma = ka,\ \gamma_0 = ka_0,\ S(\gamma) = J_0(\gamma) I_1(\gamma) + I_0(\gamma) J_1(\gamma) \tag{7}$$

and

$$\eta_0 = -\frac{f_0}{Bk^4} \qquad k^2 = \omega \left[\frac{M}{B}\right]^{\frac{1}{2}}, \tag{8}$$

where $M = \varrho h$ denotes a mass of plate divided by the unit of area. The time term, defined by the notation of $\exp(i\omega t)$ is omitted in text begining from Eq. (5).

In the particular case for which the whole surface of plate is excited to vibration by a factor different from zero ($a_0 = a$), Eq. (5) and Eq. (6) are reduced to the following form

$$\eta_1(r)/\eta_0 = 1 - \frac{1}{S(\gamma)} [I_1(\gamma) J_0(kr) + J_1(\gamma) I_0(kr)] \tag{9}$$

and $\eta_2(r)/\eta_0 = 0$

3. Acoustic pressure in the Fraunhofer zone

A distribution of acoustic pressure in the Fraunhofer zone of the source vibrated in a rigid, planer baffle is calculated based on the relation, [3]

$$p(R, \theta, \varphi) = \frac{i\varrho_0 \omega}{2\pi} \frac{\exp(-ik_0 R)}{R} \int_{\delta_0} v(r_0, \varphi_0) \times \exp[ik_0 r_0 \sin\theta \cos(\varphi - \varphi_0)]\, d\delta_0 \tag{10}$$

for $\frac{1}{2} k_0 r_0 \left(\frac{r_0}{R}\right) \ll 1$, furthermore R, θ, φ denote the spherical coordinates of a point of field, r_0, φ_0 denote the polar coordinates of a point of the source, ϱ_0 denotes a density of fluid medium, $k_0 = \frac{2\pi}{\lambda}$, $\delta_0 = \pi a^2$.

In the case of circular plate excited to axially symmetric vibration, Eqs. (3), (4) the rate of vibration is independent of the angular variable φ_0. Assuming also relation

$$v(r_0) = i\omega\eta(r_0) \tag{11}$$

Eq. (10) defined for acoustic pressure is reduced to the form

$$p(R, \theta) = -\varrho_0 \omega^2 \frac{\exp(-ik_0 R)}{R} \Big[\int_0^{a_0} \eta_1(r_0) J_0(k_0 r_0 \sin\theta) r_0\, dr_0 + \int_{a_0}^{a} \eta_2(r_0) J_0(k_0 r_0 \sin\theta) r_0\, dr_0 \Big]. \tag{12}$$

After integration we obtain relation

$$p(R,\theta)=\frac{\varrho_0 f_0 \varepsilon^2 a^2}{2M}\frac{\exp(-ik_0 R)}{R}$$
$$\times\frac{2J_1(\varepsilon x)/(\varepsilon x)-U(\varepsilon,\gamma)J_1(x)x/\gamma-W(\varepsilon,\gamma)J_0(x)}{1-(x/\gamma)^4\sin^4\theta}, \tag{13}$$

where $\varepsilon_0=a_0/a$, $x=k_0 a\sin\theta$ and

$$U(\varepsilon,\gamma)=\frac{2}{\varepsilon\gamma S}[J_1(\varepsilon\gamma)I_0(\gamma)-I_1(\varepsilon\gamma)J_0(\gamma)], \tag{14}$$

$$W(\varepsilon,\gamma)=\frac{2}{\varepsilon\gamma S}[J_1(\varepsilon\gamma)I_1(\gamma)+I_1(\varepsilon\gamma)J_1(\gamma)]. \tag{15}$$

For the principal direction i.e. $\theta=0$, we obtain the following relation for acoustic pressure

$$p_0=\frac{\varrho_0 f_0 \varepsilon^2 a^2[1-W(\varepsilon,\gamma)]}{2M}\frac{\exp(-ik_0 R)}{R}, \tag{16}$$

the form of which we apply for calculation of the directionality coefficient, [3]

$$K(\theta)=\frac{|p|}{|p_0|} \tag{17}$$

if $p_0\neq 0$. But for

$$1-W(\varepsilon,\gamma)=0, \tag{18}$$

the state of vibratory system is such, that a volumen displacement of the vibrated plate is equal to zero (compare with [1]), then a directionality coefficient must be defined in another way. It can be achieved by referring the value of pressure $p(R,\theta)$ to that of pressure $p'(R,\theta_0)$ in such direction θ_0 for which this value reaches maximum.

In the case of coincidence between a frequency factor forcing vibration and a frequency of proper vibration, the damping effects arr negligible, i.e.

$$\gamma=\gamma_n,\quad S(\gamma_n)=0 \tag{19}$$

we obtain relation

$$K_n(\theta)=\lim_{\gamma\to\gamma_n}K(\theta)=\frac{|J_0(x)-xJ_1(x)J_1(\gamma_n)/(\gamma_n J_1(\gamma_n))|}{|1-(x/\gamma_n)^4|}, \tag{20}$$

identical with this published in [5].

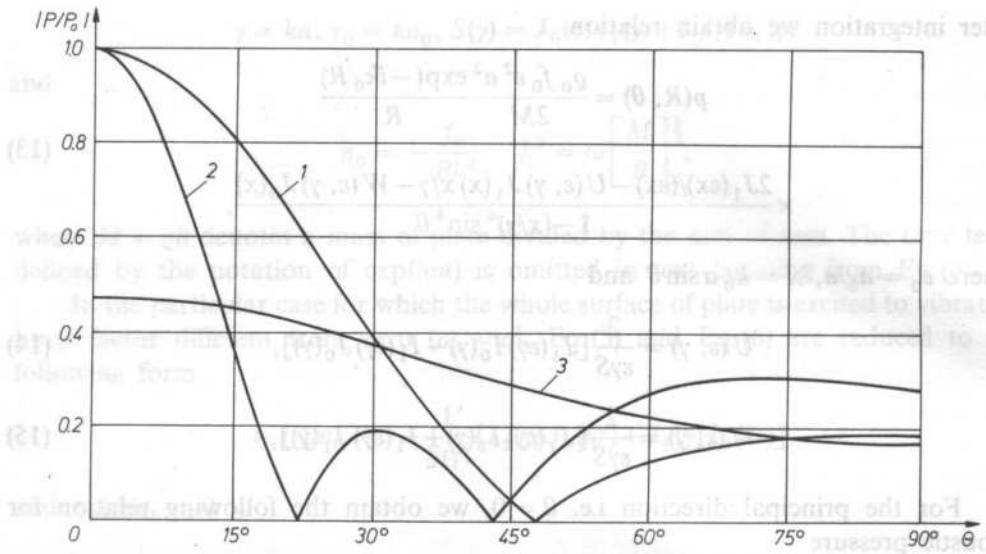

FIG. 1. The directionality coefficient of the radiation of a circular plate with different values of ka. Curve 1 — $ka = 10$, $k_0/k = 0.5$; curve 2 — $ka = 10$, $k_0/k = 1$, curve 3 — $ka = 5$, $k_0/k = 1$. It has been assumed that p_0 denotes the pressure on the principal direction with $ka = 10$, $a_0/a = 1$

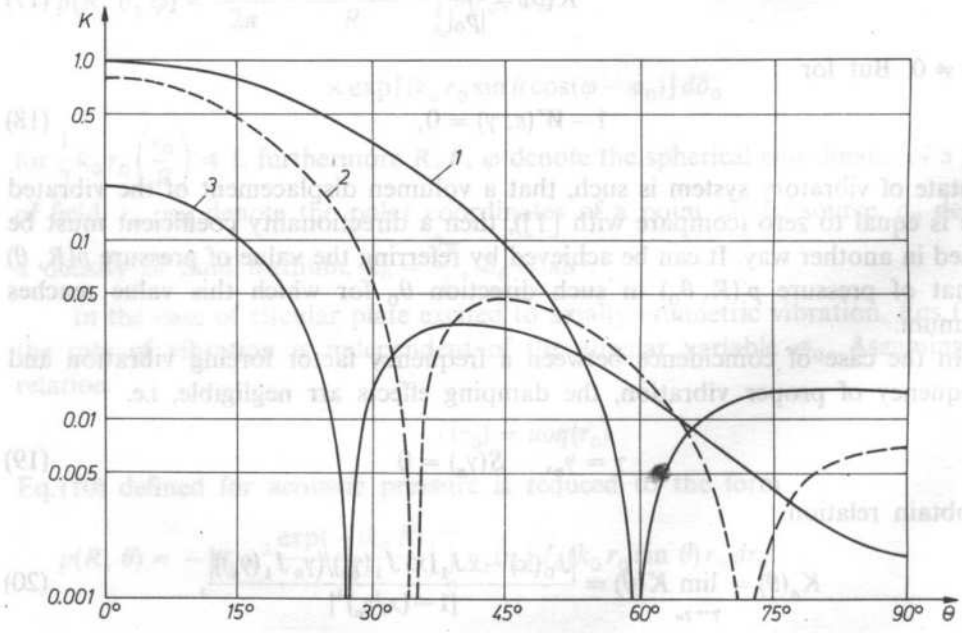

FIG. 2. The directionality coefficient of the radiation of a circular plate with different values of a_0/a. Curve 1 — $a_0/a = 1$, curve 2 — $a_0/a = 0.5$, curve 3 — $a_0/a = 0.2$. It has been assumed that $ka = 5$, $k_0/k = 2$

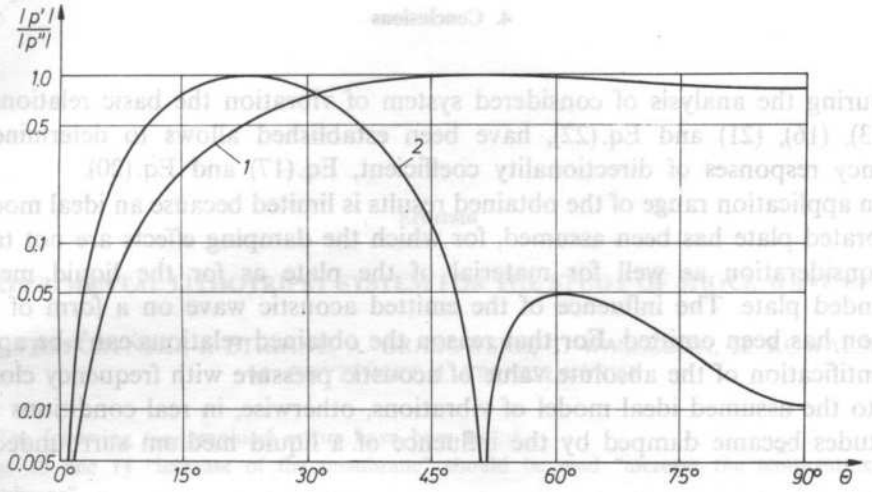

FIG. 3. The relative acoustic pressure $p'/p_{\max}$ depended on the direction of radiation, θ with $ka = 6.3064$. Curve 1 – $k_0/k = 1$, curve 2 – $k_0/k = 2$. It has been assumed that $p_{\max}$ denotes the pressure on the direction of the maximal radiation, θ_0

If a volumen displacement of plate is equal to zero, then

$$p'(R,\theta) = \frac{\varrho_0 f_0 \varepsilon^2 a \exp(-ik_0 R)}{2M} \frac{}{R} \times$$
$$\times \frac{2J_1(\varepsilon x)/(\varepsilon x) + xJ_1(x)\,[J_0(\gamma) - 2J_1(\varepsilon\gamma)/(\varepsilon\gamma)]/(\gamma) - J_0(x)}{1-(x/\gamma)^4}, \tag{21}$$

moreover, if we assume $\gamma = \gamma_n$, then Eq. (21) is adequate to the description of vibration state, for which the resonance coincides with antiresonance [1]

Diagrams of directionality coefficient of the radiation of a plate stimulated to the forced vibration are shown in Fig. 1, 2 and 3. In Fig. 2, the value $p(R, \theta)$ of the acoustics pressure, Eq. (13), was referred to the value p_0 on the principal axis, moreover it was assumed that $a_0 = a$, i.e.

$$p_0 = \frac{\varrho_0 f_0 a^2 [1 - W(\gamma)]}{2M}, \quad W_0(\gamma) = \frac{4J_1(\gamma) I_1(\gamma)}{\gamma S} \tag{22}$$

In Fig. 1 the pressure p_0 has been determined for $\gamma = 10$ in the principal direction, but the value of $p_{\max}$ shown in Fig. 3, has been defined for $\gamma = \gamma_2 = 6.3064\ldots$ in direction of maximal radiation θ_0

4. Conclusions

During the analysis of considered system of vibration the basic relations, i.e. Eqs. (13), (16), (21) and Eq. (22), have been established allows to determine the frequency responses of directionality coefficient, Eq. (17) and Eq. (20).

An application range of the obtained results is limited because an ideal model of the vibrated plate has been assumed, for which the damping effects are not taking into consideration as well for material of the plate as for the liquid medium surrounded plate. The influence of the emitted acoustic wave on a form of plate vibration has been omitted. For that reason the obtained relations can't be applied for identification of the absolute value of acoustic pressure with frequency close or equal to the assumed ideal model of vibrations, otherwise, in real conditions these magnitudes became damped by the influence of a liquid medium surrounded the plate.

The loss rigorous criterion of estimation of the relative value of pressure are considered for example for the directionality coefficient.

References

[1] T. HAJASAKA, *Electroacoustics* (in Russian), Mir Moscow 1982.
[2] S. KALISKI, *Vibration and waves*, (in Polish), PWN, Warszawa 1986.
[3] I. MALECKI, *Theorie of waves and acoustic systems*, PWN, Warsaw 1964.
[4] W. RDZANEK, *Directional characteristic of a circular membrane vibrating under the effect of a force with uniform surface distribution*, Archives of Acoustics, **10**, 2, 179–190 (1985).
[5] W. RDZANEK, *Mutual and total acoustic impedance of a system of sources with a variable surface distribution of particle velocity* (in Polish) WSP, 1979.
[6] E. SKUDRZYK, *Simple and complex vibratory systems*, University Park and London, 1968.
[7] E. SKUDRZYK, *The foundations of acoustics*, Springer Verlag, Vien-New York, 1971.

This work is part of the CPBP 02.03 Program

Received on December 29, 1988

Erratum

AN EXPERIMENTAL LITHOTRIPSY SYSTEM FOR THE STUDY OF SHOCK WAVE EFFECTS

L. FILIPCZYŃSKI, J. ETIENNE, A. GRABOWSKA, T. WASZCZUK, H. KOWALSKI, M. GRYZIŃSKI, J. STANISŁAWSKI

The following typographical errors have been noted:

1. Page 15 line 14 "increase of the membrane" should be read "increase the temperature of the membrane".
2. Page 16 line 14 "critical is" should read "critical point is".
3. Page 20 line 1 "its metal" should read "its metal plate".
4. Page 20 line 4 "3%" should read "3 Mpa".

Erratum

ACOUSTICAL SHADOW OF A SPHERE IMMERSED IN WATER. I

L. FILIPCZYŃSKI, T. KUJAWSKA

The following typographical errors have been noted:

1. In the formula 12 $h_m^2 ka$ should read h_m^2 and $p_m \cos x$ should read $P_m \cos$.
2. In the formula 17 h_m^2 ka should read $h_m ka$.

Erratum

PERCEPTION ASPECTS OF A RULE SYSTEM FOR CONVERTING MELODIES FROM MUSICAL NOTATION INTO SOUND

L. FRYDEN, J. SUNDBERG AND A. ASKENFELT

Archives of Acoustics **13**, 3–4, 269–280 (1988).

The following missprints have been noted:

1. Page 269, line 12: "an amplitudes" should read "and amplitudes".
   Line 12: "have been formulated" should read "has been formulated".
2. Page 273, line 17: "inversly" should read "inversely".
3. Page 275, line 1: "time window of two or three notes" should read "time window of one, two or three notes".
   Line 4: "marks cues" should read "mark cues".
4. Page 276, line 11: "negligeable" should read "neligible".

Line 25: "where" should read "were".

5. Page 278, line 38: "increases" should read "increased".
6. Page 279, line 39: "pronounciation" should read "pronunciation".
   Line 40: "a analysis – synthesis" should read "an analysis by synthesis".
7. Page 280, line 10: "epistalar" should read "epistlar".
   Line 12: "Finnskoga" should read "Finnskogarna".
   Line 14: "Fruelingstraum" should read "Frühlingstraum".
   Line 27: "vam" should read "van".

After line 15 following should be added:

A. Tegner: Ekorn satt i granen, from „Sjung med oss, Mamma" (nursery tune).

The reference list should be supplemented by the following:

[10] R. Carlson, A. Friberg, L. Fryden, B. Granstrom and J. Sundberg, *Speech and music performance: Parallels and contrasts*, Contemporary Music Review, **4**, 389–402 (1989).

[11] J. Sundberg, L. Fryden, and A. Askenfelt, *What tells you the player is musical?* [In:] J. Sundberg (ed.), Studies of Music Performance, publ. 39 issued by The Royal Swedish Academy of Music, Stockholm, 61–75 (1983).

[12] J. Sundberg, A. Friberg and L. Fryden, *Rules for automated performance of ensamble music*, Contemporary Music Review, **3**, 89–109 (1989).

[13] J. Sundberg, *Computer synthesis of music performance*, [In:] J. Sloboda (ed.) Generative Processes in Music, Clarendon Press, Oxford, 52–69 (1988).

The following acknowledgements should be added:

Acknowledgements

This paper was presented at the Summer Workshop on Psychoacoustics of Music, Jablonna, July 5–11, 1982 and so far not published. Since that time some rules have been modified, and thoughts around the results have cleared somewhat. Sound examples have been published in Sundberg & al., (10); rules for ensemble music performance are presented in Sundberg & al., (11); parallels between speech and music performance are discussed in Carlson & al., (12); a recent description of the rules is presented in Sundberg [13].